

**University of Strathclyde**

**Strathclyde Institute of Pharmacy and Biomedical Sciences**

**DISCOVERY OF NOVEL  
ANTIBACTERIAL AND ANTI-  
TUBERCULAR COMPOUNDS USING  
CHEMICAL GENETICS AND  
COMPUTATIONAL APPROACH  
TARGETED AT PHOSPHOLIPID  
BIOSYNTHESIS**

**JOHN TIONG**

Thesis presented in fulfilment of the requirements for the degree of  
Doctor of Philosophy

2012

## **Declaration**

This thesis is the result of the author's original research. It has been composed by the author and has not been previously submitted for examination which has led to the award of a degree.

The copyright of this thesis belongs to the author under the terms of the United Kingdom Copyright Acts as qualified by University of Strathclyde Regulation 3.50. Due acknowledgement must always be made of the use of any material contained in, or derived from, this thesis.

Signed:

Date:

## **Acknowledgements**

I am truly indebted and thankful to the many people whose help, encouragement and support made this thesis possible. First and foremost, I would like to thank both my supervisors, Dr Geoff Coxon and Dr Paul Herron for their continuous guidance and patience throughout my entire PhD. Thank you both for advising, encouraging and throwing your support behind me when experiments were failing, things got challenging and when everything seemed to fall apart. Thanks for not giving up on me. Thanks also to Dr Paul Hoskisson and Dr Nick Tucker for dispensing your advice and expertise in times of need. I still don't remember what happened on my stag do though!

To all my current and ex-colleagues in Medicinal Chemistry Lab and Molecular Microbiology lab especially Leena, Giacomo, Jessica, Sabin, Audrey, John, David, Rachael, Zhenyu, Laura, Alison, Charles, Maeidh, Tai, Vartul and Gillian, thank you very much for your help and all the nice fun in the lab. Can't imagine how dull things would have been without your good company.

I would like to thank my family, most importantly my parents and my wife, Amy for their unconditional support. Thanks especially to Amy for being with me through thick and thin, for leaving behind everything just to keep me accompanied throughout my PhD, for being an understanding wife, for putting up with the extremely frugal living knowing that we don't have much to spend and for your unconditional love. This thesis is dedicated especially to you. I love you!

## Abstract

Bacterial membranes undergo dynamic rearrangements during cell division with lateral heterogeneity in phospholipid distribution. An understanding of the synthesis of the cell membrane can provide a basis for the rational design of new antibacterial compounds which will ultimately be developed towards potential new antibiotics. Mounting evidence is implicating the importance of phospholipid in the viability of mycobacteria. The genetically tractable and related organism, *Streptomyces coelicolor* represents an ideal model for analogous studies on *Mycobacteria tuberculosis* for the purpose of designing novel classes of anti-tuberculosis drugs targeting the phospholipid biosynthesis pathways.

Genetic and biochemical studies carried out on phosphatidylserine synthase (Pss) and phosphatidylserine decarboxylase (Psd) demonstrated the essentiality of these membrane proteins in *S. coelicolor*. Alteration of *pss* expression affects the overall growth and morphology of *S. coelicolor* (i.e. hyphal growth, branching, septation and sporulation) therefore verified the potential of these proteins as drug targets. Although, the early stage “hit identification” approach using a modest collection of compounds was unsuccessful, further screening of relevant compounds should continue. Structural modifications should be carried out on some of the initial compounds which were devoid of antibacterial activity in order to address the possible pharmacodynamic issues. Protein X-ray crystallography or saturation transfer difference - nuclear magnetic resonance (STD-NMR) spectroscopy of these proteins should also be considered in the event of further futile attempts.

## Table of Contents

<b>1.0 Introduction and project rationale</b> .....	3
1.1 Global prevalence and mortality rate of tuberculosis.....	4
1.2 Tuberculosis: The disease.....	6
1.3 Drugs used in current TB treatment and new anti-TB drug development.....	9
1.4 Computer-Aided Drug Discovery and Development (CADD).....	12
1.5 <i>Streptomyces coelicolor</i> .....	14
1.5.1 <i>S. coelicolor</i> as the model bacteria for analogous study on <i>M. tuberculosis</i> .....	14
1.5.2 Cell division in <i>S. coelicolor</i> .....	16
1.5.3 Lifecycle of <i>S. coelicolor</i> .....	17
1.6 Phospholipid biosynthesis in prokaryotes.....	21
<b>2.0 Project aims</b> .....	29
<b>3.0 Materials and methods</b> .....	32
3.1 Media and antibiotics.....	33
3.2 Strains, plasmids, cosmids, bacterial cultivation and storage.....	36
3.3 Growth of <i>S. coelicolor</i> mycelium in liquid culture and measurement of growth by dry weight.....	40
3.4 <i>S. coelicolor</i> antibiotic production and measurement.....	40
3.4.1 Determination of actinorhodin (Act) concentration in liquid culture.....	40
3.4.2 Determination of undecylprodigiosin (Red) concentration in liquid culture.....	40
3.5 Spore sensitivity assays.....	41
3.5.1 Lysozyme, DMSO, SDS, sonication and temperature sensitivity.....	41
3.5.2 Osmotic stress test (KCl & sucrose).....	41
3.6 Antimicrobial susceptibility testing via Disc diffusion assay.....	41
3.7 Production of electrocompetent <i>E. coli</i> .....	42
3.8 Electrotransformation of competent cells.....	43
3.9 Intergeneric transfer of plasmid/cosmid from <i>E. coli</i> to <i>S. coelicolor</i> M145 by conjugation.....	44
3.10 DNA isolation.....	45
3.10.1 Modified Birnboim and Doly DNA Isolation Protocol.....	45
3.10.2 Wizard <sup>®</sup> Plus SV Minipreps DNA Purification System.....	46
3.10.3 <i>S. coelicolor</i> Genomic DNA Isolation Protocol.....	47
3.11 RNA extraction from <i>Streptomyces</i> .....	47
3.12 Restriction digest of DNA.....	49
3.13 Dephosphorylation of digested DNA and heat inactivation of Thermosensitive Alkaline Phosphatase, TSAP.....	50

3.14	Phosphorylation of digested DNA and heat inactivation of T4 Polynucleotide Kinase.....	51
3.15	Ethanol precipitation of DNA.....	51
3.16	Ligation of vector and insert DNA.....	52
3.17	Agarose gel electrophoresis of DNA.....	53
3.18	Gel extraction of DNA.....	54
3.19	PCR product purification protocol.....	55
3.20	Klenow polymerase for blunting a 5' overhang.....	56
3.21	Design of primers and DNA sequence analysis.....	56
3.22	Polymerase Chain Reaction (PCR).....	57
3.23	Reverse-transcription PCR (RT-PCR).....	60
3.24	Redirect© Technology: PCR-targeting system in <i>S. coelicolor</i> .....	62
3.25	Transposon inactivation of target gene.....	63
3.26	Enhanced green fluorescent protein ( <i>egfp</i> ) - gene fusion as a mode to report protein localization within bacterial cells.....	63
3.27	DNA cloning/subcloning.....	64
3.28	Phospholipid extraction and identification via thin layer chromatography (TLC).....	64
3.29	Microscopy.....	65
3.30	Bioinformatics.....	66
3.30.1	Inter-species protein sequence alignment and phylogenetic analysis.....	66
3.30.2	Two-dimensional (2D) similarity searching of potential inhibitor of target protein.....	66
3.31	Chemical synthesis of 2-amino-5-methylthiazole-4-carboxylate (ATC) derivatives.....	66
3.31.1	Synthesis of methyl 2-amino-5-methylthiazole-4-carboxylate (QAB004).....	67
3.31.2	Synthesis of 2-amino-5-methylthiazole-4-carboxylic acid (QAB004A).....	68
3.31.3	Synthesis of methyl 2-amino-5-benzylthiazole-4-carboxylate (QAB008).....	69
3.31.4	Synthesis of methyl 2-heptanamido-5-methylthiazole-4- carboxylate (QAB014).....	70
3.32	Chemical Analysis.....	71
3.32.1	Melting point determination.....	71
3.32.2	Elemental analysis (CHN).....	71
3.32.3	Infrared spectroscopy (IR).....	71
3.32.4	Nuclear magnetic resonance (NMR) spectroscopy.....	71
3.32.5	Mass spectrometry (MS).....	72

<b>4.0 Results: Phylogenetic analysis and protein sequence alignment</b> .....	73
4.1 Introduction.....	74
4.2 Phylogenetic analysis of Psd and Pss homologues.....	74
4.3 Prediction of membrane spanning region and orientation of Psd and Pss.....	84
4.4 Discussion and conclusion.....	86
<b>5.0 Results: Disruption of <i>psd</i> and <i>pss</i> in <i>S. coelicolor</i></b> .....	88
5.1 Introduction.....	89
5.2 Transposon, Tn5062 inactivation of <i>psd</i> and <i>pss</i> in <i>S. coelicolor</i> .....	90
5.3 Cloning of <i>psd</i> and <i>pss</i> into $\Phi$ BT1 based integrating vector, pAV11b.....	95
5.4 Transposon inactivation of <i>psd</i> and <i>pss</i> post-complementation.....	104
5.5 Controlled-expression of <i>pss</i> in LSM105 ( <i>pss</i> ::Tn5062/ <i>tcp830-pss</i> <sup>+</sup> ).....	106
5.6 RT-PCR profile of M123A ( <i>psd</i> <sup>+</sup> <i>pss</i> <sup>+</sup> / <i>tcp830-psd</i> <sup>+</sup> <i>pss</i> <sup>+</sup> ) to verify the nature of gene transcription by <i>tcp830</i> promoter.....	108
5.7 Cloning of <i>psd</i> and <i>pss</i> into pSAM2 based integrating vector, pPM927.....	111
5.8 Construction of the deletion vector for PCR-directed mutagenesis of <i>psd</i> and <i>pss</i> in <i>S. coelicolor</i> .....	118
5.9 PCR-directed mutagenesis of <i>psd</i> and <i>pss</i> post-complementation.....	123
5.10 PCR-verification of JT672 ( $\Delta$ <i>pss</i> :: <i>apra</i> <sup>r</sup> / <i>ptipAps</i> <sup>+</sup> ).....	125
5.11 Controlled-expression of <i>pss</i> on minimal medium and MS agar.....	128
5.12 Discussion and conclusion.....	133
<b>6.0 Results: Phenotypic characterization of <i>pss</i> mutant, JT672</b> .....	138
6.1 Introduction.....	139
6.2 RT-PCR and thin layer chromatography profiles of JT672.....	139
6.2.1 Introduction.....	139
6.2.2 Identifying appropriate solvent system for phospholipid TLC.....	140
6.2.3 Controlled –expression of <i>pss</i> and corresponding phospholipid and RT-PCR profiles of JT672 ( $\Delta$ <i>pss</i> :: <i>apra</i> <sup>r</sup> / <i>ptipA-pss</i> <sup>+</sup> ).....	145
6.2.3.1 Phospholipid and RT-PCR profiles of 3MA grown JT672.....	145
6.2.3.2 Phospholipid and RT-PCR profiles of YEME grown JT672.....	149
6.2.4 Metabolism of the anionic and zwitterionic phospholipids in <i>S. coelicolor</i> .....	156
6.3 Screening for mutant phenotypes on 3MA under different growth conditions (temperature, KCl and sucrose concentrations).....	158
6.4 Spore sensitivity assay.....	165

6.5	Dry weight growth curve and antibiotics production of JT672.....	171
6.6	Enhanced green fluorescent protein (EGFP) tagging of Psd and Pss as a mode to analyse protein localization within bacterial cells.....	174
6.6.1	Introduction.....	174
6.6.2	Construction of the <i>egfp</i> -tagged cosmids of <i>psd</i> and <i>pss</i> .....	174
6.6.3	C-terminal <i>egfp</i> -tagging of <i>psd</i> or <i>pss</i> in <i>S. coelicolor</i> .....	179
6.7	PCR-verification of ME67 ( <i>pss-egfp</i> ).....	181
6.8	Microscopy analysis of ME67 and JT672.....	183
6.9	Discussion and conclusion.....	194
6.9.1	Effect of varying expression of <i>pss</i> on RT-PCR and phospholipid profiles of <i>S. coelicolor</i> .....	194
6.9.2	Adaptation of JT672 to different external growth pressures.....	197
6.9.3	Effect of varying expression of <i>pss</i> on growth curve and antibiotic production of JT672.....	199
6.9.4	Microscopy analysis of ME67 and JT672.....	200
<b>7.0</b>	<b>Results: Screening for novel anti-TB compounds targeting Psd and Pss in <i>S.coelicolor</i></b> .....	<b>204</b>
7.1	Introduction.....	205
7.2	The rationale behind choosing natural substrate of target protein as template for virtual screening.....	206
7.3	2D similarity screening of potential inhibitor(s) of Psd.....	207
7.4	Analogues of thiolactomycin (TLM): 2-amino-5-methylthiazole-4-carboxylate (ATC) derivatives.....	216
7.4.1	Introduction.....	216
7.4.2	Chemical synthesis of ATC derivatives.....	217
7.5	Screening of compounds for antibacterial activities.....	221
7.6	Discussion and conclusion.....	224
7.6.1	Chemical mechanism involved in the synthesis of ATC derivatives.....	224
7.6.2	Screening for potential inhibitors of Psd.....	228
<b>8.0</b>	<b>Conclusion and future work</b> .....	<b>232</b>
<b>9.0</b>	<b>References</b> .....	<b>235</b>



## Abbreviations

3MA	Minimal medium + mannitol
Apra	Apramycin
Amp	Ampicillin
ATC	2-amino-5-methylthiazole-4-carboxylate
atc	Anhydrotetracycline
CADD	Computer-Aided Drug Discovery and Development
CDP-DAG	Cytidine-diphosphate-diacylglycerol
Cds	CDP-diglyceride synthetase
CFU	Colony forming unit
Chp	Chaplin
CL	Cardiolipin
CL3	Containment level 3
Cls	Cardiolipin synthase
CR3	Complement receptor type 3
CS	Cycloserine
DOT	Directly observed treatment
DST	Drug susceptibility testing
EGFP	Enhanced green fluorescent protein
FVYE	Fab-1, YGL023, Vps27, and EEA1
GOLD	Genetic Optimisation for Ligand Docking
Hyg	Hygromycin
LB	Luria- Bertani
MDR	Multi drug resistant
MIC	Minimal inhibitory concentration
MS	Mannitol soy flour
NMR	Nuclear magnetic resonance
OD	Optical density
PA	Phosphatidic acid
PCR	Polymerase chain reaction
PE	Phosphatidylethanolamine
PG	Phosphatidylglycerol
PG3P	Phosphatidylglycerol-3-phosphate
PgP	Phosphatidylglycerol phosphate phosphatase
PgsA	Phosphatidylglycerol-3-synthase
PI	Phosphatidylinositol
PI3P	Phosphatidylinositol 3-phosphate
Pis	Phosphatidylinositol synthase
PknG	Protein kinase G
PLC	Phospholipase C
PS	Phosphatidylserine
Psd	Phosphatidylserine decarboxylase
Pss	Phosphatidylserine synthase
qPCR	Quantitative real time polymerase chain reaction
QSAR	Quantitative-structure activity relationship
Rdl	Rodlin
RPM	Revolution per minute

RT-PCR	Reverse transcription-polymerase chain reaction
Spec	Spectinomycin
Str	Streptomycin
TACO	Tryptophan aspartate-containing coat protein
TB	Tuberculosis
TLC	Thin layer chromatography
TLM	Thiolactomycin
XDR	Extensively drug resistant

## **1.0 Introduction and project rationale**

## 1.1 Global prevalence and mortality rate of tuberculosis

Tuberculosis (TB) is a debilitating disease that has plagued mankind for many millenia. The disease is caused by the slow growing bacterial species of *M. tuberculosis* which was first discovered by a German physician, Robert Koch in 1882. The disease is so contagious that approximately a third of the world population was infected by TB in the 20<sup>th</sup> century (Kochi, 1994) with an estimate of 8 million new cases and 2 million deaths each year (Harries & Dye, 2006). There were an estimated 8.8 million new and recurrent cases of TB reported in 2010 with 59% being reported in Asia. Approximately 40% of total global cases were found in China and India alone followed by 26% in Africa. The global TB death rate and prevalence of Mtb/ HIV co-infection were 23% and 0.18% respectively but in some African nations, TB fatality was more than 50% due to higher incidence of AIDS. While more than half of global TB cases occurred in developing nations in Asia (Dye *et al.*, 1999; WHO, 2008; WHO, 2011), resurgence is on the rise in highly industrialized countries in Europe and United States (12% and 3% of total global cases in 2010) owing to factors like international migration, strong epidemiological coexistence between TB with HIV and drug resistance (Parry & Davies, 1996; Mori, 2007; WHO, 2011).

As TB endemic area, the disease burden in China was dramatically reduced between 1990 and 2010 where prevalence, mortality and annual incidence rates declined by 50%, 80% and 3.4% respectively. This was on track with the Millenium Development Goal target that projected the reduction of TB incidence rates by 2015 (WHO, 2011). However, just when the conventional TB pandemic appears to be slowing, there are now reports of emergence of multi drug resistant (MDR) strain of *M. tuberculosis* which has decreased susceptibility to first-line drugs such as isoniazid and rifampicin (Espinal, 2003; Zager & McNerney, 2008) making disease eradication more challenging. A total of 272,906 cases of MDR-TB were reported globally in 2000, increasing alarmingly to 424,203 cases in 2004 (Zignol *et al.*, 2006) and further trending upwards to 650,000 cases in 2010 (WHO, 2011). Collectively, India and China accounted for approximately half of world MDR-TB cases (WHO,

2011). Even though MDR-TB has long been recognized as a serious threat in TB treatment, it is not prioritized by the developing nations in particular due to national financial constraint as well as lack of expertise in this area (Mori, 2007).

This is further complicated by the emergence of extensively drug resistant (XDR)-TB (which constitutes up to 20% of the reported MDR-TB cases in some regions) defined as resistance to rifampicin, isoniazid, any fluoroquinolone and one or more of the intravenous second-line drugs (capreomycin, kanamycin and amikacin). XDR-TB is particularly prevalent in several countries of the former Soviet Union, Africa and South East Asia (Lawn & Wilkinson, 2006; Wright *et al.*, 2009; WHO, 2011). This is a major global health concern that needs be addressed immediately and if left unattended is expected to cost the lives of millions in the coming decades. Thus, development of new potent drugs is of paramount importance in combating the scourge of this deadly disease.

## 1.2 Tuberculosis: The disease

TB is a contagious disease which is spread via inhalation of aerosolized water droplets from the cough or sneeze of a TB patient. Once in the lung, the bacteria are internalized into macrophage phagosomes via receptor-specific interactions (Houben *et al.*, 2006). One of such receptors which has been identified *in vitro* is the cholesterol-dependent complement receptor type 3 (CR3) that allows the uptake of *Mycobacterium sp* into macrophages while preventing lysosomal degradation of the internalized bacterium (Gatfield & Pieters, 2000; Peyron *et al.*, 2000). In addition, Peste (Pes) which is member of the CD36 family of scavenger receptors is also important for similar internalization and survival processes of the pathogen (Philips *et al.*, 2005).

*M. tuberculosis* is capable of secreting the acid phosphatases (e.g. SapM) which might prevent the fusion of phagosome with the lysosome by depleting the phosphatidylinositol 3-phosphate (PI3P) molecules. PI3P molecules are generated by phosphatidyl 3-kinases which are normally recruited by the endosomes (Vergne *et al.*, 2005). Since PI3P is required to bind with the so-called Fab1, YOTB, Vac1, and endosome autoantigen 1, EEA1 (FVYE) domain for the fusion of early and late endosomes (Gruenberg & Stenmark, 2004), elimination of PI3P will in turn obstruct the fusion of *M. tuberculosis* containing phagosomes to lysosomes thereby ensuring their survival within the macrophage.

Other factors that can modulate the intracellular trafficking include a eukaryotic like serine/threonine kinase, the protein kinase G (PknG) of *M. tuberculosis* that stalls the maturation of phagosomes (Walburger *et al.*, 2004), preservation of a collection of host molecules such as tryptophan aspartate-containing coat protein (TACO) needed to circumvent the fusion of phagosomes to lysosomes (Ferrari *et al.*, 1999) and glycosylated phosphatidylinositol lipoarabinomannan (ManLAM) that restrains maturation of phagosomes (Fratti 2003). Therefore, even with most of the *M. tuberculosis* killed via alveoli macrophages engulfment, the remnants which survived through the evasion of this

immune defense mechanism will continue to replicate in the established niche within the macrophage.

Multiplication of *M. tuberculosis* persists with eventual lysis of the infected cells by the bacterial phospholipase C<sub>s</sub> (PLC) (Cotes *et al.*, 2008; Bakala N'Goma *et al.*, 2010), releasing the pathogens which are then phagocytosed by further macrophages and blood monocytes. Additional immune cells, especially T-cells, may be mobilised against the infected macrophages when they move into tissues to form the granuloma. Central area of necrosis then develop, resulting in the death of majority of the bacteria as well as the surrounding lung tissues. Some however may lie dormant for months or even years after the initial contact with the possibility to be reactivated as latent TB if immunity of the host dampens (Grosset, 2003). Hence, an effective antimicrobial compound must be able to target not only the viable bacteria but the ones in dormancy for complete eradication of the disease from a patient.

While the lungs are the initial infection site (pulmonary TB), the disease is capable of spreading throughout the body (extra-pulmonary TB) such as the bones, the nervous systems, colon, intestine etc. Nevertheless, it is pulmonary TB that is known to be the most contagious form of the disease. There are 3 possible outcomes following initial infection. The first and the most optimistic outcome would be where sufficient immunity is mounted to rid the host of the bacteria and the host fully recovers from the disease. The other possibility will be where complete eradication of the bacteria cannot be achieved by host's immune system but a defense barrier is formed against the disease. The patient maybe symptomless while the bacteria enter into dormancy but if the host's immune system weakens at some point of his/her life, active TB will develop. This is known as latent TB. In the full blown stage of the disease, the bacteria will spread around the lungs causing destruction to the lung tissues resulting in death if it goes untreated.

The disease can be prevented by BCG vaccination which confers immunity in 70 to 80% of immunized individuals. Current treatment is divided into 2 phases; the

initiation phase and the continuation phase which can be given either supervised (also known as directly observed treatment (DOT)) (Bayer & Wilkinson, 1995) or unsupervised for several months. Current anti-TB drugs are often said to be ineffective by modern standards due to the lengthy and complicated regimen. This often leads to patient non-compliance which may result in the emergence of resistant strain of bacteria (Sumartojo, 1993; Volmink & Garner, 2007).

Hence, it is clear that unlike the current anti-TB medicines, new classes of compounds are required to be potent to reduce the treatment duration, selective against the pathogen to avoid side effects and more importantly, novel in their cellular targets for potential integration into existing regimen. Recent work in genetically-related Actinobacteria i.e. *S. coelicolor* and *M. tuberculosis* has revealed that membrane phospholipid biosynthesizing enzymes in both bacteria are promising targets for drug development. Our exciting research endeavours are based on this scheme where both chemical and computational approaches are utilized in conventional screening of compounds which could potentially target these enzymes.



### 1.3 Drugs used in current TB treatment and new anti-TB drug development

Limitation with current TB treatment is its complexity which entails a cocktail of anti-TB drugs which have to be taken at a precise combination over a stipulated duration that might compromise patient compliance (Xu *et al.*, 2009). Given the fact that *M. tuberculosis* grows only very slowly together with its robust waxy cell wall defense barrier, anti-TB drugs have to be taken for a long time by the patients in order to exert their full antimicrobial effect to completely eradicate the pathogens. Such is the reason behind the complicated and lengthy nature of the conventional chemotherapeutic regimen for the treatment of TB.

The ultimate aims of the treatment regimen are to contain the infection by clearing the pathogens as quickly as possible from the body and to prevent the emergence of drug resistance. The treatment involves the administration of a combination of different drugs with their own mode of actions over several months. These drugs are categorized into either first-line; isoniazid, rifampicin, pyrazinamide, ethambutol and streptomycin or second-line; para-aminos salicylic acid, fluoroquinolone such as moxifloxacin, prothionamide, ethionamide, amikacin, kanamycin, cycloserine etc, with the former generally having better efficacy and safety index (WHO, 2010). The molecular targets of the first-line and some of the second-line drugs are summarized in Table 1.

The therapy starts off with an initial 2 months of intensive treatment involving the administration of isoniazid which is effective against actively growing *M. tuberculosis*, killing approximately 95% of the pathogen within the first 2 days, rifampicin that kills the sporadically active bacterial population and pyrazinamide that eliminates those with low metabolic activity. The bacteriostatic agent, ethambutol should be added to the treatment regimen in case of known risk of resistance to isoniazid. The intensive eradication stage is followed by a 4-month continuation phase using isoniazid and rifampicin, each with its own purpose. Rifampicin is important to prevent possible relapse since it is effective against persistor whereas isoniazid is used to preclude the possibility of rifampicin resistance

Table 1: First-line and several second-line anti-TB agents with the molecular targets in *M. tuberculosis* (adapted from Dover & Coxon, 2011)

<b>Drug</b>	<b>Drug targets</b>
Isoniazid	Enoyl-ACP reductase involved in mycolic acid elongation
Rifampicin	DNA-dependent RNA polymerase $\beta$ -subunit
Pyrazinamide	Membrane depolarization, fatty acid synthesis, protein translation and ribosomal protein S (RpSA)
Ethambutol	Arabinosyl transferase, embB involved in cell wall arabinan polymerization
Streptomycin	30S subunit of prokaryotic ribosomes
Para amino salicylic acid	Salicylate kinase enzyme Dhbe involved in the synthesis of iron regulating molecules called siderophores
Fluoroquinolones (eg. moxifloxacin)	DNA gyrase
Ethionamide/prothionamide	Enoyl-ACP reductase involved in mycolic acid elongation
Aminoglycosides (eg. kanamycin, capreomycin)	30S subunit of prokaryotic ribosomes

(Mitchison, 2000). None of the current anti-TB agents are effective against target ATP synthase (Andries *et al.*, 2005) and nitroimidazole PA-824 from PathoGenesis Corporation (Stover *et al.*, 2000). Both compounds exhibit activity against non-replicating bacteria which could potentially shorten the conventional anti-TB regimen.

In addition, other approaches have to be taken in view of extensive amount of time and funds required in developing new chemical entities, one of which involves re-evaluation of existing drugs. Phase II clinical trials conducted to investigate the possibility of substituting ethambutol with moxifloxacin (Burman *et al.*, 2006) or isoniazid with moxifloxacin (Dorman *et al.*, 2009) in the initial 2-month phase have yielded promising outcomes. Other examples include evaluating the non-indicated use of thioridazine (sedative drug) as an anti-TB which has shown activity against XDR-TB (Amaral *et al.*, 2010) as well as the antiprotozoal agent, nitazoxanide which shows bactericidal activity against both replicating and non-replicating *M. tuberculosis* (De Carvalho *et al.*, 2009).

With the emergence of the almost untreatable XDR-TB and XXDR-TB, it has become clear that the rate of development of bacterial resistance has outpaced the rate of anti-TB/antibiotic discovery. The urgent need of new generation of anti-TB agents should not be downplayed in view of an impending global plague. A global TB framework should be drawn to foster multidisciplinary collaborations among drug industries and academia to ensure channeling of sufficient funds and support into drug discovery programme for sustained supply of new anti-TB agents.

## 1.4 Computer-Aided Drug Discovery and Development (CADD)

CADD (with other similar terms like computer-aided drug design, computer-aided molecular modeling, *in silico* drug design etc); (Kapetanovic, 2008) is a term that defines the combination of biology and chemistry theories with computational methods in designing ligands that inhibit or mimic the activities of biological molecules *in vivo*. Computer-assisted drug design offers an inexpensive alternative as well as a complementary procedure to the traditional drug discovery techniques i.e. random screening and chance observation based on molecular diversity of compounds from natural sources which can be costly and time-consuming. It is widely employed in the chemical, biomedical, pharmaceutical and agrochemical industries to expedite hit identification as well as hit-to-lead optimization, to predict the toxicity/safety profiles of the potential drug compounds and to ease drug delivery system formulation.

Several approaches are available depending on the drug design scenario explored. There are generally four different design scenarios which may necessitate the employment of different techniques. When both protein and ligand structures are known, both ligand-based (3D spatial orientation of important pharmacophores presence within a ligand) and structure-based design (protein target docking) are used concurrently; when protein structure is known but ligand structure is unknown, *de novo* structure-based technique is employed; when protein structure is not identified whereas the ligand structure is established, quantitative-structure activity relationship (QSAR) and 2D similarity design will be applied; when both ligand and protein structures are unknown which is the trickiest of all scenarios (this project), this may draw on various experiments to identify the target protein as well as the screening of the large library of compounds for potential ligands which could be expensive and challenging. It is worth pointing out that the matching of different techniques to different drug design scenarios mentioned above is just a proposition of the probable starting approach. In fact, all techniques can be used in each scenario depending on the stage of development. In other words, there is no exclusivity of techniques in any drug design scenario.

Generally, the computational techniques are applied at different stages of the drug discovery process for several purposes i.e. visualizing the protein structure and the physicochemical properties of its active site, identifying new ligands for the target protein using virtual screening, predicting and optimizing the binding mode of known active ligands as well as the binding affinities of related series of compounds. Thereafter, *in silico* filters are used to sort the list of compounds with the purpose of eliminating ligands with unwanted properties such as poor biological activity or high toxicity based on QSAR (Kapetanovic, 2008; Acharya *et al.*, 2011).

In the modeling of protein-ligand interactions, several programs such as Genetic Optimisation for Ligand Docking (GOLD), FlexX, Fitted, Glide and Surflex have become regularly used tools (Corbeil & Moitessier, 2009). The scoring functions commonly used in these programs for the quantification of ligand-protein interactions are force-field based, knowledge-based and empirical scoring functions (Ferrara *et al.*, 2004). Nevertheless, none of the docking programs in current use can guarantee screening with no false negative and/or false positive even with the employment of such sophisticated scoring functions.

There is little doubt that CADD has gained importance and implementation in drug design arena. It complements and improves the role of traditional techniques like chemical synthesis and biological experimentation which require a great deal of time and resources. As a matter of fact, it normally takes 14 to 20 years to develop and to bring a new drug to market with a huge cost which can range from hundreds of millions to almost a billion dollars (Shankar 2006). Such is the huge investment which is normally absorbed by end users like us since new drugs are almost always highly priced. At present, CADD accounts for approximately 10% of research and development expenditure of pharmaceutical companies. However, this is expected to rise to 20% in year 2016 with its increasing application in drug discovery and development (Van de Waterbeemd 2003).

## 1.5 *Streptomyces coelicolor*

### 1.5.1 *S. coelicolor* as the model bacteria for analogous study on *M. tuberculosis*

*S. coelicolor* is a Gram positive soil-dwelling, saprophytic bacterium of the actinobacteria phylum although some also inhabit aquatic niches. Other members of this group include the mycobacteria and corynebacteria which all possess the characteristic of high genomic content of Guanine and Cytosine bases; 72.12% *S. coelicolor* (Bentley *et al.*, 2002). *Streptomyces* spp are of great industrial relevance due to their capability to produce numerous types of secondary metabolites that possess antimicrobial, antiviral, antitumor, antiparasitic, and immunosuppressive effects. Approximately two-thirds of all naturally-derived antibiotics of current medicinal use are produced by *Streptomyces* spp. Of all these useful compounds, *S. coelicolor* is known to produce 4 antibiotics i.e. actinorhodin (Act), undecylprodigiosin (Red), methylenomycin (Mmy) and calcium-dependent antibiotic (CDA) (Bentley *et al.*, 2002).

*S. coelicolor* is a model for analogous study on *M. tuberculosis* due to the lack of pathogenicity, well-sequenced genetic map with 7,825 predicted genes, bioinformatics tools available that provide us with knowledge of the degree of synteny to *M. tuberculosis* (Bentley *et al.*, 2002) as well as the availability of genetic tools and sensitive screens for identifying defects in cell division in genetically modified mutants. The genomic synteny between *S. coelicolor* and *M. tuberculosis* is shown in Figure 1. Recent studies have also revealed significant similarity in the developmental and morphological stages in both species (Scherr & Nguyen, 2009) further supporting the use of *S. coelicolor* as model for study on *M. tuberculosis*. Finally, the structural and biochemical differences between mammalian and bacterial proteins can very often be exploited to our advantage in identifying targets for novel anti-bacterial drug design.

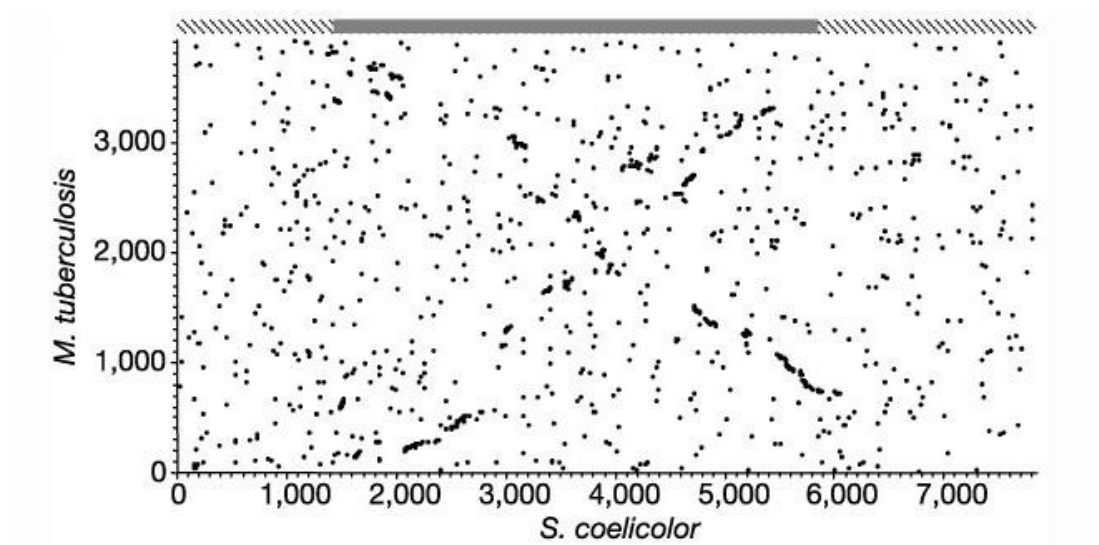


Figure 1: Comparison of chromosome structure between *S. coelicolor* and *M. tuberculosis* (reproduced from Bentley *et al.*, 2002). The two axes represent the coded proteins in the genomic order for the chromosome. DnaA is located centrally in the core region (*SCO1440 to 5869*) as represented by the solid bar above the plot. The core region is flanked by the arms as shown in hatched line. The x-dots represent a region of synteny between the two bacteria. Such synteny in the core region points to the fact that *S. coelicolor* and *M. tuberculosis* hailed from common ancestor with subsequent evolutionary acquisition of DNA of the arms. In *S. coelicolor*, the central core region comprises of almost half of the whole chromosome and nearly all genes located here are found to be essential genes i.e. involving in critical processes like cell division, DNA replication, transcription, translation etc. The non-essential genes are mostly found in the arms that flanked the two sides of the core

### 1.5.2 Cell Division in *S. coelicolor*

There are generally two known types of cell division in the lifecycle of *S. coelicolor* (McCormick, 2009). The first division involves the infrequent formation of single-layered bacterial cell wall that does not engage in cell constriction and separation. Such infrequent process is the reason behind the widely-spaced septa (cross walls) in filamentous like hyphal cells; each of these containing tens of copies of chromosomes (Prosser & Tough, 1991; Flardh *et al.*, 2000). The second division which is synchronized within each aerial hypha itself whilst asynchronous between hyphae requires the remodeling of synthesized cell wall material into double-layered septa for the purpose of sporulation. Unlike the first division, each prespore compartment contains only a single copy of chromosome needed for dispersion (McCormick, 2009).

Septation generally necessitates the assembly of FtsZ proteins at multiple foci along the hyphae marking the sites to which other division proteins will be recruited. Long spiral swirls are then formed followed by their construction into the ring like structure known as the Z-ring at the inner cytoplasmic membrane completing the binary fission process (McCormick *et al.*, 1994; Schwedock *et al.*, 1997). *ftsZ* mutants are still viable under normal growth conditions though no vegetative division and sporulation are observed. This points to the fact that mycelium branching and hyphal tip extension do not require cell division (McCormick *et al.*, 1994; Flardh & Buttner, 2009). This was proven later via time-lapse microscopy (Jyothikumar *et al.*, 2008).



### 1.5.3 Lifecycle of *S. coelicolor*

The general lifecycle of *Streptomyces* spp is shown in Figure 2. *S. coelicolor* establishes a lifecycle that is both complex and similar to that of filamentous fungi. Apical growth at hyphae tips occurs via *de novo* incorporation of peptidoglycan precursors at the extending cell wall (Braña *et al.*, 1982; Gray *et al.*, 1990; Prosser & Tough, 1991 & Miguélez *et al.*, 1992). The AfsK-regulated DivIVA protein plays a fundamental role in steering tip extension and initiation of new branches of hyphae which collectively form the vegetative mycelium. Hence, it indirectly determines the shape of this bacterium (Flardh, 2003a; Hempel *et al.*, 2008; Flardh & Buttner, 2009; Hempel *et al.*, 2012). Mycelium is an important vegetative structure that normally plies across and deep down into media scavenging for substrate, giving rise to a vegetative colony. Unlike most bacteria, cell division is dispensable during vegetative growth of *S. coelicolor* as described previously. The importance of cell division is however observed in the developmental and differentiation stage i.e. the formation of aerial hyphae for the purpose of sporulation (McCormick, 2009).

Perhaps, the deteriorating environmental condition such as the depletion of nutrients marks the advent of change of phase in the life cycle of *S. coelicolor*; shifting from the vegetative growth phase to dormant spore phase (Flardh & Buttner, 2009; Scherr & Nguyen, 2009). Reproductive spores are crucial for the purpose of dispersion when its survival is deemed challenged. The imperative biological adaptation will be triggered by several sigma factors, principally by those responsible for aerial hyphae formation ( $\sigma^B$ ) and sporulation ( $\sigma^L$  and  $\sigma^M$ ) (Lee *et al.*, 2005). Aerial hyphae grow up to the surface of the colony at the expense of substrate hyphae lysis (Willey *et al.*, 2006) and such morphological differentiation normally coincides with biosynthesis of important secondary metabolites including antibiotics such as actinorhodin and undecylprodigiosin (Takano *et al.*, 1992; Bystrykh 1996; Kang *et al.*, 1998).

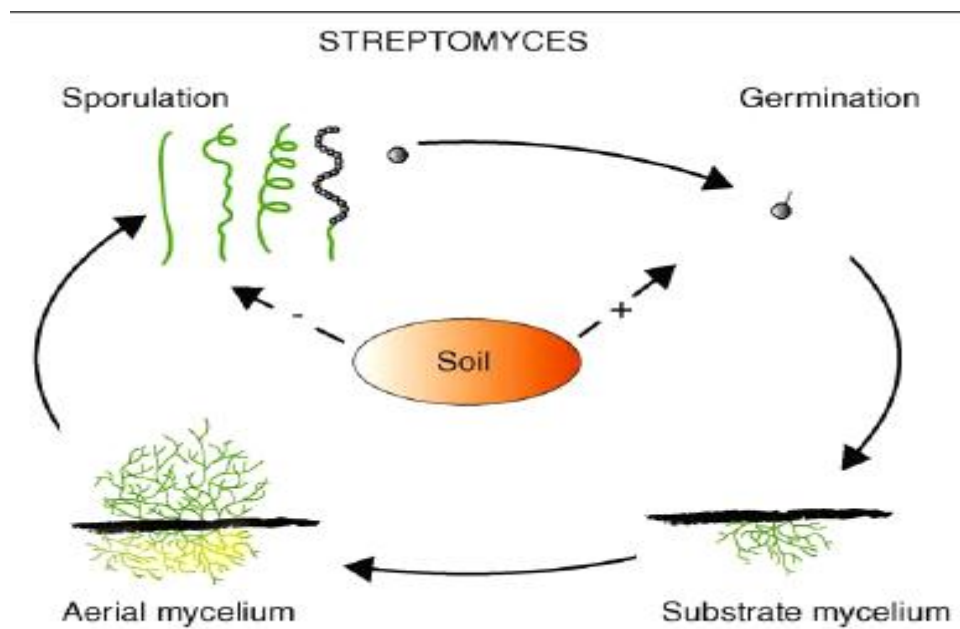


Figure 2: General lifecycle of *Streptomyces* spp (adapted from Scherr & Nguyen 2009). Favourable conditions (arrow with positive sign) will trigger the germination of spores that give rise to vegetative mycelia which grow by means of hyphal tip extension and branching. When survival is challenged (arrow with negative sign), important secondary metabolites will be secreted in conjunction with morphological differentiation resulting in erection of aerial hypae and subsequent septation to form robust spores for dispersion. The cycle will continue thereafter.

In rich media such as R2YE, surfactant peptide, SapB which is specified by the rapid aerial mycelium (*ram*) formation gene cluster (derived from *ramS* under the control of regulatory gene, *ramR*); (Kodani *et al.*, 2004) plays a vital role as a scaffolding protein that allows the efficient formation of aerial hyphae into the air. In *bld* mutants, SapB production is impaired with blockade at the stage of formation of aerial hyphae therefore these mutants acquire a smooth bald colony surface phenotype. Other defects in *bld* mutants include faulty cell-cell signaling, carbon catabolite repression and lack of antibiotic production (Kelemen & Buttner, 1998). In wild type strains, the formation of aerial hyphae will lead to their septations to form chains of uninucleoid cells (also called sporogenic cells) that will shape into spores (Willey *et al.*, 1991; Capstick *et al.*, 2007).

In minimal media, chaplins (Chp's) are found to be the key alternative contributors to the formation of aerial hyphae that is found to be independent of SapB (Capstick *et al.*, 2007). In order for aerial hyphae to ply through the surface tension of the solid medium in which it grows, *S. coelicolor* has to coat its aerial hyphae with hydrophobic sheath which is made from both Chp and rodlin (Rdl) proteins. In *S. coelicolor*, there are 8 types of Chp proteins, ChpA -H which can be divided into two groups; 3 long and 5 short Chp's. Short Chp attaches itself to the aerial hyphae via heteropolymerization with the aerial hyphae cell wall-anchored long Chp forming the hydrophobic filaments (Elliot *et al.*, 2003; Flardh & Buttner, 2009). *chp* genes are expressed prior to the formation of aerial mycelium and mutants of all the 8 genes are deprived of aerial mycelium on both rich and minimal media (Capstick *et al.*, 2007; Claessen *et al.*, 2004). Double mutants which are unable to synthesize both SapB and Chp appear bald under any conditions which they are grown in (Capstick *et al.*, 2007). Rdl proteins on the other hand are subdivided into two types, A and B (Claessen *et al.*, 2002). Mutants of both genes are observed to form disordered network of fine filaments despite the fact that hydrophobic sheath and aerial mycelium are still formed (Claessen *et al.*, 2003).

In a way similar to the vegetative growth phase, aerial hyphae grow by way of tip extension driven by DivIVA foci with occasional cross-wall formation

(Flardh *et al.*, 1999; Xu *et al.*, 2008). Subsequently, the *whi* genes (especially *whiA* and *whiB*) initiate a shift from elongation phase to division stage in the multichromosomal (50 or more copies of chromosomes in each) sporogenic cells (Flardh *et al.*, 1999; Flardh & Buttner, 2009). Nevertheless, the mechanism underlying this switch remains to be investigated. However, it is speculated that the *crgA* gene which is located in the vicinity of origin of replication in the genomes of all actinomycete might play a role in the phase shift. Its gene product CrgA might be involved in coordinating aerial hyphae extension and septation via cell division inhibition at the precise timing (De Sol *et al.*, 2003; Del Sol *et al.*, 2006).

A large number of the regularly spaced Z-rings are formed through the assembly of FtsZ along the aerial hyphae (Schwedock *et al.*, 1997; Flardh *et al.*, 2000; Grantcharova *et al.*, 2005) and *S. coelicolor* FtsK which is located at the sporulation septa pumps chromosomes through septa (Wang 2007) thereby completing the process of forming unigenomic prespore units. Maturation in these units eventually leads to their dispersion as spores. Mutations in the early *whi* genes prevent sporulation septation whereas null *whiD* mutant is able to sporulate albeit at a lower level compared to wild type with irregular septum placement along the spore chain (Molle *et al.*, 2000).

Spores are robust entities that ensure the survival of the species through environment hardship and when a favourable condition is encountered, germination of spores will take place spontaneously. Germination is a process that involves swelling of spore and growth polarization directed by DivIVA (Flardh & Buttner, 2009). Emergence of germ tubes is very much dependent on the association of DivIVA focus, where it forms a large focus at each growing hyphal tip (Flardh *et al.*, 2003). The deposition of  $\beta$ -linked glucan in the cell envelope at hyphal tips arises following interaction between cellulose synthase-like protein CslA with DivIVA (Xu *et al.*, 2008). The whole life cycle then restarts thereafter.

## 1.6 Phospholipid biosynthesis in prokaryotes

The fluid mosaic model of the membrane structure was first proposed by Singer and Nicolson in 1972 and went on to become the most widely accepted model in modern science. The model described the thermodynamically-feasible organization of homogenous phospholipid bilayer and the embedded amphipathic proteins within the cell membrane as shown in Figure 3 (Singer & Nicolson, 1972). More importantly, it provides a comprehensive insight into the general structure of the protective cell barrier of all organisms, although it falls short of mentioning the presence of other essential membrane components in the eukaryotes especially cholesterol which plays a fundamental role in determining the fluidity of the mosaic. Moreover, mounting evidences from extensive studies over the recent years have also resulted in the revision of the fluid mosaic model to account for the discovery of the heterogeneity of phospholipid distribution in both eukaryotic (Metcalf *et al.*, 1986; Emoto *et al.*, 1996; Munro, 2003) and prokaryotic membranes (Mileykovskaya and Dowhan 2000; Kawai *et al.*, 2004; Huang *et al.*, 2006; Jyothikumar *et al.*, 2012).

Although the permeability barrier of cells which serves as matrix for the assembly of vast array of proteins may define the non-catalytic role of phospholipids in a whole range of membrane-associated processes, it has now become clear that these major membrane building blocks are actively involved in some of these cellular functions in prokaryotes such as regulation of protein kinase C activity (Rando, 1988), cell division (Barak *et al.*, 2008), protein targeting and trafficking (Romantosov 2007), osmotic stress response (Miller, 1985; Lopez *et al.*, 2006; Romantosov 2008;), lactose permease active transport system (Bogdanova *et al.*, 2010), morphogenesis (Jyothikumar *et al.*, 2012) etc.

The function of each phospholipid hence its dispensability differs across the species just as there is variation in the overall membrane composition in different bacteria. Nevertheless, the prokaryotes shared a common phospholipid biosynthetic pathway (Figure 4) which was first mapped out based on extensive biochemical studies of phospholipid metabolism in *E. coli* (Kanfer & Kennedy, 1963;

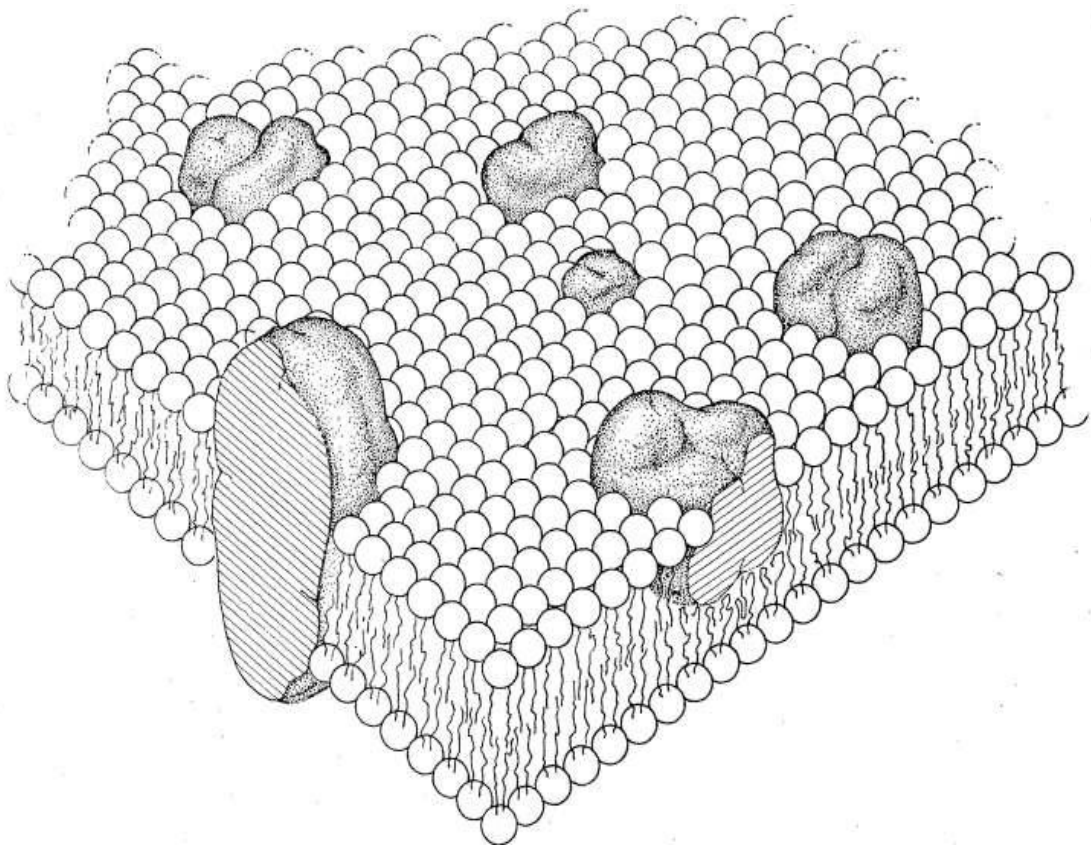


**Figure 3:** The original Fluid Mosaic model (reproduced from Singer and Nicolson, 1972). A bilayer of phospholipids (spheres with tails) with embedded proteins (shaded structures).

Kanfer & Kennedy, 1964) and subsequently verified via radiolabelling studies and genetic analyses over the years.

Phospholipids biosynthesis begins with the formation of phosphatidic acid (PA) through two-steps acylation of sn-glycerol-3-phosphate by fatty acyl coenzyme A-glycerol 3-phosphate acyltransferase and fatty acyl coenzyme A-lysoPA acyltransferase in the presence of fatty-acyl-CoA and magnesium ion (Pieringer *et al.*, 1967; Okuyama & Wakil, 1973). PA is rapidly converted to central liponucleotide intermediate, cytidine-diphosphate-diacylglycerol (CDP-DAG) by CDP-diglyceride synthetase, Cds. The enzyme exhibits a high degree of substrate specificity characteristic recognizing only long chain CDP and cytidine nucleotides in its reversible catalysis which favours the formation of CDP-DAG (Sparrow & Raetz, 1985).

*E. coli*, *cds* mutants accumulate up to 50 times more PA compared to wild type largely at the expense of the anionic phospholipids phosphatidylglycerol (PG) and cardiolipin (CL) whereas phosphatidylethanolamine (PE) content remains largely unaffected. The overall lipid-to-protein ratio also remains fairly close to that of the wild type (Ganong *et al.*, 1980). The observation points to a possible gene lesion bypass since *cds* mutants are presumably non-viable due to obstruction in phospholipid synthesis. CDP- DAG is an important activated intermediate since it is located at the branch point where it is ready to donate its phosphatidyl moiety to 3 other important phospholipid biosynthetic pathways.

In the first branch, phosphatidylinositol synthase, Pis catalyzes the formation of phosphatidylinositol (PI) via an inositol molecule substitution into the CDP-DAG molecule (Nikawa *et al.*, 1988). Although this pathway is essentially missing in most bacteria including *E. coli* (Nikawa *et al.*, 1988; Xia & Dowhan, 1995), Pis is found to be essential for the viability of *Mycobacterium smegmatis* (Jackson *et al.*, 2000).

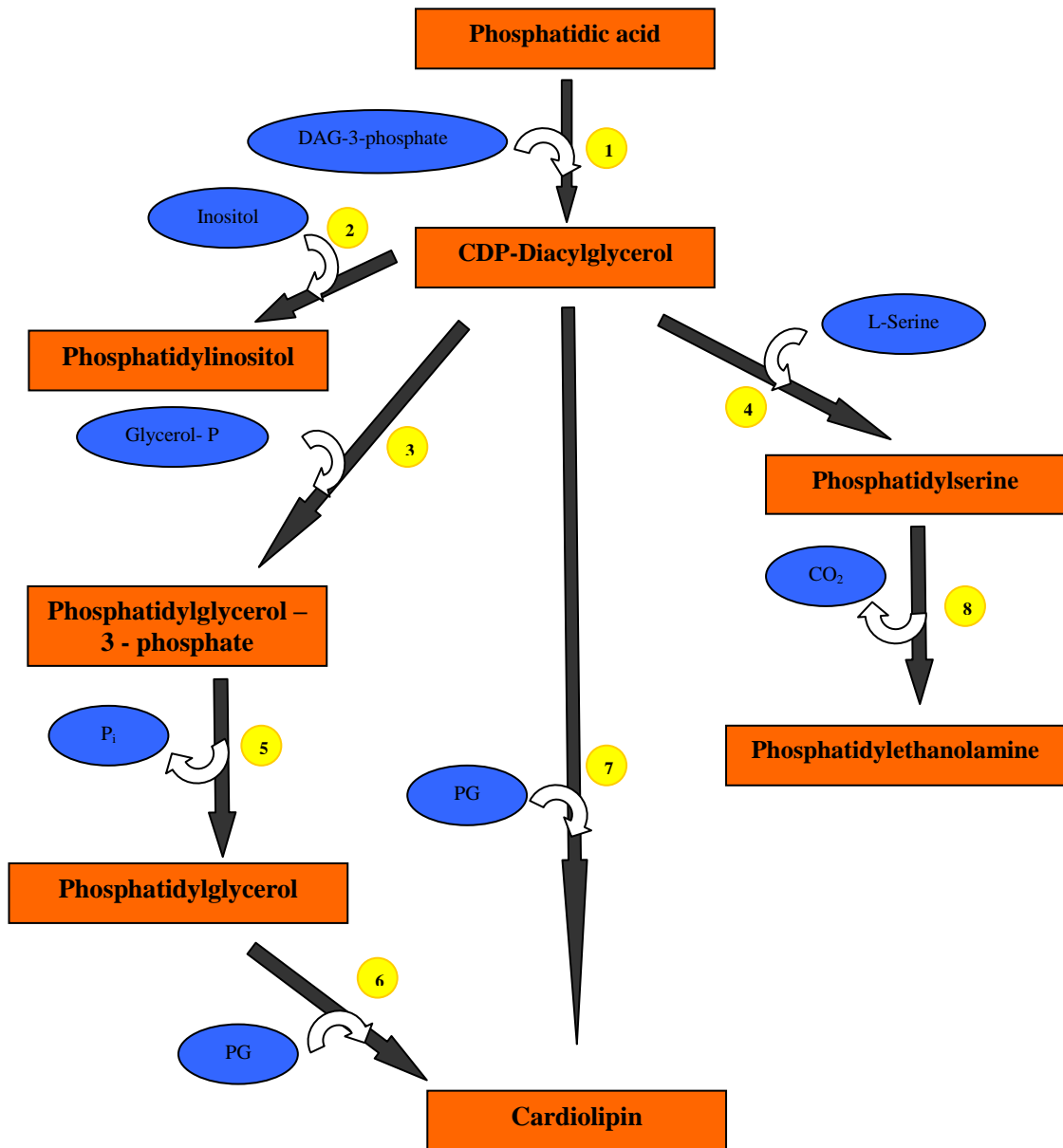


Figure 4: The major phospholipid biosynthetic pathway found in prokaryotes. The enzymes and substrates involved in the pathway are all indicated. (1) CDP-diglyceride synthetase, Cds; (2) Phosphatidylinositol synthase, Pis; (3) Phosphatidylglycerol-3-phosphate synthase, PgsA; (4) Phosphatidylserine synthase, Pss; (5) Phosphatidylglycerol phosphate phosphatase, PgpA or PgpB; (6) Bacterial type cardiolipin synthase, Cls-I; (7) Eukaryotic type cardiolipin synthase, Cls-II; (8) Phosphatidylserine decarboxylase, Psd.



In another branch, bacterial cardiolipin is formed via a multi-steps pathway. First, a phosphatidylglycerol-3-phosphate (PG3P) intermediate is formed when Phosphatidylglycerol-3-phosphate synthase, PgsA catalyzes the condensation of a glycerolphosphate with CDP- DAG, releasing CMP as a by-product (Chang & Kennedy, 1967a). The reaction then proceeds with the removal of the phosphate group from PG3P by phosphatidylglycerol phosphate phosphatase, PgpA or PgpB to yield PG. Subsequently, prokaryotic cardiolipin synthase, Cls-I (phospholipase D superfamily) catalyzes the reversible formation of CL via the transfer of a phosphatidyl group from one PG to another PG molecule (Rampini *et al.*, 1970; Hirschberg & Kennedy, 1972).

It is reported that *E. coli* *pgsA* null mutants are non-viable and defective in the synthesis of both PG and CL (Heacock & Dowhan, 1987). The absolute need of PgsA may also stem from the fact that PG is an important precursor for the synthesis of various membrane-bound oligosaccharides (Jackson & Kennedy 1984) and lipoproteins (Yu *et al.*, 1986). Mutants with disrupted *pgpA* and *pgpB* on the other hand are still viable with no significant phenotypic change although there is a slight increase in the level of PG3P. This suggests the presence of a third copy of the gene which accounts for the additional catalytic activity required to maintain the biosynthesis of the anionic phospholipids in *E. coli* *pgpA* and *pgpB* mutants (Funk *et al.*, 1992). CL is also dispensable in *E. coli* since *cls* mutant is still viable and does not display any distinctive phenotype compared to the wild-type (Pluschke *et al.*, 1978).

In eukaryotic cells and some actinobacteria such as *S. coelicolor* (Sandoval - Calderon *et al.*, 2009; Jyothikumar *et al.*, 2012), the synthesis of cardiolipin in cell membrane is rather straightforward. The eukaryotic type Cls-II (CDP-alcohol phosphatidyltransferase superfamily) brings about the condensation of CDP-DAG and PG to generate CL with cytidine monophosphate as the by-product. In *S. coelicolor*, Cls-II is shown to be essential in morphogenesis of this bacterium as *clsA* mutants are unable to erect aerial hyphae and sporulate whilst ClsA null mutants are non-viable on MS agar with only weak growth on 3MA. Over-expression of this

gene, on the other hand, results in aberrant hyphae, anucleated spores as well as weakend tips (Jyothikumar *et al.*, 2012).

The final branch of the phospholipid synthesis pathway involves the production of an anionic phosphatidylserine (PS) from the transfer of the phosphatidyl moiety from the CDP-DAG to the hydroxyl group of L-serine by Pss followed by a terminal step decarboxylation of PS by Psd to give the zwitterionic PE (Kanfer & Kennedy, 1964; Dowhan *et al.*, 1974; Voelker, 1997). PS is a minor membrane component in *E. coli* due to its rapid conversion to zwitterionic PE by Psd found in the inner cytoplasmic membrane. Unlike Gram positive bacteria such as *B. subtilis* where Pss is an integral membrane protein (Dutt & Dowhan, 1981; Okada *et al.*, 1994), *E. coli* Pss is a soluble protein (Kanfer & Kennedy, 1964) which is tightly associated with ribosomal fraction of the cell lysates whereas 10 to 30% are dissolved in the cytoplasm (Raetz & Kennedy, 1972; Ishinaga 1974). Nonetheless, it was shown that association of soluble cytosolic Pss to the acidic phospholipid components of the membrane is essential for its catalytic property (Saha *et al.*, 1996a).

The *E. coli pss* mutation is only conditionally lethal since the suppression of phenotypic defect i.e. temperature-dependant growth/cell division without the restoration of normal PE production is observed when the appropriate concentrations of cations ( $Mg^{2+}$ ,  $Si^{2+}$  or  $Ca^{2+}$ ) and/or sucrose are added to the growth culture (Ohta & Shibuya, 1977; DeChavigny *et al.*, 1991). Since PE is believed to be involved in the formation of an inverted hexagonal phase ( $H_{II}$ ) in the membrane (Cullis & De Kruijff, 1978b), its role is believed to be substituted by CL (but not PG) which has the similar  $H_{II}$  phase-forming ability in the presence of the divalent cation (Cullis *et al.*, 1978a; Vasilenko *et al.*, 1982). Similar to *pss* mutation, *E. coli psd* mutants are also conditionally viable where growth arrest can be avoided with the addition of the divalent cations. Death due to incubation at non-permissive temperature of above 42°C is likely caused by toxic accumulation of PS rather than loss of Psd function since the mutant continues to grow at normal rate over several generations before growth arrest is observed with huge increase of overall PS content (Hawrot &

Kennedy, 1978). In both mutants, there is an overall increase in CL content at the expense of PG (Hawrot & Kennedy, 1978; DeChavigny *et al.*, 1991) presumably due to the triggering of a natural compensatory mechanism needed to maintain the overall membrane function and fluidity. PE is therefore dispensable in *E. coli* (DeChavigny *et al.*, 1991)

*M. tuberculosis* possesses a complex cell envelope comprising an inner membrane barrier made up of 3 covalently-linked components; mycolic acids (hallmark of the waxy manifestation of the bacterial coat), arabinogalactan and peptidoglycan (Figure 5). These components represent the key factors responsible for virulence and intracellular survival of the pathogen (Dubnau *et al.*, 2000; Gao *et al.*, 2003) where the enzymes involved in their synthesis are also the target of current anti-TB agents (i.e. mycolic acid: isoniazid, ethionamide and prothionamide; arabinogalactan and lipoarabinomannan: ethambutol; peptidoglycan: cycloserine). Hence, interference with the biosynthesis of other essential constituents within the cell envelope especially the cell membrane would presumably also affect the viability of *M. tuberculosis*. This serves as the basis to initiate a guided drug design program.

Pss and Psd which are involved in a 2 steps PE synthesis process are localized in plasma membrane (PM<sub>f</sub>) fraction and the plasma membrane – cell wall (PM-CW) fraction. PM<sub>f</sub> subdomain of the plasma membrane may be the main site of PE biosynthesis in actively dividing mycobacteria, it is however deprived of PE vis-à-vis the PM-CW fraction suggestive of a theoretical mechanism that actively transports PS, PE and other phospholipids between the two compartments (Morita *et al.*, 2005). In addition to the two major phospholipids mentioned, PI and its metabolic derivatives are also known to be essential in structure, physiology and possibly host infection in this genus of prokaryotes (Jackson *et al.*, 2000). Therefore, three important drug targets (i.e. Psd, Pss and Pis) have been identified within the phospholipid biosynthesis pathway.

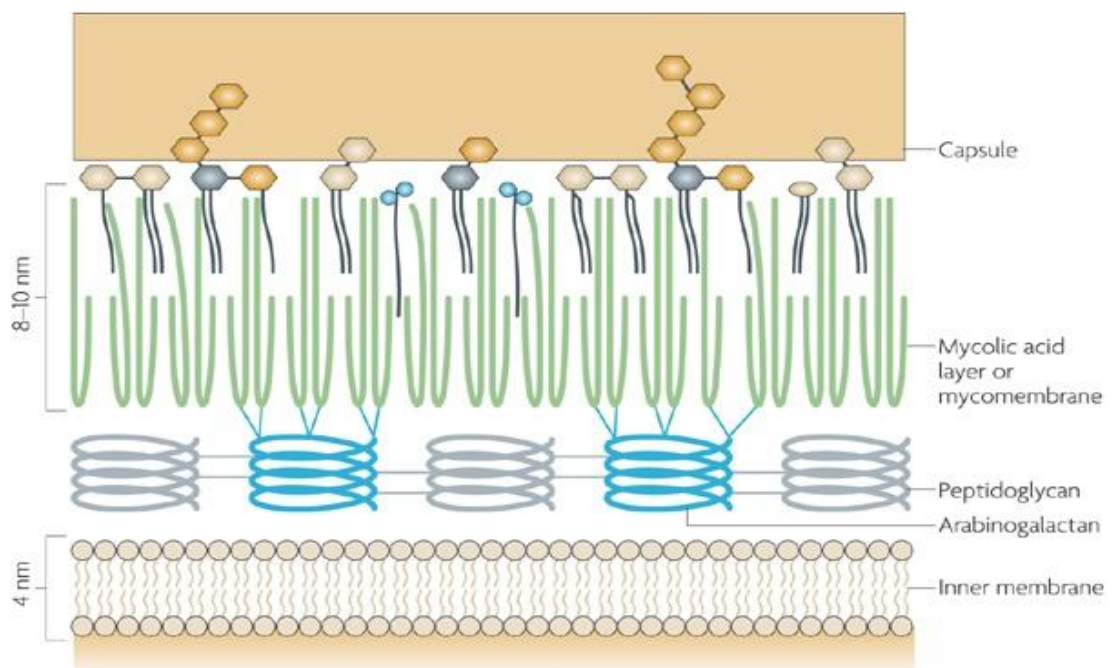


Figure 5: Cell wall of *Mycobacterium tuberculosis* (adapted from Abdallah *et al.*, 2007).

## **2.0 Project aims**

## 2.0 Project aims

Since experimental work on the virulent bacteria is often restricted to the confine of containment level 3 (CL3) facilities, our preliminary research has to be carried out on a genetically-related “surrogate” which is both safe and faster growing. With emerging evidence which revealed the significantly high degree of resemblance in the developmental stages in the life cycles of both streptomycetes and mycobacteria (Scherr & Nguyen, 2009), it has become clear recently that the saprophytic *S. coelicolor* could be used as a model for analogous study of *M. tuberculosis*. Genome sequencing studies coupled with bioinformatic predictions have also concluded the seemingly high degree of genetic synteny and sequence homology at the level of individual gene or gene clusters between the two species (Bentley *et al.*, 2002). This further substantiates the applicability of *S. coelicolor* as a model.

The project requires the combined approach of both molecular microbiology and medicinal chemistry disciplines. The aims of the projects are:

1. verifying the essentiality of both *Pss* and *Psd* in *S. coelicolor* as the potential drug targets in the phospholipid biosynthesis pathways.
2. construction of *pss* and *psd* mutants where the expression of their gene products are inducer-dependent to elucidate the overall gene functions ( in terms of growth and morphogenesis). The mutants are also used concurrently as sensitive “screens” for the purpose of compound testing.
3. *in silico* screening of the library of compounds for the analogues of natural substrates which could possibly inhibit the target proteins.
4. chemical synthesis and testing of compounds against *S. coelicolor* for possible antibacterial activity. Further testing of relevant compounds which possess the desired antibacterial profile against mutants described in 2.

5. Optimization of the lead ligands to improve their potency and toxicity profiles.

## **3.0 Materials and methods**



### 3.0 Materials and methods

#### 3.1 Media and antibiotics

Table 2: Composition of various growth media. All media (except those specified by \*\*) were sterilised by autoclaving at 120 KPa for 30 minutes.

\* Components sterilised individually then mixed aseptically.

\*\*Components sterilized by filtration with a 0.22 µm filter.

\*\*\* Trace element solution: 40 mg ZnCl<sub>2</sub>, 200 mg FeCl<sub>3</sub>.2H<sub>2</sub>O, 10 mg CuCl<sub>2</sub>.2H<sub>2</sub>O, 10 mg MnCl<sub>2</sub>.4H<sub>2</sub>O, 10 mg NaB<sub>4</sub>O<sub>7</sub>.10H<sub>2</sub>O, 10 mg (NH<sub>4</sub>)<sub>6</sub>Mo<sub>7</sub>O<sub>24</sub>.4H<sub>2</sub>O in 1 L deionised water.

Media	Composition (per litre)
2x YT broth (Kieser <i>et al.</i> , 2000)	10 g tryptone 10 g yeast extract 5 g NaCl Make up to 1L using distilled water
Luria-Bertani (LB) agar (Sambrook <i>et al.</i> , 1989)	10 g tryptone 5 g yeast extract 20 g agar (omit for broth) 5 g NaCl Make up to 1L using distilled water
Mannitol soy flour (MS) agar (Hobbs <i>et al.</i> , 1989)	20 g soya flour 20 g mannitol 20 g agar Make up to 1L using tap water
Minimal medium agar with mannitol (3MA) (Hopwood, 1967)	0.5 g L-asparagine/ NH <sub>2</sub> SO <sub>4</sub> 0.5 g K <sub>2</sub> HPO <sub>4</sub> 0.2 g MgSO <sub>4</sub> .7H <sub>2</sub> O 0.01g FeSO <sub>4</sub> .7H <sub>2</sub> O 10 g agar Make up to 1L using distilled water After autoclaving add 5 g mannitol
Minimal medium agar with glucose (Hopwood, 1967)	0.5 g L-asparagine/ NH <sub>2</sub> SO <sub>4</sub> 0.5 g K <sub>2</sub> HPO <sub>4</sub> 0.2 g MgSO <sub>4</sub> .7H <sub>2</sub> O 0.01g FeSO <sub>4</sub> .7H <sub>2</sub> O 10 g agar Make up to 1L using distilled water After autoclaving add 10 g glucose
Nutrient agar (Oxoid)	13 g nutrient broth 20 g agar 1 L distilled water
SOC*	20 g tryptone

(Hanahan, 1983)	5 g yeast extract 10 mM NaCl 2.5 mM KCl 10 mM MgCl <sub>2</sub> ** 10 mM MgSO <sub>4</sub> ** 20 mM glucose** Make up to 1L using distilled water
R2YE/R2 (Okanishi <i>et al.</i> , 1974; Hopwood & Wright, 1978; Thompson <i>et al.</i> , 1980)	103 g sucrose 10.12 g MgCl <sub>2</sub> .6H <sub>2</sub> O 0.25 g K <sub>2</sub> SO <sub>4</sub> 10 g glucose 0.1 g casamino acids 800 ml distilled water 2.2 g agar per 80 ml solution At time of use add: 1 ml KH <sub>2</sub> PO <sub>4</sub> (0.5 % w/v) 8 ml CaCl <sub>2</sub> .2H <sub>2</sub> O (3.68 % w/v) 1.5 ml L-proline (20 % w/v) 10 ml TES buffer (5.73 % w/v, pH5.2) 0.2 ml trace element solution*** 0.5 ml NaOH (1N) To make R2YE add 5 ml yeast extract (10 % w/v)
Müller-Hinton agar (Oxoid)	2.0 g beef extract 17.5 g digest of casein 1.5 g starch 17.0 g agar 1 L distilled water

All media were prepared based on the composition in Table 2. Suppliers of different ingredients of various media were Fisher, Oxoid and Sigma. The media or their component(s) were either sterilised by autoclaving at 120KPa for 30 minutes or filtration through a 0.22 µm filter. Where necessary, antibiotics were added to the media to enable the selection of a specific strain of bacteria. The stock and working concentrations of different antibiotic used were shown in Table 3.

Table 3: Stock and working concentrations of various antibiotics used in the laboratory. To prepare, dissolve in: <sup>1</sup>100% ethanol, <sup>2</sup>0.25 M NaOH, <sup>3</sup>80% Ethanol. They were all stored at - 20°C.

<b>Antibiotics</b>	<b>Stock concentration (mg/ml)</b>	<b>Working concentration (µg/ml)</b>
Ampicillin (Amp)	50	50
Apramycin (Apra)	100	50
Chloramphenicol (Chl) <sup>1</sup>	25	25
Kanamycin (Km)	25	50
Nalidixic acid (NAL) <sup>2</sup>	20	20
Tetracycline (Tet) <sup>3</sup>	12.5	12.5
Spectinomycin (Spec)	200	50
Streptomycin (Str)	25	25

### 3.2 Strains, plasmids, cosmids, bacterial cultivation and storage.

The different strains of bacteria and intrinsic plasmid characteristics were shown in Table 4. *E. coli* was grown (in the presence of appropriate antibiotic if required) at 37 °C for 16 to 18 hours before cultivation unless stated otherwise. Liquid culture was incubated with shaking at 225 r.p.m. Glycerol stock was prepared by diluting 670 µl of fresh overnight culture with 330 µl of sterile 80% glycerol before being stored at -80 °C

*S. coelicolor* was grown (in the presence of appropriate antibiotic if required) at 30 °C unless stated otherwise. *S. coelicolor* grown on solid media was cultivated after 3 to 5 days or until greyish spores were observed. Spore stock could be prepared by flooding an MS agar plate containing the dense greyish confluent of *S. coelicolor* with 10 ml of sterile 20 % glycerol and the spores were scraped from the surface of the agar using sterile cotton buds. The suspension was vortexed to break the spore chains and filtered through a syringe containing sterile cotton wool. The spore suspension was stored at either – 20 °C or - 80 °C. Liquid culture was incubated with shaking at 250 r.p.m in Erlenmeyer flask containing sterile spring to aid dispersal of mycelia and aeration. The culture was typically harvested after 48 hours or until the onset of undecylprodigiosin production.

Table 4: Bacterial strains, cosmids and plasmids. *amp<sup>r</sup>*, *apra<sup>r</sup>*, *chl<sup>r</sup>*, *hyg<sup>r</sup>*, *km<sup>r</sup>*, *spc/str<sup>r</sup>* and *tsr<sup>r</sup>* represent ampicillin, apramycin, chloramphenicol, hygromycin, kanamycin, spectinomycin/streptomycin and thiostrepton resistant genes respectively.

Strain or plasmid	Characteristics	Source
<i>E. coli</i> DHF $\alpha$	General cloning host. F <sup>+</sup> , <i>endA1</i> , <i>hsdR17</i> ( <i>r<sub>K</sub></i> . <i>m<sub>K+</sub></i> ), <i>supE44</i> , <i>thi-1</i> $\lambda^-$ , <i>recA1</i> , <i>gyrA96</i> , <i>relA1</i> , <i>deoR</i> , $\Delta$ ( <i>lacZYA-araF</i> )U169, $\phi$ 80 <i>dlacZ</i> $\Delta$ M15	Grant <i>et al.</i> , 1990
<i>E. coli</i> JM109	General cloning host. e14 <sup>-</sup> ( <i>McrA</i> <sup>-</sup> ), <i>recA1</i> , <i>endA1</i> , <i>gyrA96</i> , <i>thi-1</i> , <i>hsdR17</i> ( <i>r<sub>K</sub></i> . <i>m<sub>K+</sub></i> ), <i>supE44</i> , <i>relA1</i> , $\Delta$ ( <i>lac-proAB</i> ) [F <sup>+</sup> <i>traD36</i> , <i>proAB</i> , <i>lac<sup>q</sup>Z</i> $\Delta$ M15]	Vaillancourt <i>et al.</i> , 1994
<i>E. coli</i> ET12567 (pUZ8002)	Host for mobilization of DNA to <i>Streptomyces</i> via intergeneric conjugation. Contains non-transmissible <i>oriT</i> mobilising plasmid pUZ8002. <i>tet<sup>r</sup></i> , <i>chl<sup>r</sup></i> , <i>km<sup>r</sup></i>	Kieser <i>et al.</i> , 2000
St9C7	Supercos-1 containing <i>S. coelicolor</i> chromosomal DNA including <i>pss</i> and <i>psd</i> . <i>amp<sup>r</sup></i> , <i>km<sup>r</sup></i>	Redenbach <i>et al.</i> , 1996
St9C7.1.H05 (abbrev. H05)	St9C7 containing <i>pss</i> ::Tn5062 insertion. <i>amp<sup>r</sup></i> , <i>km<sup>r</sup></i> , <i>apra<sup>r</sup></i>	Bishop <i>et al.</i> , 2004
St9C7.2.C03 (abbrev. C03)	St9C7 containing <i>psd</i> ::Tn5062 insertion. <i>amp<sup>r</sup></i> , <i>km<sup>r</sup></i> , <i>apra<sup>r</sup></i>	Bishop <i>et al.</i> , 2004
St9C7.1.G12 (abbrev. G12)	St9C7 containing <i>SCO6469</i> ::Tn5062 insertion. <i>amp<sup>r</sup></i> , <i>km<sup>r</sup></i> , <i>apra<sup>r</sup></i>	Bishop <i>et al.</i> , 2004
pMS82	Integrative vector for <i>Streptomyces</i> containing <i>ori<sub>TRK2</sub></i> <i>int attP<sub>ΦBT1</sub></i> . <i>hyg<sup>r</sup></i>	Gregory <i>et al.</i> , 2003
pAV11b	pMS82 containing tetracycline-inducible <i>tcp830</i> promoter and <i>tetris</i> . <i>hyg<sup>r</sup></i>	Khaleel <i>et al.</i> , 2011
pUC19	<i>E. coli</i> cloning vector. <i>lacZ<math>\alpha</math></i> , <i>amp<sup>r</sup></i>	Yanisch-Perron <i>et al.</i> , 1985
pPM927	Integrative vector for <i>Streptomyces</i> containing <i>ori<sub>TRK2</sub></i> , <i>int attP<sub>pSAM</sub></i> , <i>ptipA</i> promoter. <i>spc/str<sup>r</sup></i> <i>tsr<sup>r</sup></i>	Smokvina <i>et al.</i> , 1990
pJL101	<i>SCO6469</i> ::Tn5062 insertion, <i>pss</i> and <i>psd</i> from G12 in pUC19. <i>apra<sup>r</sup></i> , <i>amp<sup>r</sup></i> .	This work
pJL102	<i>SCO6469</i> ::Tn5062 insertion, <i>pss</i> and <i>psd</i> from G12 in pUC19 with a reversed orientation compared to pJL101. <i>apra<sup>r</sup></i> and <i>amp<sup>r</sup></i> .	This work
pJT101	<i>pss</i> & <i>psd</i> from G12 in pMS82. <i>hyg<sup>r</sup></i>	This work
pSM102	<i>psd</i> in pUC19. <i>amp<sup>r</sup></i>	This work
pAT135 (A)	<i>pss</i> in pUC19. <i>amp<sup>r</sup></i>	This work
pST246 (B)	<i>psd</i> & <i>pss</i> in pUC19. <i>amp<sup>r</sup></i>	This work

pJA868 (A)	<i>pss</i> (sense orientation) in pAV11b. <i>hyg<sup>r</sup></i>	This work
pJA868 (B)	<i>pss</i> (antisense orientation) in pAV11b. <i>hyg<sup>r</sup></i>	This work
pSV101 (A)	<i>psd</i> (sense orientation) in pAV11b. <i>hyg<sup>r</sup></i>	This work
pSV101 (B)	<i>psd</i> (antisense orientation) in pAV11b. <i>hyg<sup>r</sup></i>	This work
pIP123 (A)	<i>psd</i> & <i>pss</i> (sense orientation) in pAV11b. <i>hyg<sup>r</sup></i>	This work
pIP123 (B)	<i>psd</i> & <i>pss</i> (antisense orientation) in pAV11b. <i>hyg<sup>r</sup></i>	This work
pPM67S	<i>pss</i> (sense orientation) in pPM927. <i>spc/str<sup>r</sup>, tsr<sup>r</sup></i>	This work
pPM67A	<i>pss</i> (antisense orientation) in pPM927. <i>spc/str<sup>r</sup>, tsr<sup>r</sup></i>	This work
pPM68S	<i>psd</i> (sense orientation) in pPM927. <i>spc/str<sup>r</sup>, tsr<sup>r</sup></i>	This work
pPM68A	<i>psd</i> (antisense orientation) in pPM927. <i>spc/str<sup>r</sup>, tsr<sup>r</sup></i>	This work
pPM68+67S	<i>psd</i> & <i>pss</i> (sense orientation) in pPM927. <i>spc/str<sup>r</sup>, tsr<sup>r</sup></i>	This work
RD6467	St9C7 with <i>pss::apra<sup>r</sup>.amp<sup>r</sup>, km<sup>r</sup>, apra<sup>r</sup></i>	This work
RD6468	St9C7 with <i>psd::apra<sup>r</sup>.amp<sup>r</sup>, km<sup>r</sup>, apra<sup>r</sup></i>	This work
RD6467+68	St9C7 with <i>psd</i> & <i>pss::apra<sup>r</sup>.amp<sup>r</sup>, km<sup>r</sup>, apra<sup>r</sup></i>	This work
<i>S. coelicolor</i> M145	Wild type SCP1 <sup>-</sup> SCP2 <sup>-</sup> Pgl <sup>+</sup>	Kieser <i>et al.</i> , 2000
<i>S. coelicolor</i> LSM101	M145::H05 single cross-over. <i>km<sup>r</sup>, apra<sup>r</sup></i>	This work
<i>S. coelicolor</i> LSM104	M145::H05::pJA868(A) single cross-over. <i>km<sup>r</sup>, apra<sup>r</sup>, hyg<sup>r</sup></i>	This work
<i>S. coelicolor</i> LSM105	M145 <i>pss::Tn5062::pJA868(A)</i> double cross-over. <i>km<sup>s</sup>, apra<sup>r</sup>, hyg<sup>r</sup></i>	This work
<i>S. coelicolor</i> TJL101	M145::C03 single cross-over. <i>km<sup>r</sup>, apra<sup>r</sup></i>	This work
<i>S. coelicolor</i> TJL104	M145::C03::pSV101(A) single cross-over. <i>km<sup>r</sup>, apra<sup>r</sup>, hyg<sup>r</sup></i>	This work
<i>S. coelicolor</i> JA101	M145::C03::pIP123(A) single cross-over. <i>km<sup>r</sup>, apra<sup>r</sup>, hyg<sup>r</sup></i>	This work
<i>S. coelicolor</i> AJ101	M145::H05::pIP123(A) single cross-over. <i>km<sup>r</sup>, apra<sup>r</sup>, hyg<sup>r</sup></i>	This work
<i>S. coelicolor</i> M123A	M145::pIP123A. <i>hyg<sup>r</sup></i>	This work
<i>S. coelicolor</i> JT671	M145::RD6467::pPM67S single cross-over. <i>km<sup>r</sup>, apra<sup>r</sup>, spc/str<sup>r</sup>, tsr<sup>r</sup></i>	This work
<i>S. coelicolor</i> JT672	M145Δ <i>pss</i> ::pPM67S double cross-overs. <i>km<sup>s</sup>, apra<sup>r</sup>, spc/str<sup>r</sup>, tsr<sup>r</sup></i>	This work
<i>S. coelicolor</i> AL681	M145::RD6468::pPM68S single cross-over. <i>km<sup>r</sup>, apra<sup>r</sup>, spc/str<sup>r</sup>, tsr<sup>r</sup></i>	This work
<i>S. coelicolor</i> M67A	M145::pPM67A. <i>spc/str<sup>r</sup> tsr<sup>r</sup></i>	This work

<i>S. coelicolor</i> M67S	M145::pPM67S. <i>spc/str<sup>r</sup> tsr<sup>r</sup></i>	This work
<i>S. coelicolor</i> M927	M145::pPM927. <i>spc/str<sup>r</sup> tsr<sup>r</sup></i>	This work

### **3.3 Growth of *S. coelicolor* mycelium in liquid culture and measurement of growth by dry weight** (Kieser *et al.*, 2000)

YEME broth (400 ml) in a 2 L baffled flask was inoculated with approximately  $4 \times 10^7$  pregerminated spores of *S. coelicolor*. The culture was incubated at 30 °C in a shaking incubator. At designated time point, 5 ml culture was withdrawn and vacuum filtered through pre-weighed Whatman filter paper. The filter paper was then dried for 5 minutes at mid-low power in a microwave and the filter paper with the dried biomass was reweighed. The dry weight of the biomass was calculated by subtracting the weight of the filter paper from the final weight. This was repeated for all pre-determined time points and a growth curve was then plotted.

### **3.4 *S. coelicolor* antibiotic production and measurement**

#### **3.4.1 Determination of actinorhodin (Act) concentration in liquid culture** (Kang *et al.*, 1998)

An equal volume of 1 M NaOH was added to the liquid culture containing the mycelia followed by 5 minute centrifugation at 1000 g. The supernatant was collected and the absorbance was measured at 633 nm. The concentration of Act was calculated using the molar extinction coefficient,  $\epsilon_{633}$  of  $15135 \text{ M}^{-1}\text{CM}^{-1}$ .

#### **3.4.2 Determination of undecylprodigiosin (Red) concentration in liquid culture** (Williams *et al.*, 1956)

An aliquot (10 ml) of liquid culture containing the mycelia was centrifuged for 5 minutes at 1000 g. The supernatant was discarded and 10 ml of absolute methanol was added to the cell pellet followed by gentle mixing in a shaker for 24 hours. After centrifugation at 1000 g for 5 minutes, the absorbance of the supernatant at 530 nm was measured and the concentration of Red was calculated using the molar extinction coefficient  $\epsilon_{530}$  of  $100150 \text{ M}^{-1}\text{CM}^{-1}$



### **3.5 Spore sensitivity assays**

#### **3.5.1 Lysozyme, DMSO, SDS, sonication and temperature sensitivity** (adapted from Hoskisson *et al.*, 2000)

A square Petri plate (12 cm x 12cm) containing 3MA was divided into 8 columns and 8 rows. The columns were marked with the dilution series  $10^0$  to  $10^{-5}$  whereas the rows were marked with variables; the duration of exposure to a particular temperature/sonication, different concentrations of lysozyme, DMSO and SDS. An aliquot (5  $\mu$ l) of post treatment spore suspension (initial concentration of  $5 \times 10^5$  cfu/ $\mu$ l for  $10^0$  and diluted accordingly up to  $10^{-5}$ ) was spotted onto each column based on the predetermined dilution. The plate was incubated at 30° C and examined daily for signs of growth change.

#### **3.5.2 Osmotic stress test (KCl & sucrose)**

Aliquots (1 ml) of 3MA with different concentration of KCl/sucrose were added to a 24-well plate. An aliquot (5  $\mu$ l) of spore suspension (initial concentration of  $5 \times 10^5$  cfu/ $\mu$ l for  $10^0$  and diluted accordingly up to  $10^{-5}$ ) was spotted onto each column based on the predetermined dilution. The plate was incubated at 30° C and examined daily for signs of growth change.

### **3.6 Antimicrobial susceptibility testing via Disc diffusion assay** (Bauer *et al.*, 1966)

An overnight culture of the test bacteria was diluted accordingly using broth to give a bacterial suspension of approximately  $1 - 2 \times 10^8$  CFU/ml. A sterile cotton bud was dipped into the bacterial suspension before swabbing the entire surface of a Müeller-Hinton agar plate. This was repeated twice, rotating the plate 60° each time to ensure the inoculum was spread evenly throughout the entire surface. Finally, the rim of the agar was swabbed to complete the spreading process. The plate was left to dry for 5

minutes before applying the 6 mm sterile paper discs (Whatman filter paper no. 1) impregnated with 100 µg/ml of each test compound onto the surface of the agar. The discs must be pressed down onto the agar to ensure complete contact. The plate was then inverted and incubated at the temperature ideal for the growth of the test bacteria. The presence of any zone of inhibition was then noted.

### 3.7 Production of electrocompetent *E. coli* (Sambrook *et al.*, 1989)

A single colony of the bacteria was inoculated in a 5 ml L-broth and incubated overnight at 250 rpm at 37°C. Aliquot of fresh LB-broth (50 ml) was inoculated with 0.5 ml of the fresh overnight culture and incubated until it reached OD<sub>600</sub> of 0.4 to 0.6. All the reagents, apparatus and the cells were chilled on ice prior to the start of the experiment. The culture was then transferred to a 50 ml chilled Falcon tubes and centrifuged at 2500 rpm, 4 °C for 15 minutes. The supernatant was removed and the pellet was gently resuspended in 50 ml of ice-cold 10% (w/v) glycerol, followed by recentrifugation at 2500 rpm, 4°C for 15 minutes. The process was repeated twice. After the final resuspension using 200 µl of ice-cold 10% (w/v) glycerol, the cell suspension was aliquoted into chilled Eppendorf tubes, with 50 µl in each tube. These tubes were then transferred to a liquid nitrogen bath followed by storage at -80°C prior to use. The transformation efficiency of the competent cells was tested via transformation using pUC19 and should be in the range of 10<sup>8</sup> to 10<sup>9</sup> cfu/µg for efficient transformation assay. The transformation efficiency could be calculated based on the following formula:

Transformation efficiency (cfu/µg) =

$$\frac{\text{cfu on control plate}}{\text{ng of supercoiled vector plated}} \times \frac{10^3 \text{ ng}}{1 \text{ } \mu\text{g}} \times \text{final dilution plated}$$

### **3.8 Electrotransformation of competent cells (Dower *et al.*, 1988)**

Electrocuvette and SOC solution to be used in the experiment should be pre-chilled at 4°C. The Eppendorf tube containing the electrocompetent cells was thawed on ice immediately before the start of the transformation procedure. An aliquot of DNA (1 µl) to be used for the transformation was added to the thawed competent cells and mixed briefly with pipette tip. The mixture was incubated on ice for 1 minute. The cells/DNA mixture was then added to the bottom of the electrocuvette and with the Bio-Rad Micropulser apparatus set at 2.5 kV:25 mf:200 Ω, the mixture was zapped. An aliquot (1 ml) of ice-cold SOC was immediately added to the mixture with gentle mixing via pipetting. The mixture was then transferred to a 5 ml sterile universal and incubated for either 1.5 hours (JM109 and DHFα) or 3 hours (ET12567) at 225 rpm. The culture was then plated onto LB-agar plate containing the appropriate antibiotic(s). The culture should be spread evenly on the agar and allowed to air dry prior to overnight incubation at 37°C.

### **3.9 Intergeneric transfer of plasmid/cosmid from *E. coli* to *S. coelicolor* M145 by conjugation (Kieser *et al.*, 2000)**

A colony of *E.coli* ET12567/pUZ8002 with the plasmid of interest was inoculated in 5ml LB broth in the presence of kanamycin and chloramphenicol to maintain the selection of pUZ8002 and the dam mutation respectively as well as antibiotic used to select the *oriT*-containing plasmid. The culture was incubated overnight at 37 °C, 225 rpm. The overnight culture was diluted 1:100 in fresh LB broth with the appropriate antibiotic as above and grown at 37°C, 225 rpm to an OD<sub>600</sub> of 0.4 – 0.6. The culture was then centrifuged at 4000 rpm for 5 minutes and the supernatant was discarded. The supernatant was resuspended in an equal volume of fresh LB broth followed by centrifugation at 4000 rpm for 5 minutes. The washing was repeated for another time to ensure the traces of antibiotics were completely removed prior to resuspension in 1ml of LB. While the washing was done, 100 µl of *S. coelicolor* M145 spore suspension was added to 500 µl of 2 x YT broth and heat shocked at 50°C for 10 minutes and allowed to cool. Then, 500 µl of the resuspended *E.coli* ET12567/pUZ8002 culture was added to 500µl of the heat- shocked spore suspension and the mixture was mixed briefly by vortexing. The mixture was then centrifuged at 4000 rpm for 5 minutes and the supernatant was removed. Aliquot (200 µl) of 2 x YT was then used to resuspend the mixture before plating out on MS agar containing 10 mM MgCl<sub>2</sub> and incubated at 30°C for 16 hours. The plate was then overlaid with 1 ml of water containing nalidixic acid and the appropriate plasmid/cosmid selecting antibiotic(s) and the incubation at 30°C was resumed. When sporulation had taken place, the colonies were patched on Nutrient/MS agar containing nalidixic acid and the appropriate antibiotic to select for the wanted exconjugants.

### 3.10 DNA isolation

#### 3.10.1 Modified Birnboim and Doly DNA Isolation Protocol (Birnboim & Doly, 1979)

Table 5: Composition of Solutions I, II and III used in Modified Birnboim and Doly DNA Isolation Protocol. All solutions sterilised by autoclaving at 120 KPa for 30 minutes. Solution II was freshly prepared on the day of use.

Solution name	Components
Solution I	50 mM glucose 25 mM Tris CL (pH 8) 10 mM EDTA (pH 8)
Solution II	0.2 N NaCl 1% SDS
Solution III	0.3 M potassium acetate 11.5% glacial acetic acid 28.5% distilled water

The compositions of solution I, II and III were shown in Table 5. Aliquot (3 ml) of overnight *E.coli* LB broth culture was harvested and centrifuged for 30 seconds at 12000 g in a tabletop centrifuge. The supernatant was discarded and the pellet was blotted on a tissue. The bacterial pellet was then resuspended in 100 µl of ice - cold solution I by vigorous vortexing. Freshly prepared ice - cold solution II (200 µl) was then added to the bacterial suspension and the content of the microcentrifuge tube was mixed via rapid inversion. This was followed by the addition of 150 of ice – cold solution III and the viscous bacterial lysate was then mixed by gentle vortexing. The microfuge tube was then stored on ice for 3 to 5 minutes prior to 5 minutes of centrifugation at 12000 g. The supernatant was then transferred to a fresh tube and an equal volume of phenol:chloroform was added to the supernatant followed by mixing of content via gentle vortexing. The mixture was centrifuged at 12000 g for 2 minutes. The top layer (aqueous phase) was transferred to a fresh tube and the DNA precipitated with the addition of double volume of ethanol. After vortexing, the mixture was allowed to stand for 2 minutes at room temperature. After 10 minutes of

centrifugation at 12000 g, the supernatant was poured off and the pellet of DNA was dried in a speed vacuum concentrator for 20 to 30 minutes. Appropriate volume of TE buffer (pH 8)/sterile distilled water and 1-2  $\mu$ l of RNAase were added to the pellet and the extracted DNA could be stored at  $-20^{\circ}\text{C}$ .

### **3.10.2 Wizard<sup>®</sup> Plus SV Minipreps DNA Purification System (Promega)**

Aliquots of 1 to 5 ml (high copy number plasmid) or 10 ml (low copy number plasmid) of overnight *E.coli* LB broth culture were harvested and centrifuged for 5 minutes at 10000 g in a tabletop centrifuge. The supernatant was discarded and the cell pellet was resuspended in 250  $\mu$ l of Cell Resuspension Solution via vortexing. The cells were lysed by the addition of 250  $\mu$ l of Cell Lysis Solution. As soon as the cell suspension cleared, 350  $\mu$ l of Neutralization Solution was added and the bacterial lysate was then centrifuged at maximum speed (around 14000 g) for 10 minutes at room temperature. The supernatant was decanted into the provided spin column followed by 1 minute of maximum speed centrifugation. The flowthrough from the collection tube was discarded and 750  $\mu$ l of Column Wash Solution (previously diluted with 95% of ethanol) was added to the spin column prior to 1 minute of maximum speed centrifugation. This was repeated with another 250  $\mu$ l of Column Wash Solution followed by a further 2 minutes of maximum centrifugation. The spin column was then transferred to a new sterile 1.5 ml microfuge tube and the DNA was eluted using the appropriate amount of Nuclease Free Water. The isolated DNA could be stored at  $-20^{\circ}\text{C}$ .

### 3.10.3 *S. coelicolor* Genomic DNA Isolation Protocol (Kieser *et al.*, 2000)

Aliquot (50 ml) of *Streptomyces coelicolor* YEME culture (pink) was harvested after 36 to 48 hours and centrifuged at 4K r.p.m for 10 minutes. The supernatant was discarded and the cell pellet was resuspended in 20 ml of solution I (from Birnboim and Doly DNA Isolation Protocol) before the addition of 0.4 ml of 30mg/ml lysozyme and 5mg/ml RNaseA. The mixture was incubated in a 37 °C water bath for 30 – 60 minutes. Aliquot (1 ml) of 20 % SDS solution was added to it and the mixture was inverted for 8 to 10 times (gentle mixing). Phenol solution (10 ml) was then added followed by 10 minutes of gentle shaking. To aid the separation of organic and aqueous phases, the mixture was centrifuged at 4K r.p.m for 10 minutes. The aqueous layer was transferred to a new tube and the phenol extraction step described above was repeated. After centrifugation at 4K r.p.m for 10 minutes, the aqueous layer was transferred to a new tube and this time 20 ml of absolute ethanol was added to precipitate the genomic DNA. The genomic DNA was harvested via spooling using a sealed Pasteur pipette. The genomic DNA was transferred into a sterile centrifuge tube and resuspended in sterile distilled water/TE buffer prior to storage at – 20 °C.

### 3.11 RNA extraction from *Streptomyces* (Qiagen; Mersinias, 2003; Bucca *et al.*, 2009)

Pregermination of *S. coelicolor* spores was carried out by adding the spore suspension to 2 x YT 100 followed by 6 - 8 hours incubation at 30°C/250 r.p.m. Pregerminated spores were pelleted at 3000 rpm for 10 minutes and resuspended in 10 ml of sterile distilled water. The suspension was vortexed briefly to disperse the clumped mycelia before measuring the OD<sub>450</sub>. The equation below was used to calculate the volume (V) of spore suspension required to inoculate 3 x 10<sup>6</sup> spores.

$$V = (3 \times 10^6 / [\text{OD}_{450} \times 10^8]) \times 1000 \mu\text{l}$$

*S. coelicolor* spore suspension was inoculated in 50 ml of YEME for 24 hours at 30°C/250 r.p.m prior to harvesting. The culture was centrifuged at 4000 r.p.m for 5 minutes and the pellet was then transferred to RNase-free tube. Alternatively, pregerminated spores could be inoculated on sterile cellophane disc laid on 3MA between 48 to 60 hours before being scraped into a sterile falcon tube. RNAprotect Bacteria Reagent (2 volumes) was immediately added to it followed by 5 seconds of vortexing. The mixture was incubated for 5 minutes at room temperature before centrifugation at 4000 r.p.m for 10 minutes. After the removal of supernatant, 200 µl of 1 x TE containing 3mg/ml of lysozyme was added to the tube before vortexing it for 10 seconds. The tube was incubated at room temperature for 30 minutes or more. 700 µl of buffer RLT was added and the tube was vortexed vigorously. The mixture was then centrifuged at 4000 r.p.m for 10 minutes and before transferring the supernatant to a fresh tube. 1 volume of phenol/chloroform/isopropyl alcohol was added and the tube was inverted several times prior to centrifugation at 4000 r.p.m/4°C for 15 minutes. The aqueous (upper) phase was extracted and transferred to a fresh tube and extraction was repeated this time using phenol. The aqueous layer was transferred to a fresh tube. An aliquot (500 µl) of ethanol was added to it and then mixing was done via pipetting. The mixture (including any precipitate which had formed) was then applied to an RNeasy mini column in a 2 ml collection tube followed by a 30 seconds centrifugation at 10K r.p.m. The flow-through was discarded and 700 µl buffer RW1 was added to the column prior to another 30 seconds of centrifugation at 10K r.p.m. The RNeasy column was then transferred to a new 2 ml collection tube before the addition of 500 µl buffer RPE. Centrifugation was done at 10K r.p.m for 2 minutes and the column was then transferred to a new 1.5 ml microcentrifuge tube. The RNA was eluted using 50 µl of RNase-free water via centrifugation at 10K r.p.m for 1 min. The RNA could then be quantified using NanoDrop 2000<sup>TM</sup> Spectrophotometer or stored at – 20°C.



### 3.12 Restriction digest of DNA

Table 6: The different components in a restriction enzyme digest mix. One unit of restriction enzyme could digest 1  $\mu\text{g}$  of DNA in one hour.

Composition	Volume ( $\mu\text{l}$ )		
	Single digest	Single digest	Double digest
DNA sample	1	5	5
10 x buffer	2	2	2
Restriction enzyme	5 u	5 u	5 u
BSA (if required)	1	1	1
Sterile distilled water to	20	20	20

Restriction digest reactions were set up based on Table 6. Restriction enzymes and their related buffers were from Promega, Invitrogen and New England Biolab (NEB). The mixture was incubated at 37 °C water bath for an appropriate length of time depending on the amount of DNA/enzyme added into the reaction. Loading dye (4  $\mu\text{l}$ ) was added at the end of the reaction and the digested DNA could be analyzed via gel electrophoresis.

### 3.13 Dephosphorylation of digested DNA and heat inactivation of Thermosensitive Alkaline Phosphatase, TSAP (Promega)

Table 7: The different components in a DNA dephosphorylation mixture.

Composition	Volume ( $\mu$ l)
DNA	Up to 1 $\mu$ g
Multicore 10 x buffer	1x
TSAP	1u
Sterile distilled water to	20 to 50

The DNA dephosphorylation mix was set up based on Table 7. Multicore 10 x buffer was diluted by addition of sterile distilled water to give a final buffer concentration of 1 x at a volume of 20  $\mu$ l or 50  $\mu$ l. The reaction was incubated at 37 °C for 15 minutes to dephosphorylate all vector DNA overhang types (3', 5' or blunt). TSAP was then heat -inactivated by incubating the reaction mixture at 74 °C for a further 15 minutes. The mixture was then left on ice briefly. The final step involved purification of the DNA using DNA purification systems such as PCR clean up system. The digested DNA could be stored at -20°C.

### 3.14 Phosphorylation of digested DNA and heat inactivation of T4 Polynucleotide Kinase (Promega)

Table 8: The different components in a DNA phosphorylation mixture.

Composition	Final concentration
DNA (average size of 1.5kb)	250 ng
10 x kinase buffer	1x
ATP 0.1 mM	2 $\mu$ l
T4 PNK	10 – 20 units
Sterile distilled water to	40 $\mu$ l

The reaction mixture was set up based on Table 8. The mixture was incubated at 37 °C for 30 minutes. The reaction could be stopped by adding 2  $\mu$ l of 0.5 M EDTA or purification of the DNA using DNA purification systems such as PCR clean up system. The digested DNA could be stored at – 20°C.

### 3.15 Ethanol precipitation of DNA

One tenth volume of 3 M sodium acetate pH 5.2 was added to the DNA solution. This was followed by the addition of 2 volumes of ice-cold ethanol to the mixture. The ethanolic solution was stored on ice for 15 to 30 minutes to allow the precipitation of DNA. The DNA was then recovered by centrifugation at 12,000 g for 10 minutes at 0 °C. The supernatant was carefully removed before half-filling the tube with 70 % ethanol followed by a further centrifugation at 12,000 g for 2 minutes at 4°C. The supernatant was then carefully removed and the tube was bloated dry on a tissue. The tube was placed in a speed vacuum for 30 minutes to ensure complete evaporation of the remaining ethanol. The dried DNA pellet was then dissolved in a desired volume of TE buffer pH 8.0/sterile distilled water and the DNA solution could be stored at -20°C.

### 3.16 Ligation of vector and insert DNA (Promega)

The amount of insert DNA (normally in excess) required to be used for ligation with 100 ng of vector DNA was calculated using the formula below. A 1:3 or 1:5 molar ratio of vector:insert was utilized in most cloning processes.

$$\frac{\text{ng of vector} \times \text{kb size of insert DNA}}{\text{kb size of vector DNA}} \times \text{molar ratio of } \frac{\text{insert}}{\text{vector}} = \text{ng of insert}$$

A ligation mixture consisted of the following components:

Vector DNA	100 ng
Insert DNA	50 ng
T4 DNA Ligase	1 u
Ligase 10 x Buffer	1 $\mu$ l
Sterile Distilled water to	10 $\mu$ l

The ligation mixture was then left at 4°C for 16 hours before the recombinant plasmid could be used to transform competent cells.

### 3.17 Agarose gel electrophoresis of DNA

Table 9: Composition of 50 x TAE buffer. The buffer should be diluted to 1 x for use in agarose gel electrophoresis of DNA.

<b>Composition</b>	<b>Amount</b>
Tris base	242 g
Disodium EDTA dihydrate	37.2 g
Glacial acetic acid	57.1 ml
Sterile distilled water to	1 L

The appropriate amount of agarose was added to the right volume of 1 x TAE buffer to prepare 0.8 to 1.2 % of agarose gel. The mixture was heated in a microwave oven to allow the agarose to dissolve before cooling it in a 50 °C water bath. Ethidium bromide was added to the gel and mixed evenly to give a final concentration of 0.1 mg/L. Then the mixture was poured into an agarose tray with the comb in place. The gel was allowed to set before the removal of the comb. The gel was placed in an electrophoresis chamber and sufficient amount of 1 x TAE buffer was added to the chamber to cover the surface of the gel. DNA samples with loading dye were then loaded into the wells and appropriate voltage (~ 70V) was applied to the chamber. Finally, the post-electrophoretic gel was visualised under UV transillumination at 100 % intensity and images recorded using Syngene GelDoc system.

### 3.18 Gel extraction of DNA (Qiagen)

Post electrophoresis, gel extraction was performed using the UV transilluminator on a low intensity (50% or less) setting for ethidium bromide-stained gels or the DarkReader (Clare Chemical Research) for gels stained with SYBR GOLD (Invitrogen). The DNA fragment was excised from the agarose gel with a clean and sharp scalpel. The gel slice was weighed in a pre-weighed microcentrifuge tube. Buffer QG (3 volumes) was added to 1 volume of gel and the mixture was incubated at 50°C with continuous vortexing every 2 to 3 minutes until complete dissolution of the gel. An aliquot (10 µl) of 3 M sodium acetate pH 5.2 could be added if the mixture was orange or violet in colour to ensure efficient adsorption of DNA to the QIAquick membrane. One gel volume of isopropanol was added to the sample to increase the yield of DNA fragments with the size of less than 500bp or more than 4kbp. The sample was then applied to the QIAquick column and centrifuged for 1 minute at 13,000 rpm. The flow – through was discarded. To ensure all the traces of agarose was removed, 0.5 ml of Buffer QG was added to the QIAquick column. This was centrifuged for 1 minute at 13,000 rpm and the flow – through was discarded. 0.75 ml of Buffer PE was added and centrifugation was carried out at 13,000 rpm for 1 minute to clean up the DNA. To ensure the residual ethanol from the Buffer PE would be completely removed, an additional 1 minute centrifugation at 13,000 rpm was done. The collection tube was replaced with a clean 1.5 ml microcentrifuge tube and 30 µl of nuclease free water was added to the center of the QIAquick membrane and the column was allowed to stand for 1 minute prior to centrifugation at 13,000 rpm for 1 minute. The eluted DNA could be stored at – 20°C.

### **3.19 PCR product purification protocol (Qiagen)**

Buffer PBI (5 volumes) was added and mixed with 1 volume of the PCR sample. The colour of the mixture was checked to ensure it remained yellow. Aliquot (10 µl) of 3M sodium acetate pH 5.2 could be added if the mixture was orange or violet in colour to ensure efficient adsorption of DNA to the QIAquick membrane. The sample was then applied to the QIAquick column and centrifuged for 1 minute at 13,000 rpm. The flow – through was discarded and 0.75 ml Buffer PE was added to the QIAquick column. This was centrifuged for 1 minute at 13,000 rpm and the flow – through was discarded. To ensure the residual ethanol from the Buffer PE would be completely removed, an additional 1 minute centrifugation at 13,000 rpm was done. The collection tube was replaced with a clean 1.5 ml microcentrifuge tube and 30 µl of nuclease free water was added to the center of the QIAquick membrane and the column was allowed to stand for 1 minute prior to centrifugation at 13,000 rpm for 1 minute. The eluted DNA could be stored at – 20°C.

### 3.20 Klenow polymerase for blunting a 5' overhang (Promega)

Table 10: The 5' overhang blunting reaction mix using Klenow polymerase from Promega.

Composition	Amount
DNA template	1 to 4 $\mu\text{g}$
10x Klenow Buffer	2 $\mu\text{l}$
Acetylated BSA (10 $\mu\text{g}/\mu\text{l}$ )	0.2 $\mu\text{l}$
dNTPs (1mM each)	0.8 $\mu\text{l}$
Klenow Polymerase	1 $\mu\text{l}$
Nuclease free water	to 20 $\mu\text{l}$

Following DNA purification process of the restriction enzyme digestion or PCR products which left 5' overhangs, blunting of the overhang could be carried using the reaction set up show in Table 10. The mixture was then incubated at room temperature for 10 minutes before a further DNA purification process outlined in section 3.19

### 3.21 Design of primers and DNA sequence analysis

The nucleotide sequences of genes of interest were analyzed using Clone Manager. Primers for PCR and DNA sequencing were designed based on these sequences using Primer3 (Rozen & Skaletsky, 2000), link: <http://frodo.wi.mit.edu/primer3/>. The primers could then be scored using Premier Biosoft Net Primer, link: <http://www.premierbiosoft.com/servlet/com.pbi.crm.clientside.FreeToolLoginServlet#>. The prediction of the presence of hairpin loop in a particular sequence was done using Softberry FOLDRNA, link: <http://linux1.softberry.com/berry.phtml?topic=foldrna&group=programs&subgroup=rnastrut>. When necessary, restriction digest recognition sequences could be



engineered onto the primers to aid later cloning procedures. The experimentally determined DNA sequences could be aligned with the bioinformatically predicted sequences using EMBOSS Pairwise Alignment Algorithms, link: <http://www.ebi.ac.uk/Tools/emboss/align/index.html>.

### 3.22 Polymerase Chain Reaction (PCR)

PCR was first carried out using GoTaq® DNA polymerase kit (Promega) or Accuzyme™ Mix DNA polymerase kit (Bioline) if a proof-reading system was required to prevent possible point mutations. The general PCR mix set ups for both were shown in Table 11 and 13. The thermocycling conditions were shown in Table 12 and 14. Primers used in various amplification processes were summarized in Table 15. All the reagents were completely thawed, vortexed and centrifuged briefly before the start of the procedure. A mastermix of the PCR mix could be prepared before aliquoting to minimize pipetting errors and contamination.

Table 11: The PCR reaction mix using GoTaq® DNA polymerase kit from Promega.

Composition	Final Concentration
5x Green GoTaq® Reaction Buffer	1x
PCR Nucleotide Mix 20mM	0.8mM
Upstream primer	0.1-1.0µM
Downstream primer	0.1-1.0µM
GoTaq® DNA Polymerase (5u/µl)	1.25 u
DNA template	<250ng
DMSO	4%
Magnesium Chloride (25mM)	1.5 – 3.0mM
Nuclease Free Water to	Final volume

Table 12: The Thermal Cycling Condition for GoTaq® DNA Polymerase Mediated PCR Amplification.

<b>Step</b>	<b>Temperature (°C)</b>	<b>Time</b>	<b>Number of cycles</b>
Initial denaturation	95	5 minutes	1
Denaturation	95	1 minute	30
Annealing	55 - 65	1 minute	30
Extension	72	2 minute	30
Final extension	72	5 minutes	1
Soak	10	Indefinite	

Table 13: The PCR reaction mix using Accuzyme™ Mix DNA polymerase kit from Bioline

<b>Composition</b>	<b>Final Concentration</b>
2x Accuzyme™ Mix (2.5u/μl )	31.25 unit
Upstream primer	0.1-1.0μM
Downstream primer	0.1-1.0μM
DNA template	<250ng
DMSO	4%
Magnesium Chloride (50mM)	1.5 – 3.0mM
Nuclease Free Water to	To final volume

Table 14: The Thermal Cycling Condition for Accuzyme™ DNA Polymerase Mediated PCR Amplification.

<b>Step</b>	<b>Temperature (°C)</b>	<b>Time</b>	<b>Number of cycles</b>
Initial denaturation	95	5 minutes	1
Denaturation	94 - 97	1 minute	30
Annealing	68	1 minute	30
Extension	72	0.5 – 1 min/Kb	30
Final extension	72	5 minutes	1
Soak	10	Indefinite	

Table 15: PCR oligonucleotides sequences

Oligo Name	Description	Sequence ( 5' to 3')	Melting Temperature (°C)
6468L1(A)	EcoRV flanked <i>psd</i>	CGATATCATGCCCCACAGCCAAACC	66.3
6468R1(B)	EcoRV flanked <i>psd</i>	CGATATCAGAGCGGCATCTCCTCCTC	68.0
6467L1(C)	EcoRV flanked <i>pss</i>	CGATATCATGCCGCTCTCGCTCCG	67.8
6467R1 (D)	EcoRV flanked <i>pss</i>	CGATATCGGCCTCGTCCTCAAACGC	67.9
PPM68L (E)	BamHI flanked <i>psd</i>	CGGATCCATGCCCCACAGCCAAACC	69.5
PPM68R (F)	BamHI flanked <i>psd</i>	CGGATCCAGAGCGGCATCTCCTCCTC	71.1
PPM67L(G)	BamHI flanked <i>pss</i>	CGGATCCATGCCGCTCTCGCTCCG	71.3
PPM67R(H)	BamHI flanked <i>pss</i>	CGGATCCGGCCTCGTCCTCAAACGC	71.2
JT672 (R1)	Primed from 3' end of <i>ptipA</i>	GCTTGACCTCACGTCAC	53.0
JT672 (L1)	Primed from 5' end of <i>pss</i>	TGAAGTACACCGCCATGAAG	57.2
JT672 (R2)	Primed from 3' end of <i>pss</i>	GGTGACTCGAATTGACCGTG	59.9
JT672 (L2)	Primed from 5' end of <i>SCO6469</i>	CGATATCGGCCTCGTCCTCAAACC	68.2
ME67 (L1)	Primed from mid of <i>egfp</i>	GGGTTGTCGGGCAGCAGCA	68.7

### 3.23 Reverse-transcription PCR (RT-PCR) (Sambrook *et al.*, 1989)

The RT-PCR reaction setup was shown in Table 15 unless stated otherwise. The reaction mix (50  $\mu$ l) was prepared using Qiagen® OneStep RT-PCR kit in two steps as shown in Table 16 (a) and (b). All RNA samples were normalized at 100 ng per reaction using Nanodrop ND-1000 (Thermo Fischer Scientific) prior to the start of the assay. The thermocycling was carried out using Biorad PTC-100 DNA engine with conditions shown in 16 (c). Primers used for the assay is shown in Figure 16 (d). The generated complementary DNA (cDNA) was then electrophoresed on a 1.4% agarose at 70V for 1.5 hours. The entire assay was done in an RNase-free condition to prevent degradation of the samples.

Table 16: RT-PCR reaction mix, thermocycling conditions and primers for *psd* and *pss*.

(a)

Component	Final concentration
RNase-free water	13.5 $\mu$ l
5x RT-PCR buffer	1x
5x Q - solution	1x
RNA (100 ng/ $\mu$ l)	100 ng
DNase (5u/ $\mu$ l)	2.5u

Placed in thermal cycler for 37 °C for 30 mins and 1  $\mu$ l of 25 mM EDTA was added. The mixture was then incubated at 75 °C for 10 mins before cooling at 4 °C.

(b)

Component	Final concentration
RNase-free water	15 $\mu$ l
5x RT-PCR buffer	1x
5x Q - solution	1x
dNTPs (10mM)	400 $\mu$ M
Primer 1 (10pM)	0.6 $\mu$ M
Primer 2 (10pM)	0.6 $\mu$ M
Qiagen® OneStep RT-PCR enzyme mix	2 $\mu$ l

(c)

Step	Time (min)	Temperature (°C)
Reverse transcription	30	50
Initial PCR activation	15	95
3-step cycling		
Denaturation	1	94
Annealing	1	*
Extension	1	72
Number of cycles	35	
Final extension	10	72

\*61 °C for *psd* and *pss* primers; 66.1 °C for *hrdB* primers

(d)

Oligo Name	Sequence (5' to 3')	Temperature (°C)
6468F (L1); <i>psd</i>	AGCCAAACCTCTGCACCTC	58.83
6468R (R1); <i>psd</i>	CTCTACATCCACCTCGACACC	58.04
6467F (L2); <i>pss</i>	CTTCATGGCGGTGTACTTCA	58.15
6467R (R2); <i>pss</i>	GACAGGACGATCCAGGACAG	59.06

### **3.24 Redirect© Technology: PCR–targeting system in *S. coelicolor* (Gust *et al.*, 2003)**

General protocol is outlined here. See result section for detailed strategy employed.

The plasmid DNA was digested using appropriate restriction enzymes and the PCR template containing the resistance cassette was gel - purified. Two long primers (58 nt and 59 nt), each containing 39 nt matching the *S. coelicolor* sequence adjacent to the gene to be disrupted at the 5' end and 20 nt or 19 nt matching the left or right end of the disruption cassette at the 3' end were used to PCR amplify the extended resistance cassette. A gel electrophoresis was carried out to check the fragment size to confirm the amplification. The PCR product was then cleaned via DNA purification process.

*E. coli* BW25113/pIJ790 was grown overnight at 30°C in 10 ml LB broth containing chloramphenicol (25 µg/ml). Aliquot of (100 µl) of the *E. coli* BW25113/pIJ790 overnight culture was inoculated in 10 ml of SOB containing 20 mM and chloramphenicol (25 µg /ml). This was grown for 3-4 h at 30°C shaking at 200 rpm to an OD600 of ~ 0.6. Electrocompetent *E. coli* BW25113/pIJ790 was prepared as described previously. Electrotransformation of cosmid DNA into *E. coli* BW25113/pIJ790 was carried out and the culture was incubated for 1.5 hours at 30°C. The culture was spread onto LB agar containing carbenicillin (100 µg/ml), kanamycin (50 µg/ml) to select for the Supercos1-derived cosmids and chloramphenicol (25 µg/ml) for λ RED recombination plasmid, pIJ790 before overnight incubation at 30°C.

A single colony of the transformants was transferred to 5 ml LB broth containing carbenicillin (100 µg/ml), kanamycin (50 µg/ml) and chloramphenicol (25 µg/ml) prior to overnight incubation at 30°C. This culture was then used as a pre-culture for generating competent cells to be transformed with the PCR- amplified resistance cassette. Transformation was carried out and the mixture was then incubated for 1.5 hours at 30°C. The culture was spread onto LB agar containing carbenicillin (100 µg/ml), kanamycin (50 µg/ml) and hygromycin (100 µg/ml). It was incubated

overnight at 37°C to promote the loss of pIJ790 if no further gene disruption was required. A single colony obtained from the plate was transferred to 5ml LB broth containing carbenicillin (100 µg/ml), kanamycin (50 µg/ml) and hygromycin (100 µg/ml). This was incubated overnight at 37°C for isolation of the mutagenised cosmid. After confirmation via restriction digestion, the recombinant cosmid was conjugally transferred into *S. coelicolor*. Double crossover exconjugant apra<sup>r</sup>, km<sup>s</sup> was picked via replica patching.

### 3.25 Transposon inactivation of target gene

See result section for detailed strategy employed in transposon-mediated gene mutagenesis.

### 3.26 Enhanced green fluorescent protein (*egfp*) - gene fusion as a mode to report protein localization within bacterial cells (adapted from Gust *et al.*, 2003).

General protocol is outlined here. See result section for detailed strategy employed. The plasmid pIJ786 was digested using EcoRI and HindIII and the PCR template containing the resistance cassette was gel - purified. Two long primers (89 nt forward primer and 58 nt reverse primer), each containing 19 nt or 20 nt matching the left or right end of the *egfp* cassette at the 3' end and 39 nt *S. coelicolor* sequence at the end of (forward primer) or adjacent to the gene of interest at the 5' end (reverse primer) were used to PCR amplify the extended *egfp* cassette (with the forward primer also containing a 10 amino acids linker). A gel electrophoresis was then conducted to check the fragment size to confirm the amplification. *S. coelicolor* cosmid containing the gene of interest and the extended *egfp* cassette were introduced into *E. coli* BW25113/pIJ790. The mutagenised cosmid was then verified via PCR and restriction digestion. The mutant cosmid was then transformed into electrocompetent *E. coli* ET12567/pUZ8002 prior to conjugal transfer to *S. coelicolor*. The colonies were patched on replica plates containing apramycin (50 µg/ml) or kanamycin (50 µg/ml). Apra<sup>r</sup>, km<sup>s</sup> colonies were chosen for verification via PCR/Southern blot prior to microscopy.

### **3.27 DNA cloning/subcloning**

See result section for individual cloning strategies. All cloning experiments were done using various DNA modification enzymes from Promega, Bioline and New England Biolabs according to manufacturers' instructions.

### **3.28 Phospholipid extraction and identification via thin layer chromatography (TLC); (Bligh & Dyer, 1959)**

Phospholipid extraction was done according to Bligh & Dyer (1959) with slight modifications. Cultures with 25 mg of dry mass or 100 mg of wet mass was weighed out and transferred to a fresh appendorf tube. The mycelia were resuspended in 100  $\mu$ l chloroform, 200  $\mu$ l methanol and 80  $\mu$ l water followed by vigorous vortexing for 10 minutes. Aliquot (100  $\mu$ l) of chloroform was added to the mixture and the sample was vortexed for an additional minute. Aliquot (100  $\mu$ l) of water was then added again to the mixture prior to another minute of vortexing. The sample was then centrifuged at 13K r.p.m for 1 minute which resulted in phase separation (mycelial disc forming in the middle of the mixture separating the aqueous (upper) and organic (lower) layers). The organic layer was carefully removed and dried in a vacuum centrifuge. The sample could be stored at  $-20$  °C or used immediately by resuspending it in chloroform prior to application onto a K6 60A porosity silica gel TLC plate with a dimension of 200mm x 200mm x 250 $\mu$ m (stationary phase). Phospholipid standards ( $\alpha$ -phosphatidyl-DL-glycerol sodium salt from egg yolk lecithin (PG); 3-sn-phosphatidylethanolamine from bovine brain (PE); cardiolipin solution from bovine heart (CL) from Sigma) dissolved in ethanol (5 $\mu$ g/ml) were also spotted onto the plate to aid in identification of the resolved spots on the plate. The plate was put into TLC tank with various solvent mixtures (mobile phase) which would move up the plate via capillary action. The plate was then allowed to dry and the phospholipid spots were then visualized by spraying the plate with Molybdenum blue (Sigma).



### **3.29 Microscopy** (Kieser *et al.*, 2000; Jyothikumar *et al.*, 2012)

Samples were inoculated on coverslips inserted 45° diagonally into 3MA plate. The inoculum was incubated at 30 °C for the required amount of time before the removal of the coverslips for methanol fixing (and staining if necessary) and mounting onto microscope slides. Microscopy was carried out on a Nikon TE2000S inverted microscope at 100x magnification using different filters. Images were captured using Hamamatsu Orca-285 Firewire Digital CCD camera and further image processing was done using IPLabs 3.7 image processing software (BD Biosciences Bioimaging, Rockville, Maryland, USA). Both Pss-EGFP in ME67 and Vancomycin-FL staining of JT672 were visualized with FITC filter (Ex 492/18; Em 520/20), Syto42 staining with DAPI filter (Ex 403/12; Em 455/10) and FM4-64 staining with TRITC filter (Ex 572/23; Em 600/20). Measurement of morphological parameters (apical tip to first lateral branch distance, inter-branch distance, inter-septum distance and spore width) were done using IPLabs 3.7 image processing software. The multiple data sets were analysed using Minitab (ANOVA) and bar charts with their standard errors were constructed using Microsoft Excel 2003.

### **3.30 Bioinformatics**

#### **3.30.1 Inter-species protein sequence alignment and phylogenetic analysis**

The amino acid sequence for a particular protein encoded for by the gene of interest from different species could be obtained from Uniprot, link: <http://www.uniprot.org/>. The different amino acid sequences were then saved into .txt format before being imported into the CLC Sequence Viewer 6 (freeware) for sequence alignment and phylogenetic analysis.

#### **3.30.2 Two-dimensional (2D) similarity searching of potential inhibitor of target protein**

The 2D chemical structure of a particular known ligand/substrate of the target protein was drawn using ChemBioDraw Ultra 12.0 (Mills, 2006). The 2D chemical structure could be divided into substructures to refine search. Both the structure/substructures and the library of chemical compounds were then imported into Accelrys' scientific informatics platform, Pipeline Pilot (Morrison, 2012) for database querying. After the completion of the 2D similarity searching, the output file could be exported and viewed using MarvinSketch.

### **3.31 Chemical synthesis of 2-amino-5-methylthiazole-4-carboxylate (ATC) derivatives (Al-Balas *et al.*, 2009)**

The chemical synthesis of the four ATC derivatives was achieved via the Darzens reaction between methyl dichloroacetate and the appropriate aldehyde. Detailed synthetic strategy is outlined as followed.

### 3.31.1 Synthesis of methyl 2-amino-5-methylthiazole-4-carboxylate (QAB004)

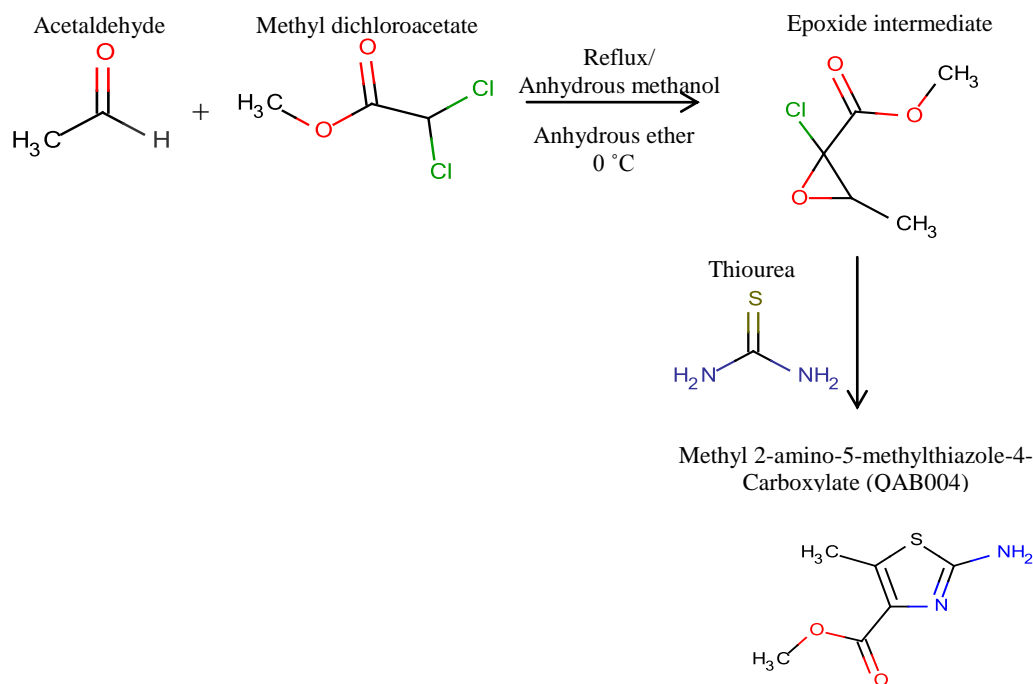


Figure 6: The strategy employed in the chemical synthesis of methyl 2-amino-5-methylthiazole-4-carboxylate from acetaldehyde and methyl dichloroacetate

The general synthetic strategy of QAB004 is shown in Figure 6. Acetaldehyde (3.2 g, 72 mmol, 1 eq) and methyl dichloroacetate (10.3 g, 72 mmol, 1 eq) were added to a stirring anhydrous ether at 0 °C prior to the addition of NaOMe (5.80 g, 108 mmol, 1.5 eq) previously dissolved in anhydrous methanol, in a dropwise manner. After a further 1 hour stirring at 0 °C, brine solution was added and the product was extracted from the organic layer with ether followed by drying using MgSO<sub>4</sub>. The ether layer was concentrated *in vacuo* using rotary evaporator prior to the addition of thiourea (5.48 g, 72 mmol, 1 eq) pre-dissolved in anhydrous methanol. The mixture was refluxed for 4 hours before concentrated *in vacuo* using rotary evaporator and neutralized with 0.5 M NaOH. The mixture was washed and extracted with ethylacetate before drying using MgSO<sub>4</sub>. After concentrating *in vacuo*, the product was purified from MeOH/H<sub>2</sub>O.

### 3.31.2 Synthesis of 2-amino-5-methylthiazole-4-carboxylic acid (QAB004A)

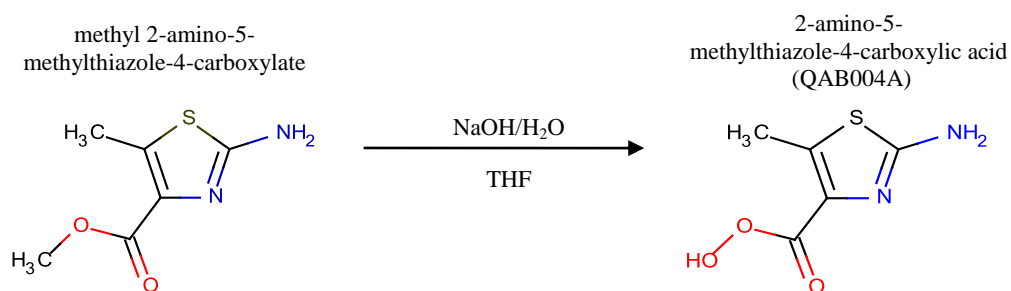


Figure 7: The strategy employed in the chemical synthesis of 2-amino-5-methylthiazole-4-carboxylic acid from methyl 2-amino-5-methylthiazole-4-carboxylate.

The general synthetic strategy of QAB004A is shown in Figure 7. Methyl 2-amino-5-methylthiazole-4-carboxylate (1 g, 5.8 mmol, 1 eq) was added to a stirring solution of NaOH at 50 °C until the compound dissolved completely. The mixture was left to stir at room temperature for 24 hours prior to neutralization using 1M HCl to pH 4. The precipitated product was then filtered and dried in a dessicator.

### 3.31.3 Synthesis of methyl 2-amino-5-benzylthiazole-4-carboxylate (QAB008)

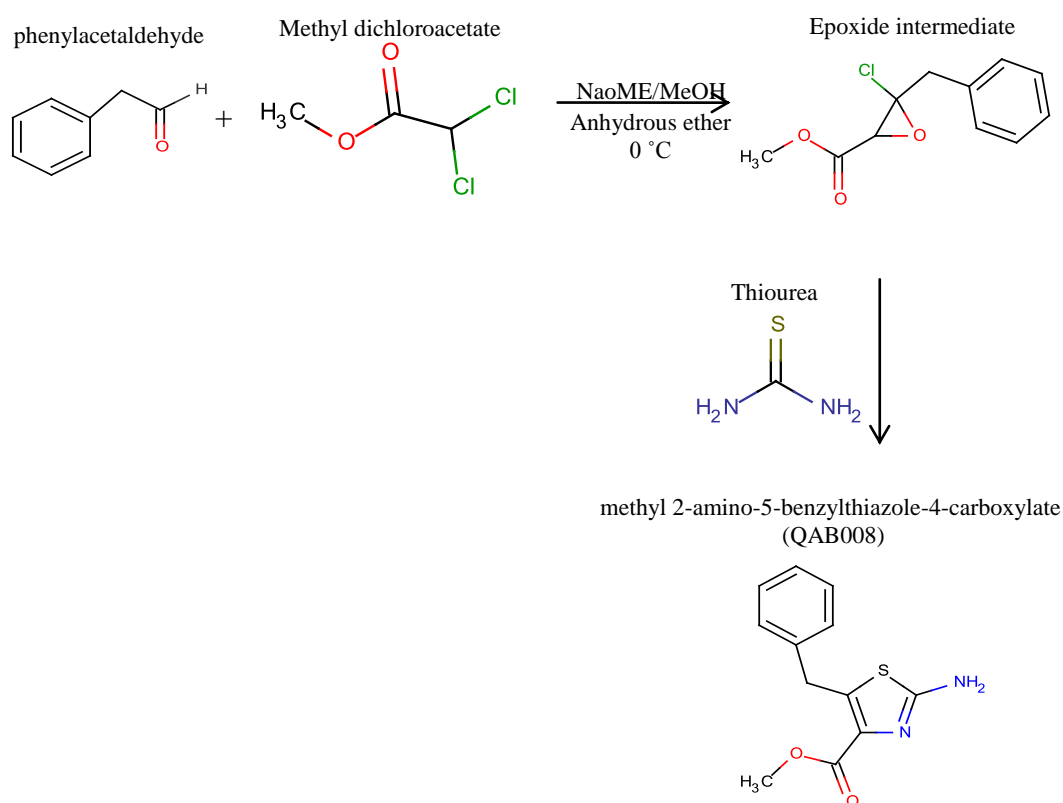


Figure 8: The strategy employed in the chemical synthesis of methyl 2-amino-5-benzylthiazole-4-carboxylate from methyl dichloroacetate and phenylacetaldehyde.

The general synthetic strategy of QAB008 is shown in Figure 8. Phenylacetaldehyde (1.45 g, 12 mmol, 1 eq) and methyl dichloroacetate (1.72 g, 15 mmol, 1 eq) were added to a stirring anhydrous ether at 0 °C prior to the addition of NaOMe (0.98 g, 18 mmol, 1.5 eq) pre-dissolved in anhydrous methanol, in a dropwise manner. After a further 1 hour stirring at 0 °C, brine solution was added and the product was extracted from the organic layer with ether followed by drying using MgSO<sub>4</sub>. The ether layer was concentrated *in vacuo* using rotary evaporator prior to the addition of thiourea (0.91 g, 12 mmol, 1 eq) pre-dissolved in anhydrous methanol. The mixture was refluxed for 4 hours before concentrated *in vacuo* using rotary evaporator and neutralized with 0.5M NaOH. The mixture was washed and extracted with ethylacetate before drying using MgSO<sub>4</sub>. After concentrating *in vacuo*, the product was purified from MeOH/ether.

### 3.31.4 Synthesis of methyl 2-heptanamido-5-methylthiazole-4-carboxylate (QAB014)

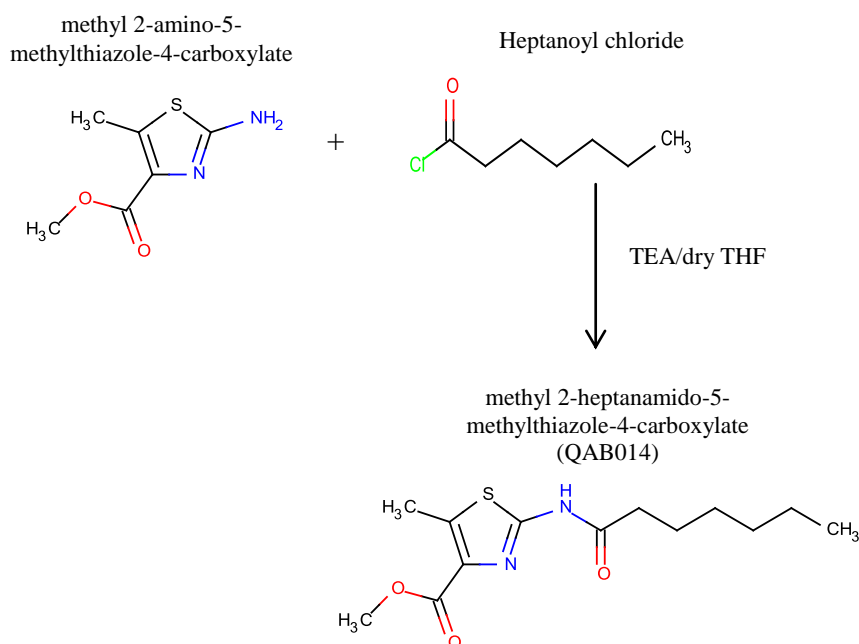


Figure 9: The strategy employed in the chemical synthesis of methyl 2-heptanamido-5-methylthiazole-4-carboxylate from methyl 2-amino-5-methylthiazole-4-carboxylate and heptanoyl chloride.

The general synthetic strategy of QAB014 is shown in Figure 9. Methyl 2-amino-5-methylthiazole-4-carboxylate (1 g, 5.8 mmol, 1 eq) was dissolved in a stirring solution of anhydrous tetrahydrofuran within a cooled bath (0 °C) after which triethylamine (1.17 g, 11.6 mmol, 2 eq) was added to the mixture. Heptanoylchloride (1.72 g, 11.6 mmol, 2 eq) was then added in a dropwise manner into the reaction. The reaction was stirred for a further 4 hours. The mixture was then concentrated *in vacuo* using rotary evaporator followed by basicification with 0.5M of ammonium hydroxide. The organic layer was extracted using dichloromethane (DCM) and this layer was purified further via extraction with 0.5M HCl. The DCM layer was then dried using MgSO<sub>4</sub> and concentrated *in vacuo* prior to recrystallization from methanol.

### **3.32 Chemical Analysis**

#### **3.32.1 Melting point determination**

Melting point (°C) determination of a particular compound was carried out using Stuart Scientific Melting Point SMP1 apparatus.

#### **3.32.2 Elemental analysis (CHN)**

Elemental analysis of compound was conducted using Perkin Elmer 2400 Analyzer to determine the percentage content of C, H, N and other halogens.

#### **3.32.3 Infrared spectroscopy (IR)**

Infrared spectra of compounds were obtained from Jasco FT-IR-4200 ATR (Attenuated Total Reflection Mode) and Mattson Genesis Series FT-IR spectrometers where samples were compressed together with KBr into disks prior to IR analysis. Readings were expressed as Wavenumbers,  $\nu_{\max}$  (cm<sup>-1</sup>).

#### **3.32.4 Nuclear magnetic resonance (NMR) spectroscopy**

Proton (<sup>1</sup>H NMR) and carbon (<sup>13</sup>C NMR) spectra of compounds were obtained from JEOL EX 270 (270MHz), Bruker AMX-400 (400MHz) and JEOL Lambda delta 400 (400MHz) spectrometers. Data were reported as chemical shifts in parts per million (ppm) whereas coupling constants (J) were quoted in hertz (Hz). Samples were dissolved in appropriate deuterated solvents in NMR tubes prior to analysis.

### **3.32.5 Mass spectrometry (MS)**

High-resolution mass spectroscopy (ms) was conducted using electron impact (EI), chemical impact (CI), and fast atom bombardment (FAB) ionizations on a JEOL JMS-700 Dual-sector High-resolution Mass Spectrometer. Analysis of the samples was reported as mass-to-charge ratio ( $m/z$ ) and relative abundance.



**4.0 Results**  
**Phylogenetic analysis and protein sequence alignment**

## 4.1 Introduction

Phylogenetic analysis is a useful tool in reconstructing the tree of life for gauging the divergence of evolutionary relationship of organisms with regards to a particular molecular entity i.e. gene or gene product. The underlying principle is to group different organisms according to their level of similarity which could further unravel the chain of events and evolutionary forces (such as mutation, deletion, duplications) involved in the process of evolution.

Since the crystal structures of the target proteins have not been determined, this method is the major source of information regarding the primary structures and the degree of conservation of interspecies Psd and Pss, ultimately validating the use of *S. coelicolor* as our model bacteria for analogous studies on other bacteria/pathogens especially *M. tuberculosis*. The aim is to ensure that there is parallel activity of the identified antibacterial compounds against *S. coelicolor* and other genetically related pathogens with selective toxicity/inhibitory effect only against the proteins of these bacteria.

## 4.2 Phylogenetic analysis of Psd and Pss homologues.

The importance of aminophospholipids (PE and PS) as the major building blocks in the plasma membrane of mycobacteria (Morita *et al.*, 2005) coupled with the essentiality of PI and its metabolic derivatives in structure, physiology as well as host infection by member of this genus (Jackson *et al.*, 2000) suggest that enzymes involved in the biosynthesis of these phospholipids could be potential drug targets for anti-TB drug discovery program. It was hypothesized that the structural and functional organization of the mycobacterial plasma membrane would be detrimentally altered following the depletion of some of these phospholipids, consequently affecting the cell viability and virulence.

Phylogenetic analysis was carried out on Psd and Pss homologues of various prokaryotic and eukaryotic taxa. The amino acid sequences were exported from Uniprot as FASTA file and multiple sequence alignments as well as phylogenetic trees computed in ClustalW (Larkin *et al.*, 2007) using Neighbour-joining algorithm (Saitou & Nei, 1987). Subsequently, the robustness of the tree topology was assessed by comparing it to a phylogenetic tree generated using the Unweighted Pair Group Method with Arithmetic Mean (UPGMA); (Michener & Sokal, 1957; Sneath & Sokal, 1973) algorithms.

The analysis was conducted on a number of prokaryotes including *S. coelicolor*. The purpose was to determine the applicability of *S. coelicolor* as a model for the analogous study of *M. tuberculosis* based on the degree of similarity of the interspecies protein sequences. The mammalian (mouse and human) and yeast (*S. cerevisiae*) proteins were included in the global alignment process in order to gauge the degree of dissimilarity between eukaryotic and prokaryotic Psd and Pss thus the likelihood of circumventing the issue of non-specific targeting of the host proteins.

The proteins are generally larger in the eukaryotes compared to prokaryotes and there is significant difference in terms of amino acid sequences even within the identified motifs (highlighted in Figure 10: Psd & Figure 13: Pss). Presumably, their secondary and tertiary structures might also differ substantially. The corresponding phylogenetic trees further established the low degree of genetic relationship between the two domains of life i.e. prokaryotes versus eukaryotes (Figure 11: Psd & Figure 14: Pss).

Human Psd only showed 14% and 9% identity with *S. coelicolor* and *M. tuberculosis* proteins respectively whereas a significantly high homology was observed between Psd of *S. coelicolor* and *M. tuberculosis* (36% identity). The putative conserved LGST sequence found in the eukaryotic Psd (highlighted by black rectangle in Figure 10) is thought to be involved in pyruvoyl prosthetic group formation and endoproteolysis (Trotter *et al.*, 1993). The cleavage of the proenzyme to liberate the catalytic  $\alpha$ -chain from  $\beta$ -subunit (Li & Dowhan, 1988) was proposed

to occur between the Gly and Ser residues within the conserved motif of mammalian and yeast Psd (Voelker, 1997). In both *Mycobacteria* and *Streptomyces*, the LGST sequence is substituted by the FGSR motif found within the highly conserved GLIRXGSRXD motif of both genera (highlighted by black rectangle in Figure 10 & 12) where *S. coelicolor* and *M. tuberculosis* displayed 90% identity. The detailed alignment of Psd of several members of the actinobacteria phylum also revealed the highly conserved domain near the C-terminal end of the protein (Figure 12).

Another consensus motif, FxFxLKxxxKxR located in the  $\alpha$ -subunit of the eukaryotic protein is also absent in their prokaryotic counterparts (highlighted by orange rectangle in Figure 10). This domain which is located in close vicinity to the catalytic carbonyl is thought to be important in facilitating the interaction between PS and eukaryotic Psd (Igarashi *et al.*, 1995; Schuiki & Daum, 2009). The absence of this substrate recognition site in the prokaryotes suggests the difference in the prokaryotic and eukaryotic Psd substrate affinity which could be exploited to our advantage in the drug discovery program.

The phylogenetic tree generated using the Neighbour-Joining algorithm (Figure 11) indicated that Psd of both *Mycobacteria* and *Streptomyces* genera were in fact sister taxa which hailed from a common ancestor before diverging to form their own clades. The topology of the phylogenetic tree constructed using Neighbour-Joining algorithm was also similar to the one computed via UPGMA algorithm (data not shown) hence confirming the robustness of the analysis.

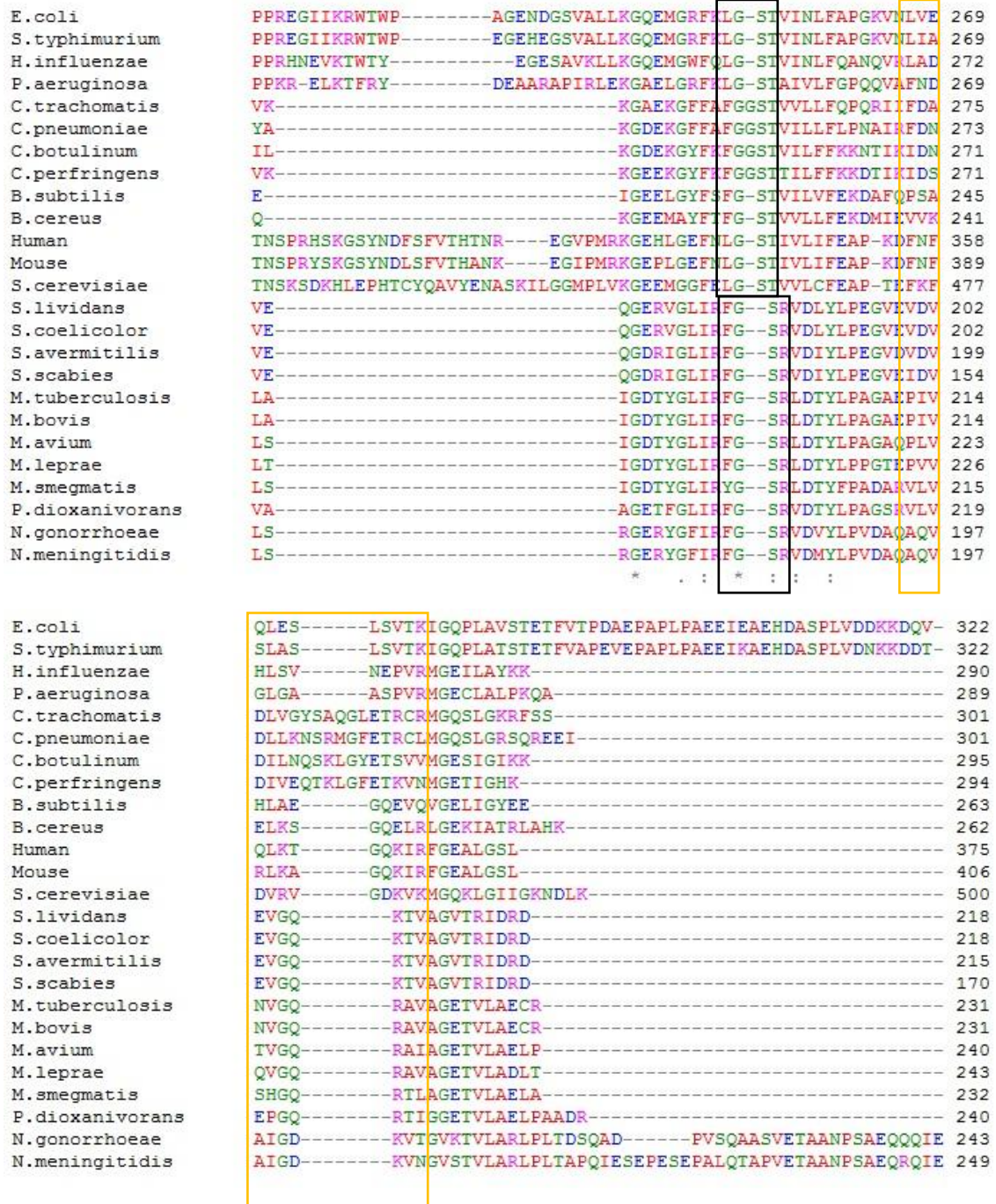


Figure 10: Multiple sequence alignment of the prokaryotic and eukaryotic Psd using ClustalW. There is little sequence homology between the prokaryotic and eukaryotic proteins even within the catalytic domain of the protein. The putative conserved LGST motif (black rectangle) is thought to be involved in pyruvoyl prosthetic group formation and endoproteolysis in the eukaryotes. In both *Mycobacteria* and *Streptomyces*, the LGST sequence is substituted by the FGSR motif. The FxLKxxxKxR motif (orange rectangle) which is believed to be important for substrate recognition in eukaryotic proteins was not found in their prokaryotic counterparts.

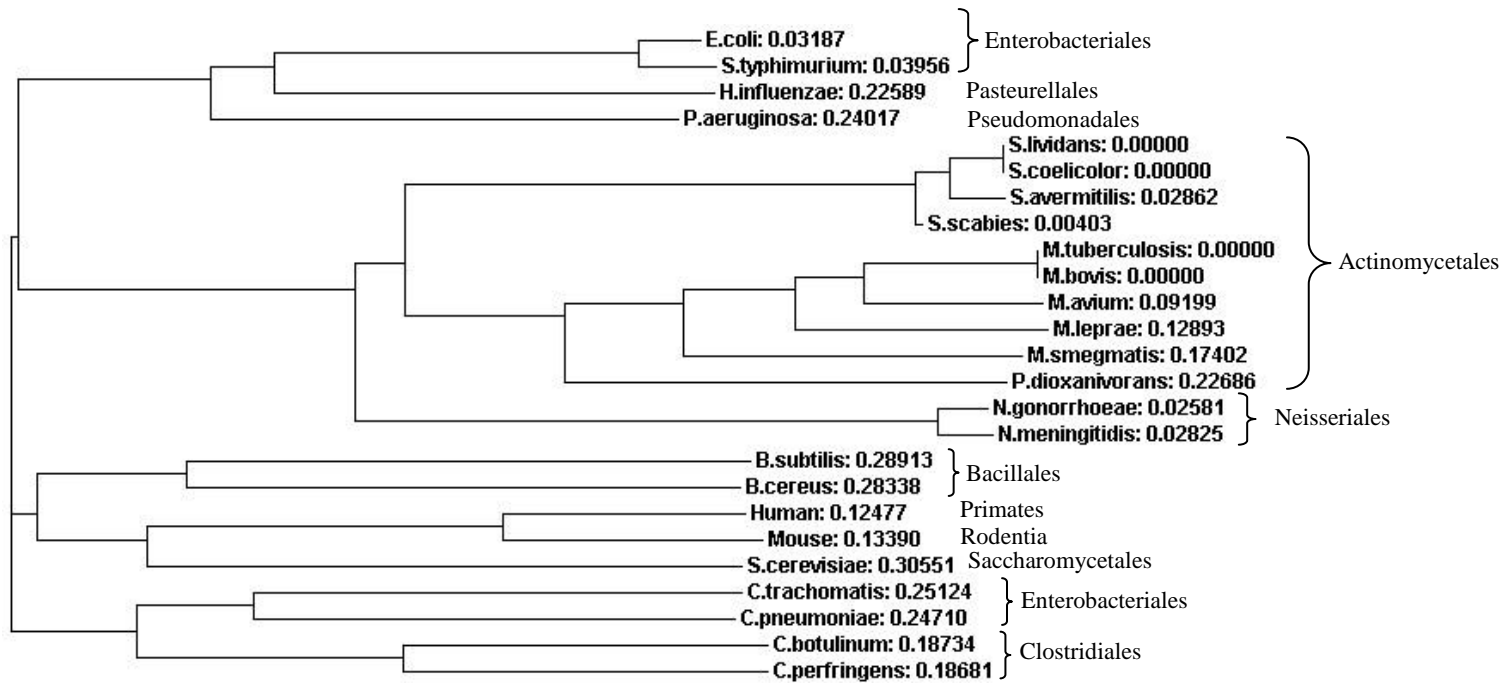


Figure 11: Evolutionary relationships of Psd in 25 taxa inferred using Neighbour-Joining algorithm.



M. tuberculosis	PLPRVSIFLSILDAHVQRAPVSGEVIQVQHRPGRFGSADLPEASDDNERTSVRIRMPNGA	162
M. bovis	PLPRVSIFLSILDAHVQRAPVSGEVIQVQHRPGRFGSADLPEASDDNERTSVRIRMPNGA	162
M. avium	ALPRVSIFLSLLDAHVQRAPVSGEVIDVQHRPGRFGSADLAAASTENERTSLRIRTPGGA	171
M. leprae	SLPRVSIFLSLLDVHVQRAPISGEVIQVQYQPGFGAADLAPASTENERTSVRIRTAGGT	174
M. smegmatis	PMQRVSIFLSVLDDAHVQRAPIGGEVVAVRHRPGRFHSAELEAAASEDNERNVSVVIRIPEGL	163
P. dioxanivorans	PVPRVSVFLSVLDVHVQRPVVDGRVVAVVEYRPGVFLSADLDKASEDNERNAVLFEATDGH	167
S. lividans	GRTRVAIFMSPLNVHVNRAPLAGTIVTSVEHVPGGFVPA-FNKESENNERVVWHFDTELG-	150
S. coelicolor	GRTRVAIFMSPLNVHVNRAPLAGTIVTSVEHVPGGFVPA-FNKESENNERVVWHFDTELG-	150
S. avermitilis	GRTRVAIFMSPLNVHVNRAPLSGTIVTSVEHIPGGFVPA-FNKESENNERVVWHFDTELG-	147
S. scabies	GRTRVAIFMSPLNVHVNRAPLSGTIVTSVEHIPGGFVPA-FNKESENNERVVWHFDTELG-	102

\*\*\*:\*\* \* :.\*\*\*:\* : \* \* \* .: \* \* \* . \* : \* :\*\*\* : \*

M. tuberculosis	EVVAVQIAGLVARRIVCDAHVGDKLAI GDTYGLIRFGSRLD TYLPAGAEPIVNVGQRAVA	222
M. bovis	EVVAVQIAGLVARRIVCDAHVGDKLAI GDTYGLIRFGSRLD TYLPAGAEPIVNVGQRAVA	222
M. avium	EVVAVQVAGLLARRIICDAHVGDKLSIGDTYGLIRFGSRLD TYLPAGAQPLVTVGQRAIA	231
M. leprae	EVVVVQIAGLLARRIVCYAHIGDKLTIGDTYGLIRFGSRLD TYLPPGTEPVVQVQRAVA	234
M. smegmatis	HIIAVQIAGLIARRIVCDVHVGDKLSIGDTYGLIRYGSRLD TYFPADARVLVSHGQRTLA	223
P. dioxanivorans	RVGVLQIAGLLARRIVCEVAQGDEVAAGETFGIRFGSRVD TYLPAGSRVLVEPGQRTIG	227
S. lividans	DIEMIQIAGAVARRIVPYVPQGTKVEQGERVGLIRFGSRVD LYLPPEGVEVDVEVGQKTVA	210
S. coelicolor	DIEMIQIAGAVARRIVPYVPQGTKVEQGERVGLIRFGSRVD LYLPPEGVEVDVEVGQKTVA	210
S. avermitilis	DIEMIQIAGAVARRIVPYVPQGTKVEQGDRI GLIRFGSRVDIYLPPEGVDVDEVGQKTVA	207
S. scabies	DIEMIQIAGAVARRIVPYIPEGTKVEQGDRI GLIRFGSRVDIYLPPEGVEIDVEVGQKTVA	162

: :\*\*\* :\*\*\*\*: \* : : \* : \*\*\*\*\*:\*\* \* . \* \*\*\*\*:



Pfam domain  
88-216

Figure 12: The sequence of the conserved catalytic region of actinomycetes Psd as well as its location in Pfam. The highly conserved motif, GLIRXGSRXD (black rectangle) containing the FGSR motif (in *S. coelicolor* and *M. tuberculosis*) thought to be involved in pyruvoyl prosthetic group formation and endoproteolysis is located near the C-terminal end of the protein. There is 90% identity for this highly conserved motif between *S. coelicolor* and *M. tuberculosis*.

Human Pss1 and Pss2 exhibited a very low homology with that of *S.coelicolor* and *M. tuberculosis* proteins with overall identity of less than 10% whereas Pss of both *S.coelicolor* and *M. tuberculosis* showed 20.4% identity. The four aspartic acid residues – containing motif,  $\text{DX}_2\text{DGX}_9(\text{S/T})\text{X}_2\text{GX}_3\text{DX}_3\text{D}$  located near the N-terminal end of the mycobacteria and streptomycetes proteins (Jackson *et al.*, 2000; Karnezis *et al.*, 2002) believed to be associated with the catalytic activity of this enzyme (Saha *et al.*, 1996b; Karnezis *et al.*, 2002) is conserved within the two genera (highlighted in Figure 13 & 15). This motif was not as conserved in the mammalian proteins based on the protein alignment analysis (highlighted Figure 13). This is not surprising given the fact that mammalian Pss1 and Pss2 utilize different substrates, phosphatidylcholine and PE respectively in the biosynthesis of PS (Kuge, *et al.*, 1986). The same motif was also not observed in *E. coli* but showed homology with *E. coli* PgsA (data not shown) (Saha *et al.*, 1996b).

Although the phylogenetic tree generated using the Neighbour-Joining algorithm (Figure 14) showed the low degree of genetic relationship between both *Mycobacteria* and *Streptomyces* genera, the applicability of *S. coelicolor* as model for analogous studies on *M. tuberculosis* should not be ruled out. This is due to the fact the domain near to the catalytic site is highly conserved between the two genera (Figure 15). Therefore, there is likelihood of cross-reactivity of any potential inhibitors for Pss of both groups. Finally, the tree topologies for both algorithms (Neighbour-joining vs UPGMA) were found to be grossly similar (data not shown).

In conclusion, highly conserved regions were observed for the two proteins (Pss and Psd) of both *S. coelicolor* and *M. tuberculosis* especially near the catalytic domains which concurred with previous studies (Bentley *et al.*, 2002). Therefore, the use of *S. coelicolor* for analogous study on *M. tuberculosis* looked promising although the data generated thereafter remain to be validated in the pathogen itself.



```

S.cerevisiae      AHFFILLGMCDFD---LDGRVARLRNRSSLMGQELDSLADLVVSFGVAPAAIAFAIGFQIT 172
C.perfringens    AAIFILLAGLYDR---YDGRVARYLNVSSDLGKELDSLADLVVSFGVAPSVLTFVF----- 84
S.coelicolor     AVILMLCAAIFDL---FDGLVARKLRSS-PMGAELDNLSLISFGLAPAYFVLVYG----- 104
S.lividans       AVILMLCAAIFDL---FDGLVARKLRSS-PMGAELDNLSLISFGLAPAYFVLVYG----- 104
S.avermitilis    AVILMLCAAVFDL---FDGLVARKLRSS-PMGAELDNLSLISFGLAPAYFVLVYG----- 104
S.scabies        AVILMLCAAIFDL---FDGLVARKLRSS-PMGAELDNLSLISFGLAPAYFVLVYG----- 116
B.subtilis       AVLFIITGMFLDF---FDGMAARKLNAVSDMGRELDSPADLVTFVGVAPSM LAYS----- 81
M.tuberculosis  AMALIAAAAILDG---LDGRVARILDAQSRMGAEIDSLADAVNFGVTPALVLYVSM----- 95
M.bovis          AMALIAAAAILDG---LDGRVARILDAQSRMGAEIDSLADAVNFGVTPALVLYVSM----- 95
M.leprae         AIALIAAAAILDG---LDGRVARILGAESRMGEEIDSLADAVNFGVAPAVLYATM----- 95
N.gonorrhoeae   AAIAVFI SMLLDG---MDGRVARLTNSQSAFGEQLDSLADMVVSFGVAPALIA YKWQ---- 99
N.meningitidis  AAIAVFI SMLLDG---MDGRVARLTNSQSAFGEQLDSLADMVVSFGVAPALIA YKWQ---- 99
P.aeruginosa    AAIAIFVAMVLDG---LDGRVARLTNTQSAFGEYDLSLIMVAFGVAPALVAFENA---- 122
H.pylori        ACWLVAASLILDG---LDGRVARLTNTTSKFGIEFDLADVIAFGVAPSLIAYFYV---- 88
Human_Pss1      NCHVITWERIISH---FDIFAFGHFWGWAMKALLIRSYGICWTISITWELTELFFMHL LP 208
Mouse_Pss1      NCHVITWERIVSH---FDIFAFGHFWGWAMKALLIRSYGICWTISITWELTELFFMHL LP 208
Human_Pss2      DNETDPFHNIWDK---LDGFVPAHFLGWYLKTLMIRDWWMCMII SVMFEFLEYSLEHQLP 236
Mouse_Pss2      DNKTDPFHNIWDK---LDGFVPAHFIGWYLKTLMIRDWWMCMII SVMFEFLEYSLEHQLP 214
E.coli          LGVLHFKGFIIDDSVLYSGASLNDVYLHQHDKYRYDRYQIIRNRKMSDIMFEVWTQNIMN 193
S.typhimurium   LGVLHFKGFIIDDSVLYSGASLNDVYLHQHDKYRYDRYQIIRNRQADIMFDVWTQNLMN 193
H.influenzae    FGVLVKGFVDDTVLYSGASINNVYLHQFEKYRYDRYQIITHAELADSMVNFINDYLLD 194

```

Figure 13: Multiple sequence alignment of the prokaryotic and eukaryotic Pss using ClustalW. There is little sequence homology between the prokaryotic and eukaryotic proteins even within the catalytic domain of the protein. The catalytic motif containing the quadruple aspartic acids,  $Dx_2DGx_9(S/T)x_2GX_3Dx_3D$  of the prokaryotic proteins (highlighted by black rectangle) is not conserved in the mammalian proteins.

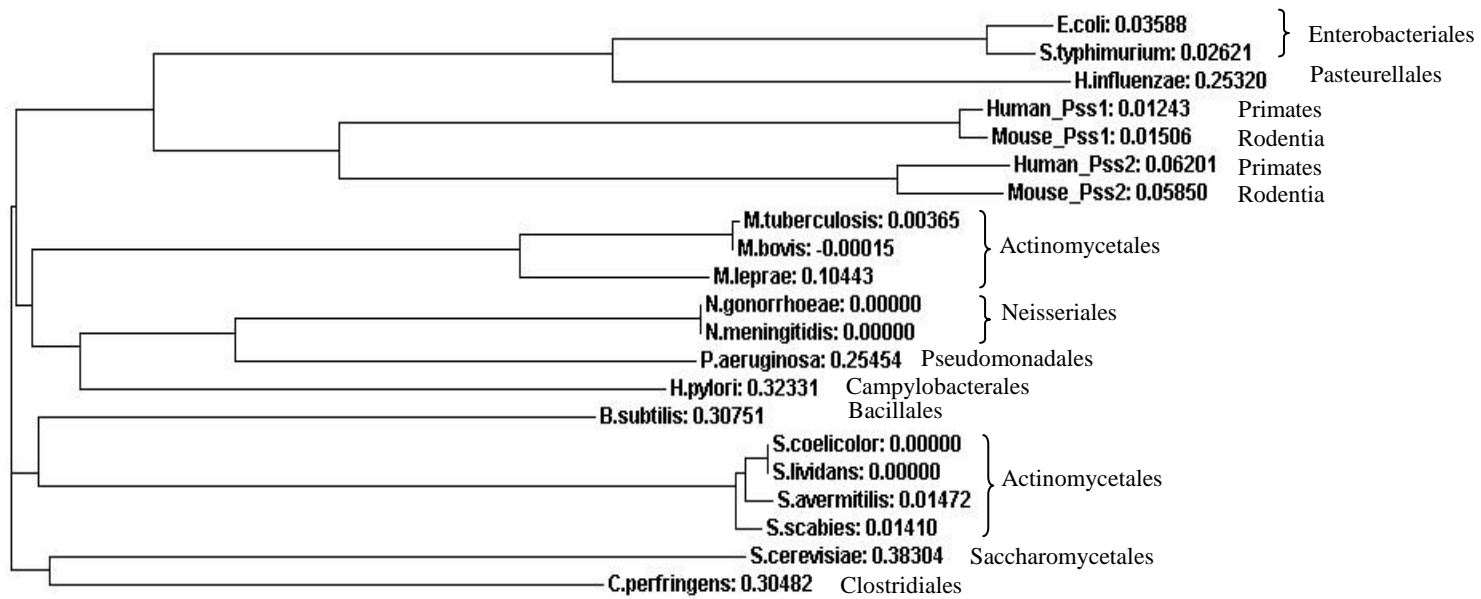


Figure 14: Evolutionary relationships of Pss in 25 taxa inferred using Neighbour-Joining algorithm.



### 4.3 Prediction of membrane spanning region and orientation of Psd and Pss

Querying of RCSB Protein Data Bank revealed that Psd and Pss crystal structures for both *S. coelicolor* and *M. tuberculosis* have yet to be determined. This had proven to be a challenge in the drug discovery scenario since the substrate binding moieties within the active sites of the proteins as well as the binding mechanism of any compounds to the amino acid could not be confirmed or predicted immediately. At the time of writing, Pss of *H. influenzae* was the only crystal structure available in the database. However, both phylogenetic analysis and protein sequence alignment divulged the high degree of dissimilarity between the proteins of *H. influenzae* and the actinobacteria, *S. coelicolor* and *M. tuberculosis* rendering the crystal structure useless in our hope to carry out a parallel analysis based on the ligand binding moieties of Pss *H. influenzae*.

The use of SOSUI Classification and Secondary Structure Prediction of Membrane Proteins software (Hirokawa, 1998) revealed 7 transmembrane helices for Pss of *S. coelicolor* with the C-terminal found on the cytoplasmic side (Figure 16) whereas *S. coelicolor* Psd was predicted to be a soluble protein hence with no transmembrane domain.

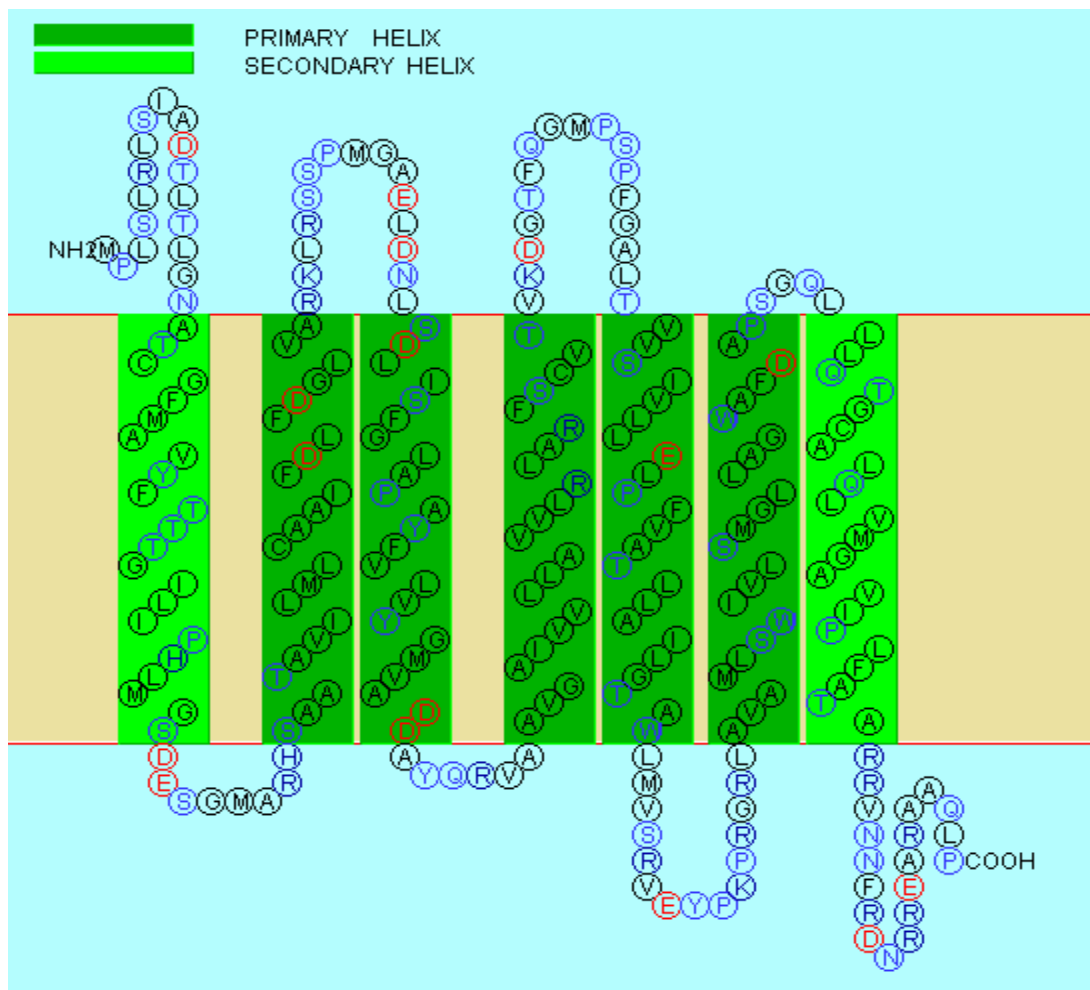


Figure 16: SOSUI prediction of topological organisation of membrane spanning domains of Pss in *S. coelicolor*. The membrane-bound protein has 7 membrane-spanning domains with the N-terminal found in the extracellular side whereas C-terminal in the intracellular leaflet.

#### 4.4 Discussion and conclusion

Psd in its native form is an inactive proenzyme made up of the  $\alpha$  and  $\beta$  subunits linked by the putative LGST motif in human, yeast and *E. coli* and perhaps the FGSR motif within the highly conserved GLIRXGSRXD sequence in *S. coelicolor* and *M. tuberculosis*. These putative motifs were proposed to be involved in pyruvoyl prosthetic group formation and endoproteolysis (Trotter *et al.*, 1993). Liberation of the functional  $\alpha$  chain involved in the decarboxylation of PS occurred through the cleavage of the amide bond between Gly and Ser residues (Voelker, 1997). The proposed catalytic mechanism is described in the discussion section of Chapter 7. The absence of the eukaryotic substrate recognition domain, FxFxLKxxxKxR in the prokaryotic proteins implicates the difference in substrate affinity of this enzyme between the two groups which gives further credence to our drug discovery endeavour. Although this protein was predicted to be a soluble entity within *S. coelicolor*, it is believed to be associated to the cell membrane for its catalytic purpose in a similar way observed in mycobacteria (Morita *et al.*, 2005).

In Pss, the conserved region, Dx<sub>2</sub>DGx<sub>9</sub>(S/T)x<sub>2</sub>Gx<sub>3</sub>Dx<sub>3</sub>D containing the quadruple aspartic acid residues involved in the catalytic activity of this enzyme (Saha *et al.*, 1996b; Jackson *et al.*, 2000; Karnezis *et al.*, 2002) is located near the N-terminal end of the mycobacterial and streptomycetes proteins. The low degree of conservation of this motif in human and mouse proteins implicates the difference in substrate and catalytic mechanism between the mammalian and prokaryotic enzymes which concurred with previous findings (Kuge, *et al.*, 1986; Kuge, *et al.*, 1997). Nonetheless, little is known about the ligand binding properties of Pss in both prokaryotes and eukaryotes. Finally, the membrane-spanning characteristic of *S. coelicolor* Pss permitted the use of enhanced green fluorescence protein reporter system (C-terminal end tagging) to visualize the cellular localization of this protein (Chapter 6).

Although the phylogenetic tree showed the low degree of genetic relationship between Pss of both *Mycobacteria* and *Streptomyces* genera, protein sequence

alignment showed Psd and Pss of both *S. coelicolor* and *M. tuberculosis* to be highly conserved near the catalytic domains. This substantiated the use of *S. coelicolor* as model for analogous studies of *M. tuberculosis* for the purpose of designing novel classes of anti-TB drugs targeting the phospholipid biosynthesis pathway. The prokaryotic Psd and Pss are generally different from their eukaryotic counterparts with the latter being larger proteins. The proposed conserved catalytic and/or substrate recognition motifs in *S. coelicolor* and *M. tuberculosis* proteins are also grossly different or absent in the eukaryotes as described previously. Hence, the dissimilarity between the mammalian and the prokaryotic proteins would be exploited to our advantage where the potential inhibitors could be optimized to specifically target the proteins within both *S. coelicolor* and *M. tuberculosis* with little toxicity to host cells.

Trimethoprim which is commonly used in treatment of urinary tract infection is one good example of an antibiotic that targets a protein which is present in both human and prokaryotic cells. However, due to structural differences, the inhibitory action of trimethoprim on *E.coli* dihydrofolate reductase is 1,000 times higher compared to human enzyme (Katzung, 2004) hence does not incur significant toxicity to human cells. The basis of this project is to emulate such a successful example.

**5.0 Results**  
**Disruption of *psd* and *pss* in *S. coelicolor***



## 5.0 Disruption of *psd* and *pss* in *S. coelicolor*

### 5.1 Introduction

Recombinant DNA technology is a collection of indispensable tools which are already contributing substantially to molecular biology research, medicine, industry, agriculture and possibly more fields in the near future. In the context of microbial genetic engineering, two commonly used methods in *S. coelicolor* are transposon and PCR-mediated mutagenesis. Transposon-mediated gene disruption is a form of insertional mutagenesis where transposon cassettes are introduced via homologous recombination into the middle of the coding sequences of genes. The presence of stop codons or termination sequences will result in gene inactivation due to translational and transcriptional block (Prescot 2005). This forms the basis of this project where a minitransposon Tn5062 derived from the 'cut and paste' transposon Tn5 (Herron *et al.*, 2004) was used in the attempt to disrupt both *psd* and *pss* in order to elucidate their functions by demonstrating the connection of the mutant phenotypes to the gene lesion.

PCR-directed mutagenesis (Gust *et al.*, 2003) is another useful alternative for engineering a gene lesion at a defined site of bacterial genome. It shares a similar homologous recombination concept to transposon insertional inactivation. Its general advantage over transposon-directed mutagenesis is its ability to circumvent the polar effects incurred by the stop codon within transposon cassette hence does not affect the transcription of the downstream gene in an operon. Therefore, any phenotypic consequences of the disruption can be safely attributed to the loss of the target gene function.

Initially, transposon mediated mutagenesis was attempted to gauge the essentiality of these genes in *S. coelicolor*. To demonstrate the connection between the mutant phenotypes and the gene lesion, complementing vectors containing *psd/pss* were constructed and introduced into the bacterial genome pre- or post- gene disruption depending on the essentiality of the genes. The ability to disrupt the

parenteral gene only in the presence of a second copy of the gene introduced into the ectopic site of the bacterial genome may suggest the essential nature of the target gene hence validating the gene product as potential drug target. Finally, construction of similar mutants was attempted using PCR-directed mutagenesis.

## **5.2 Transposon, Tn5062 inactivation of *psd* and *pss* in *S. coelicolor***

Bioinformatic analysis suggested that (*SCO6468; psd*) and (*SCO6467; pss*) encode the putative phospholipid biosynthesis enzymes, Psd and Pss responsible for the physiological production of PE and PS respectively. A genetic approach was undertaken to investigate their functions in *S. coelicolor* and disruption of individual gene was attempted using cosmids containing fragments of *S. coelicolor* genome (Redenbach *et al.*, 1996) which were mutagenised by random insertion of the Tn5 - based transposon, Tn5062 obtained from the *S. coelicolor* transposon insertion library of University of Wales, Swansea (Bishop *et al.*, 2004).

The mutagenised cosmids (H05 and C03) as well as transposon insertion sites for *psd* and *pss* are shown in Figure 17. H05 and C03 were transferred individually into *S. coelicolor* M145 via intergeneric conjugation by co-culturing *E. coli* ET12567/pUZ8002 + individual cosmid with *S. coelicolor* M145 on MS agar. Exconjugants (1000 colonies) were then patched onto two replica MS agar plates with either 50 µg/ml of kanamycin or apramycin to screen for potential double crossover exconjugants *apra*<sup>r</sup>, *km*<sup>s</sup> which had undergone the allelic replacement (*pss*::Tn5062). For both *psd* and *pss*, the selection for a Tn5062 insertion only gave rise to single crossover exconjugants *apra*<sup>r</sup>, *km*<sup>r</sup> designated TJL101(M145::C03) and LSM101 (M145::H05) respectively (Figure 18) throughout the entire screening process despite repeating the conjugation several times.

Single crossover indicated that the entire Tn5062 containing cosmid was integrated into the *S. coelicolor* genome via single homologous recombination event thus retaining an intact copy of the gene of interest (one disrupted copy from the

mutagenised cosmid and one parenteral copy of the gene). The inability to obtain double crossover exconjugant suggests that either the allelic exchange could not take place easily or both *psd* and *pss* are essential for the viability of *S. coelicolor* which reinforced the belief of these proteins being good drug targets. Therefore, the transposon inactivation experiment was repeated in the presence of a second copy of the gene of interest in an ectopic site of *S. coelicolor* genome.

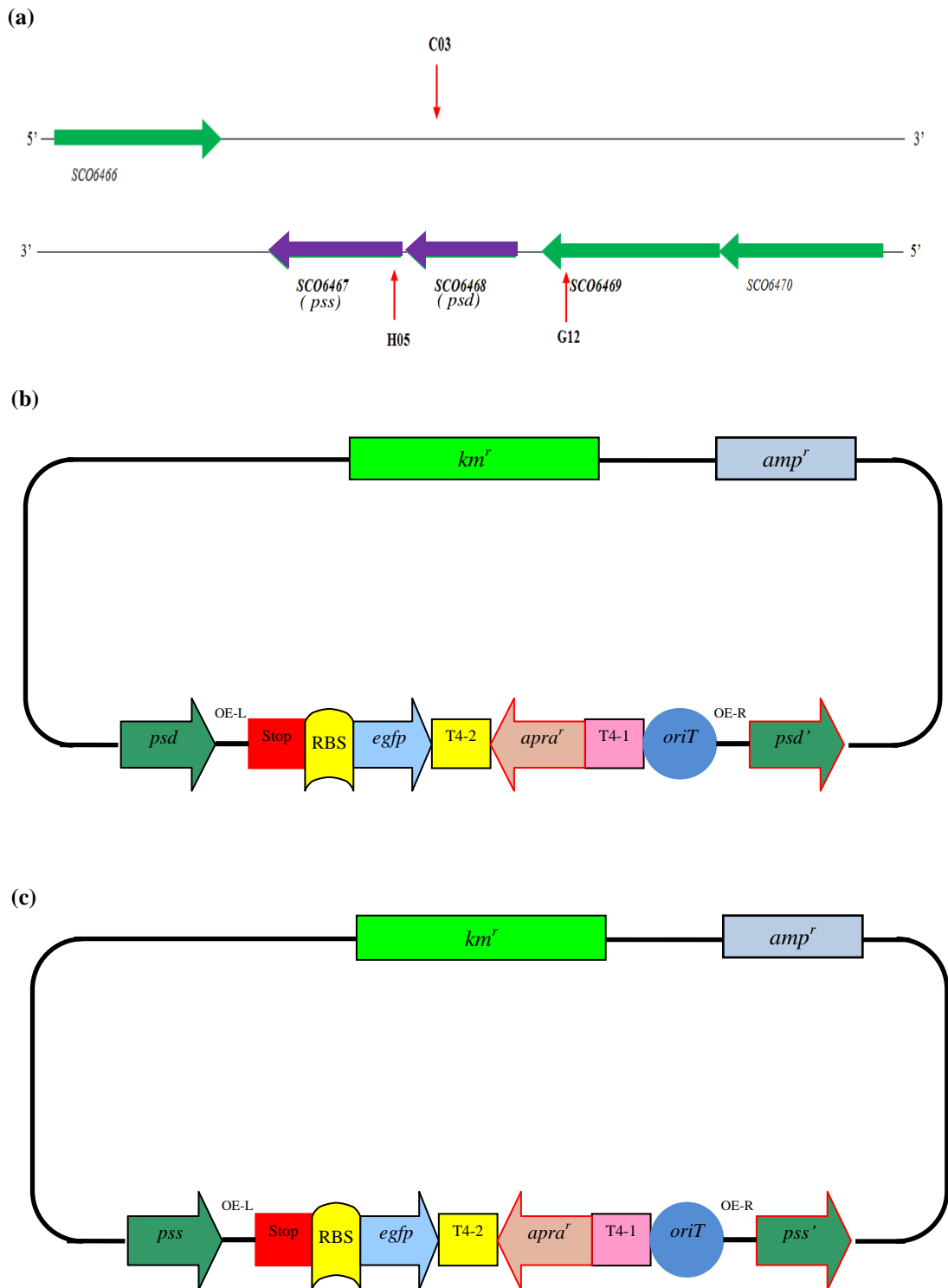


Figure 17: (a) Genome positions of *SCO6467* (*pss*) and *SCO6468* (*psd*) with transposon insertion sites and the upstream and downstream genes flanking them. (b) Mutagenised cosmid C03. (c) Mutagenised cosmid H05.

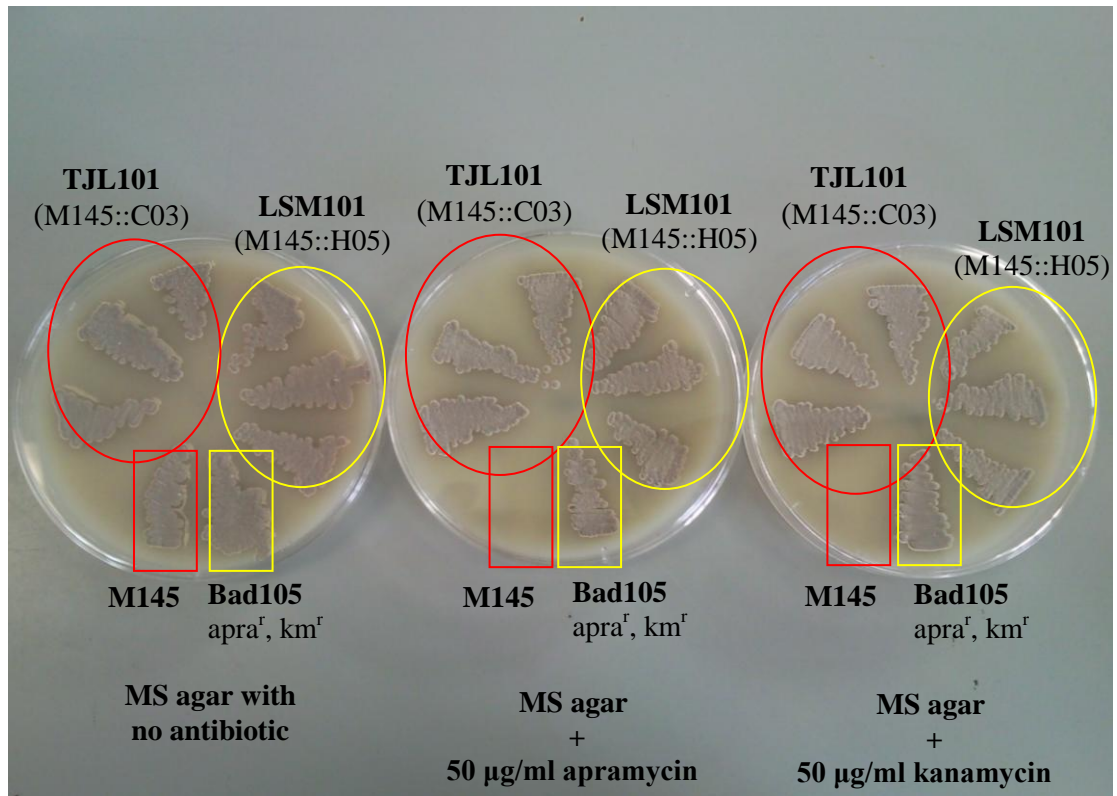


Figure 18: Single crossover exconjugants LSM101 and TJJ101 obtained from single homologous recombination event between *S. coelicolor* M145 genome with inactivation vector H05 and C03 respectively. **Red rectangle:** M145; **Yellow rectangle:** Bad105 apra<sup>r</sup>, km<sup>r</sup> as positive control (Rajaghopal & Herron unpublished); **Red Oval:** TJJ101; **Yellow Oval:** LSM101.

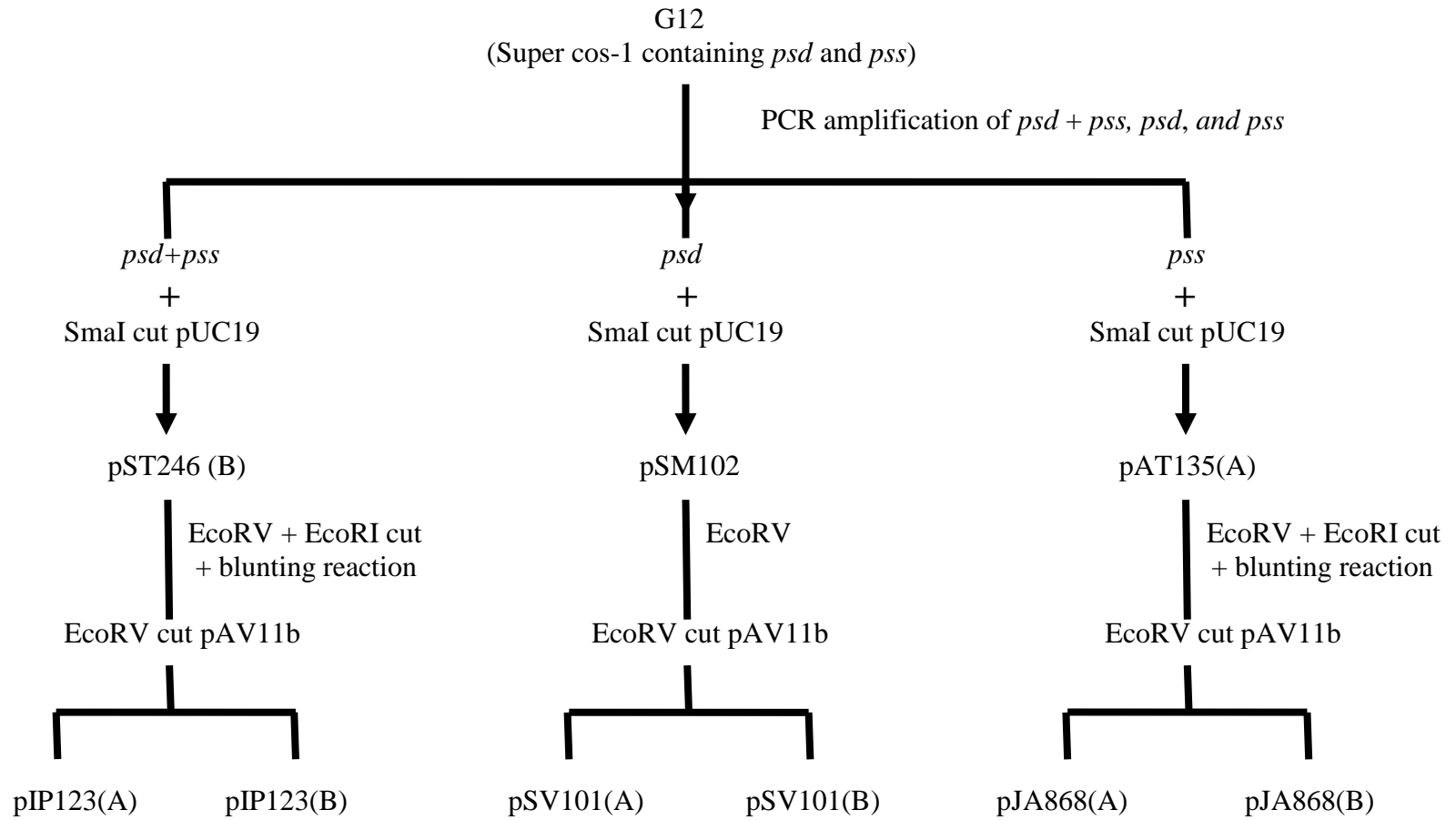


Figure 19: Cloning of *psd* and *pss* into  $\Phi$ BT1 based integrating vectors, pAV11b

### 5.3 Cloning of *psd* and *pss* into $\Phi$ BT1 based integrating vector, pAV11b

If both *psd* and *pss* are indeed essential genes, disruption of the parenteral copy of the gene could only be achieved after gene complementation. Therefore, relevant complementation vectors must be constructed. The general subcloning strategy of *psd* and *pss* into the  $\Phi$ BT1 *attP-int* locus derived integrative vector pAV11b (Khaleel *et al.*, 2011) is shown in Figure 19. Parenteral cosmid G12 was used as template for PCR amplification of *psd* and *pss* without their native promoters using combination of primers shown in Figure 20. The PCR amplification utilized high fidelity Accuzyme™ Mix DNA Polymerase (Bioline) which possesses the proofreading property to prevent possible point mutation. The blunt-ended PCR products were cloned into the SmaI site in the multiple cloning site (MCS) of pUC19 (Yanisch-Perron *et al.*, 1985) located in the middle of the open reading frame (ORF) of  $\beta$ -galactosidase, *lacZa* gene which permitted blue-white colony selection. Recombinant plasmids were then extracted and confirmed via restriction digests and gel electrophoresis.

Cloning of *psd*, *pss* and *psd+pss* into pUC19 resulted in recombinant plasmids, pSM102, pAT135(A) and pST246(B) respectively (data not shown). A series of restriction enzymes digests revealed that one of the EcoRV sites engineered onto *pss* fragment was either missing or mutated. The *psd* fragment from pSM102 was extracted via EcoRV digest whereas *pss* and *psd + pss* fragment from pAT135(A) and pST246(B) respectively were cut out using EcoRV + EcoRI double digests. Blunting reaction using Klenow fragment (Promega) was carried out prior to further subcloning into EcoRV site of pAV11b.

Such blunt-end ligation resulted in recombinant plasmids with two possible insert orientations (sense and antisense) relative to the *tcp830* promoter of the integrative vector. Cloning of *psd*, *pss* and *psd+pss* into pAV11b yielded pSV101(A) & pSV101(B) (Figure 23 & 24), pJA868(A) & pJA868(B) (Figure 21 & 22) and pIP123(A) & pIP123(B) (Figure 25 & 26) respectively with suffix (A) and (B) denoting the sense and antisense orientations of the inserts. Sequencing of these

recombinant plasmids confirmed that one of the EcoRV sites engineered onto *pss* fragment was indeed missing.

pSV101(A), pJA868(A) and pIP123(A) were then used for gene complementation in the *attB*  $\Phi$ BT1 of *S. coelicolor* (Rodriguez-Garcia *et al.*, 2005). In the case of these pAV11b derived recombinant plasmids, transcriptional control of their gene inserts was achieved via the atc inducible promoter *tcp830*. Suppression of *psd* and *pss* functions could also be achieved by complementing *S. coelicolor* genome with pSV101(B), pJA868(B) or pIP123(B) for RNA interference experiment.



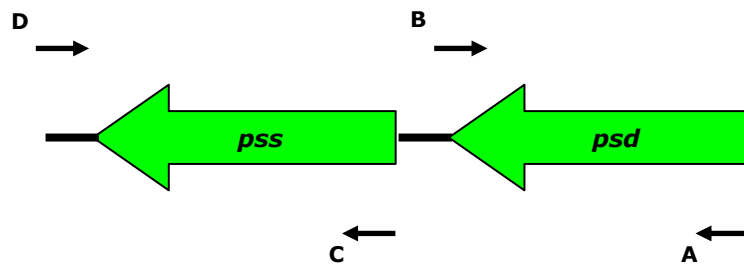
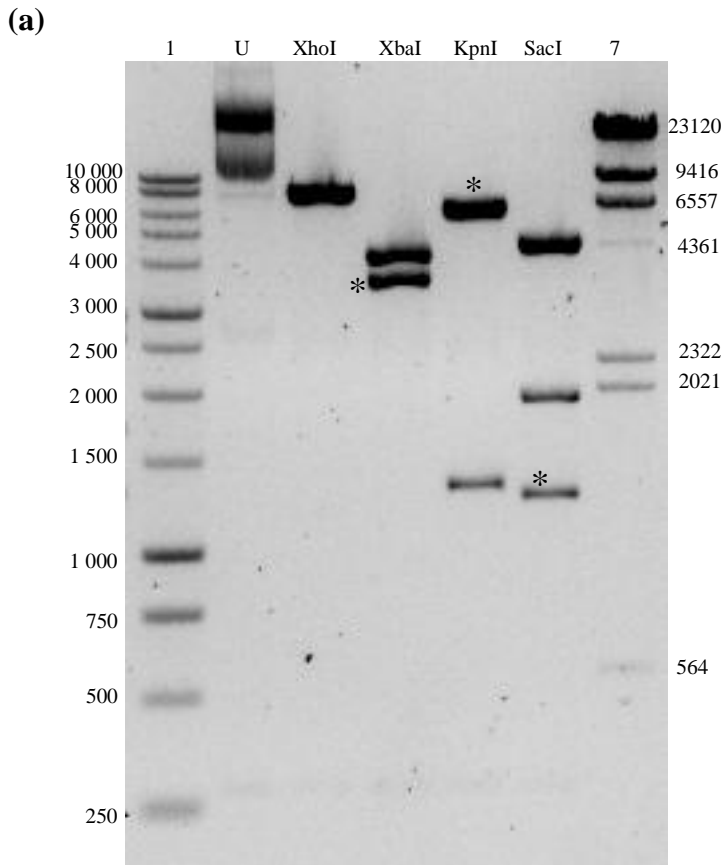


Figure 20: Primers used in PCR amplification of *psd* and *pss* for cloning into integrative vector pAV11b. The sequences of the primers are shown in Table 15, Section 3.22.



**(b)**

Restriction enzymes	Fragment sizes produced by pJA868(A) (bp)
Undigested (U)	8092
XhoI (Lane 3)	8092
XbaI (Lane 4)	4479, 3613*
KpnI (Lane 5)	6774*, 1318
SacI (Lane 6)	4886, 1947, 1259*

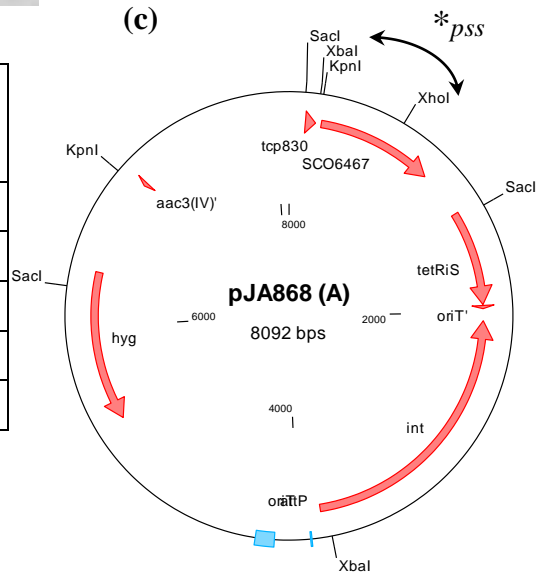
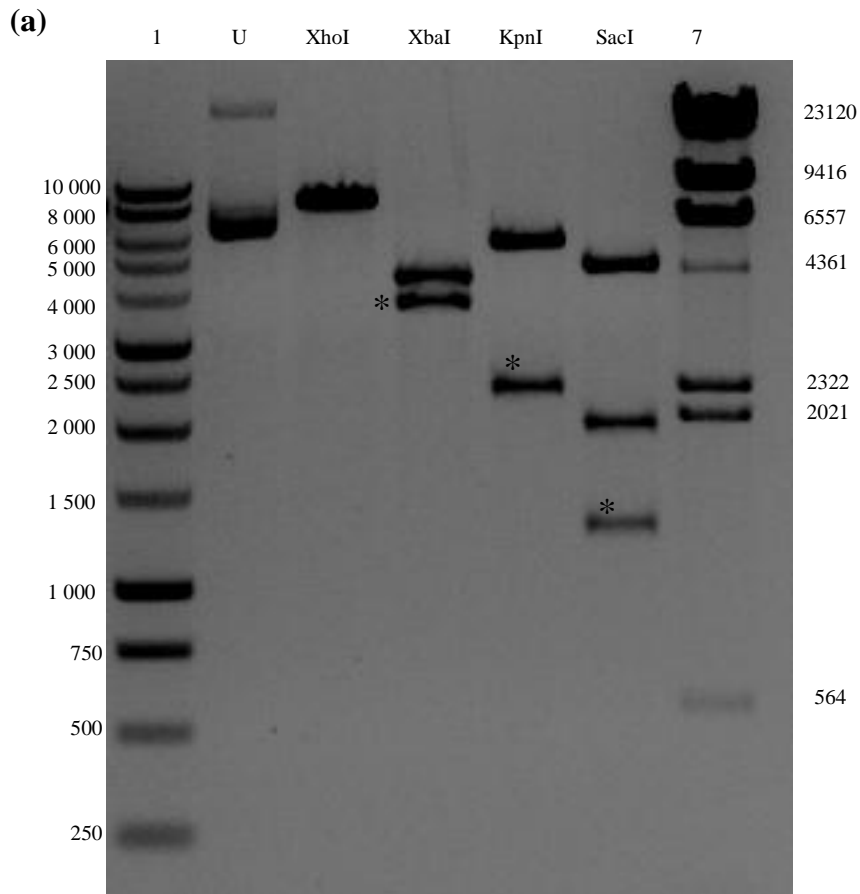


Figure 21: Electrophoresis gel of pJA868 (A) (subcloning of *pss* (*SCO6467*) from pAT135 (A) into pAV11b), map of the recombinant plasmid as well as the fragment sizes when digested with XhoI, XbaI, KpnI and SacI. **(a)** Lane 1 & 7: 1kb DNA ladder (Promega) and  $\lambda$  HindIII DNA ladder respectively; Lane 2: undigested plasmid; Lane 3: XhoI digest; Lane 4: XbaI digest; Lane 5: KpnI digest; Lane 6: SacI digest **(b)** Fragments produced by different restriction enzymes. **(c)** The map of pJA868(A) with *pss* in the sense orientation relative to *tcp830* promoter of pAV11b. The (\*) sign indicates the diagnostic band containing *pss*.



**(b)**

Restriction enzymes	Fragment sizes produced by pJA868 (B) (bp)
Undigested (U)	8092
XhoI (Lane 3)	8092
XbaI (Lane 4)	4479, 3613*
KpnI (Lane 5)	5791, 2301*
SacI (Lane 6)	4886, 1947, 1259*

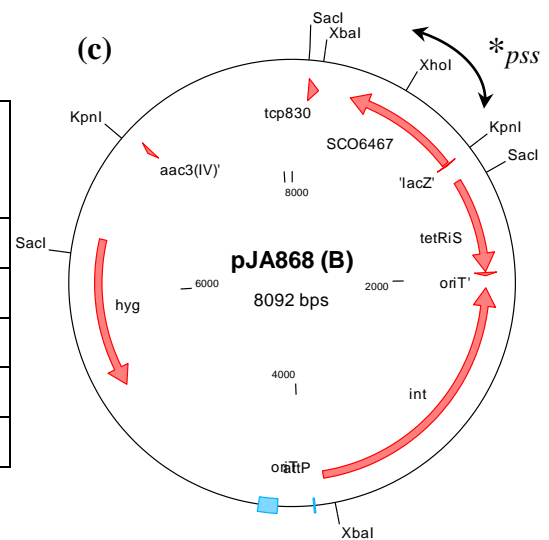
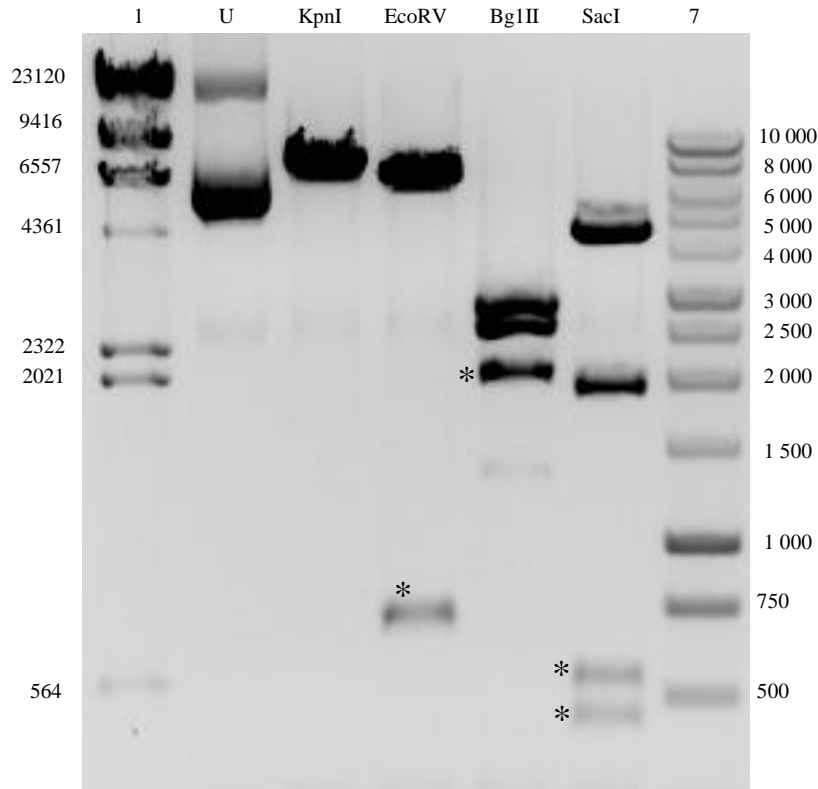


Figure 22: Electrophoresis gel of pJA868 (B) (subcloning of *pss* (*SCO6467*) from pAT135 (A) into pAV11b), map of the recombinant plasmid as well as the fragment sizes when digested with XhoI, XbaI, KpnI and SacI. **(a)** Lane 1 & 7: 1kb DNA ladder (Promega) and  $\lambda$  HindIII DNA ladder respectively ; Lane 2: undigested plasmid; Lane 3: XhoI digest; Lane 4: XbaI digest; Lane 5: KpnI digest; Lane 6: SacI digest **(b)** Fragments produced by different restriction enzymes. **(c)** The map of pJA868 (B) with *pss* in the antisense orientation relative to *tcp830* promoter of pAV11b. The (\*) sign indicates the diagnostic band containing *pss*.

(a)



(b)

Restriction enzymes	Fragment sizes produced by pSV101 (A) (bp)
Undigested (U)	7828
KpnI (Lane 3)	7828
EcoRV (Lane 4)	7097, 731*
BglIII (Lane 5)	3143, 2623, 2062*
SacI (Lane 6)	4886, 1947, 544*, 451*

(c)

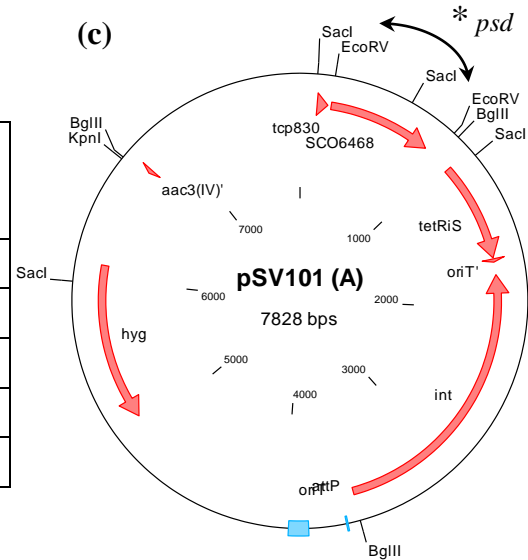


Figure 23: Electrophoresis gel of pSV101(A) (subcloning of *psd* (SCO6468) from pSM102 into pAV11b), map of the recombinant plasmid as well as the fragment sizes when digested with KpnI, EcoRV, BglIII and SacI. (a) Lane 1 & 7:  $\lambda$  HindIII DNA ladder and 1kb DNA ladder (Promega) respectively; Lane 2: undigested plasmid; Lane 3: KpnI digest; Lane 4: EcoRV digest; Lane 5: BglIII digest; Lane 6: SacI digest (b) Fragments produced by different restriction enzymes. (c) The map of pSV101(A) with *psd* in the sense orientation relative to *tcp830* promoter of pAV11b. The (\*) sign indicates the diagnostic band containing *psd*.

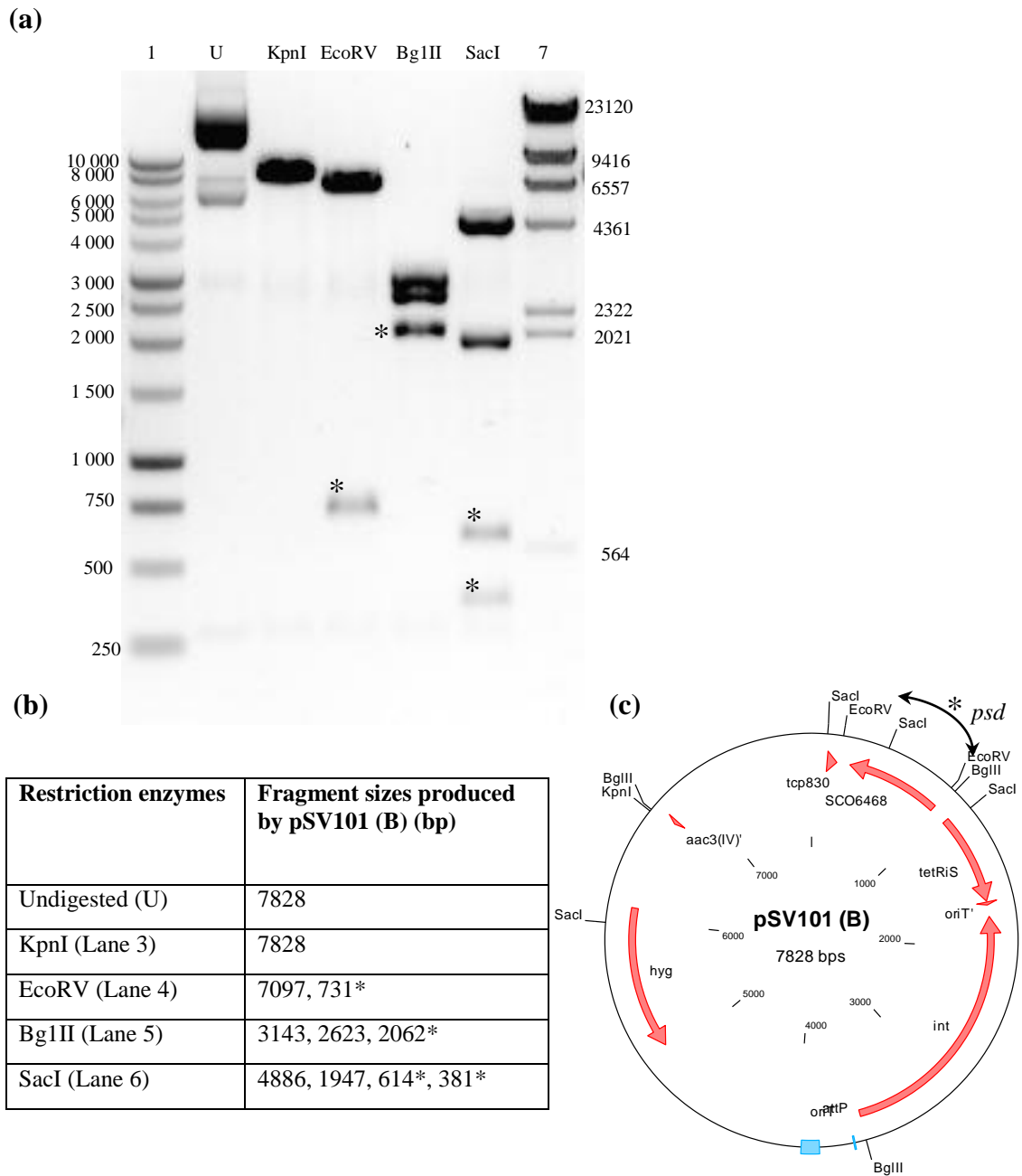


Figure 24: Electrophoresis gel of pSV101(B) (subcloning of *psd* (SCO6468) from pSM102 into pAV11b), map of the recombinant plasmid as well as the fragment sizes when digested with KpnI, EcoRV, BglII and SacI. **(a)** Lane 1 & 7: 1kb DNA ladder (promega) and  $\lambda$  HindIII DNA ladder respectively; Lane 2: undigested plasmid; Lane 3: KpnI digest; Lane 4: EcoRV digest; Lane 5: BglII digest; Lane 6: SacI digest **(b)** Fragments produced by different restriction enzymes. **(c)** The map of pSV101(B) with *psd* in the antisense orientation relative to *tcp830* promoter of pAV11b. The (\*) sign indicates the diagnostic band containing *psd*.

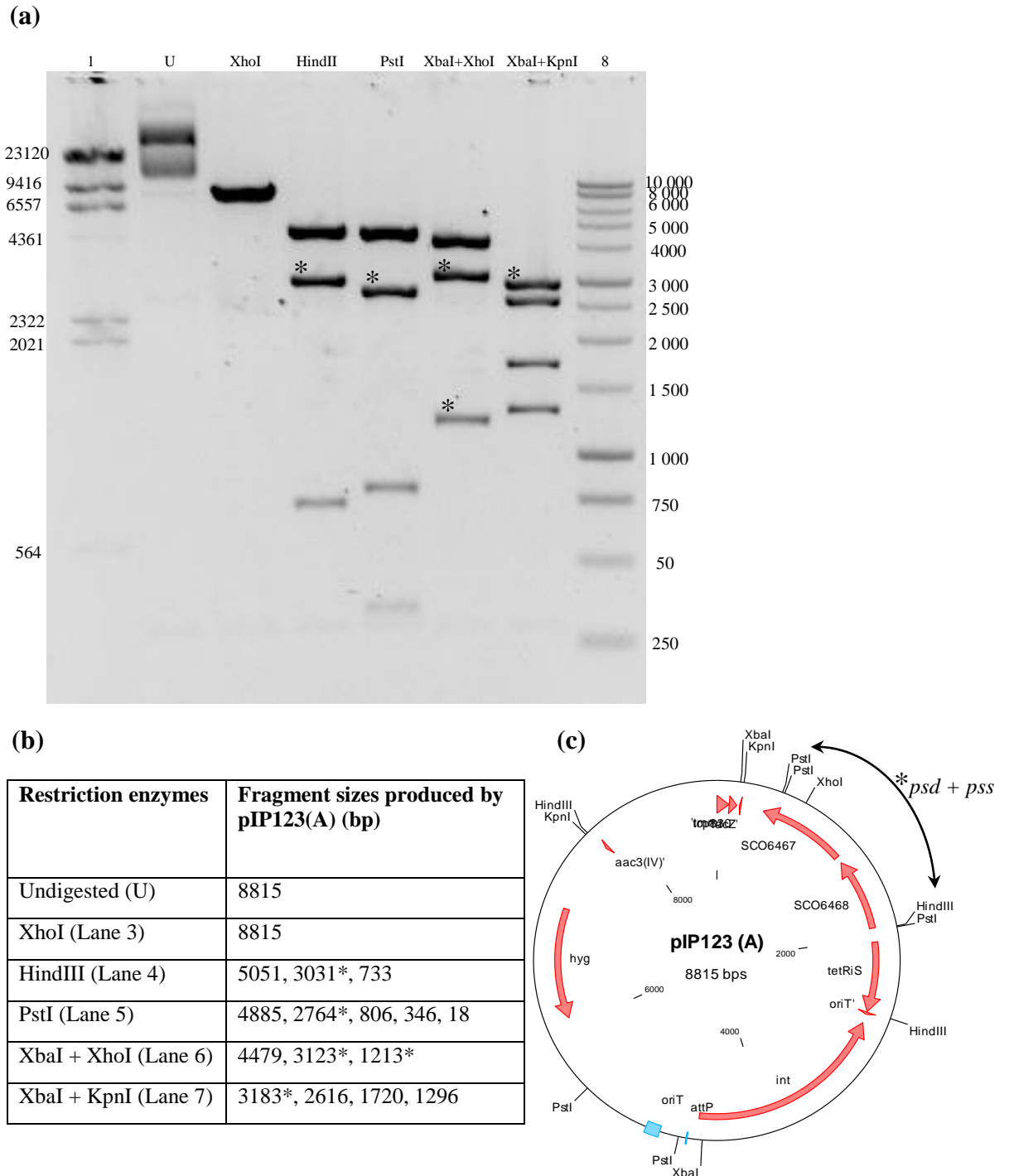


Figure 25: Electrophoresis gel of pIP123(A) (subcloning of *psd+psS* (*SCO6468+SCO6467*) from pST246(B) into pAV11b), map of the recombinant plasmid as well as the fragment sizes when digested with XhoI, HindIII, PstI, XbaI + XhoI and XbaI + KpnI. **(a)** Lane 1 & 8:  $\lambda$  HindIII DNA ladder and 1kb DNA ladder (Promega) respectively; Lane 2: undigested plasmid; Lane 3: XhoI digest; Lane 4: HindIII digest; Lane 5: PstI digest; Lane 6: XbaI + XhoI double - digests; Lane 7: XbaI + KpnI double-digests **(b)** Fragments produced by different restriction enzymes. **(c)** The map of pIP123 (A) with *psd+psS* in the sense orientation relative to *tcp30* promoter of pAV11b. The (\*) sign indicates the diagnostic band containing *psd* and *psS*.

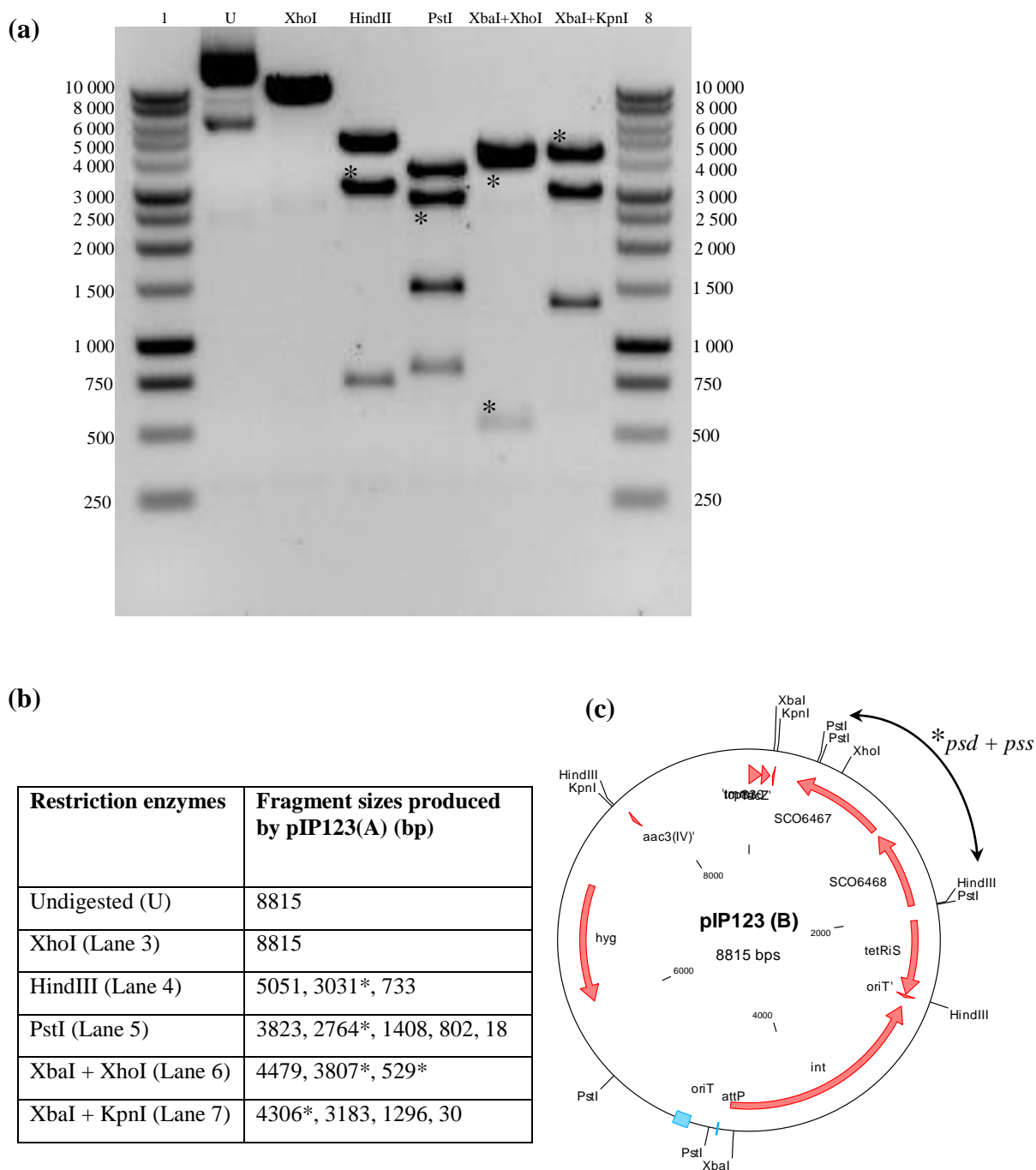


Figure 26: Electrophoresis gel of pIP123(B) (subcloning of *psd+ps* (*SCO6468+SCO6467*) from pST246(B) into pAV11b), map of the recombinant plasmid as well as the fragment sizes when digested with XhoI, HindIII, PstI, XbaI + XhoI and XbaI + KpnI. **(a)** Lane 1 & 8:  $\lambda$  HindIII DNA ladder and 1kb DNA ladder (promega) respectively; Lane 2: undigested plasmid; Lane 3: XhoI digest; Lane 4: HindIII digest; Lane 5: PstI digest; Lane 6: XbaI + XhoI double - digests; Lane 7: XbaI + KpnI double-digests **(b)** Fragments produced by different restriction enzymes. **(c)** The map of pIP123 (B) with *psd+ps* in the antisense orientation relative to *tcp830* promoter of pAV11b. The (\*) sign indicates the diagnostic band containing *psd* and *ps*.

#### 5.4 Transposon inactivation of *psd* and *pss* post-complementation

The complementing vectors pJA868 (A), pSV101 (A) and pIP123 (A) were transformed individually into *E.coli* ET12567/pUZ8002 prior to conjugal transfer into the wild type *S. coelicolor* M145. Ectopic integration of these plasmids into  $\Phi$ BT1 *attB* site located within *SCO4848* (Gregory *et al.*, 2003) introduced an extra copy of *psd/pss* under the transcriptional control of *tcp830* into the genome of *S. coelicolor*. This not only led to the possibility of post-complementation disruption of *psd* and *pss* but, in the event of successful gene disruption, allowed the demonstration of the connection between the genetic lesion and the mutant phenotypes via *tcp830* regulated transcriptional control which is an important tool for elucidation of gene function.

A single colony of each strain of the  $\text{hyg}^r$  complemented mutant was picked and streaked onto MS agar containing hygromycin and subsequently used for making a spore suspension. This was later used for further conjugation with *E. coli* ET12567/pUZ8002 containing the appropriate mutagenised cosmids (C03 or H05). 1000 exconjugants were then patched onto two replica MS agar plates with 100 ng/ml of *atc* + 50  $\mu\text{g/ml}$  hygromycin + 50  $\mu\text{g/ml}$  kanamycin or apramycin to screen for possible double crossover exconjugant  $\text{apra}^r$ ,  $\text{km}^s$  which had undergone the allelic replacement. Despite numerous attempts, only one double crossover exconjugant (LSM105: *pss*<sup>-</sup>/*tcp830*-*pss*<sup>+</sup>) which had potentially undergone replacement of parenteral *pss* with the transposon cassette (*pss*::Tn5062) was observed (Figure 27). We are still uncertain of the reason behind the failed attempt to disrupt *psd* even after gene complementation. Numerous hypotheses put forward include the incompatible ribosomal binding site of the synthetic promoter used (Rodriguez-Garcia 2005), mismatched transcriptional control by the synthetic promoter compared to the native promoter (Bateman *et al.*, 2011), aberrant gene expression out of its native locus or the polar effect incurred by the transposon-mediated inactivation of *psd* which is possibly co-transcribed with the downstream *pss*. Nevertheless, the inability to disrupt *psd* and the success of *pss* inactivation only after complementation further implied the essential nature of these genes to the viability of *S. coelicolor*.



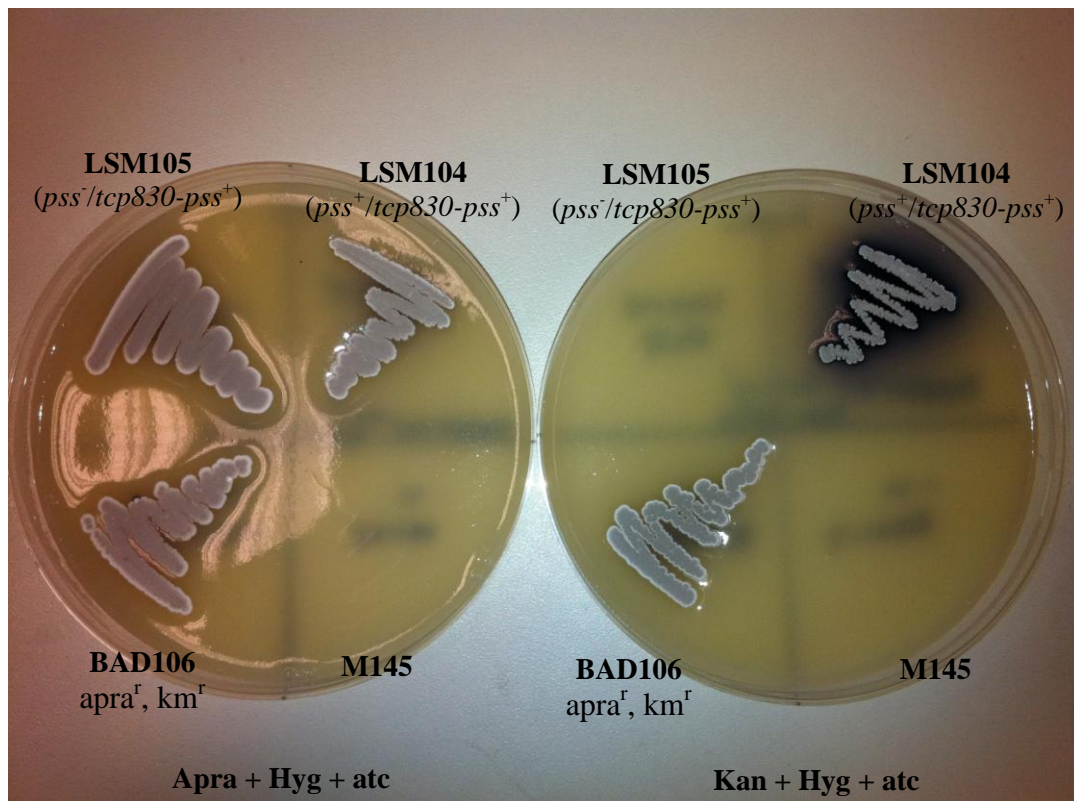


Figure 27: Single crossover exconjugant, LSM104 ( $pss^+/tcp830-pss^+$ ) and double crossover exconjugant, LSM105 ( $pss^-/tcp830-pss^+$ ) obtained from homologous recombination of *S. coelicolor* M145 genome with inactivation vector H05 post complementation with pJA868(A) (pAV11b + *pss*). **BAD106**  $apra^+$ ,  $km^+$ ,  $hyg^+$  (Rajagopal & Herron unpublished); **M145** no resistance gene; **LSM104**  $apra^+$ ,  $km^+$ ,  $hyg^+$ ; **LSM105**  $apra^+$ ,  $km^s$ ,  $hyg^+$ .

## 5.5 Controlled-expression of *pss* in LSM105 (*pss*::Tn5062/*tcp830-pss*<sup>+</sup>)

In addition to being used as an integrative vehicle, pAV11b contains the *atc* inducible promoter, *tcp830* that can regulate the expression of gene insert over a range of *atc* concentrations. The synthetic promoter was constructed (Rodriguez-Garcia *et al.*, 2005) by combining the -35 and -10 regions of *ermEp1* promoter (Bibb *et al.*, 1985) with the tetracycline repressor/operator (*tetR/tetO*) regulatable system from the *E.coli* transposon Tn10.

Repression of this promoter is achieved by the expression of the modified *tetR* gene, *tetRiS* that encodes a repressor protein that has high affinity for the *tet* operator ( $K_a$  of  $10^{11} \text{ M}^{-1}$ ). Extra repression is also provided by *S. coelicolor* innate gene *SCO0253* that encodes a similar repressor protein. In the presence of optimal concentration of *atc* for induction (100 to 1000ng/mL), the affinity of the protein for *tetO* is reduced by several orders of magnitude resulting in high level of de-repression with minimal pleiotropic effects (Rodriguez-Garcia *et al.*, 2005).

Regulated expression of the complemented copy of *pss* in the double crossover exconjugant was carried out by growing LSM105 (*pss*::Tn5062/*tcp830-pss*<sup>+</sup>) on 3MA over a concentration gradient of *atc* (0 to 100 ng/ml) using RJ118b ( $\Delta$ *clsA/tcp830-clsA*<sup>+</sup>); (Jyothikumar *et al.*, 2012) as a positive control (Figure 28). The consistent growth of LSM105 over the concentration gradient of inducer showed the absence of transcriptional control by *tcp830* promoter. The experiment was repeated with a second colony of LSM105 obtained from new batch of patching experiment which also exhibited consistent growth over the concentration gradient of *atc*. Sequencing of pJA868(A) showed that both *tcp830* promoter and *pss* were intact (data not shown). We managed to verify the constitutive nature of gene expression by *tcp830* promoter (independent of *atc* concentration) via RT-PCR (described in 5.6). To address this problem, cloning of these genes into another integrative vector with different inducible promoter was carried out.

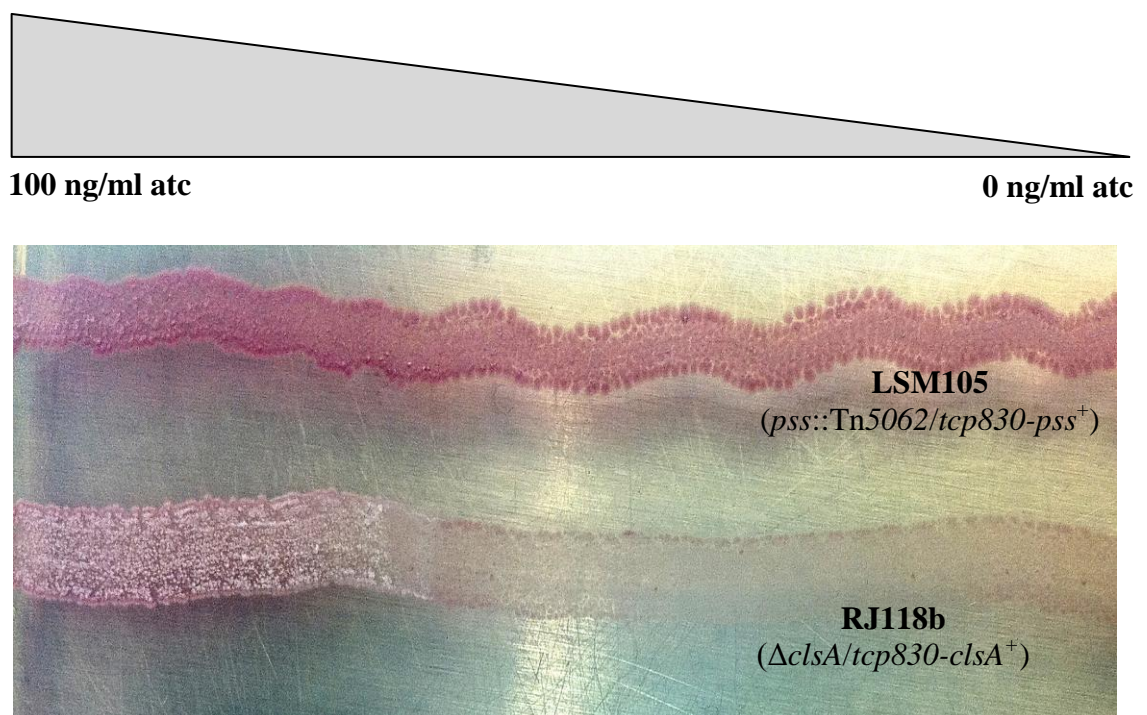


Figure 28: Controlled-expression of *pss* by *tcp830* in LSM105 (*(pss::Tn5062/tcp830-pss<sup>+</sup>)*) over a concentration gradient of *atc* using RJ118b ( $\Delta$ *clsA/tcp830-clsA<sup>+</sup>*); (Jyothikumar *et al.*, 2012) as a positive control. The mutant grew consistently over the concentration gradient implicating the loss of artificial transcriptional control by *tcp830* promoter.

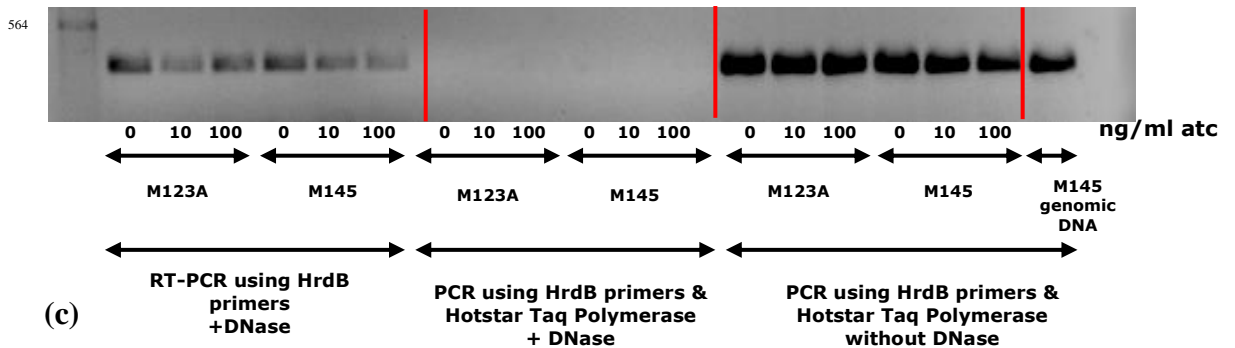
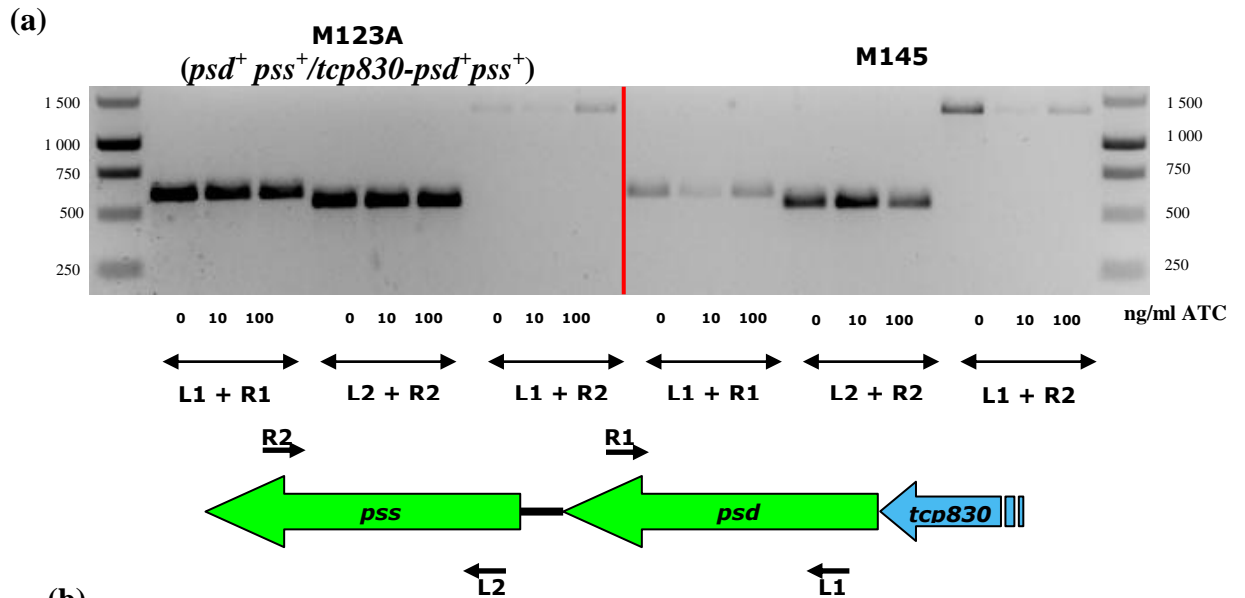
## 5.6 RT-PCR profile of M123A ( $psd^+ pss^+/tcp830-psd^+pss^+$ ) to verify the nature of gene transcription by $tcp830$ promoter

The consistent growth of LSM105 ( $pss::Tn5062/tcp830-pss^+$ ) over the concentration gradient of atc (0 to 100 ng/ml) described in 5.5 suggested the atc-independent expression of  $pss$  from the  $tcp830$  promoter. Therefore, we decided to verify this via RT-PCR analysis. The  $psd$  and  $pss$  diploids strain, M123A was constructed by delivering pIP123A ( $tcp830-psd^+pss^+$ ) into the  $\Phi$ BT1  $attB$  site of *S. coelicolor* M145 via intergeneric conjugation. The strain was then grown in YEME containing 0, 10 and 100 ng/ml of atc for 24 hours before RNA extraction. All RNA samples were normalized at 100 ng prior to amplification assay.

To gauge the transcriptional activity of  $tcp830$ , RT-PCR analysis was conducted with four primers (Figure 29(a)). Reverse transcription of  $hrdB$  encoding the constitutively-expressed principal sigma factor (Buttner *et al.*, 1990; Kang *et al.*, 1997) was used as an internal control to assess the quality of the RNA and to validate the RT-PCR assay semi-quantitatively (Figure 29(b)). A Hotstar Taq polymerase-mediated PCR assay was also conducted using  $hrdB$  primers on all the RNA samples and M145 genomic DNA in the absence and presence of RNase-free Dnase. This served as a validation control to prove that the end product obtained from the RT-PCR experiment was the reverse transcription-generated cDNA rather than the amplicon of amplified DNA contaminants which would be degraded by the Dnase as shown by the Hotstart Taq + Dnase PCR assay.

Ethidium bromide stained cDNA bands on the agarose gel were measured by densitometry using Genetools software package (Syngene) for the purpose of  $cDNA_{gene}/cDNA_{control}$  ratio calculation which served as a relative quantitative measurement for the gene transcription activity (Figure 29(c)). The calculated ratios remained fairly constant over the increasing concentration of atc indicating the inducer-independent expression of  $psd$  and  $pss$  by  $tcp830$ . This confirmed our speculation of the constitutive nature of transcription by the synthetic promoter which was rather surprising. Co-transcription of  $psd$  and  $pss$  was also observed with the generation of 1.4kb band using the combination of L1 and R2 primers. The

observation revealed that genetic polarity may indeed be an issue when it comes to transposon-mediated disruption of *psd* which is located upstream of the co-regulated *pss* within the operon i.e. the presence of a stop codon in the transposon cassette may prevent the transcription of the downstream *pss* in the operon (discussed further in discussion section). An alternative gene disruption method had to be used.



ATC concentration (ng/ml)	M123A <sub><i>psd</i></sub> /M123A <sub><i>hrdB</i></sub>	M123A <sub><i>pss</i></sub> /M123A <sub><i>hrdB</i></sub>	M123A <sub><i>psd-pss</i></sub> /M123A <sub><i>hrdB</i></sub>
0	1.30	1.29	0.48
10	1.54	1.58	0.55
100	1.27	1.35	0.53

ATC concentration (ng/ml)	M123A <sub><i>psd</i></sub> /M145 <sub>0 atc</sub>	M123A <sub><i>pss</i></sub> /M145 <sub>0 atc</sub>	M123A <sub><i>psd-pss</i></sub> /M145 <sub>0 atc</sub>
0	2.08	1.37	0.82
10	1.98	1.35	0.75
100	1.88	1.33	0.83

Figure 29: (a) RT-PCR analysis carried out on RNA extracts (100 ng) of M123A and M145 to test the transcription of *psd* and *pss* by *tcp830* over three different concentrations of atc (0, 10 and 100 ng/ml), (b) the RT-PCR validation controls using *hrdB* primers with a DNase control reaction to confirm that the generated amplicons were products of RT-PCR of RNA rather than DNA contamination and (c) the cDNA<sub>gene</sub>/cDNA<sub>control</sub> ratio calculations used as a quantitative measurement for the gene expression. Increasing the concentration of atc did not significantly alter the calculated ratios hence confirmed the constitutive nature of expression of *psd* and *pss* by *tcp830*.

## 5.7 Cloning of *psd* and *pss* into pSAM2 based integrating vector, pPM927

With the loss of transcriptional control of *tcp830* promoter in pAV11b verified, it was necessary to use an alternative integrative vector with a different inducible promoter. For this reason, the integrating vector, pPM927 derived from the self-transmissible and autonomous replicative element, pSAM2 isolated from *Streptomyces ambofaciens* ATCC23877 was chosen. pPM927 is a pSAM2-based integrative vector with no autonomous replication in *Streptomyces* (Smokvina *et al.*, 1990). It contains one of the most widely used inducible promoters in *Streptomyces* (Takano *et al.*, 1995; Enguita *et al.*, 1996), i.e. the thiostrepton inducible promoter, *ptipA* which is a useful tool for controlled-expression of gene insert (Smokvina *et al.*, 1990).

The presence of *spc/str* and *tsr* resistance genes enables transformants selection and in the case of *tsr*, allows the use of thiostrepton as the inducer for controlled-expression of *psd* and *pss* in this project. The general cloning strategy employed in construction of various pPM927-derived recombinant plasmids containing *psd* and *pss* was shown in Figure 20. The mutagenised cosmid G12 containing intact *psd* and *pss* was further used as template for PCR amplification of *psd* and *pss* to amplify the genes individually as well as in combination. The PCR amplification utilized high fidelity Accuzyme™ Mix DNA Polymerase (Bioline) which possesses the proofreading property to prevent possible point mutation. The amplicons were then cut with BamHI before cloning into BamHI site of pPM927. Recombinant plasmids were confirmed via different restriction enzymes and gel electrophoresis. Cloning of *psd*, *pss* and *psd+pss* into pPM927 yielded pPM68, pPM67 & pPM68+67 respectively (Figure 31 to 45). These integrating vectors were then used for gene complementation in *S. coelicolor* M145 for the purpose of PCR-directed mutagenesis of *psd* and *pss*. The use of these pPM927-derived recombinant plasmids allowed the partial repression or the overexpression of the complemented gene post-deletion of the parenteral gene in its native locus.

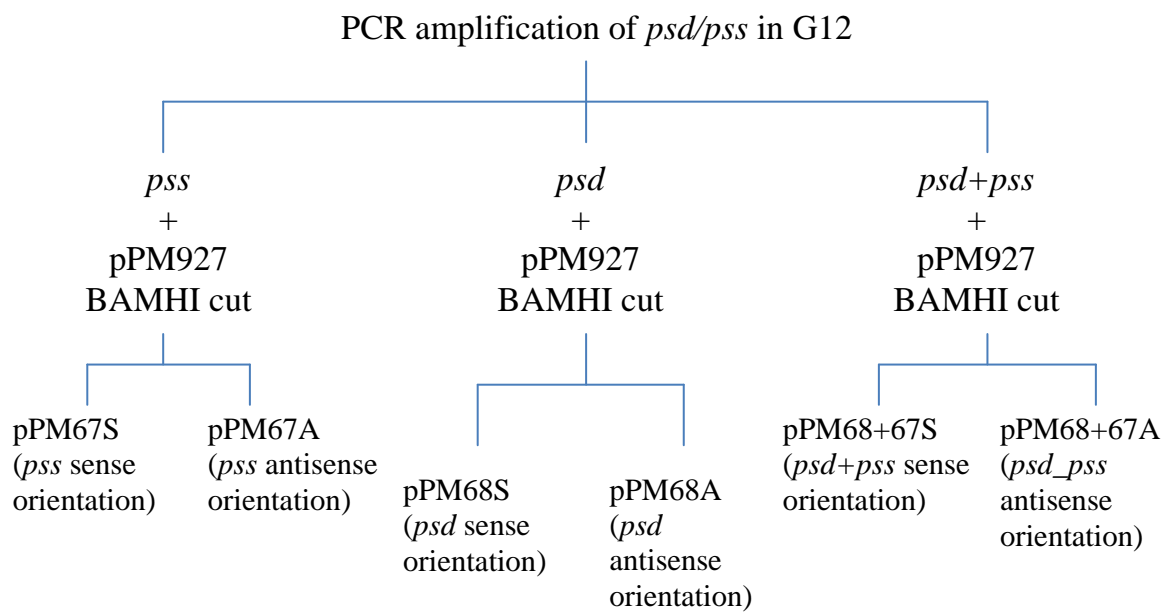


Figure 30: General cloning strategy employed in the construction of various pPM927- derived recombinant plasmids containing *psd* and *pss*.



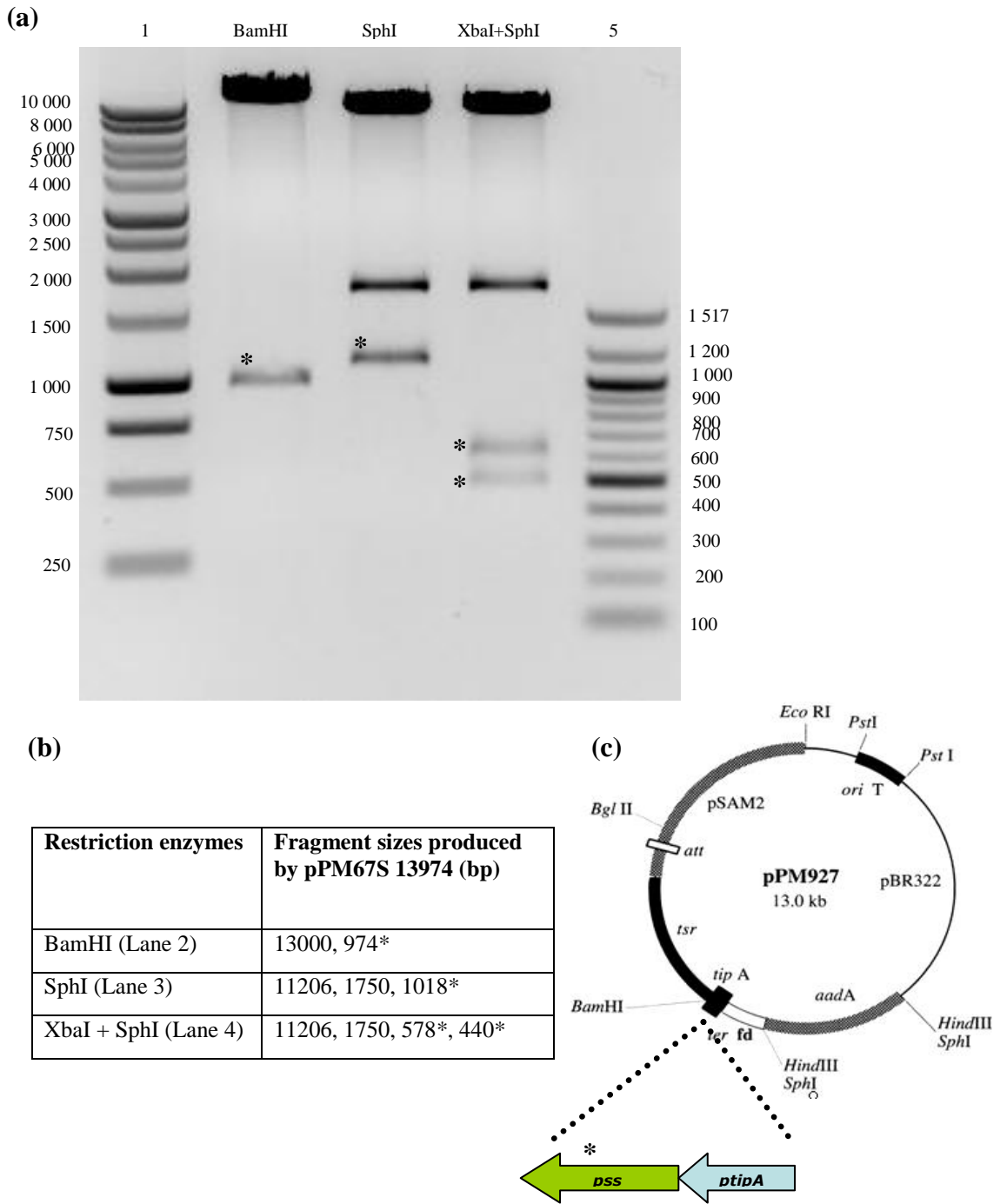


Figure 31: Electrophoresis gel of pPM67S (pPM927 + *pss*), map of the recombinant plasmid as well as the fragment sizes when digested with BamHI, SphI and XbaI + SphI. **(a)** Lane 1 & 5: 1kb DNA ladder (Promega) and 100bp ladder (NEB) respectively; Lane 2: BamHI digest; Lane 3: SphI digest; Lane 4: XbaI + SphI double digests **(b)** Fragments produced by different restriction enzymes. **(c)** The map of pPM67S with *pss* in the sense orientation relative to *ptipA* promoter of pPM927. The (\*) sign indicates the diagnostic band containing *pss*.

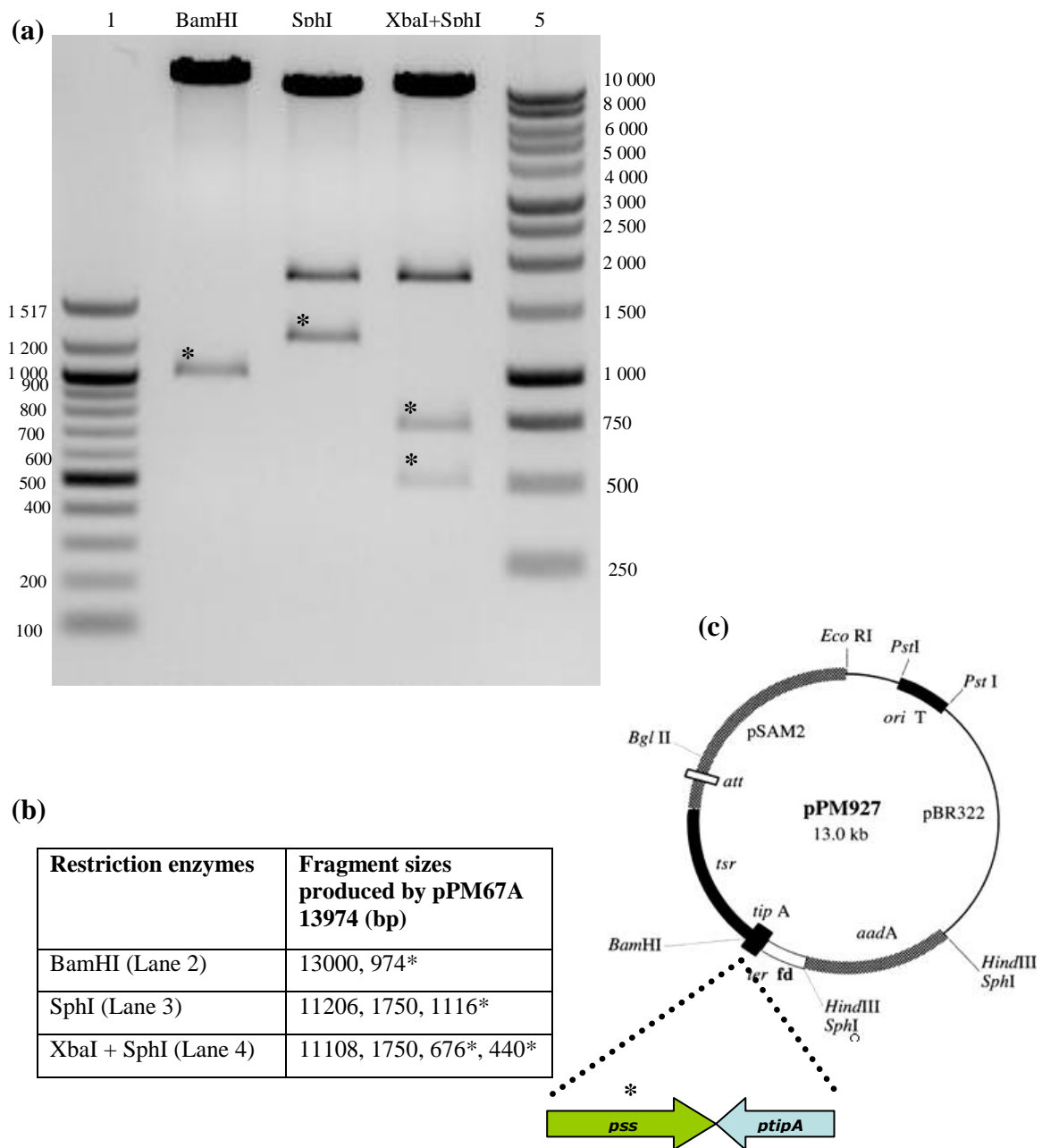


Figure 32: Electrophoresis gel of pPM67A (pPM927 + *pss*), map of the recombinant plasmid as well as the fragment sizes when digested with BamHI, SphI and XbaI + SphI. **(a)** Lane 1 & 5: 100bp DNA ladder (NEB) and 1kb DNA ladder (Promega) respectively; Lane 2: BamHI digest; Lane 3: SphI digest; Lane 4: XbaI + SphI double digests; **(b)** Fragments produced by different restriction enzymes. **(c)** The map of pPM67A with *pss* in the antisense orientation relative to *ptipA* promoter of pPM927. The (\*) sign indicates the diagnostic band containing *pss*.

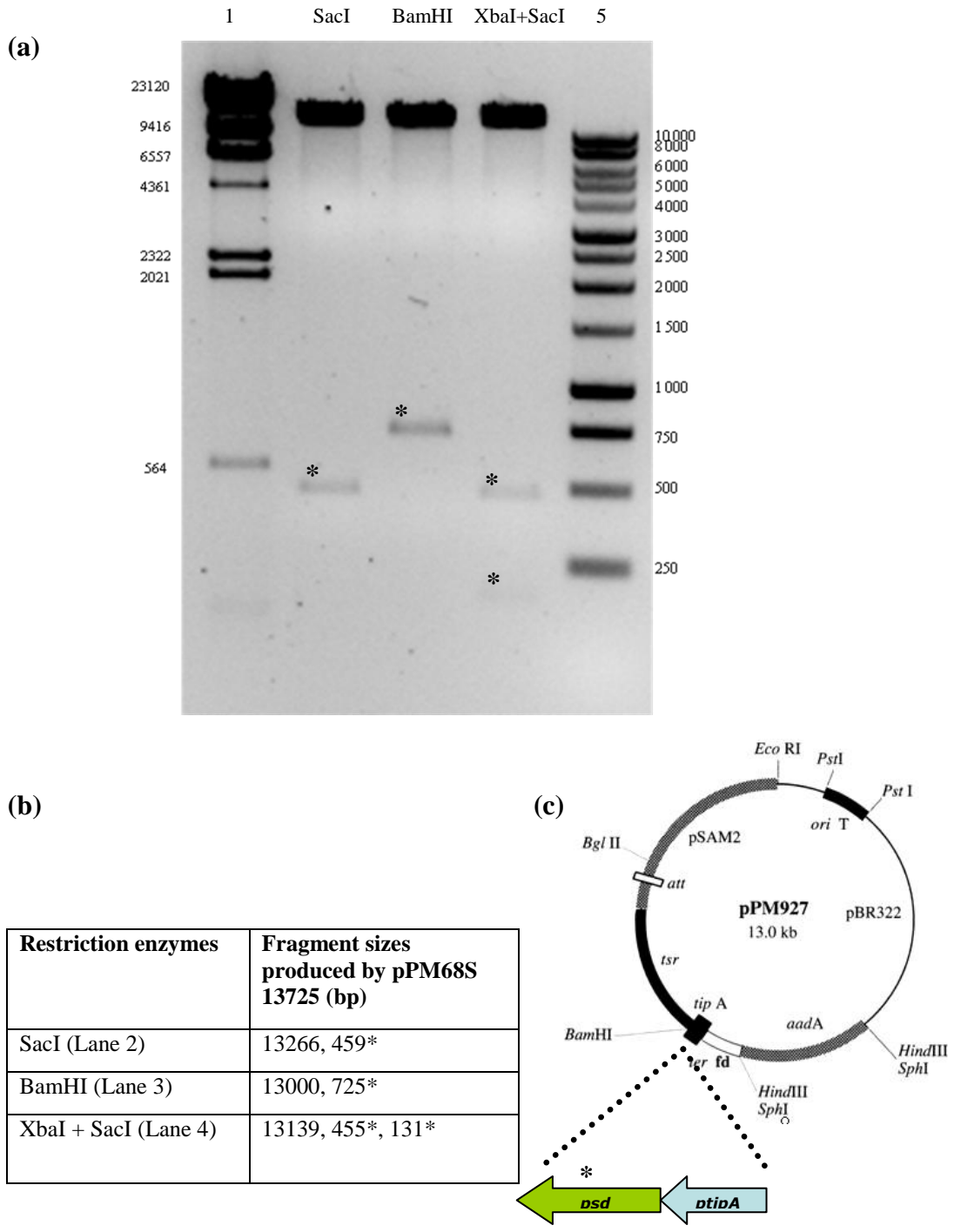


Figure 33: Electrophoresis gel of pPM68S (pPM927 + *psd*), map of the recombinant plasmid as well as the fragment sizes when digested with SacI, BamHI and XbaI + SacI. (a) Lane 1 & 5: 100bp DNA ladder (NEB) and 1kb DNA ladder (Promega) respectively; Lane 2: SacI digest; Lane 3: BamHI digest; Lane 4: XbaI + SacI double digests; (b) Fragments produced by different restriction enzymes. (c) The map of pPM68S with *psd* in the sense orientation relative to *ptipA* promoter of pPM927. The (\*) sign indicates the diagnostic band containing *psd*.

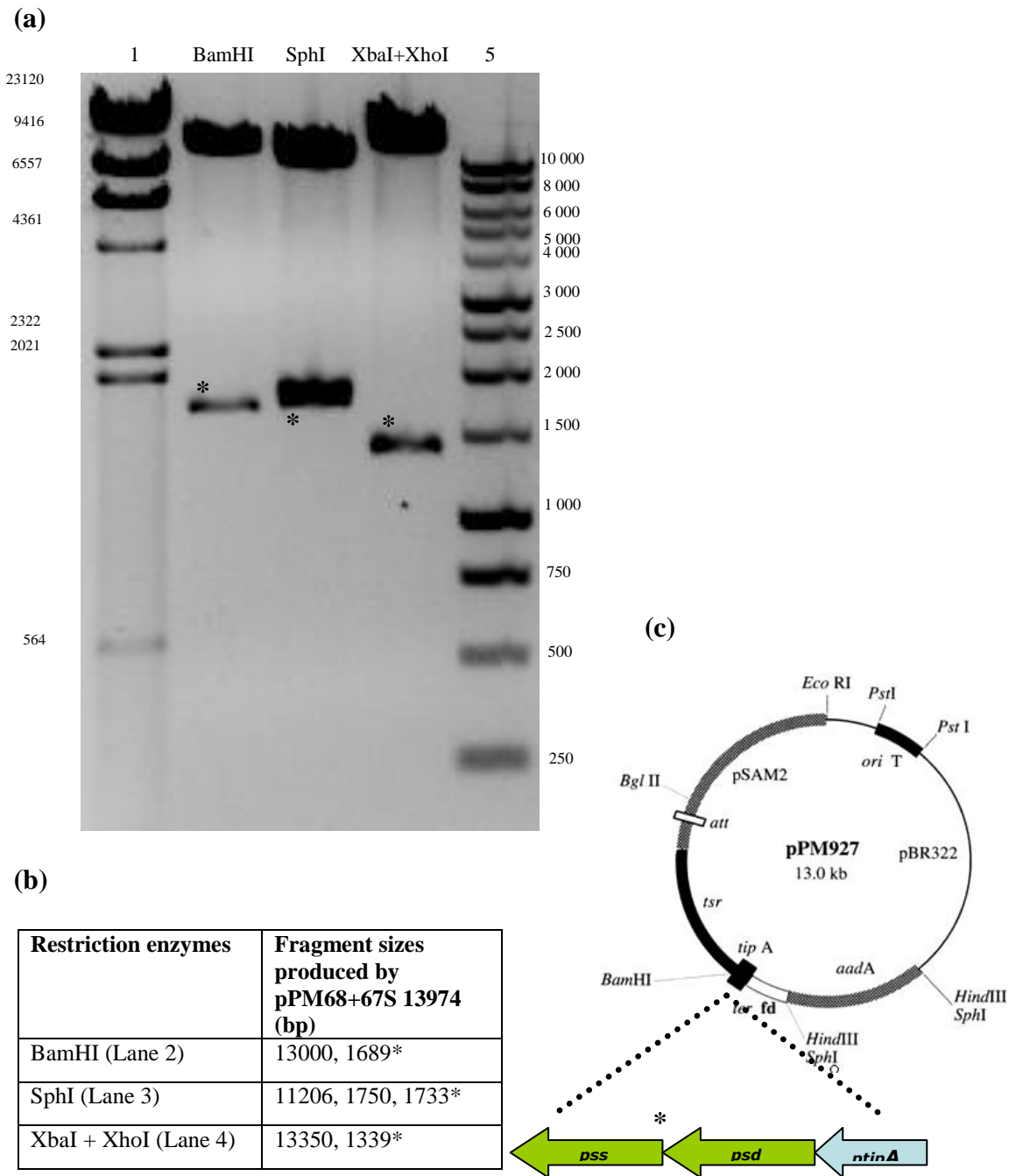


Figure 34: Electrophoresis gel of pPM68+67S (pPM927 + *psd* & *pss*), map of the recombinant plasmid as well as the fragment sizes when digested with BamHI, SphI and XbaI + XhoI. **(a)** Lane 1 & 5:  $\lambda$ HindIII DNA ladder and 1kb DNA ladder (Promega) respectively; Lane 2: BamHI digest; Lane 3: SphI digest; Lane 4: XbaI + XhoI double digests; **(b)** Fragments produced by different restriction enzymes. **(c)** The map of pPM68+67S with *psd* & *pss* in the sense orientation relative to *tipA* promoter of pPM927. The (\*) sign indicates the diagnostic band containing *psd* and *pss*.

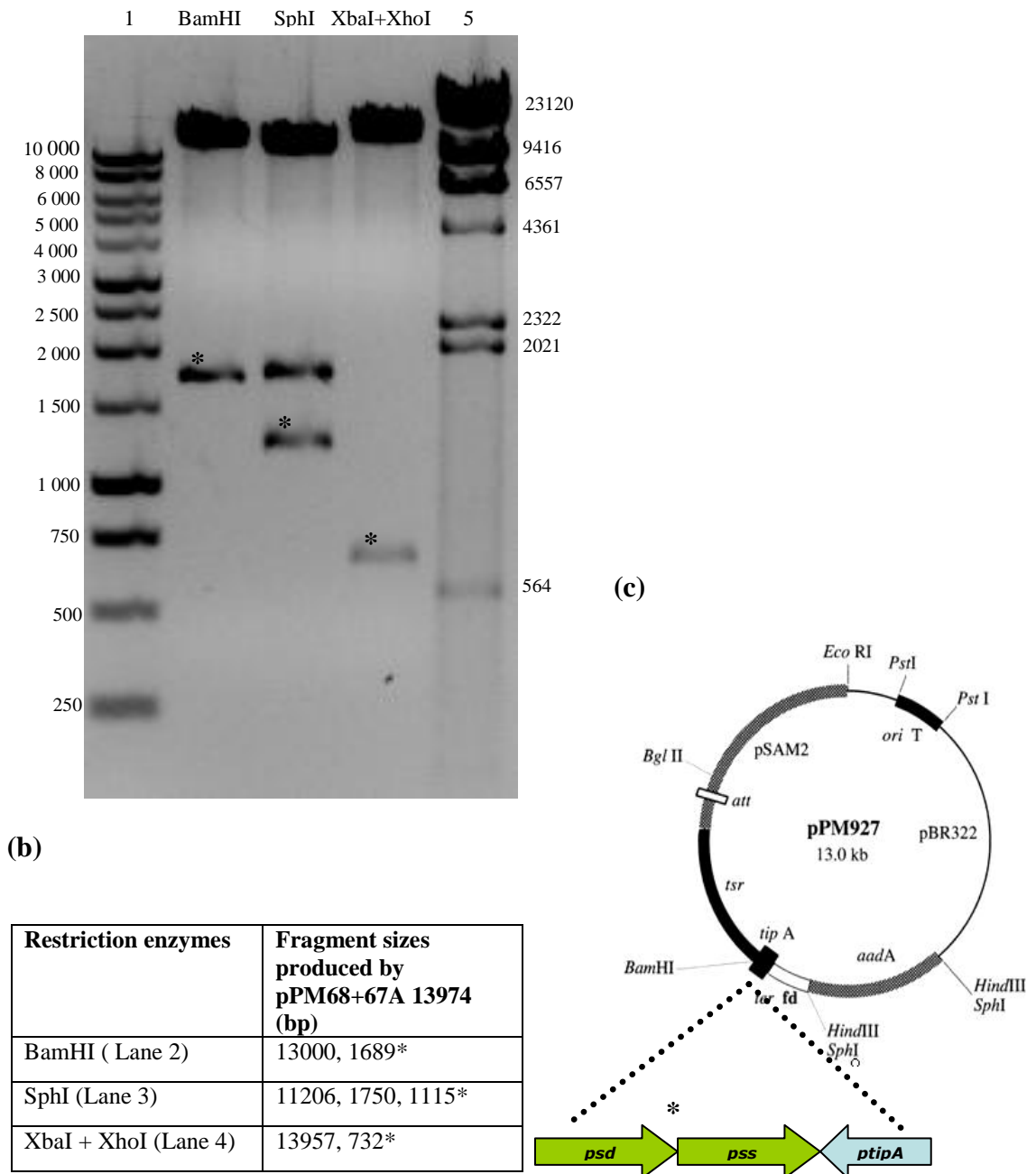


Figure 35: Electrophoresis gel of pPM68+67A (pPM927 + *psd* & *pss*), map of the recombinant plasmid as well as the fragment sizes when digested with BamHI, SphI and XbaI + XhoI. (a) Lane 1 & 5: 1kb DNA ladder (Promega) and  $\lambda$ HindIII DNA ladder respectively; Lane 2: BamHI digest; Lane 3: SphI digest; Lane 4: XbaI + XhoI double digests; (b) Fragments produced by different restriction enzymes. (c) The map of pPM68+67S with *psd* & *pss* in the antisense orientation relative to *ptipA* promoter of pPM927. The (\*) sign indicates the diagnostic band containing *psd* and *pss*.

## 5.8 Construction of the deletion vector for PCR-directed mutagenesis of *psd* and *pss* in *S. coelicolor* (Datsenko & Wanner, 2000; Gust *et al.*, 2003)

PCR-directed mutagenesis is another useful tool in molecular biology for the engineering of a gene lesion at a defined site in the bacterial genome. Its general advantage over transposon-mediated mutagenesis is its ability to circumvent the polar effect incurred by the stop codon within transposon Tn5062 cassette i.e. the in-frame deletion of the gene of interest in the bacterial genome does not terminate the transcription of the downstream gene in an operon. This is particularly important in the co-transcribed *psd* and *pss* operon.

In order to construct the relevant deletion vectors, the parenteral St9C7 cosmid (containing the *psd* and *pss* region of *S. coelicolor* genome fused with Supercos-1) had to be mutagenised by replacing the gene of interest in the cosmid with the redirect cassette ( $\Delta gene::apra^r$ ) via homologous recombination. The basis behind designing the redirect primers is shown in Figure 36. Each primer had 39 nucleotides matching the flanking sequence adjacent the gene to be deleted (*psd* and *pss*) at the 5' end and 20 or 19 nucleotides matching the left or right end of the disruption cassette at the 3' end. The primers used for PCR amplification of the extended redirect cassette are shown in Table 17.

Accuzyme™ Mix DNA Polymerase (Bioline) mediated PCR amplification of the 39nt + 39nt extended redirect cassette was done using 2938bp fragment from pIJ773 (EcoRI + HindIII digested fragment) as template. The extended redirect fragments were then gel-purified before electrotransformation into *E. coli* BW25113/pIJ790/St9C7. Double homologous recombination events between the linear DNA with the parenteral cosmid resulted in replacement of the targeted gene in the cosmid, producing RD6467 ( $\Delta pss::apra^r$ ) (Figure 37), RD6468 ( $\Delta psd::apra^r$ ) (Figure 38), and RD6467+68 ( $\Delta pss + \Delta psd::apra^r$ ) (Figure 39). These deletion vectors were then verified using various restriction enzymes before being used for in-frame deletion of *psd* and *pss* in *S. coelicolor* chromosome.

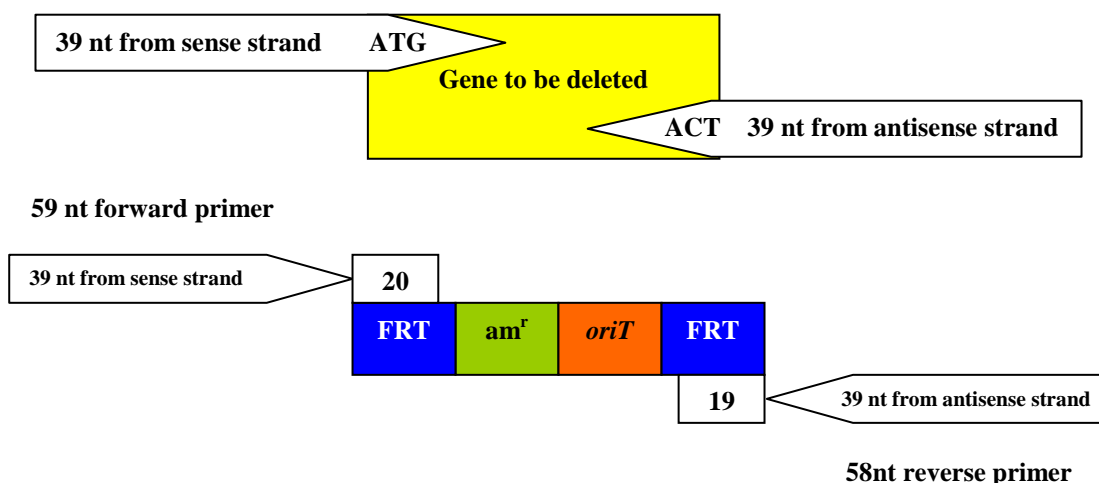


Figure 36: (a) General design of primers for PCR amplification of the redirect cassette in pIJ773. **Forward primer (59 nt):** The 5'-39 nt sequence from the sense strand that flanks the gene to be deleted ending with ATG (start codon of the gene) + 20 nt of the FLP recognition target (FRT) of pIJ773. **Reverse primer (58 nt):** The 5'-39 nt sequence from the antisense strand that flanks the gene to be deleted ending with TCA (stop codon of the gene) + 19 nt of the FRT of pIJ773.

Table 17: The sequences of primers used in PCR amplification of the extended redirect cassette. Black font: sequence flanking the gene to be deleted ending with 3 nt within the gene; blue font: 20 or 19 nt of priming site of the redirect cassette

Oligo	Sequence (5' to 3')	Temperature (°C)
RD6468L1	GTCATAGCGCGGCATCATCCGCTACGAAGGT CATCCATG <b>ATTCCGGGGATCCGTCGACC</b>	>75
RD6468R1	TCGGCCTCCGGCACCCATCCGGCCTGGGTCT GTGGATCAT <b>GTAGGCTGGAG CTGCTTC</b>	>75
RD6467L1	GTGCCGGAGGCCGACGAGGTGGACGACGAG GAGGAGAT <b>GATTCCGGGGATCCGTCGACC</b>	>75
RD6467R1	ACCCGACCCGGGTCCGGGGCCCCACCCAGC GGAGCGCTAT <b>GTAGGCTGGAGCTGCTTC</b>	>75

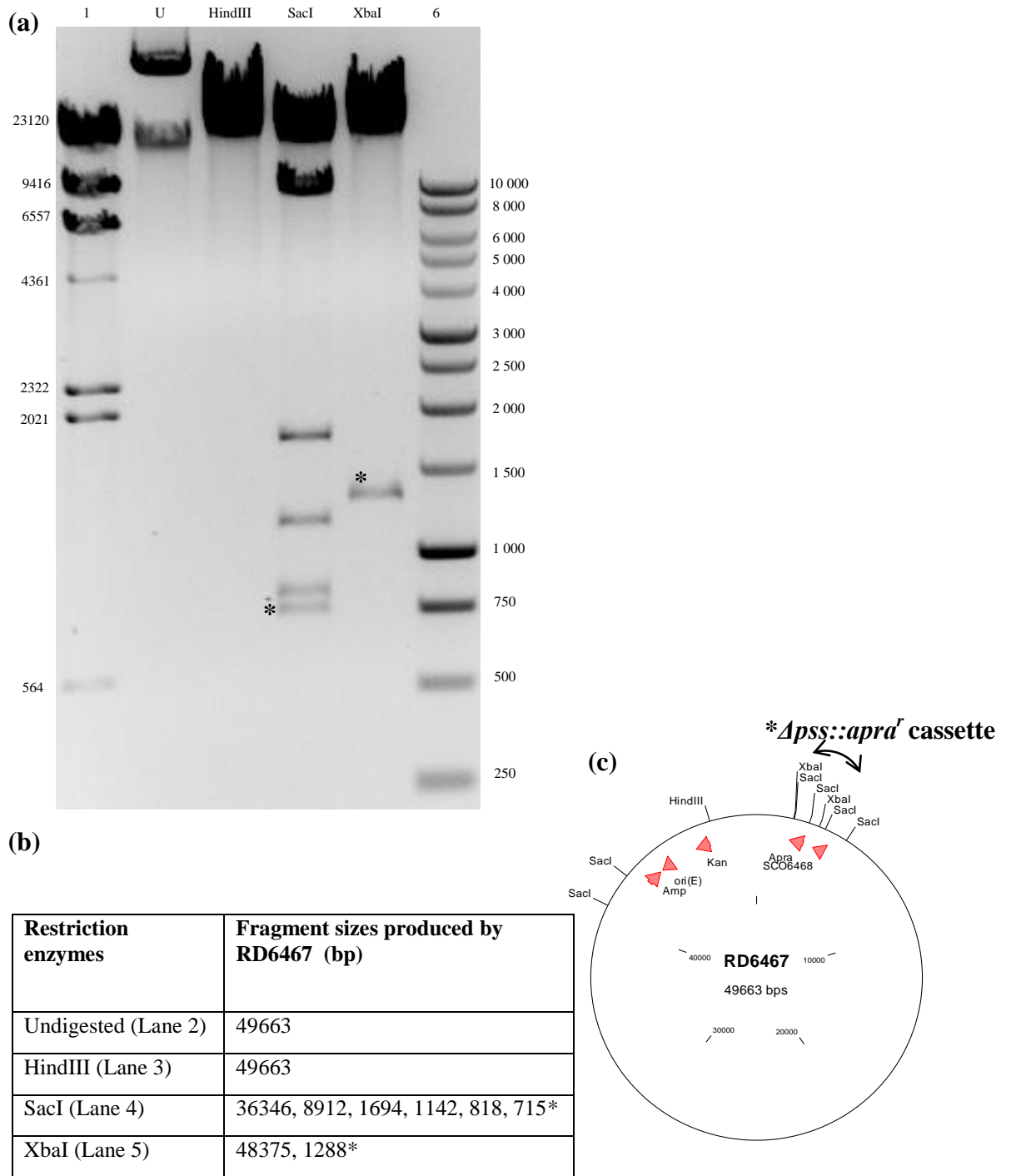


Figure 37: Electrophoresis gel of RD6467 ( $\Delta pss::apra^r$ ), map of the recombinant cosmid as well as the fragment sizes when digested with HindIII, SacI and XbaI. **(a)** Lane 1 & 6:  $\lambda$  HindIII DNA ladder and 1kb DNA ladder (Promega) respectively; Lane 2: undigested; Lane 3: HindIII digest; Lane 4: SacI digest; Lane 5: XbaI digest. **(b)** Fragments produced by different restriction enzymes. **(c)** The map of RD6467 with (\*) sign indicating the diagnostic band containing the  $\Delta pss::apra^r$  cassette.



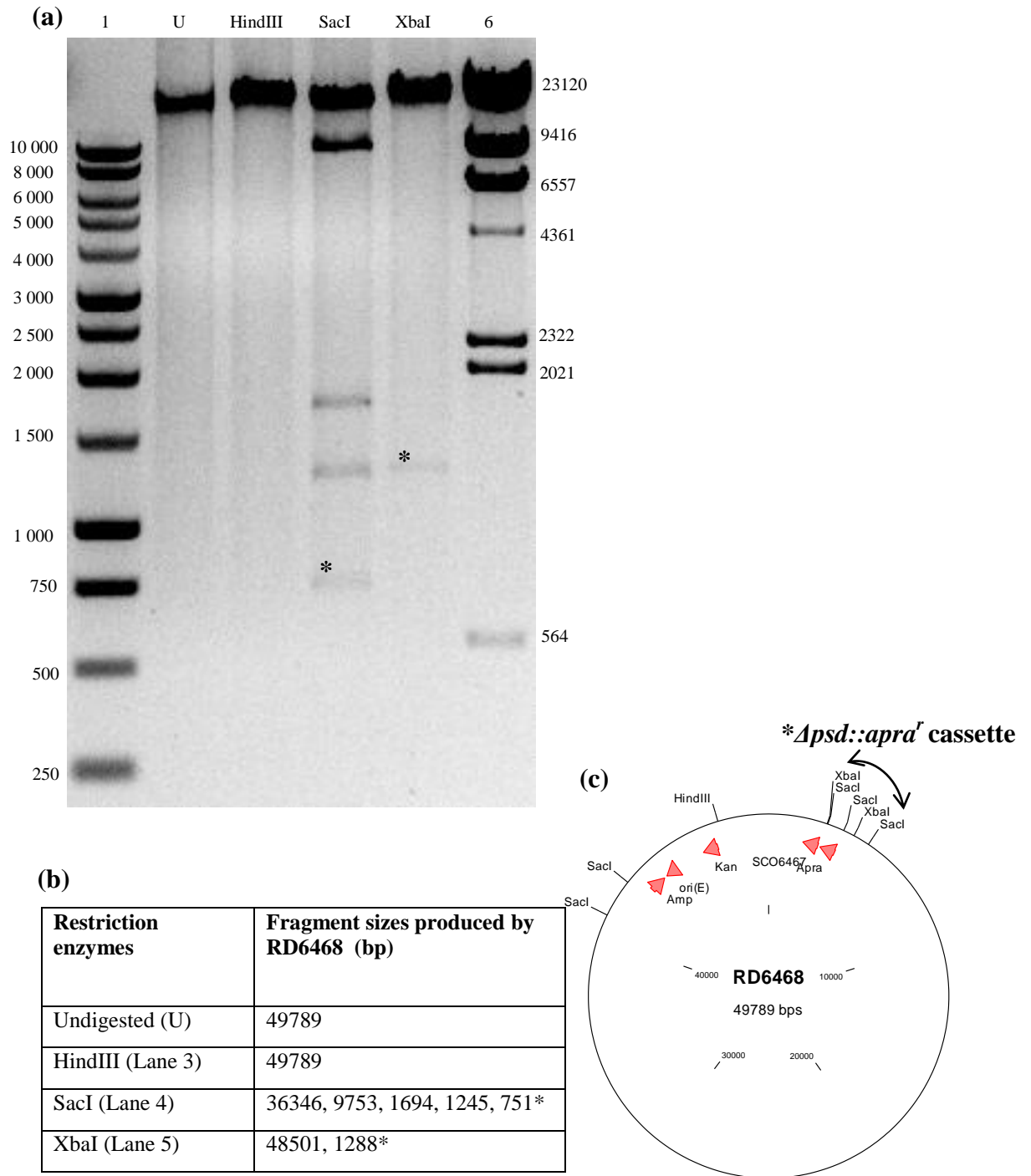


Figure 38: Electrophoresis gel of RD6468 ( $\Delta psd::apra'$ ), map of the recombinant cosmid as well as the fragment sizes when digested with HindIII, SacI and XbaI. **(a)** Lane 1 & 6: 1kb DNA ladder (Promega) and  $\lambda$  HindIII DNA ladder respectively; Lane 2: undigested; Lane 3: HindIII; Lane 4: SacI digest; Lane 5: XbaI digest. **(b)** Fragments produced by different restriction enzymes. **(c)** The map of RD6468 with (\*) sign indicating the diagnostic band containing the  $\Delta psd::apra'$  cassette.

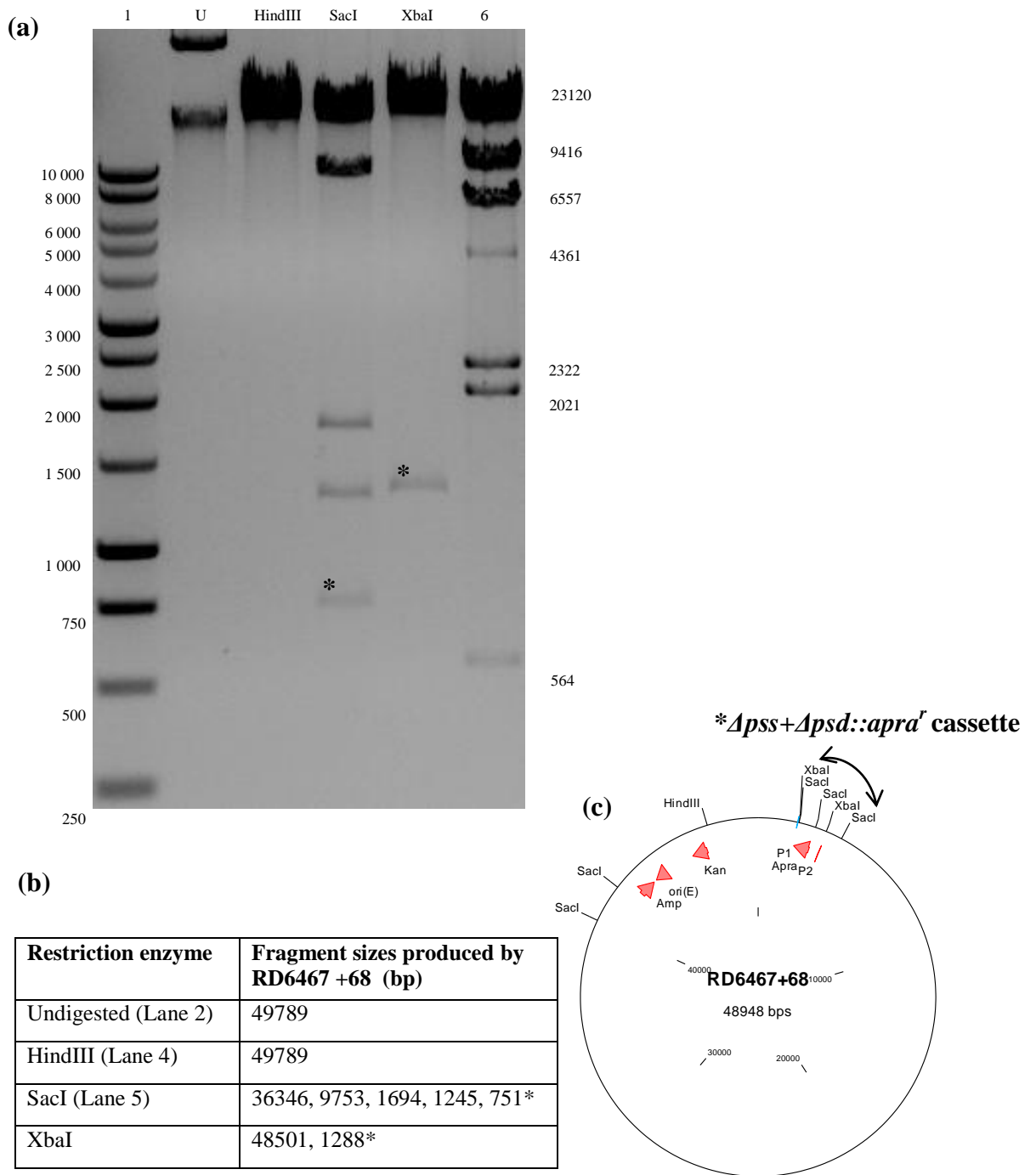


Figure 39: Electrophoresis gel of RD6467 +68 ( $\Delta pss + \Delta psd :: apra'$ ), map of the recombinant cosmid as well as the fragment sizes when digested with HindIII, SacI and XbaI. **(a)** Lane 1 & 6: 1kb DNA ladder (Promega) and  $\lambda$  HindIII DNA ladder respectively; Lane 2: undigested; Lane 3: HindIII digest; Lane 4: SacI digest; Lane 5: XbaI digest. **(b)** Fragments produced by different restriction enzymes. **(c)** The map of RD6467 +68 with (\*) sign indicating the diagnostic band containing the  $\Delta pss + \Delta psd :: apra'$  cassette.

## 5.9 PCR-directed mutagenesis of *psd* and *pss* post-complementation

As it was impossible to directly disrupt the chromosomal *psd* or *pss* in *S. coelicolor*, an extra copy of the relevant gene had to be provided *in trans* prior to deletion of the parenteral gene. For this purpose, pPM68S (pPM927 + *psd*), pPM67S (pPM927 + *pss*) and pPM68+67S (pPM927 + *psd* & *pss*), were transferred individually into *S. coelicolor* M145 via conjugation by co-culturing *E. coli* ET12567/pUZ8002 + complementing vector with M145. A recombination process catalyzed by integrase encoded by the *int* gene promotes the pSAM2 *attP* integration into the chromosomal pSAM2 *attB* site within a tRNA<sup>Pro</sup> gene (Boccard *et al.*, 1989; Mazodier *et al.*, 1990) resulting in the introduction of an extra copy of the gene of interest in the ectopic site which is transcriptionally controlled by *ptipA*.

A single colony of each strain of the exconjugants was picked and streaked onto MS agar containing thiostrepton (10 µg/ml) and spectinomycin (400 µg/ml) for confluent growth which would be used for making spore suspensions. The spore suspensions, M145 + pPM68S, M145 + pPM67S or M145 + pPM68+67S were later used for further conjugation with *E. coli* ET12567/pUZ8002 + the deletion vector RD6467, RD6468 or RD6467+68 respectively for the purpose of deletion of the targeted gene via homologous recombination. 1000 exconjugants were patched onto two replica MS agar plate with 400 µg/ml spectinomycin + 0.5 µg/ml thiostrepton + 50 µg/ml kanamycin/apramycin to screen for double crossover exconjugant *apra*<sup>r</sup>, *km*<sup>s</sup> which had undergone the allelic replacement with the redirect cassette.

Consistent with the observation made in transposon-mediated mutagenesis, only double crossover exconjugant of *pss* (JT672:  $\Delta pss::apra^r/tcp830-pss^+$ ) was observed. The *pss* mutant was generally paler in appearance compared to the wild type M145 when grown on MS agar (Figure 40). The inability to disrupt *psd* and the success of *pss* inactivation only after gene complementation further suggested the essentiality of these genes as well as the complexity of *psd* transcription which was not matched by the second copy of this gene (*ptipA-psd*) in the pSAM2 site.

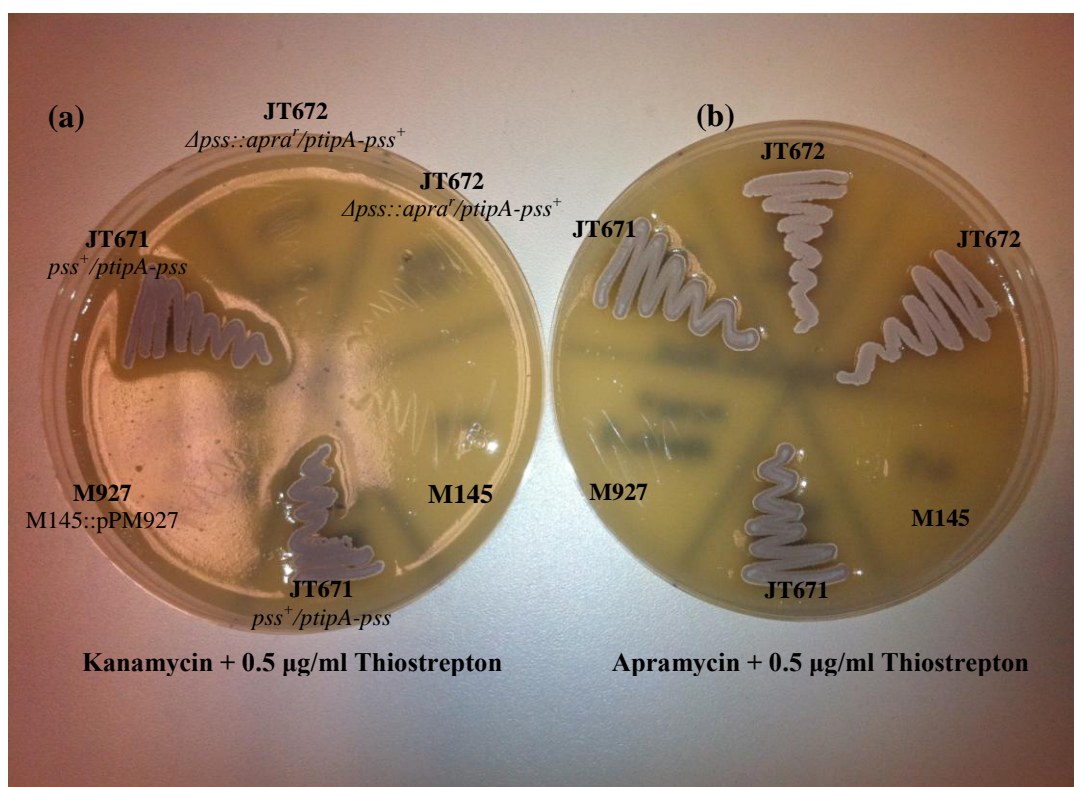


Figure 40: Single cross-over (JT671:*pss*<sup>+</sup>/*ptipA-pss*<sup>+</sup>) and double crossover exconjugants (JT672:  $\Delta pss::apra^r/ptipA-pss^+$ ) obtained from homologous recombination of *S. coelicolor* M145 genome with cosmid RD6467 after complementation with pPM67S. (a) MS agar + 50 µg/ml kanamycin + 0.5 µg/ml thiostrepton plate (b) MS agar + 50 µg/ml apramycin + 0.5 µg/ml thiostrepton plate. M145: *S. coelicolor* M145 and M927: M145::pPM927

### 5.10 PCR-verification of JT672 ( $\Delta pss::apra^r/ptipA-pss^+$ )

Two sets of primers were designed for the PCR-verification of JT672. The first pair of primers (L1 and R1) primed from the 3' of *ptipA* promoter to the 5' start of *pss* yielding a 220bp fragment. This verified the presence of the complemented copy of the gene in sense orientation with respect to the *ptipA* promoter (*ptipA-pss*<sup>+</sup>) in the bacterial chromosome. The second set of primers (L2 and R2) primed from the flanking sequences upstream and downstream of *pss* i.e. 3' end of *psd* to downstream sequence flanking *pss*. PCR-amplification of this region would give a 1.056 kbp fragment in wild type with the intact native *pss* whereas double crossover exconjugant would yield a 1.650 kbp fragment due to allelic replacement of *pss* by the *apra*<sup>r</sup> containing redirect cassette,  $\Delta pss::apra^r$ . The primers used in the verification process are shown in Figure 41.

PCR was done on JT672 against various controls (the deletion vector RD6467, the parenteral cosmid St9C7, the complementing vector pPM67S, the empty complementing vector pPM927 and the wild type *S. coelicolor* M145 (Figure 42) using both sets of primers. Priming using L1 + R1 showed the presence of 220 bp fragment in JT672 (Lane 10 and 12) which was absent in *S. coelicolor* M145 (Lane 7). The use of L2 + R2 yielded a 1.65 kb fragment in JT672 (Lane 9 and Lane 11) compared to the 1.056 kb fragment of *S. coelicolor* M145 (Lane 6) hence indicating the excision and replacement of the native *pss* by the redirect cassette.

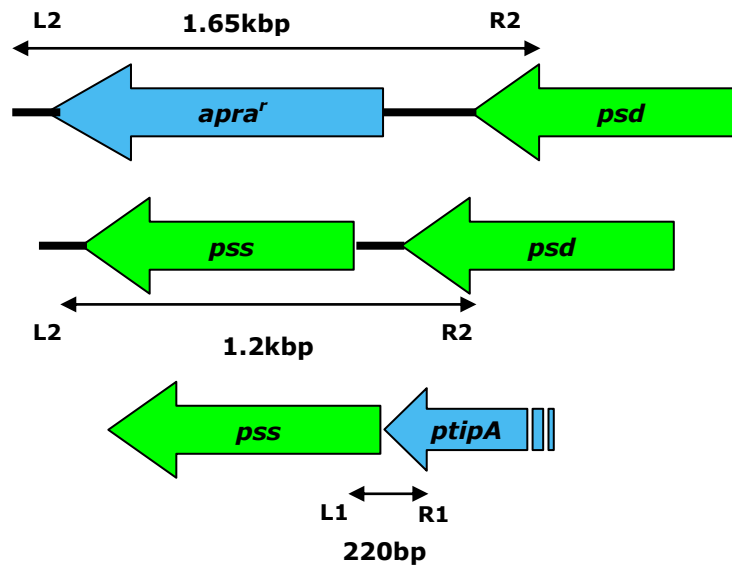
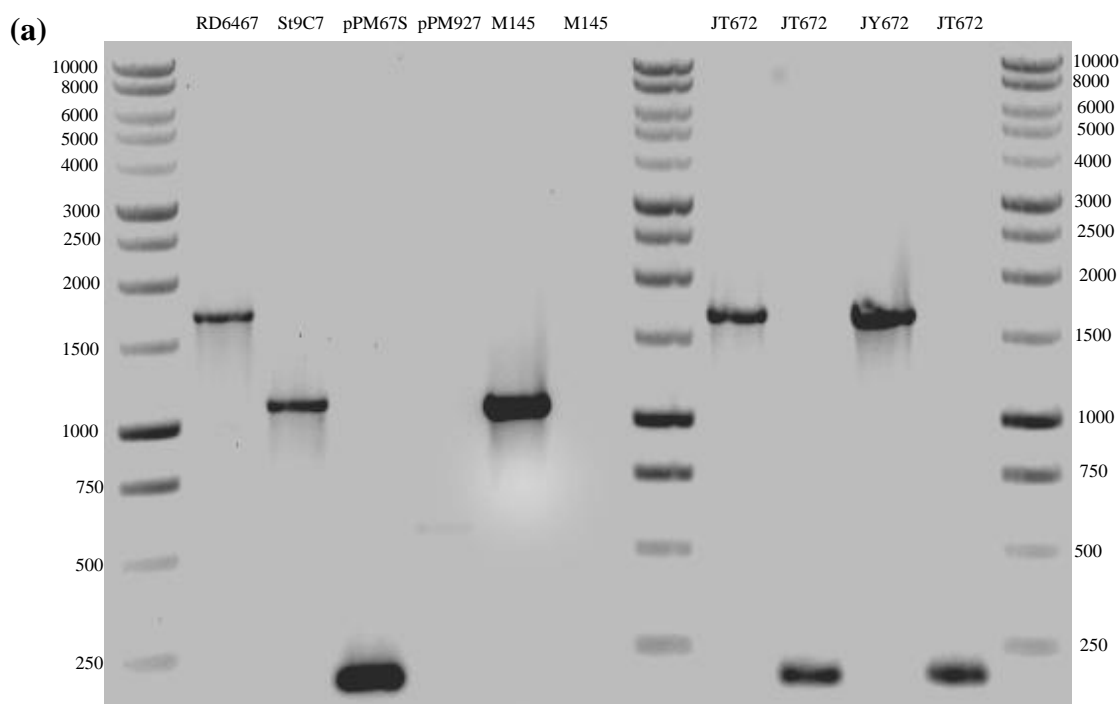


Figure 41: The priming regions of the primers used in PCR –verification of JT672. Primer L1 and R1 were used to verify the presence of *ptipA-pss<sup>+</sup>* in the bacterial chromosome whereas L2 and R2 was used to confirm the allelic replacement of *pss* by the *apra<sup>r</sup>* cassette, ( $\Delta pss::apra^r$ ). The sequences of the primers are shown in Table 15, Section 3.21.



(b)

Strain/plasmid	Primers	Expected Size (kb)	Actual size (kb)
RD6467	L2 + R2	1.650	1.650
St9C7	L2 + R2	1.056	1.056
pPM67S	L1 + R1	0.22	0.22
pPM927	L1 + R1	NIL	NIL
M145	L2 + R2	1.056	1.056
M145	L1 + R1	NIL	NIL
JT672 (colony 1)	L2 + R2	1.650	1.650
JT672 (colony 1)	L1 + R1	0.220	0.220
JT672 (colony 2)	L2 + R2	1.650	1.650
JT672 (colony 2)	L1 + R1	0.220	0.220

Figure 42: (a) PCR – confirmation of double crossover exconjugants, JT672 against various controls (RD6467, St9C7, pPM67S, pPM927 and M145) with (b) summary of different strains/plasmids, primers and size of PCR fragments generated. The presence of 0.22kb fragment showed the integration of pPM67S into *S. coelicolor* whereas the generation of 1.65kb fragment instead of 1.056kb fragment indicated the replacement of *pss* in its native locus by the redirect cassette. This confirmed the generation of *ptipA*- controlled *pss* haploid mutant.

### 5.11 Controlled-expression of *pss* on minimal medium and MS agar

The *ptipA* promoter regulates the synthesis of an mRNA transcript that encodes two proteins of different sizes, TipAL and TipAS which are 31kDa and 17kDa respectively (Murakami *et al.*, 1989; Holmes *et al.*, 1993). Induction is achieved in the presence of thiostrepton which binds covalently to the larger TipAL protein that functions as the transcriptional activator. The formation of thiostrepton-TipAL complex increases the affinity of the activator by several orders of magnitude to regions of dyad symmetry within *ptipA* thereby activating the transcription process (Chiu *et al.*, 1996; Chiu *et al.*, 1999).

Repression is modulated by the smaller TipAS protein which shares similar C-terminal thiostrepton-binding domain as the TipAL. The synthesis of TipAS in molar excess over TipAL triggered by the alternative translational initiation site for the smaller protein causes it to sequester thiostrepton that inhibits the thiostrepton-TipAL mediated transcription. However, TipAL can still bind to the transcription activation site within *ptipA* even in the absence of thiostrepton (Holmes *et al.*, 1993; Ali *et al.*, 2002; Flardh, 2003a). Hence uninduced level of promoter activity is significantly higher compared to *tcp830*.

Growth of JT672 on 3MA, minimal medium + glucose and MS agar was investigated. Partial depletion of *pss* in the absence of thiostrepton resulted in significantly reduced formation of aerial hyphae in 3MA-grown JT672. Aerial hyphae formation was thiostrepton- dependent since the density of the aerial hyphae increased with increasing thiostrepton concentration from 0 to 0.5  $\mu\text{g/ml}$ . Formation of aerial hyphae was also hindered in M67A with an antisense copy of *pss* relative to *ptipA* due to RNA interference effect causing it to appear bald at 0.5  $\mu\text{g/ml}$  thiostrepton (Figure 43). Insufficient level of *pss* expression also resulted in higher actinorhodin production in the mutant. Addition of 0.5  $\mu\text{g/ml}$  thiostrepton on the other hand, brought the level of antibiotic production down to level close to that of wild type (data not shown). Growth of M145 was inhibited at 0.5  $\mu\text{g/ml}$  of thiostrepton due to the absence of the resistance gene (Murakami *et al.*, 1989).



JT672, M145 and M927 all appeared bald when grown on minimal medium + glucose (Figure 44). Partial depletion of *pss* in JT672 caused a decrease in overall growth density and an increase in antibiotic production. Increase in the concentration of thiostrepton added from 0 to 0.5  $\mu\text{g/ml}$  raised the growth density of the mutant while reducing the antibiotic production close to that of the wild type. Unlike growth on 3MA and minimal medium + glucose, no obvious morphological defect was observed in the mutant grown on MS agar except for delayed growth in the partial *pss* depleted JT672. This was apparent with the delay in spore pigmentation in the absence of the thiostrepton (Figure 45). When left to grow for more than 5 days, the phenotypic appearance of the uninduced mutant looked similar to that of the fully-induced mutant. Nevertheless, the fully-induced/grown mutant still appeared paler in comparison to the controls (M145 and M927).

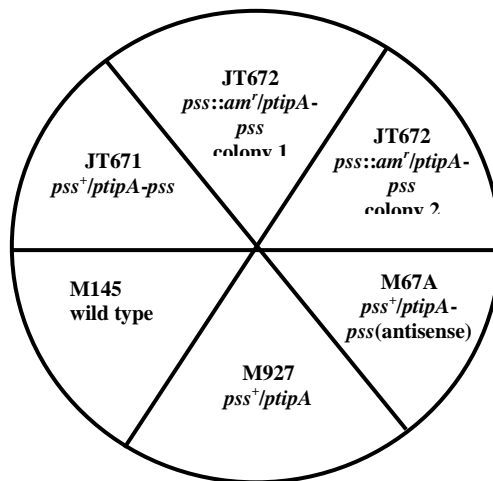
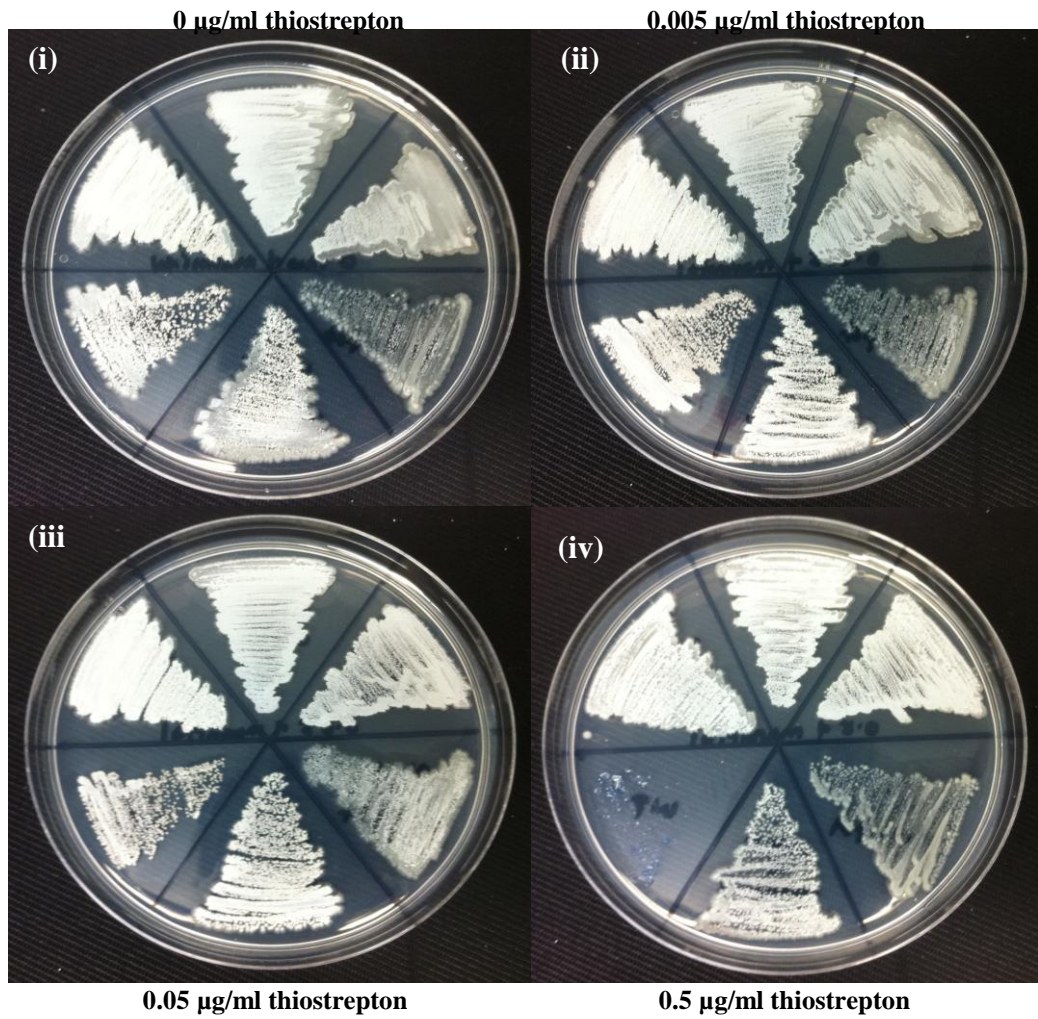


Figure 43: The phenotype of single crossover (JT671) and double crossover exconjugants (JT672) against various controls; M145, M927 and M67A grown on 3MA supplemented with (i) 0 µg/ml (ii) 0.005 µg/ml (iii) 0.05 µg/ml and (iv) 0.5 µg/ml of thiostrepton.

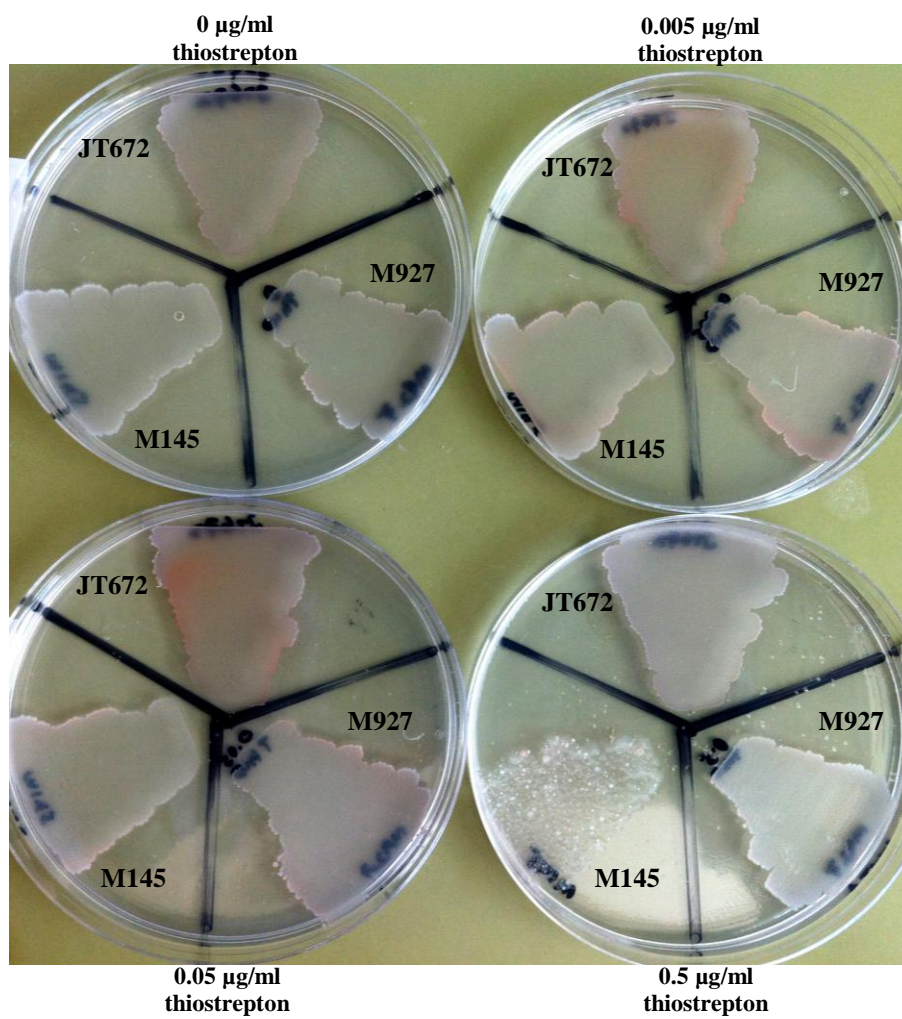


Figure 44: The phenotype double crossover exconjugants (JT672) against various controls; M145 and M927 grown on minimal media + glucose agar supplemented with 0, 0.005, 0.05 and 0.5 µg/ml of thiostrepton.



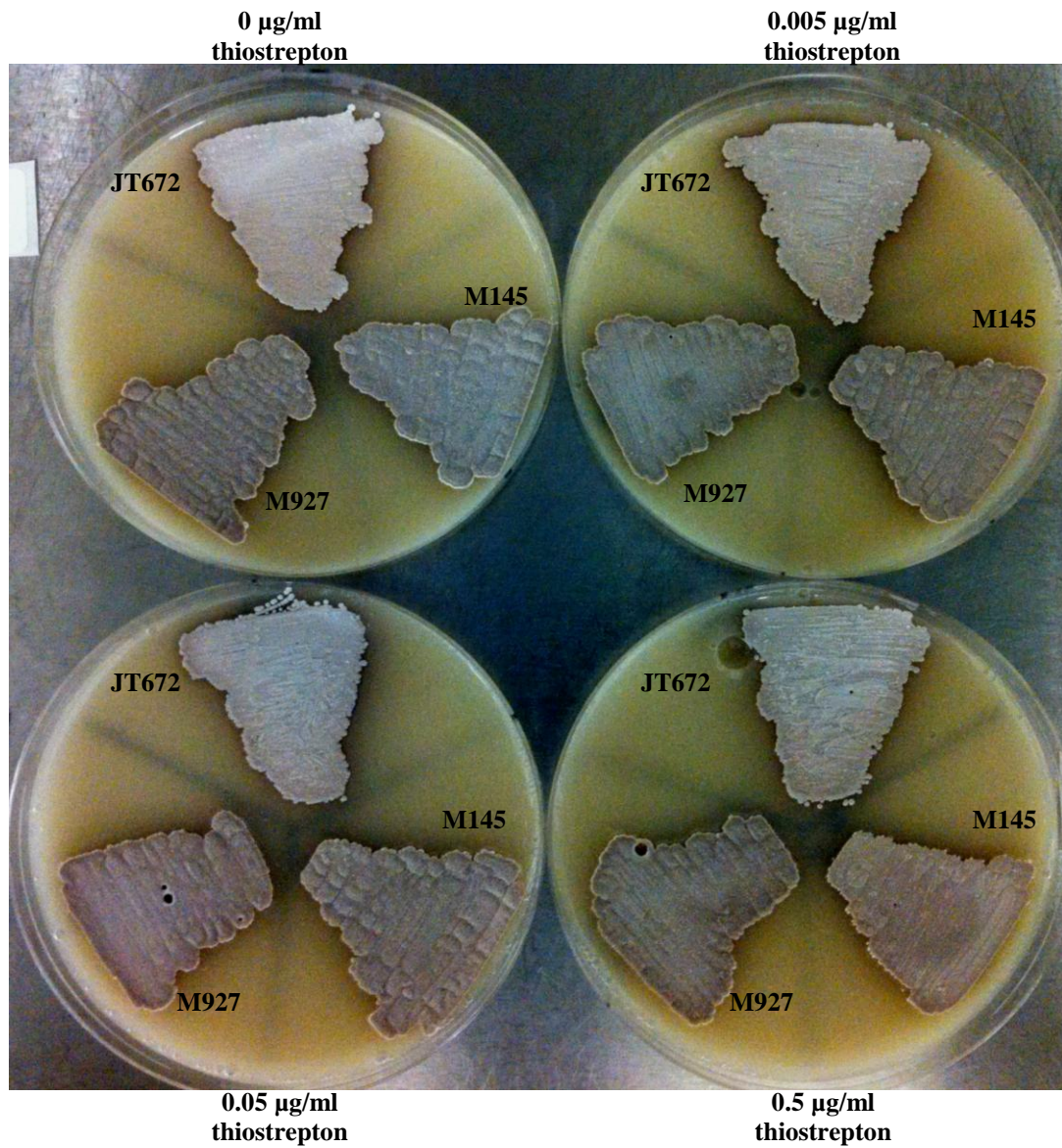


Figure 45: The phenotype of double crossover exconjugants (JT672) against various controls; M145 and M927 grown on MS agar supplemented with 0, 0.005, 0.05 or 0.5 µg/ml of thiostrepton.

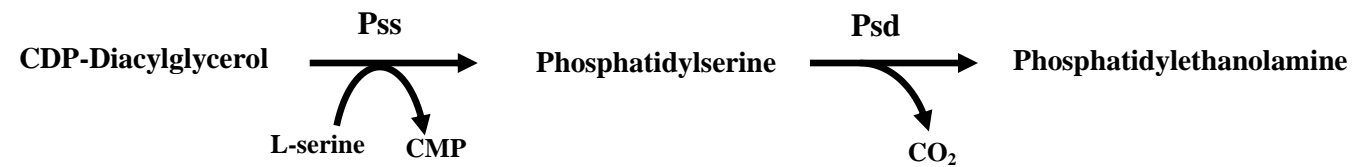
## 5.12 Discussion and conclusion

Psd and Pss are important proteins responsible for the biosynthesis of two important membrane phospholipids, PE and PS respectively. The inability to create *psd/pss* null mutants, and the futile attempt to disrupt/delete *psd* even after complementation with a second copy of the gene at an ectopic site in *S. coelicolor* genome concluded that only strain with intact Psd and Pss are able to grow. We suspect that the unsuccessful effort to delete/disrupt *psd* post-complementation was due to failure of proper expression of the second copy of the gene in the pSAM2 site.

Various reasons were proposed including the incompatible promoter/ribosomal binding site used in the complementing vector (Rodriguez-Garcia *et al.*, 2005) or more importantly the aberrant transcriptional activity of the gene out of its native locus. The latter elaborates the complexity of transcriptional regulation which was proposed to be governed by the overall architecture of the *S. coelicolor* chromosome. In other words, the dynamic structure of the bacterial chromosome may be a determinant of transcriptional activity hence there are essentially transcriptional active and inactive regions in the bacterial genome (McArthur & Bibb, 2006), a phenomenon long established in the eukaryotes (Weintraub & Groudine, 1976; Felsenfield, 1992).

The level of *psd* expression in its native locus was probably not matched by the second copy in the ectopic  $\Phi$ BT1 *attB* or pSAM2 sites therefore disruption of the parenteral gene could have been lethal to *S. coelicolor*. In addition, the genes are organized such that the second step in the pathway is encoded by the first gene of the operon (Figure 46). This could have further lent to the overall complexity.

**Biochemical pathway:**



**Genetic pathway:**

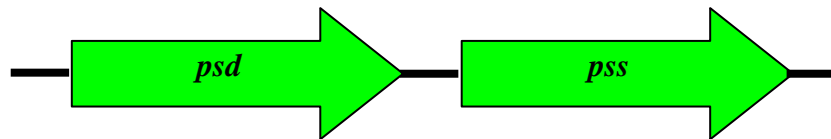


Figure 46: Biochemical and genetic orders of both *psd* and *pss* in the phospholipid biosynthetic pathway

Unlike *psd*, disruption/deletion of *pss* was possible post gene complementation. However, the transcriptional control of the ectopic *pss* by *tcp830* promoter in the double crossover exconjugant, LSM105 (*pss::Tn5062/tcp830-pss<sup>+</sup>*) appeared to be *atc*-independent. Growth and morphology were consistent over the concentration gradient of *atc* compared to the inducer dependent positive control RJ118b:  $\Delta$ *clsA::apra<sup>r</sup>/ptipA-clsA<sup>+</sup>* (Jyothikumar *et al.*, 2012). This led to the speculation of a possible suppressor mutation of the *tetR/tetO* regulatory system. RT-PCR analysis conducted on the complemented mutant M123A (*psd<sup>+</sup> pss<sup>+</sup>/tcp830-psd<sup>+</sup> pss<sup>+</sup>*) further confirmed the constitutive nature of gene expression by the synthetic promoter. This was rather surprising given the fact that previous sequencing of the complementing plasmids showed the intact sequences of both the promoter and gene inserts.

Nevertheless, we decided to restart the entire mutagenesis experiment by using a different complementing vector. A different disruption strategy was also adopted i.e. PCR- directed site mutagenesis (Gust *et al.*, 2003). This technique offered the advantage of circumventing a possible polar effect caused by transposon insertion which would otherwise hinder the expression of the co-transcribed downstream gene due to the presence of a stop codon within the transposon cassette. This is particularly important in the case of the transcriptionally-linked *psd* and *pss* operon which may partially explain the inability to transposon-inactivate *psd* (which precedes *pss* in the genetic order (Figure 46)) even after complementation.

PCR-directed mutagenesis shares similar homologous recombination concept with the transposon-mediated gene disruption. In the case of the former, replacement of the parenteral gene with an antibiotic resistance marker results in the complete excision of the native gene out of its native locus which differs from the gene truncation basis of transposon mutagenesis. The concept underlying the PCR-directed mutagenesis of *S. coelicolor* chromosomal *pss* is outlined in Figure 47. After the ectopic integration of a second functional copy of *pss* in pSAM2 *attB* site, conjugation of RD6467 to the bacteria caused the integration of the entire deletion vector into the genome via single homologous recombination event resulting in only

single crossover exconjugants *apra<sup>r</sup>*, *km<sup>r</sup>* which were partial *pss* diploid (JT671: *pss<sup>+</sup>/Δpss::apra<sup>r</sup>/ptipA-pss<sup>+</sup>*) in the first 1000 replica patched colonies. This suggested that deletion of the parenteral *pss* did not occur easily even after gene complementation and only strain with intact *pss* could grow. With subsequent replica repatching, two double crossover exconjugants *apra<sup>r</sup>*, *km<sup>s</sup>* (JT672: *Δpss::apra<sup>r</sup>/ptipA-pss<sup>+</sup>*) which had undergone a second homologous recombinant event were isolated. Due to the significant level of basal activity of the *ptipA* promoter (Holmes *et al.*, 1993; Ali *et al.*, 2002; Flardh, 2003a), *pss* mutant was still able to grow even in the absence of inducer albeit with morphological defects. In other words, only partial repression of *pss* was achievable with *ptipA* promoter.

JT672 grown on 3MA had significantly reduced aerial hyphae density showing that higher level of *pss* expression is indeed needed for proper morphological differentiation. This was further confirmed by the bald mutant obtained from the RNA interference assay done concurrently. Hence, this suggests that PE may play a role (directly or indirectly) in aerial hyphae formation and sporulation. The reduction of overall growth density of JT672 grown on minimal medium + glucose which was restored with increasing concentration of inducer further implicates the need of higher level of *pss* expression (hence adequate amount of PE) for good growth. However, all these mutant phenotypes were suppressed when grown on MS agar albeit the observed slower growth rate in the uninduced mutant. This indicates that the mutant phenotype is conditional in nature. Unlike *bld* mutants which are defective in antibiotic productions (Merrick, 1976; Champness, 1988), antibiotic production was elevated significantly in the uninduced mutant grown on both 3MA and minimal medium + glucose. This was perhaps due to physiological stress caused by insufficient production of PE in the membrane. In addition, the partial defective phospholipid biosynthesis may have caused an accumulation of precursors (such as acetyl-CoA) required to generate substrate(s) needed by the fatty acid/phospholipid biosynthetic pathways causing them to be channelled into the polyketides pathway resulting in an exaggerated antibiotic production. Nevertheless, this remains to be investigated.



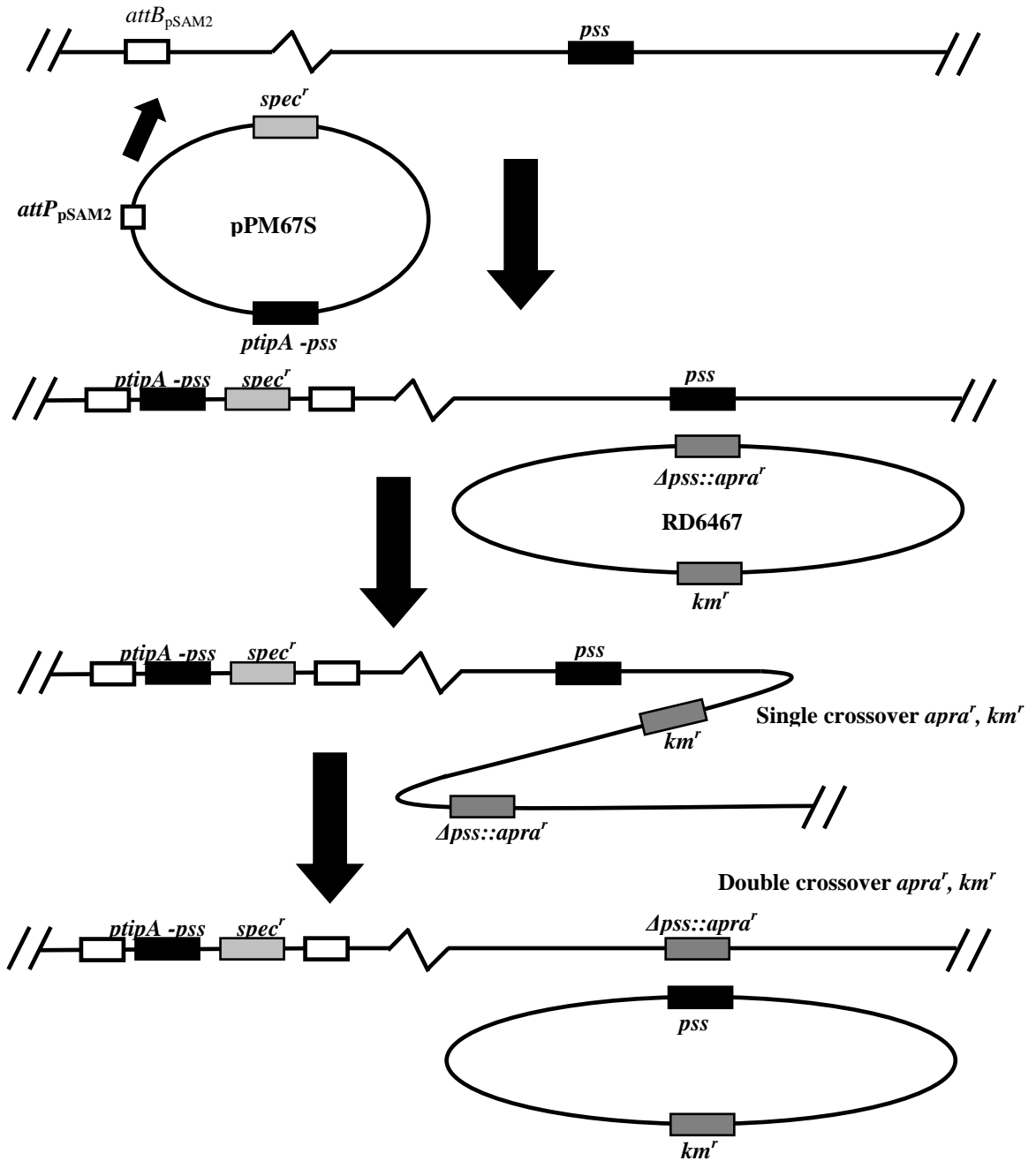


Figure 47: Integration of RD6467 and excision of *pss* post complementation using pPM67S. The conjugated pPM67S first integrated into the *attB*<sub>pSAM2</sub> site in the bacterial genome introducing an extra functional copy of *pss*. The conjugally transferred deletion vector RD6467 first integrated into the genome resulting in only single crossover exconjugant *apra<sup>r</sup>*, *km<sup>r</sup>*. Further replica patching caused allelic replacement of the native *pss* with the  $\Delta pss::apra^r$  leading to the double crossover exconjugant *apra<sup>r</sup>*, *km<sup>r</sup>* and excised cosmid lost.

## **6.0 Results**

### **Phenotypic characterization of *pss* mutant, JT672**

## **6.0 Phenotypic characterization of *pss* mutant, JT672**

### **6.1 Introduction**

In order to elucidate the function of *pss* in *S. coelicolor*, morphological and biochemical analyses were conducted on the *pss* mutant strain, JT672 under a range of growth conditions to ascertain the phenotypic changes associated with the different levels of gene expression. Observed growth anomalies which could be suppressed with the right level of *pss* expression could further establish the connection between the gene lesion and the mutant phenotypes. The information generated from these assays would be particularly useful in the context of drug discovery, since the identified antibacterial compounds which target the gene product should theoretically cause similar phenotypic change in the bacteria if not killing them altogether.

### **6.2 RT-PCR and thin layer chromatography profiles of JT672**

#### **6.2.1 Introduction**

RT-PCR is a laboratory method (a variant of PCR) commonly used to amplify a DNA sequence into high copy numbers (Rappolee *et al.*, 1988). RT-PCR however entails an additional step vis-à-vis PCR which is the reverse transcription of RNA by the enzyme, reverse transcriptase into its cDNA that acts as template for gene amplification. RT-PCR is a semi-quantitative assay (Montgomery & Dallman, 1997) with sufficient sensitivity for the detection of low copy numbers of RNA hence the need of only small amount of tissue samples (Rappolee *et al.*, 1988). Quantitative real time polymerase chain reaction (qPCR) on the other hand, has become the method of choice for detection and more accurate quantification of mRNA levels (Weis *et al.*, 1992; Winer *et al.*, 1999). It is a useful tool in molecular biology for gauging the level of gene transcription (Zamorano *et al.*, 1996). It has wide applications in molecular medicine such as clinical diagnosis (Holodniy, 1994;

Ghossein & Rosai, 1996; Hill, 1996), disease assessment especially in cancer patient (Bustin & Dorudi, 1998) and therapeutic monitoring (Desjardin *et al.*, 1999).

Thin layer chromatography (TLC) is a cheap and easy method used for the separation of compounds in mixtures based on their affinities for the adsorbent on the TLC plate (stationary phase) and the solubilities in different solvents (mobile phase). Such differences result in different rate of travel of each analyte up the plate guided by the capillary action of the solvent used. The identification can be done by comparing the retardation factor ( $R_f$  value = distance travelled by the spot /distance of the solvent front from the point of origin) of different spots with those of the standards running on the same plate. This technique is routinely used in biology for the analysis of homeostasis of lipids in prokaryotic cells with altered metabolisms (Hoischen *et al.*, 1997; Sandoval - Calderon *et al.*, 2009; Jyothikumar *et al.*, 2012).

RT-PCR analysis was conducted on JT672 to semi-quantify the controlled-expression of *pss* by *ptipA* promoter over a range of inducer concentrations. This is an important assay to ascribe the level of induction (hence the gene expression) to the added inducer in addition to validating the connection between the mutant phenotypes to the gene lesion. Finally, when carried out in combination with TLC analysis, this could help to establish the changing phospholipid profile of the mutant over different level of gene expression.

### **6.2.2 Identifying appropriate solvent system for phospholipid TLC**

In order to obtain nicely resolved spots of phospholipids on TLC plate, appropriate TLC solvent system(s) must be used. Two solvent systems were first identified i.e. (1) chloroform/methanol/water (65:25:4) (Matsumoto *et al.*, 1998) and (2) chloroform/methanol/acetic acid/water (80:12:15:4) (Jyothikumar *et al.*, 2012). The two solvent systems were used concurrently to identify/confirm several ambiguous spots resolved on either solvent system alone. Phospholipid samples were first extracted from *S. coelicolor* M145 grown for 24 hours (mid-log phase) at 30 °C

in liquid YEME (mid-log phase). The samples were then applied on three separate TLC plates each with appropriate phospholipid standards from Sigma (CL, PE, PG & PS). The first two TLC plates were then placed in tank containing either solvent system (1) or (2) whereas the third plate was run first in (1) and then (2) rotated 90° relative to the first solvent system to give a 2D TLC.

In solvent system (1) PE travelled the furthest up the plate followed by the co-migrated CL and PG spots with the least moving unknown phospholipid spot which appeared to run in parallel with the PS standard (Figure 48). We believed this spot was not the PS for two obvious reasons; firstly, PS is known to be a minor phospholipid component due to its rapid conversion to PE by Psd (Vance & Steenbergen, 2005) hence should not appear as such an intense spot. Secondly, this spot did not agree with the position of the PS standard in solvent system (2) and also in the 2D TLC (see later).

In solvent system (2), CL travelled the furthest with a certain degree of overlap with PE which appeared as the second fastest travelling phospholipid, followed by PG, a probable PS spot and finally the unknown major phospholipid spot (Figure 49). The faint PS spot seemed more agreeable with this phospholipid being a minor membrane component but remained to be verified. However, it is worth noting that a faint spot was sometimes already visible on that position before molybdenum blue staining, making its interpretation a little tricky. The slight overlap between CL and PE in solvent system (2) was confirmed via 2D TLC analysis developed in the combination of the two solvent systems (Figure 50). The 1D and 2D TLC analysis using the two solvent systems not only helped in confirming and identifying some of the uncertain spots (to rule out the unknown major spot as PS in solvent system (1) and to confirm the overlap between CL and PE in solvent system (2)) but guided us in choosing solvent system (2) for all subsequent TLC assays carried out on JT672 due to the better resolution of phospholipid spots developed in it compared to solvent system (1). Nonetheless, it was still impossible to conclusively identify all the spots by TLC.

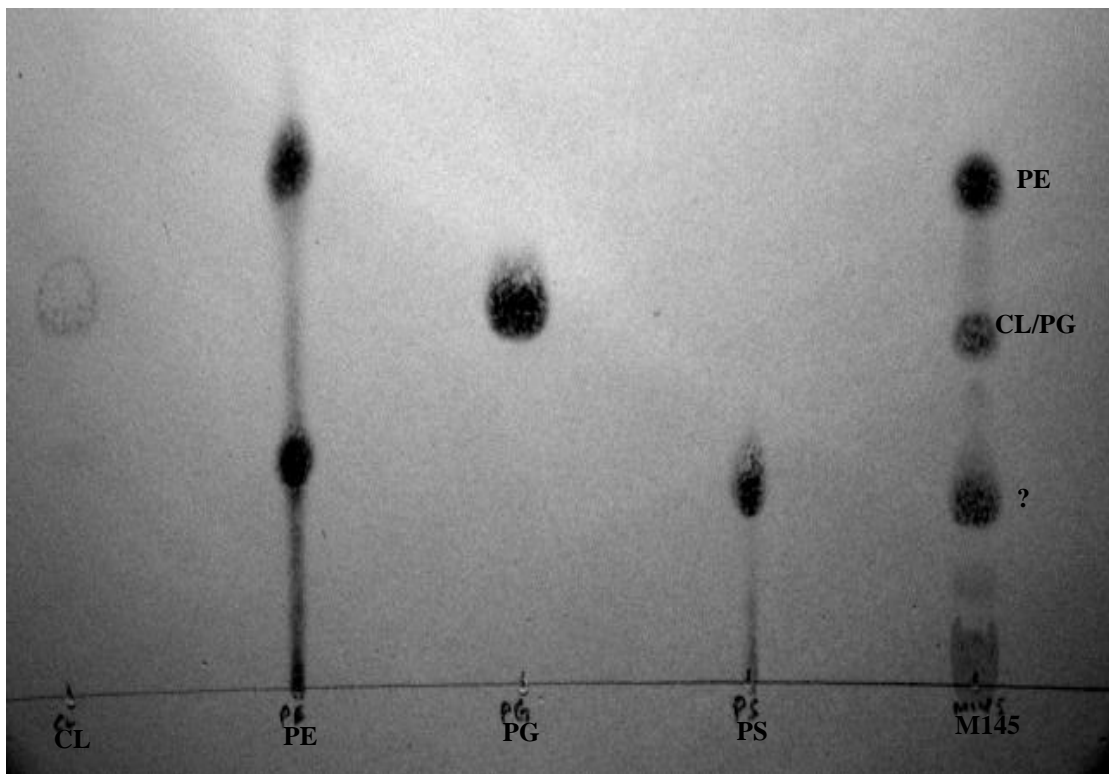


Figure 48: TLC analysis of phospholipid profile of mid-log phase M145 using four different standards, CL, PE, PG and PS developed in solvent system (1) chloroform/methanol/ water (65:25:4). PE migrated the furthest up the plate followed by CL/PG and finally an unknown phospholipid spot.

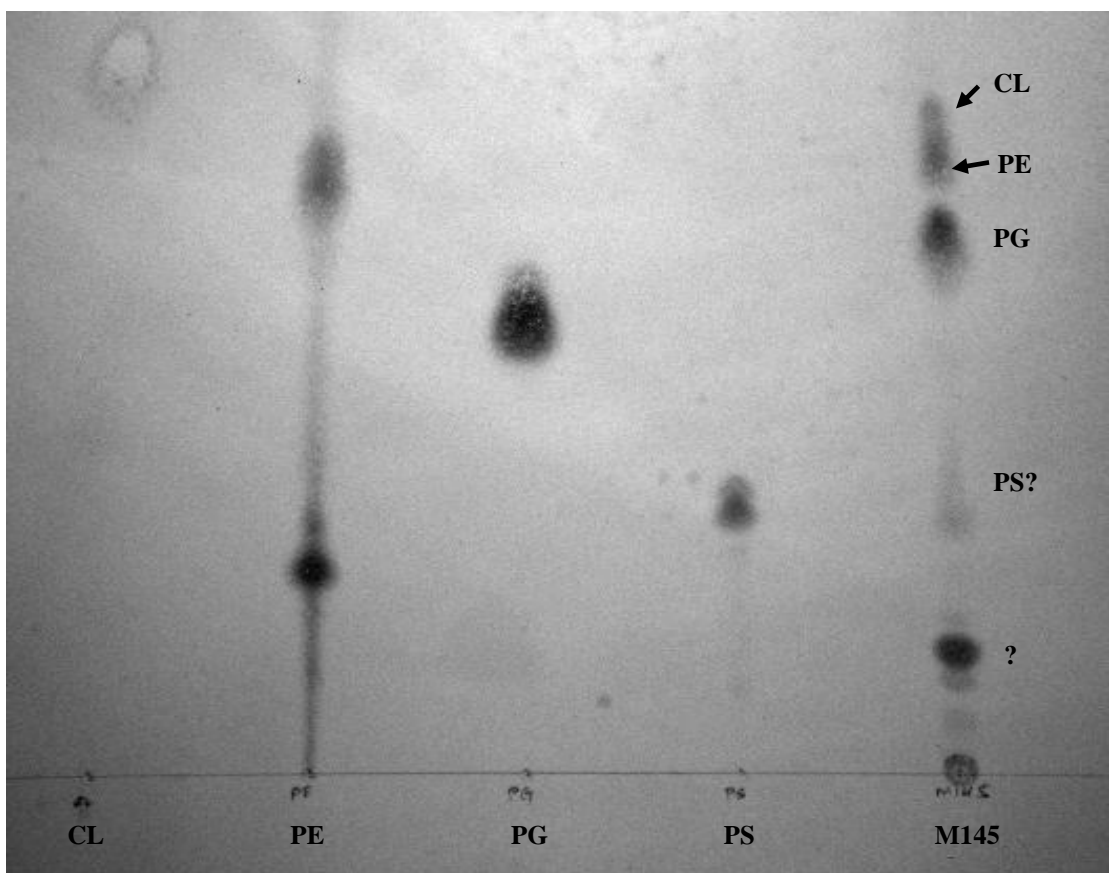


Figure 49: Thin layer chromatography analysis of phospholipids profile of mid-log phase M145 developed in solvent system (2) chloroform/methanol/acetic acid/water (80:12:15:4). CL migrated the furthest up the plate followed by PE with some degree of overlap between the two, PG, probable PS (faint spot) and finally the unknown phospholipid spot.

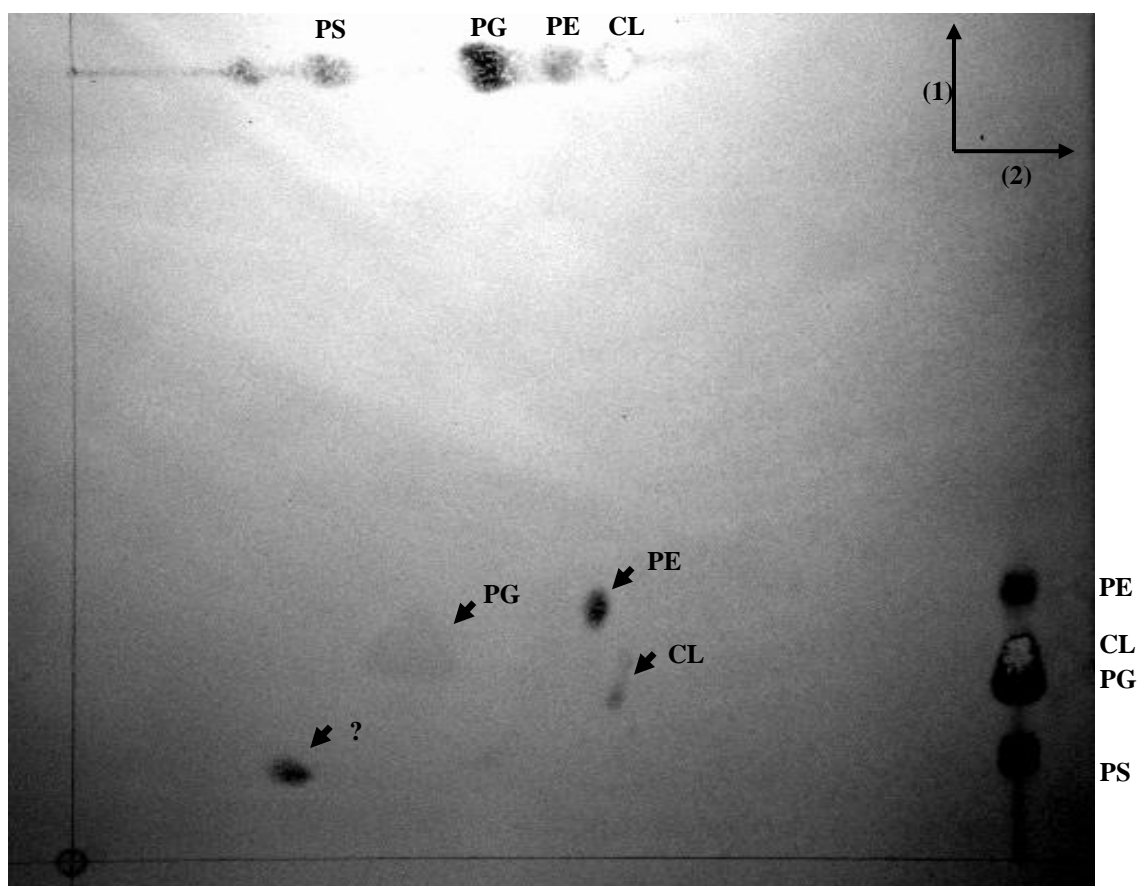


Figure 50: 2D TLC analysis of phospholipid profile of mid-log phase M145 developed in solvent system (1) chloroform/methanol/ water (65:25:4) followed by (2) chloroform/methanol/acetic acid/water (80:12:15:4). The use of the two solvent systems helped to confirm and corroborate several uncertain/unidentified spots developed in individual solvent system.



### 6.2.3 Controlled –expression of *pss* and corresponding phospholipid and RT-PCR profiles of JT672 ( $\Delta pss::apra'/ptipA-pss^+$ )

#### 6.2.3.1 Phospholipid and RT-PCR profiles of 3MA grown JT672

*S. coelicolor* mycelium grown on cellophane discs was harvested after 60 hours growth on 3MA at 30 °C. Phospholipid samples were extracted from 25mg of dry mass whereas the remaining mycelium was used for RNA extraction. All RNA samples were normalized at 100 ng per reaction prior to the start of the assay. RT-PCR was carried out using Qiagen® OneStep RT-PCR kit based on the optimized conditions described in Section 3.22. The entire assay was done in an RNase-free condition to prevent degradation of the samples. TLC analysis was conducted using solvent system (2).

RT- PCR analysis was carried out on RNA extracts of JT672 and the empty vector control M927 ( $pss^+/ptipA$ ) over four different concentrations of thiostrepton i.e. 0, 0.005, 0.05 and 0.5 µg/ml (Figure 51). The reverse transcription amplification was also done using *hrdB* primers to serve as internal control for the semi-quantitative measurements of *ptipA-pss* transcription as well as to gauge the quality of the RNA samples. Increasing concentration of thiostrepton resulted in all three sets of  $cDNA_{gene}/cDNA_{control}$  ratios being raised steadily indicating the thiostrepton-dependent induction of the *ptipA-pss*.

The non- zero values of all ratios at 0 µg/ml thiostrepton showed the significant level of basal activity of *ptipA* even in the absence of the inducer which was consistent with previous finding (Holmes *et al.*, 1993). The gene was already fully expressed at 0.05 µg/ml of thiostrepton as shown by the  $JT672_{pss}/M927_{pss}$  and  $JT672_{pss}/M927_{0\ thio}$  ratios of 1.27 and 1.20 respectively. However, the working concentration of 0.5 µg/ml was selected for use in all latter experiments (unless stated otherwise) due to previous observations of its ability to restore the phenotype of JT672 close to that of the wild type.

The concurrent TLC analysis done on the same mycelium samples revealed that the partial depletion of Pss resulted in the depletion of PE in JT672 which was restored at thiostrepton concentration of 0.05  $\mu\text{g/ml}$  or higher (Figure 52). Surprisingly, PE restoration also resulted in the simultaneous disappearance of PG spot probably because of the depletion of the common branch point substrate, cCDP-DAG needed by both the anionic and zwitterionic phospholipid biosynthetic pathways. The phospholipid profiles of both controls (M927 and M145) did not alter significantly over the different concentrations of inducer hence ruled out possible artefact in the assay. On a side note, some of the phospholipid spots appeared smeary and splotchy which is an inherent problem with TLC of solid medium grown bacteria culture (Klanbut, K. personal communication). Therefore, we decided to conduct further TLC analysis using liquid-grown JT672 instead.

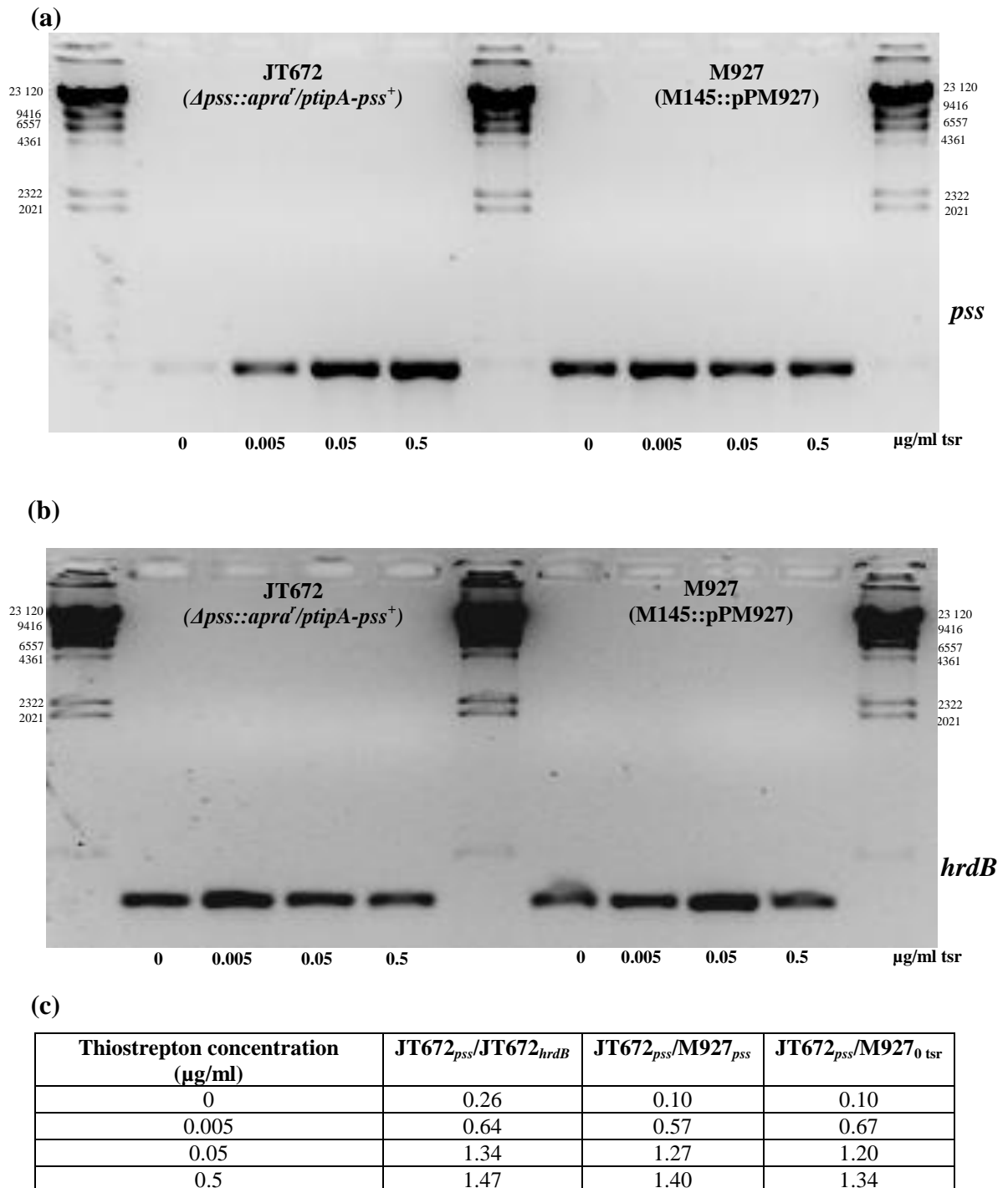


Figure 51: (a) RT-PCR profile of 3MA – grown JT672 and the empty vector control, M927 ( $pss^+/ptipA$ ) over four different concentrations of thiostrepton (0, 0.005, 0.05 and 0.5  $\mu\text{g/ml}$ ), (b) the RT-PCR validation controls using *hrdB* primers and (c) the  $\text{cDNA}_{\text{gene}}/\text{cDNA}_{\text{control}}$  ratio calculations used as a semi-quantitative measurement of the gene expression. All three sets of calculated ratios increased correspondingly with increasing thiostrepton concentration hence confirming the thiostrepton-dependent induction of the *ptipA-pss*.

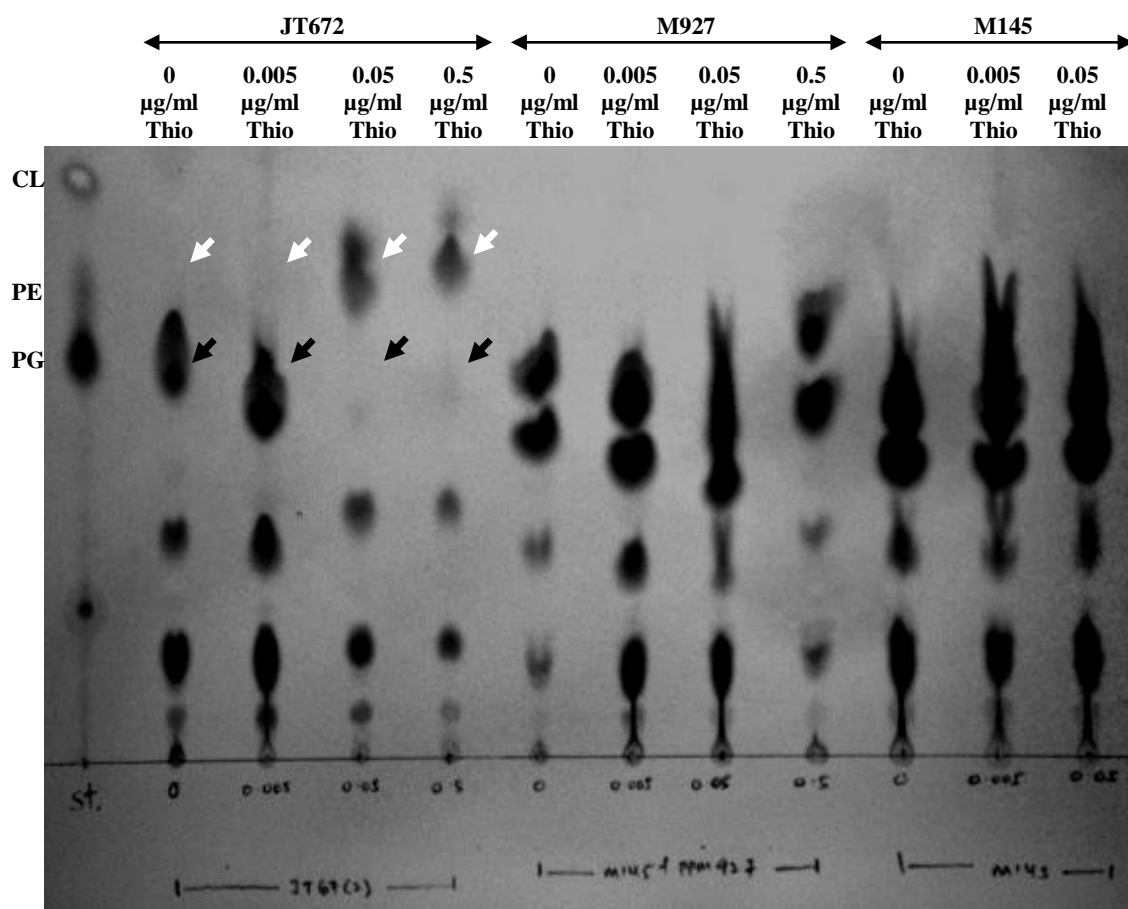


Figure 52: TLC profile of 3MA-grown JT672 over four different concentrations of thiostrepton (0, 0.005, 0.05 and 0.5  $\mu\text{g/ml}$ ). Depletion of Pss caused depletion of PE which was restored at thiostrepton concentration of 0.05  $\mu\text{g/ml}$  or higher (white arrows). Overexpression of *pss* ( $\geq 0.05$   $\mu\text{g/ml}$  thiostrepton) caused PE restoration at the expense of PG (black arrows).

### 6.2.3.2 Phospholipid and RT-PCR profiles of YEME grown JT672

After obtaining the phospholipid profile of solid-grown JT672, we were set to investigate the TLC profile of liquid-grown mutant which we believed would differ significantly based on previous work with ClsA (Jyothikumar *et al.*, 2012). *S. coelicolor* mycelium (100 mg) grown in liquid YEME was harvested after 24 hours (mid-log phase) for phospholipid extraction. TLC analysis was carried out on the liquid grown mycelium using solvent system (2). The phospholipid profile of JT672 was investigated in the absence and presence of 0.5 µg/ml thiostrepton. M145 (wild type) and M927 (empty vector control) were both used as controls in the analysis. Thiostrepton was not added to wild type M145 since it did not possess the gene that conferred resistance to this antibiotic.

Depletion of Pss in liquid-grown JT672 caused an altered phospholipid profile vis-à-vis the wild types (Figure 53). In the absence of thiostrepton, the phospholipid spot which corresponded to the PE standard was absent from JT672. The addition of 0.5 µg/ml of thiostrepton restored PE. As predicted, liquid-grown mutant displayed a different TLC pattern compared to the solid-grown mutant where depletion of Pss also caused the concurrent exhaustion of the anionic PG. The spot was not restored with the addition of 0.5 µg/ml thiostrepton. M927 displayed a phospholipid profile which resembled the wild type and remained unaltered with the addition of 0.5 µg/ml of thiostrepton further ruling out any possible artefact in the assay.

The absence of PG spot even after the restoration of the PE using 0.5 µg/ml of thiostrepton led to the same assumption of possible depletion of the natural substrate of PgsA i.e. CDP-DAG due to probable over-expression of *pss* whose gene product utilizes the same substrate for PS synthesis. Hence, matching RT-PCR of *pss* and phospholipid profiles in liquid YEME were investigated over a range of thiostrepton concentrations (0, 0.005, 0.05 and 0.5 µg/ml). RNA and phospholipids were extracted from JT672, M927 and M145 in mid-log phase for RT-PCR and TLC analyses as described previously.

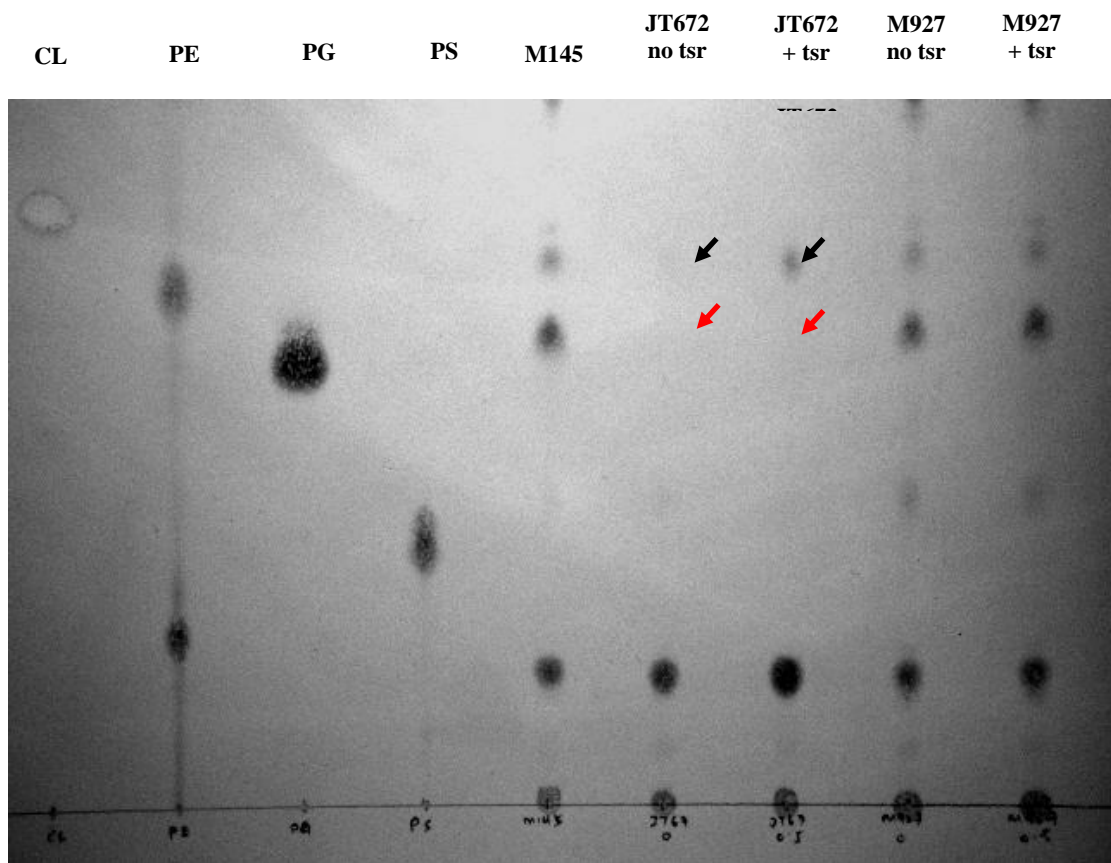
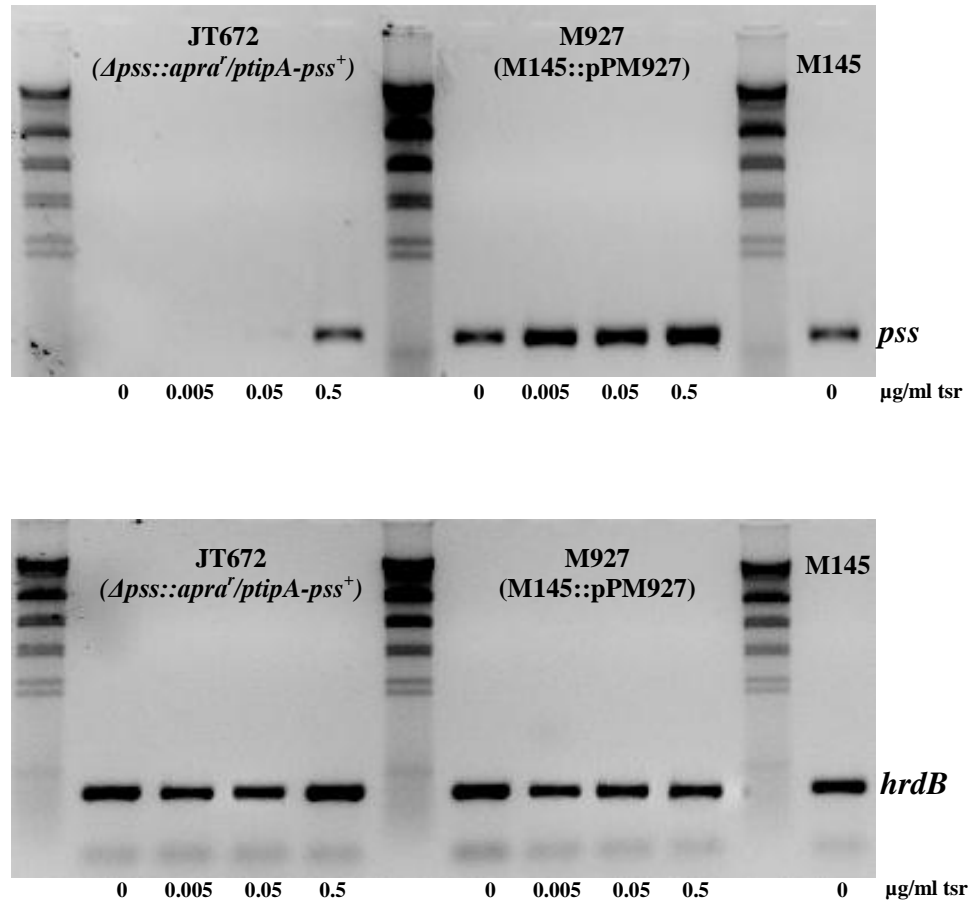


Figure 53: TLC profile of YEME-grown JT672 in the absence and presence of 0.5  $\mu\text{g/ml}$  thiostrepton. Depletion of Pss caused depletion of not only PE (black arrows) but the anionic phospholipid, PG (red arrow). The addition of 0.5  $\mu\text{g/ml}$  thiostrepton restored the PE spot in JT672 but not PG.

(a)



(b)

Thioestrepton concentration ( $\mu\text{g/ml}$ )	JT672 <sub>pss</sub> /M927 <sub>pss</sub>	JT672 <sub>pss</sub> /M927 <sub>0 tsr</sub>	JT672 <sub>pss</sub> /M145 <sub>0 tsr</sub>	JT672 <sub>pss</sub> /JT672 <sub>hrdB</sub>
0	0	0	0	0
0.005	0	0	0	0
0.05	0.07	0.06	0.11	0.08
0.5	0.55	0.85	0.99	0.48

Figure 54: Effect of alteration of *pss* expression on the RT-PCR profile of YEME-grown JT672. (a) RT-PCR analysis of JT672 over a concentration gradient of thioestrepton (0 to 0.5  $\mu\text{g/ml}$ ) using M927 and M145 as the controls with (b) the semi-quantitative measurements of *pss* expression based on various calculated expression ratios, the  $\text{cDNA}_{\text{gene}}/\text{cDNA}_{\text{control}}$ . All four sets of calculated ratios increased correspondingly with increasing thioestrepton concentration hence confirming the thioestrepton-dependent induction of the *ptipA-pss*.

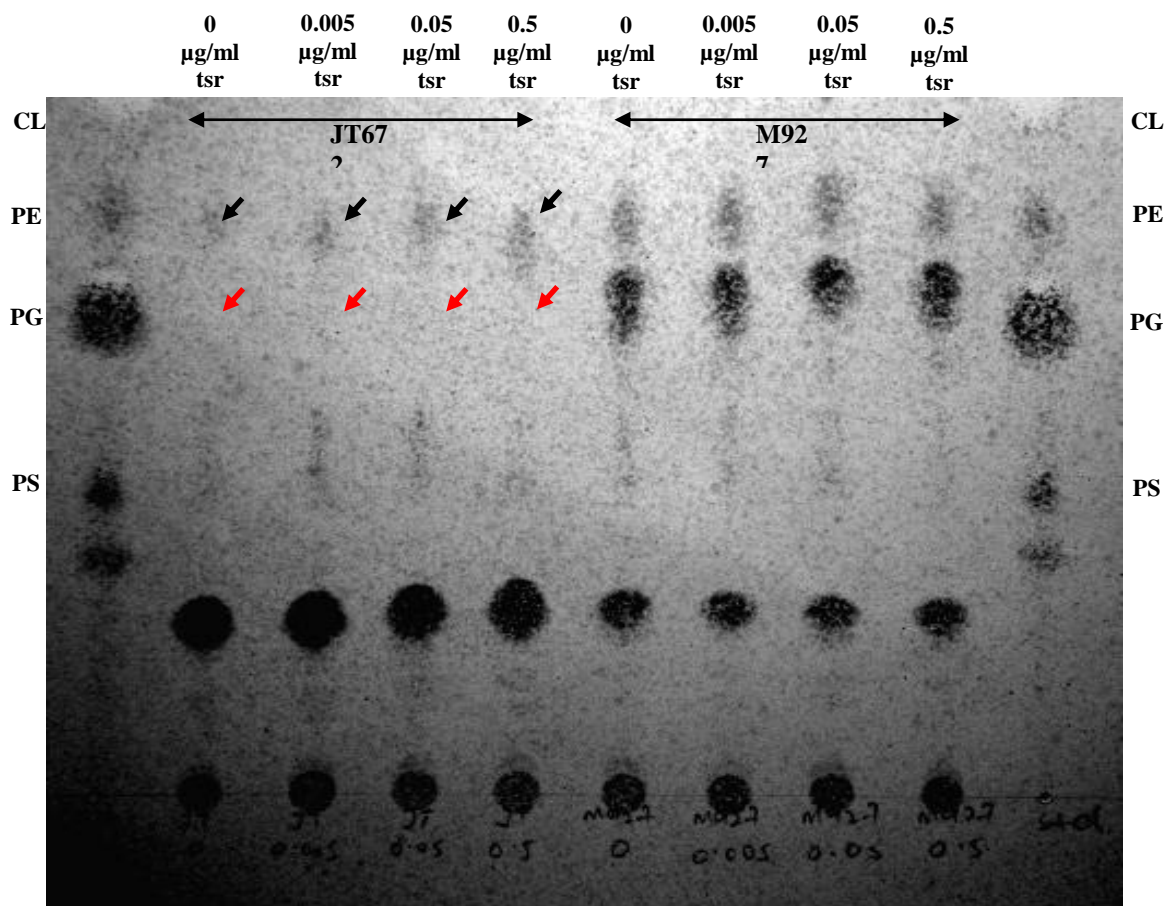


Figure 55: Effect of alteration of *pss* expression on TLC profiles of YEME-grown JT672 over four different concentrations of thiostrepton (0, 0.005, 0.05 and 0.5 µg/ml). Sequential increase in the size of PE spot (black arrows) with increasing concentration of thiostrepton was observed. PG spot was however not restored over the concentration gradient (red arrows).



RT-PCR analysis revealed the thiostrepton – dependent expression of *pss* by the *ptipA* promoter in JT672 as shown by the sequential increase of the intensity of the cDNA bands in gel electrophoresis (Figure 54). All four sets of the relative expression ratios,  $\text{cDNA}_{\text{gene}}/\text{cDNA}_{\text{control}}$  were elevated in correspond to the increase in inducer concentration. This corroborated with the TLC analysis which showed increasing size and intensity of the PE spot over the concentration gradient of thiostrepton.

Unlike the samples harvested from 3MA (Figure 51(a)), the *ptipA* promoter appeared to be fully-repressed at lower concentrations of thiostrepton ( $\leq 0.005$   $\mu\text{g/ml}$ ). Surprisingly however, PE spot was still visible on the TLC plate even at those concentrations (Figure 55). At 0.5  $\mu\text{g/ml}$  of thiostrepton, *pss* was not overexpressed unlike 3MA grown JT672 at the same concentration. With JT672<sub>*pss*</sub>/M145<sub>0 thio</sub> ratio of 0.99, the expression of *pss* was at a similar level compared to the wild type. Nevertheless, PG spot was still not replenished over the concentration gradient as revealed by the TLC analysis (Figure 55).

In view of the inability to restore the phospholipid profile to that of the wild type even at 0.5  $\mu\text{g/ml}$  of thiostrepton, three further concentrations of thiostrepton i.e. 5, 25 and 50  $\mu\text{g/ml}$  were tested on JT672 (Figure 56). Indeed, PG spot appeared over these high concentrations of inducer. Concurrent RT-PCR analysis showed the overexpression of *pss* peaking at 5  $\mu\text{g/ml}$  and declining steadily thereafter from 25 to 50  $\mu\text{g/ml}$  with JT672<sub>*pss*</sub>/M145<sub>0 thio</sub> ratio of 2.91, 2.09 and 1.78 respectively (Figure 57). The same assay also revealed that full physiological expression was achieved at 0.5  $\mu\text{g/ml}$  with the JT672<sub>*pss*</sub>/M145<sub>0 thio</sub> ratio of 1.03 implying that restoration of PG was in fact only possible in the overexpressed state.

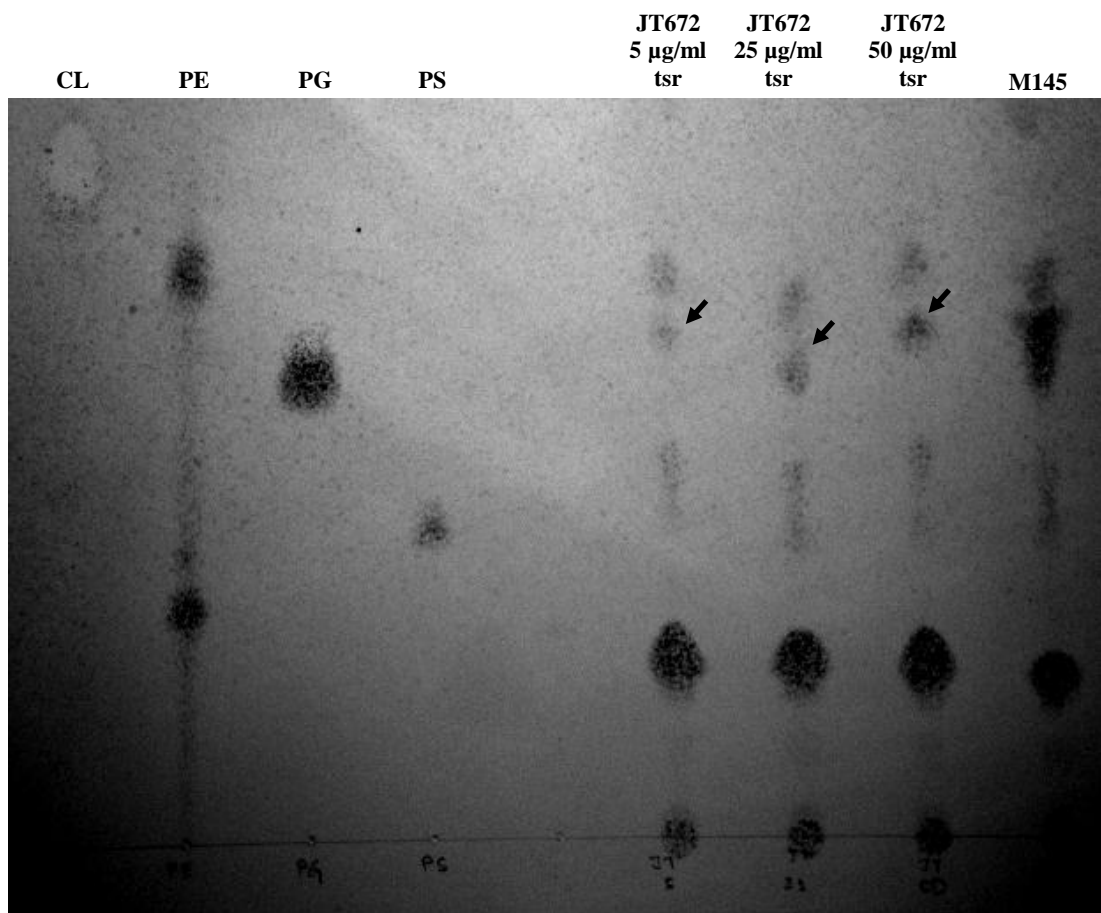
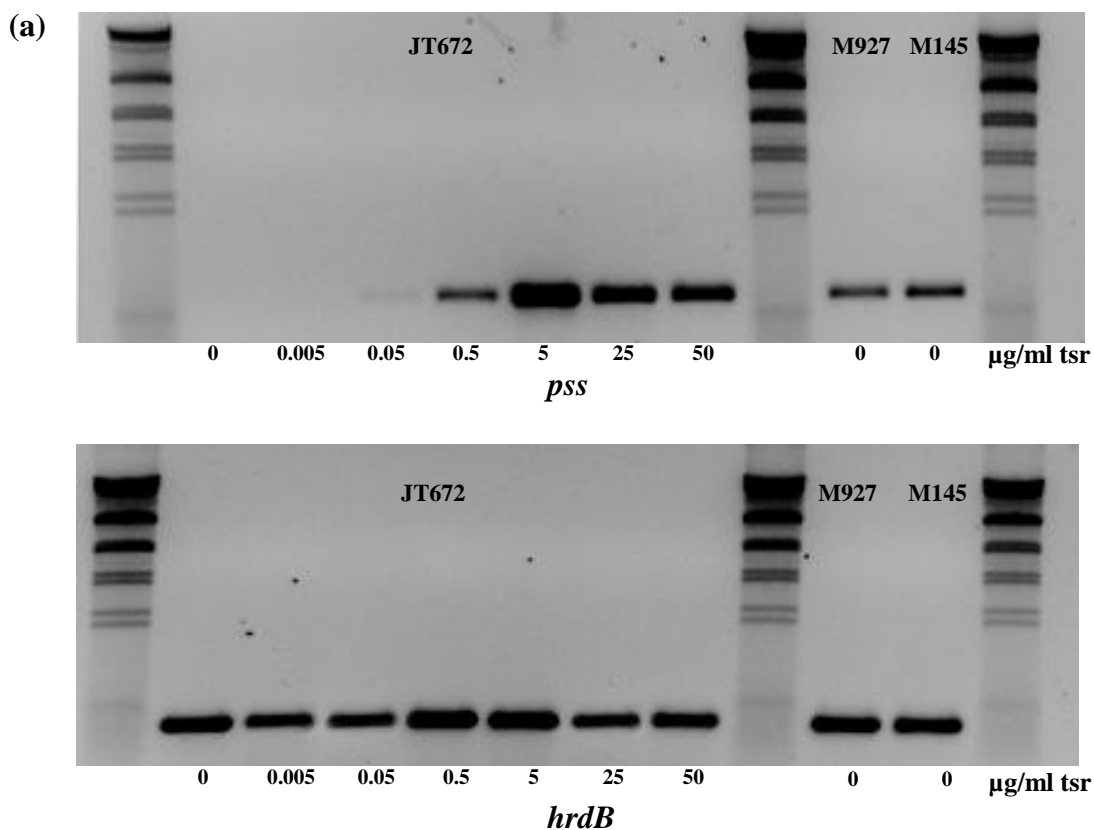


Figure 56: Thioester concentrations of 5 to 50 µg/ml restored both PE and PG productions in YEME-grown JT672 (black arrows).



(b)

Thiostrepton concentration (µg/ml)	JT672 <sub>pss</sub> /M927 <sub>0 tsr</sub>	JT672 <sub>pss</sub> /M145 <sub>0 tsr</sub>	JT672 <sub>pss</sub> /JT672 <sub>hrdB</sub>
0	0	0	0
0.005	0	0	0
0.05	0.05	0.04	0.04
0.5	1.27	1.03	0.45
5	3.55	2.91	1.29
25	2.55	2.09	1.97
50	2.17	1.78	1.02

Figure 57: (a) RT-PCR analysis of JT672 over a concentration gradient of thiostrepton (0 to 50 µg/ml) using 100 ng of RNA extract and (b) the semi-quantitative measurements of *pss* expression by *ptpA* based on various calculated expression ratios,  $\text{cDNA}_{\text{gene}}/\text{cDNA}_{\text{control}}$ . The expression of *pss* was at a similar level compared to M145 at 0.5 µg/ml of thiostrepton and the peak expression was attained at 5 µg/ml before declining steadily thereafter.

#### 6.2.4 Metabolism of the anionic and zwitterionic phospholipids in *S. coelicolor*

To understand the metabolism of the anionic (CL and PG) and zwitterionic (PE) phospholipids in *S. coelicolor*, a similar TLC analysis was carried out on the ClsA mutant, RJ118b ( $\Delta clsA::aprA^f/tcp830-clsA$ ) (Jyothikumar *et al.*, 2012). As seen in Figure 58, depletion or partial depletion of the anionic CL in the uninduced mutant caused simultaneous depletion of the zwitterionic PE and the accumulation of PG. The induction of *clsA* by *tcp830* in the presence of 100 ng/ml of atc resulted in the increased intensity of both CL and PE spots and diminishing PG which served as substrate for ClsA in the biosynthesis of CL. Taking this observation together with that seen previously in JT672, we believe a homeostatic mechanism exists to regulate the balance of the anionic/zwitterionic phospholipids in *S. coelicolor* which is crucial in maintaining the overall membrane integrity and fluidity. This concurred with observations made previously in *E. coli* (Shibuya, 1992; Saha *et al.*, 1996a).

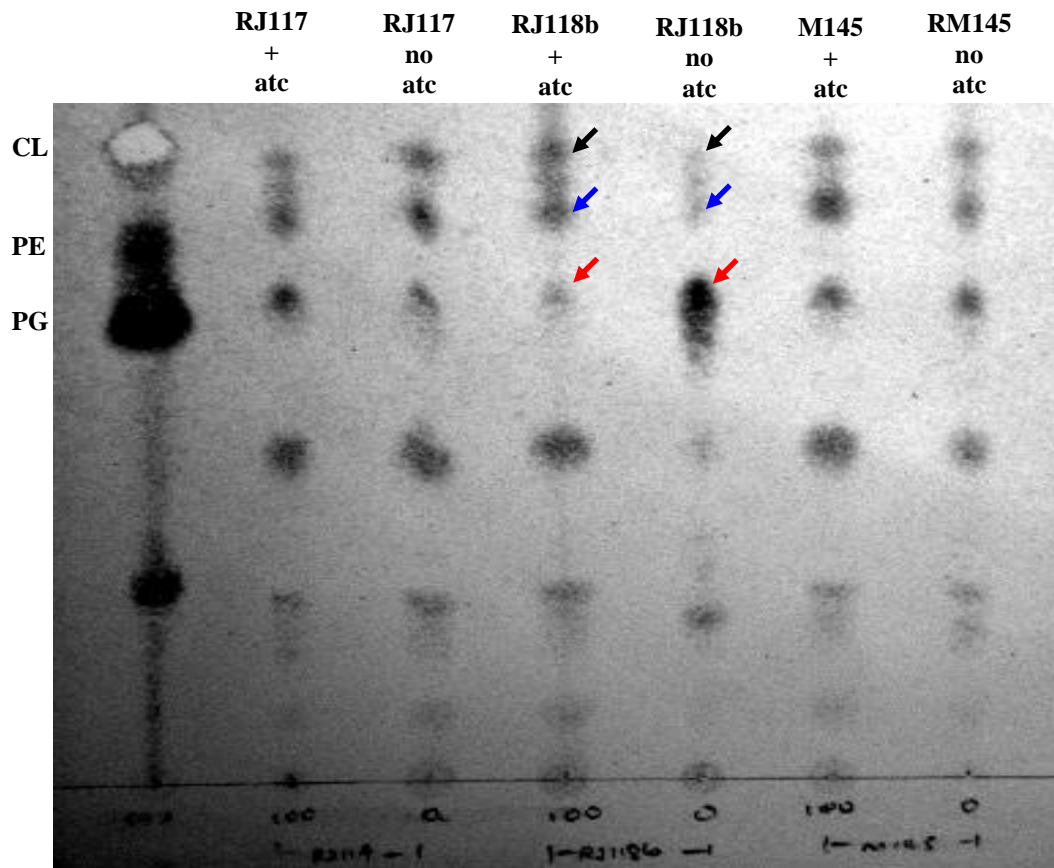


Figure 58: TLC analysis of liquid - grown mid-log phase RJ118b ( $\Delta clsA::apra^r/tcp830-clsA$ ) with or without 100 ng/ml of atc, RJ117 ( $clsA^+/tcp830$ ) and M145. In the uninduced RJ118b, both CL and PE spots were lower in intensity compared to the controls whereas the addition of 100 ng/ml of atc restored both phospholipid spots simultaneously (black & blue arrows respectively). Partial depletion of both CL and PE also caused the accumulation of PG in the uninduced RJ118b which diminished after the addition of atc due to its rapid conversion to CL in the induced mutant.

### 6.3 Screening for mutant phenotypes on 3MA under different growth conditions (temperature, KCl and sucrose concentrations)

With the clear display of morphological and physiological mutant characteristics of JT672 when grown on 3MA, this growth medium was chosen for all subsequent phenotypic characterization assays. *S. coelicolor* M145 and M927 (empty integrative vector control) were used as the controls for comparison purposes. Either 0.05 or 0.5 µg/ml of thiostrepton were used to induce the *ptipA-pss* in order to suppress any observed mutant phenotypes in JT672. Due to the inhibitory effect of thiostrepton at concentration of 0.5 µg/ml or higher, only 0.05 µg/ml was added to the growth medium if M145 had to be grown on the same plate with both JT672 and M927. In all other cases, 0.5 µg/ml would be added since this was the concentration that could restore JT672 closest to the wild phenotype.

No significant difference was observed between JT672 and the controls when grown under different temperatures in both absence and presence of thiostrepton i.e. they all grew at 37 °C and 40 °C but not at 50 °C (Figure 59). The effect of temperature on membrane fluidity would be discussed further in the discussion section. JT672 had reduced osmotolerance to KCl (Figure 60) and sucrose (Figure 61) which was evident with diminishing growth of the uninduced mutant at higher concentrations of both compounds. In the case of KCl (but not sucrose), the osmotolerance of JT672 was *pss* expression-dependence since the osmotolerance was restored at 0.5 µg/ml thiostrepton (Figure 62).

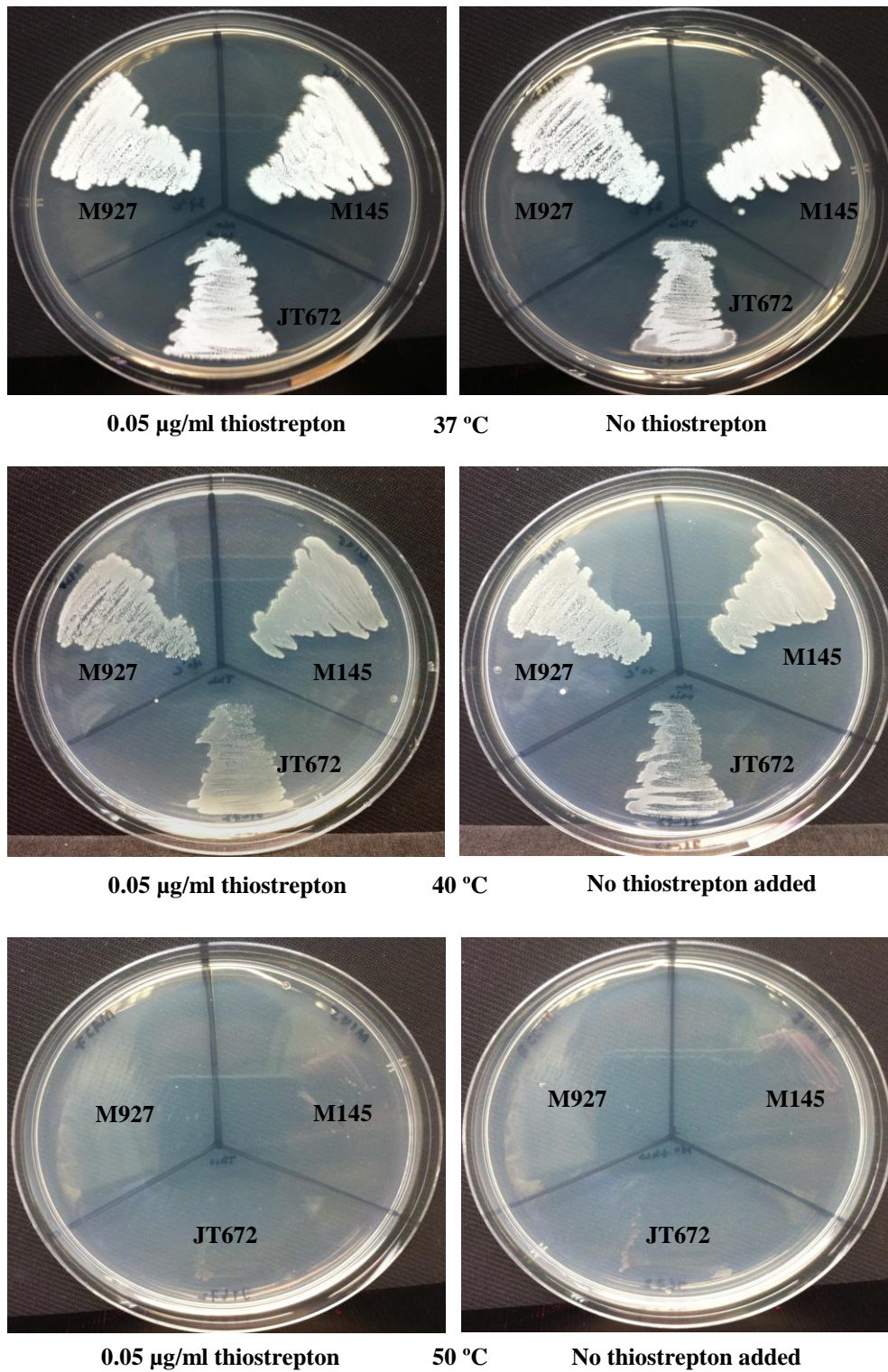
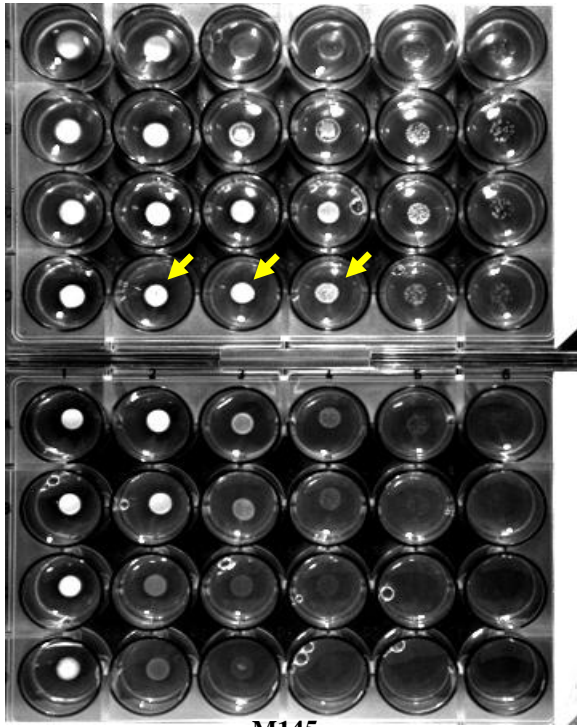


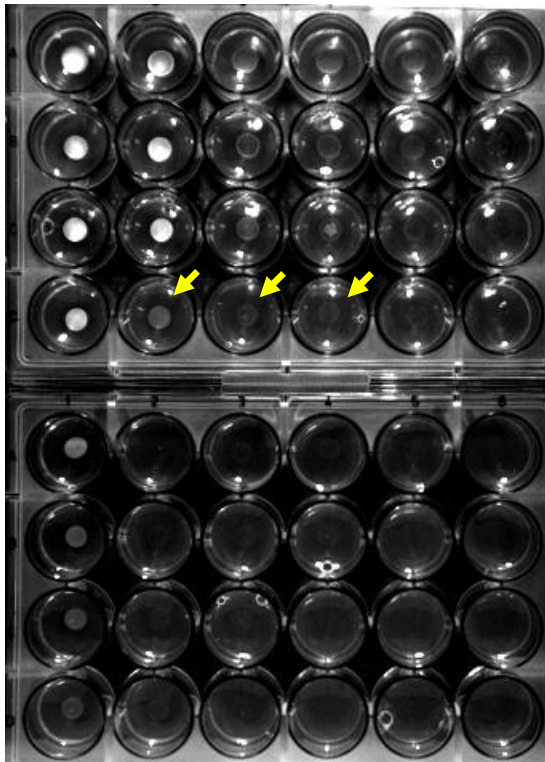
Figure 59: Effect of different incubation temperatures (37 °C, 40 °C and 50 °C) on growth of JT672 in the absence and presence of thiostrepton. JT672, M927 and M145 all grew at 37 °C, 40 °C but not 50 °C. There was no significant difference in the adaption to different growth temperature between JT672 and the controls.





M145

KCl (M)	Spore stock dilution →					
	0	10 <sup>-1</sup>	10 <sup>-2</sup>	10 <sup>-3</sup>	10 <sup>-4</sup>	10 <sup>-5</sup>
0.1						
0.2						
0.3						
0.4						
0.5						
0.6						
0.7						



JT672



JT672 + 0.5 µg/ml thiostrepton



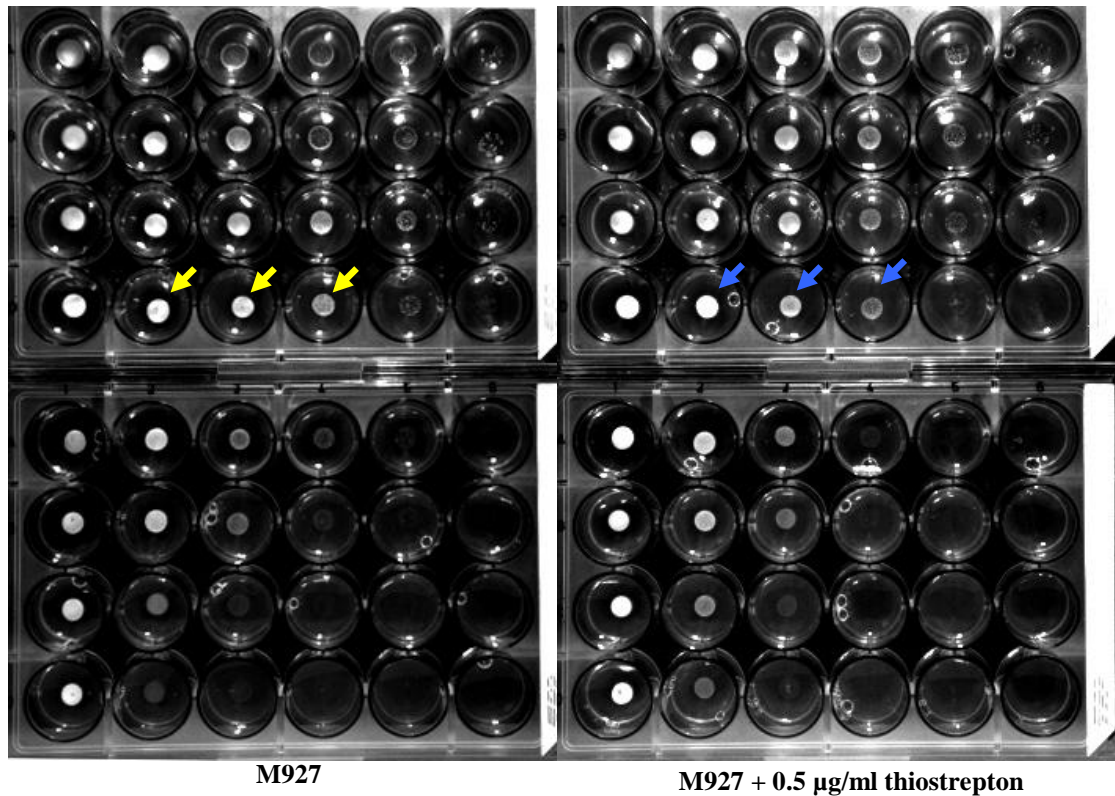
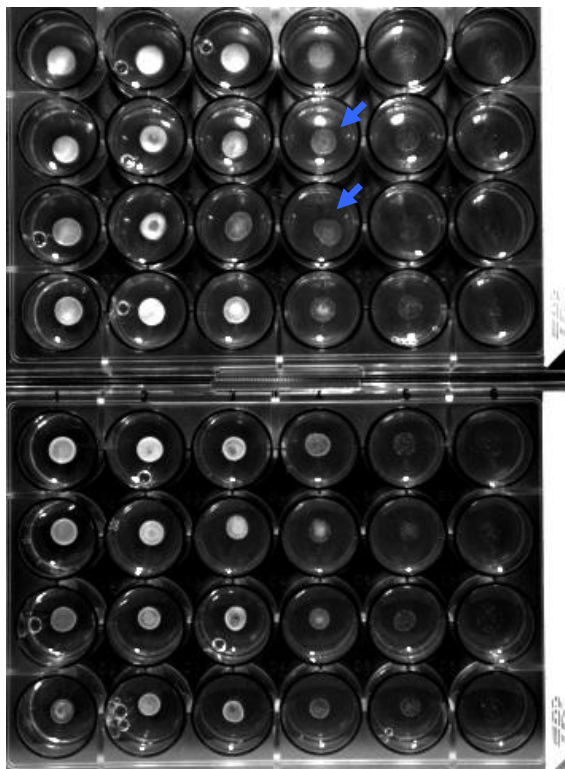
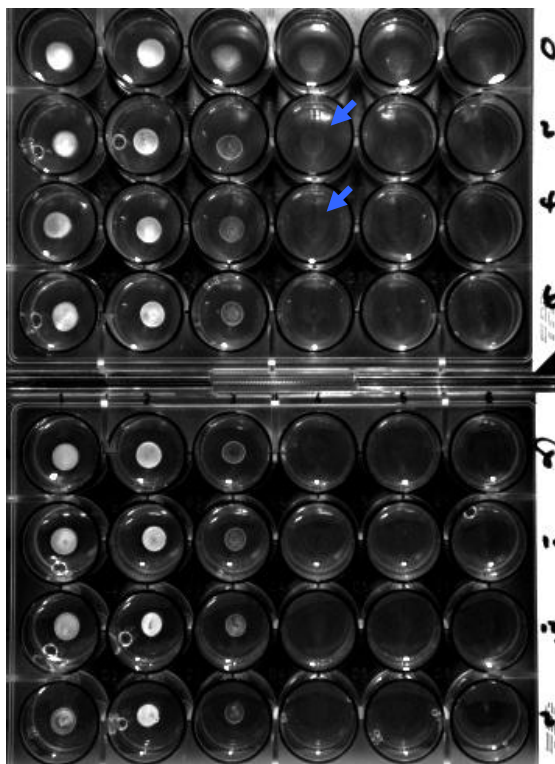


Figure 60: Effect of increasing concentration of KCl on growth of JT672 in the absence and presence of thiostrepton. Approximately  $5 \times 10^5$  starting spores of each strain were grown on 3MA with different concentrations of KCl (0, 0.1, 0.2, 0.3, 0.4, 0.5, 0.6 and 0.7 M) before being diluted accordingly ( $10^{-1}$ ,  $10^{-2}$ ,  $10^{-3}$ ,  $10^{-4}$ , and  $10^{-5}$ ) and spotted onto the respective dilution wells. JT672 had reduced tolerance to KCl with reduced growth density apparent in the dilution series (yellow arrows). Osmotolerance of this mutant was restored with the addition of 0.5 µg/ml thiostrepton (blue arrows).

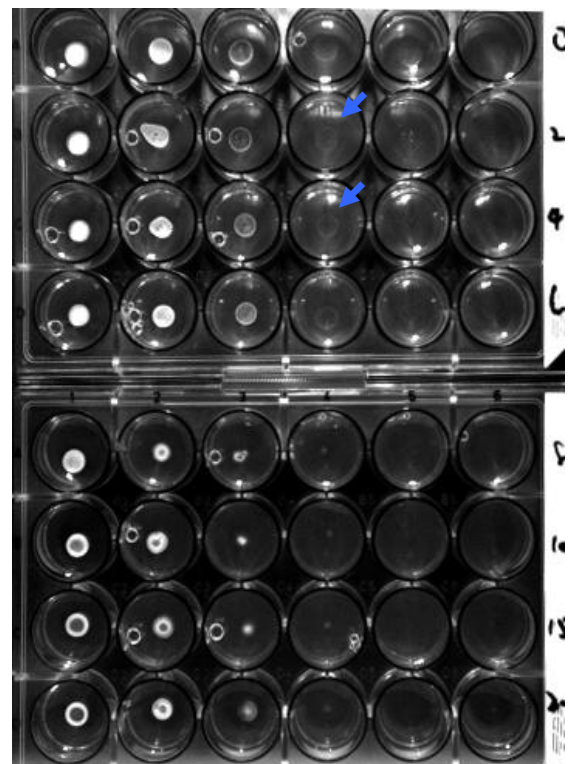


M145

Sucrose (%)	Spore stock dilution →					
	0	10 <sup>-1</sup>	10 <sup>-2</sup>	10 <sup>-3</sup>	10 <sup>-4</sup>	10 <sup>-5</sup>
2						
4						
6						
8						
10						
15						
20						



JT672



JT672 + 0.5 µg/ml thiostrepton

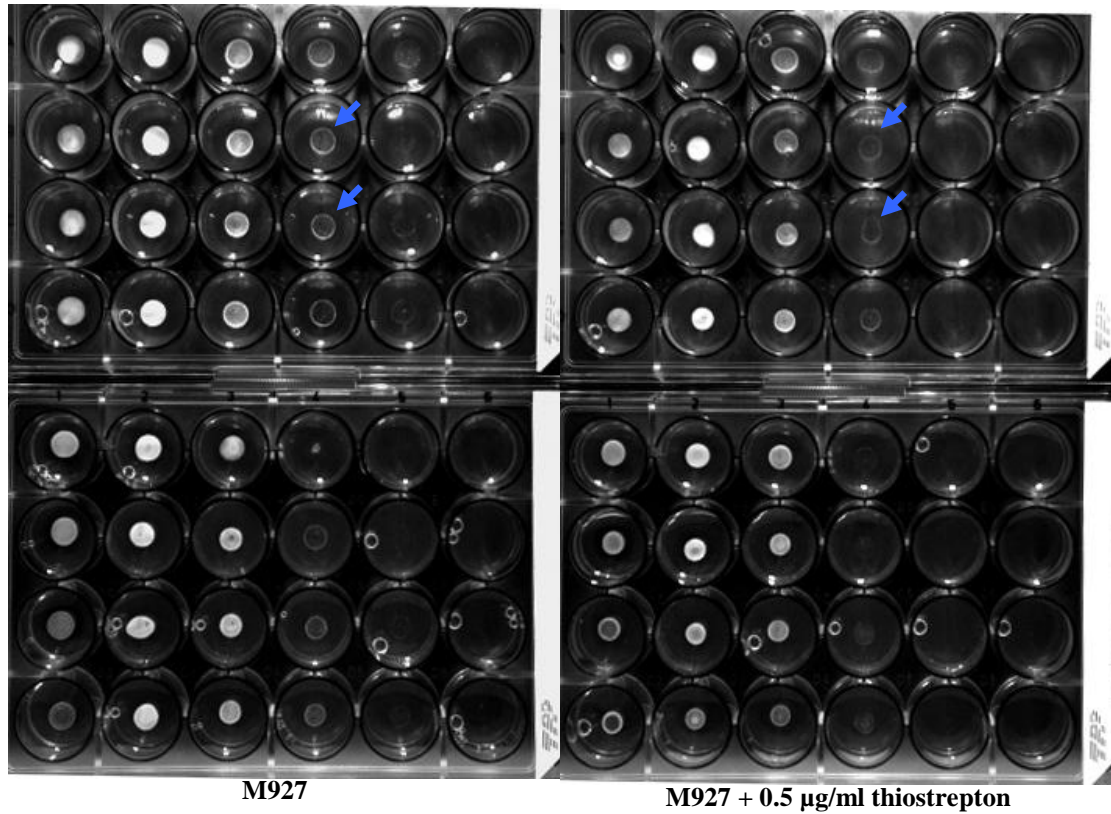


Figure 61: Effect of increasing concentration of sucrose on growth of JT672 in the absence and presence of thioestrepton. Approximately  $5 \times 10^5$  starting spores of each strain were grown on 3MA with different concentrations of sucrose (0, 2, 4, 6, 8, 10, 15 and 20 %) before being diluted accordingly ( $10^{-1}$ ,  $10^{-2}$ ,  $10^{-3}$ ,  $10^{-4}$ , and  $10^{-5}$ ) and spotted onto the respective dilution wells. JT672 had slightly reduced tolerance to sucrose with reduced growth density apparent in the dilution series (blue arrows). Such subservient phenotype was not reversed with the addition of 0.5  $\mu\text{g/ml}$  thioestrepton.



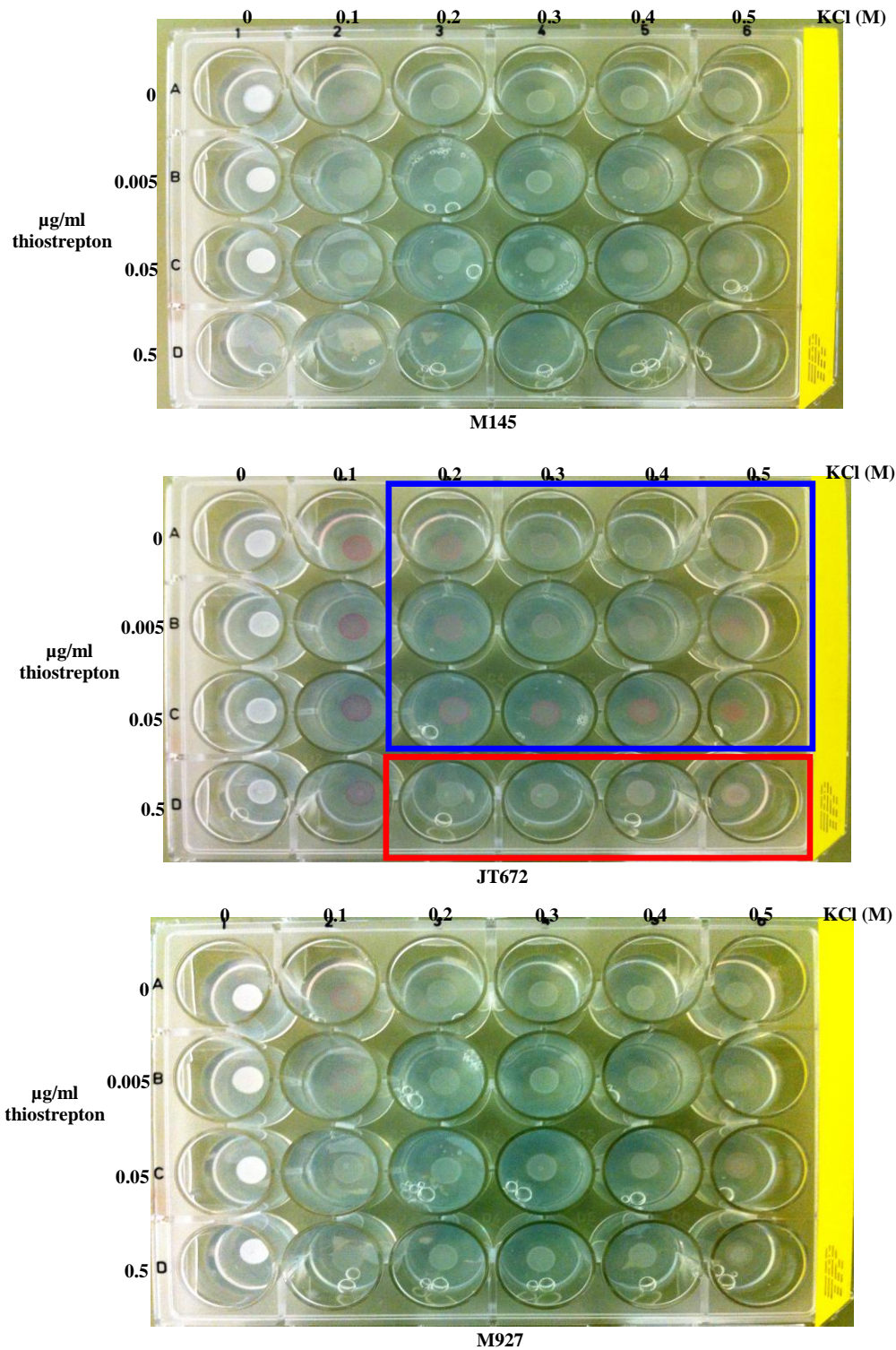


Figure 62: Effect of controlled-expression of *pss* on KCl osmotolerance in JT672. Approximately  $5 \times 10^5$  spores were grown on 3MA with increasing concentrations of KCl (0, 0.1, 0.2, 0.3, 0.4, and 0.5) against increasing concentration of thiostrepton (0, 0.005, 0.05, 0.5 µg/ml). JT672 had reduced tolerance to KCl at low level of *pss* expression ( $\leq 0.05$  µg/ml of thiostrepton) (Blue rectangle). Osmotolerance was restored with the addition of 0.5 µg/ml thiostrepton (Red rectangle). M145 could not grow in 0.5 µg/ml of thiostrepton due to absence of the resistance gene.

#### **6.4 Spore sensitivity assay**

Phospholipids play multiple roles in various cellular processes, primarily in forming the membrane bilayer that serves as permeability barrier of cell as well as the supporting matrix for vast arrays of proteins involved in important metabolic processes. Therefore, depletion or alteration of any important component, in the case of JT672, PS and PE could detrimentally affect the balance in the membrane composition causing the mutant to be more susceptible to external growth pressures. These external pressures which were thought to affect the cell membrane or cell wall integrity were investigated i.e. lysozyme sodium dodecyl sulfate (SDS), DMSO, heat treatment at 75 °C and sonication.

There was no significant difference observed between JT672 and the controls in terms of spore sensitivity to lysozyme (a peptidoglycan hydrolase) (Figure 64), DMSO (polar aprotic solvent) (Figure 65) and sonication (Figure 67). The mutant had increased sensitivity to SDS (an anionic surfactant) (Figure 63) and slightly raised tolerance to heat (Figure 66) compared to the controls. However, the adaption to both external factors was not altered by the addition of thiostrepton.

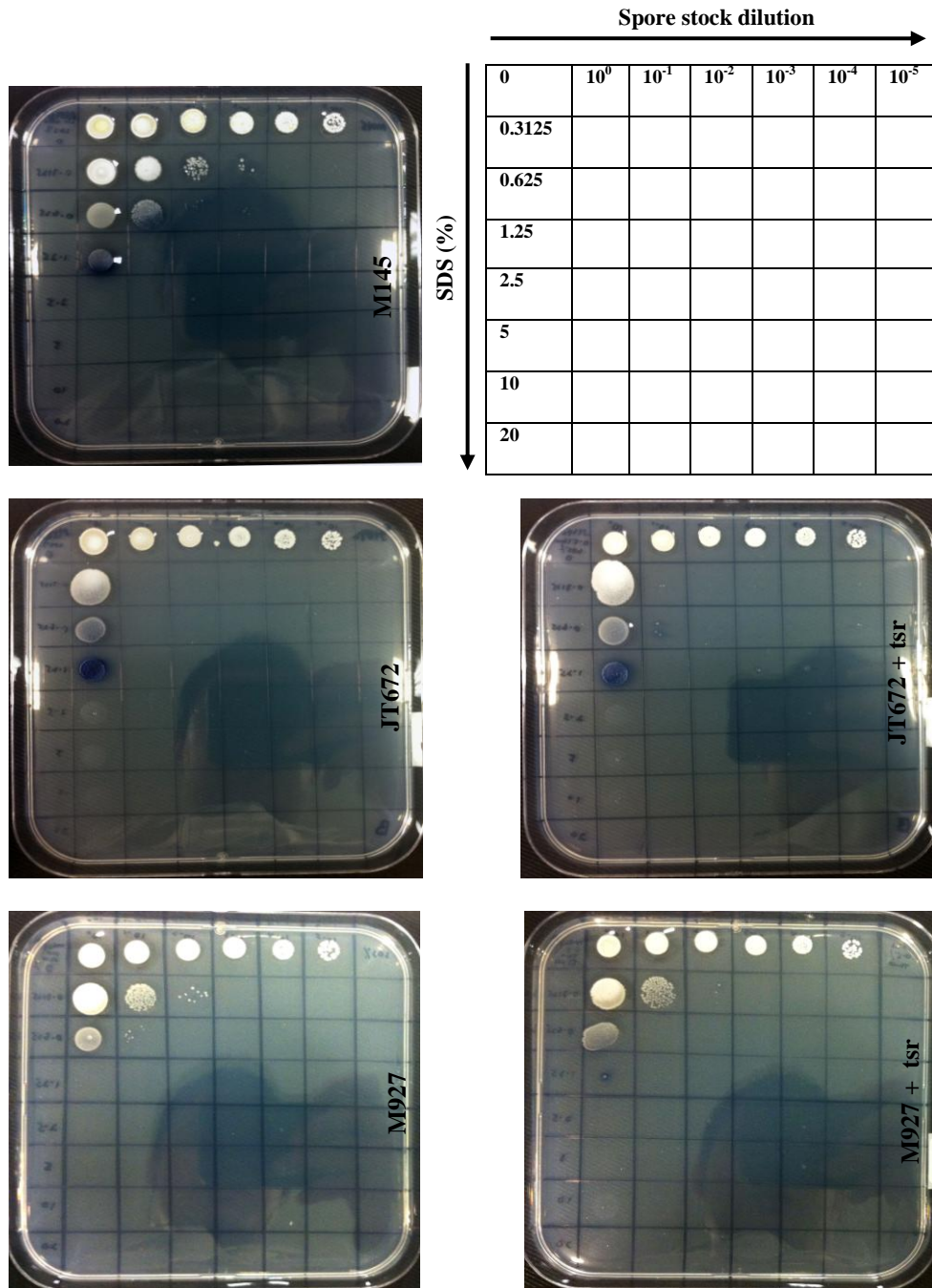


Figure 63: SDS sensitivity assay conducted on JT672 using M145 and M927 as controls. Approximately  $5 \times 10^5$  starting spores of each strain were pretreated with increasing concentration of SDS (0.3125, 0.625, 1.25, 2.5, 5, 10, 20 %) and spotted onto the  $10^0$  column. Spores serial dilutions were done accordingly ( $10^{-1}$ ,  $10^{-2}$ ,  $10^{-3}$ ,  $10^{-4}$ , and  $10^{-5}$ ) for each concentration before being spotted onto the respective dilution columns on the 3MA plates. JT672 had increased susceptibility to SDS as seen in reduction of growth density compared to M145 and M927. This was apparent with the spore dilution series corresponding to 0.3125 and 0.625% SDS. This phenotype was not reversed by the addition of 0.5  $\mu\text{g/ml}$  thiostrepton. Surprisingly, M927 did not grow beyond 0.625% SDS.

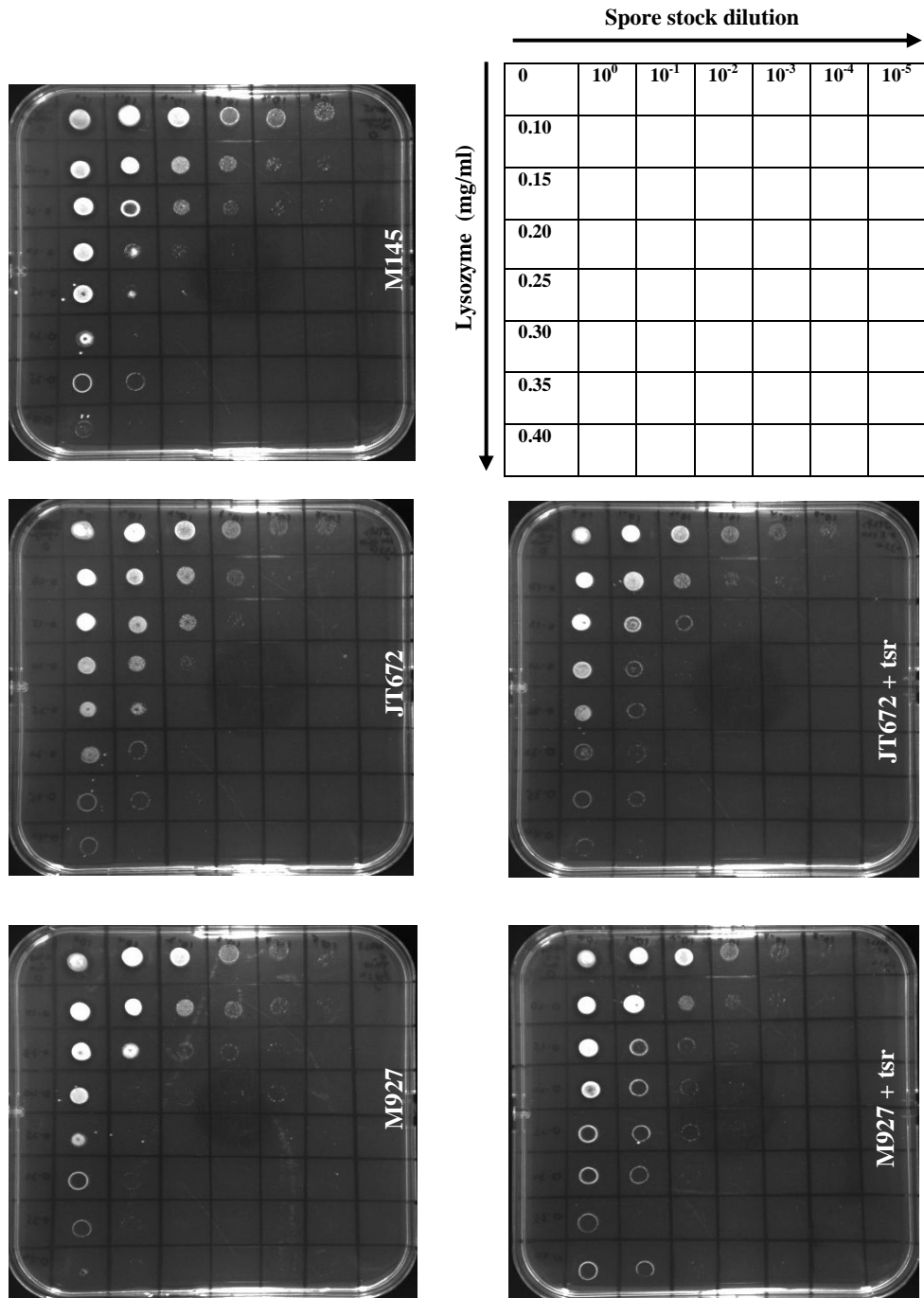


Figure 64: Lysozyme sensitivity assay conducted on JT672 using M145 and M927 as controls. Approximately  $5 \times 10^5$  starting spores of each strain were pretreated with increasing concentration of lysozyme (0, 0.10, 0.15, 0.20, 0.25, 0.30, 0.35, 0.40 mg/ml) and spotted onto the  $10^0$  column. Spores serial dilutions were done accordingly ( $10^{-1}$ ,  $10^{-2}$ ,  $10^{-3}$ ,  $10^{-4}$ , and  $10^{-5}$ ) for each concentration before being spotted onto the respective dilution columns on the 3MA plates. No significant difference was observed between JT672 and the controls.

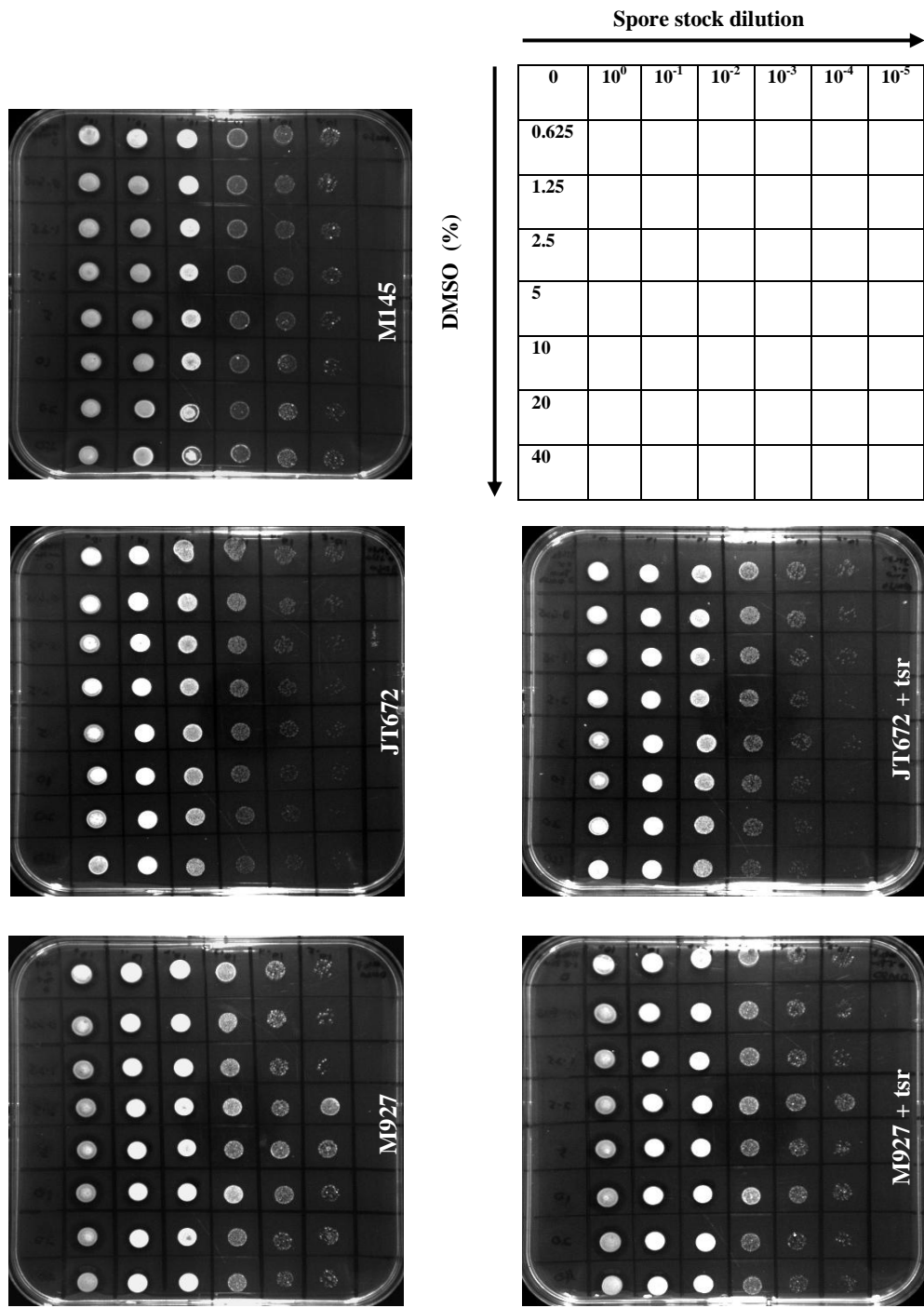


Figure 65: DMSO sensitivity assay conducted on JT672 using M145 and M927 as controls. Approximately  $5 \times 10^5$  starting spores of each strain were pretreated with increasing concentration of DMSO (0, 0.625, 1.25, 2.5, 5, 10, 20, 40 %) and spotted onto the  $10^0$  column. Spores serial dilutions were done accordingly ( $10^{-1}$ ,  $10^{-2}$ ,  $10^{-3}$ ,  $10^{-4}$ , and  $10^{-5}$ ) for each concentration before being spotted onto the respective dilution columns on the 3MA plates. No significant difference was observed between JT672 and the controls.



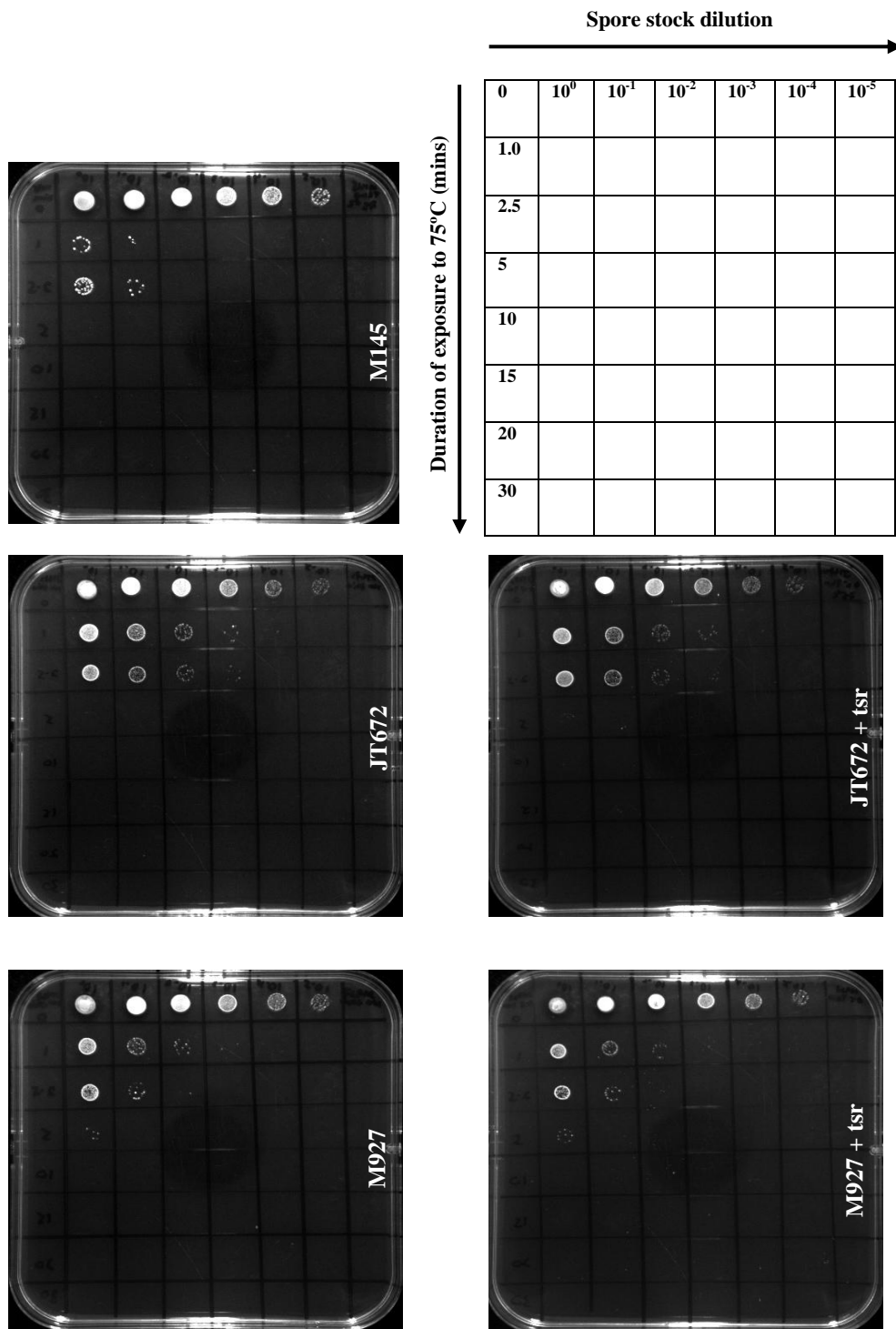


Figure 66: Heat sensitivity assay conducted on JT672 using M145 and M927 as controls. Approximately  $5 \times 10^5$  starting spores of each strain were heated at 75 °C on a heating block for a certain duration of time (0, 1, 2.5, 5, 10, 15 and 20 minutes) and spotted onto the  $10^0$  column. Spores serial dilutions were done accordingly ( $10^{-1}$ ,  $10^{-2}$ ,  $10^{-3}$ ,  $10^{-4}$ , and  $10^{-5}$ ) for each time length before being spotted onto the respective dilution columns on the 3MA plates. JT672 had slight increased resistance to heat compared to both M145 and M927 which was not altered by the addition of thiostrepton

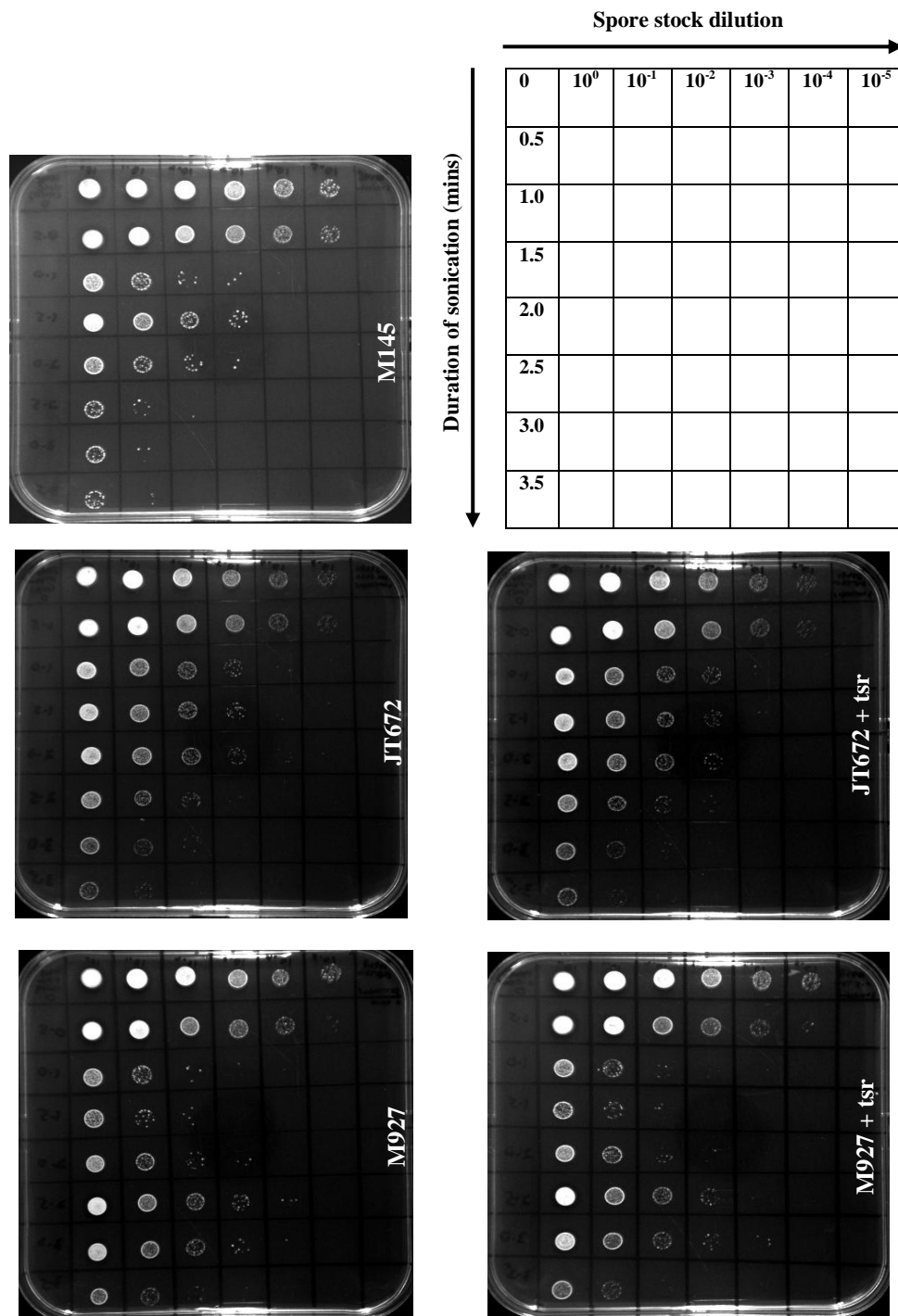


Figure 67: Sonication sensitivity assay conducted on JT672 using M145 and M927 as controls. Approximately  $5 \times 10^5$  starting spores of each strain were sonicated using Branson Sonifier 250 at output control setting 3 for a predetermined duration of time (0, 0.5, 1.0, 1.5, 2.0, 2.5, 3.0 and 3.5 minutes) and spotted onto the  $10^0$  column. Spores serial dilutions were done accordingly ( $10^{-1}$ ,  $10^{-2}$ ,  $10^{-3}$ ,  $10^{-4}$ , and  $10^{-5}$ ) for each time length before being spotted onto the respective dilution columns on the 3MA plates. No significant difference was observed between JT672 and the controls. Denser growth sometimes seen at longer duration of sonication might be due to liberation of the spores from their spore chains.

## 6.5 Dry weight growth curve and antibiotics production of JT672

In order to establish the growth pattern of JT672, it was necessary to obtain growth curve of this strain. All strains (JT672, M145 and M927) were grown in liquid YEME at 30 °C for an extended period of time and the dry biomass was measured at pre-determined time points. Cultures were harvested 8 hours after the start of incubation and every 3 (log phase) or 6 hours thereafter depending on the growth phase (8, 12, 18, 21, 24, 27, 30 and 36 hours). Samples were harvested in triplicates for every time point and all data points were mean of the three measurements (Figure 68). A growth spurt was observed between 12 to 18 hours for JT672 + 0.5 µg/ml thiostrepton compared to the uninduced mutant and other controls. This may implicate the importance of *pss* (hence PE) in the mid-log phase growth of *S. coelicolor* which is further substantiated by the slower mid-log phase growth rate observed in the partial *Pss* depleted mutant. In addition, a mid-log transition phase was observed for both induced (18 to 21 hours) and uninduced JT672 (21 to 24 hours) but not in the controls.

There was also significant difference in terms of antibiotics production between JT672 and the controls after 56 hours of incubation (Figure 69). In the absence of thiostrepton, JT672 had lower level of actinorhodin and undecylprodigiosin productions vis-à-vis M927 and M145 (~10 % for both antibiotics). The addition of 0.5 µg/ml thiostrepton increased the production of both antibiotics but was still significantly lower than that of M927 and M145 (~ 50% for actinorhodin and ~ 30% for undecylprodigiosin). Antibiotics production of both M927 and M145 were comparable but the addition of 0.5 µg/ml thiostrepton to M927 appeared to raise the production of actinorhodin but lower the undecylprodigiosin production compared to M145.

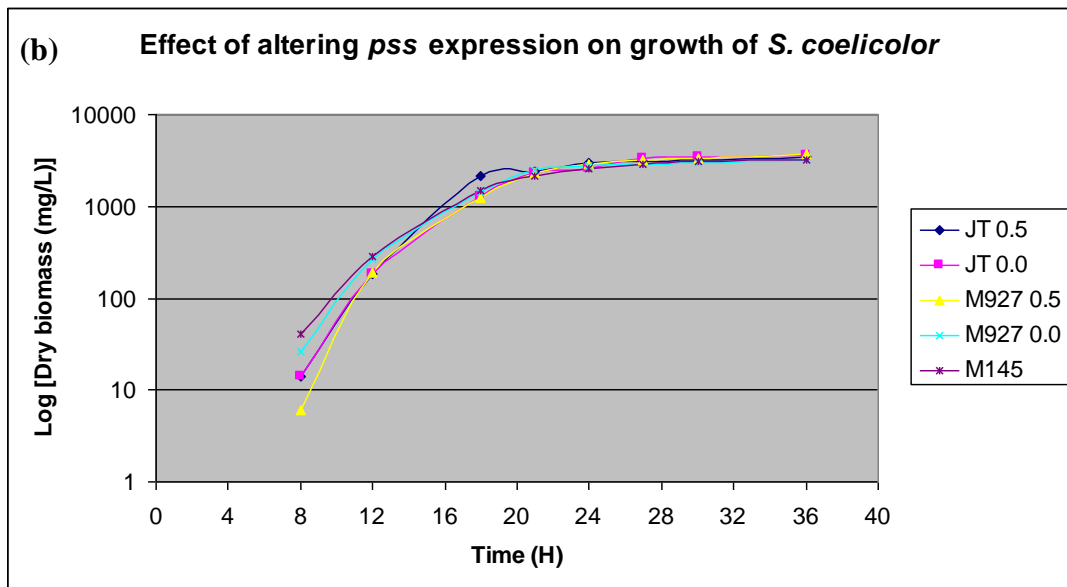
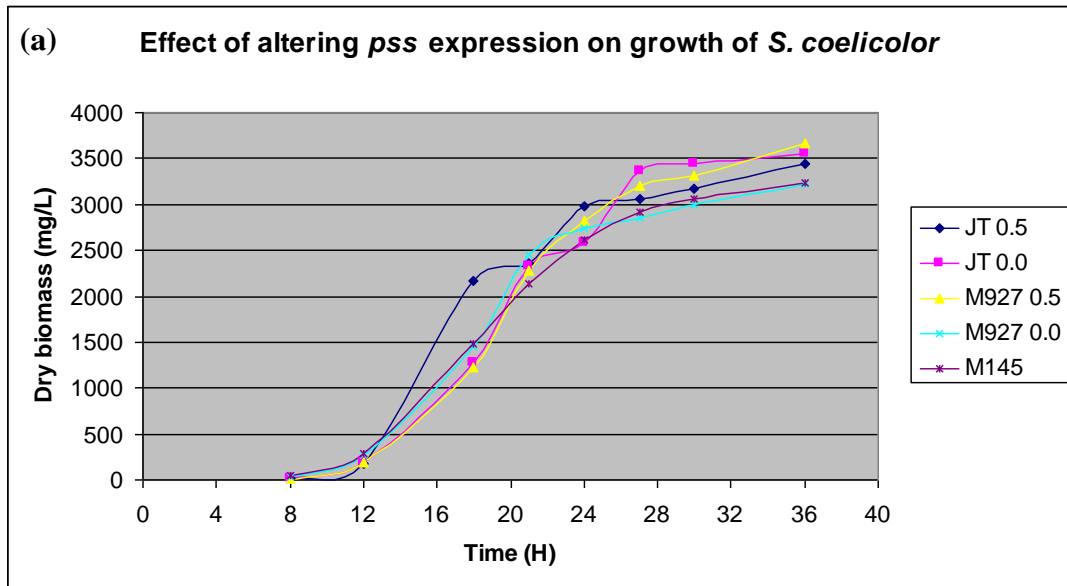
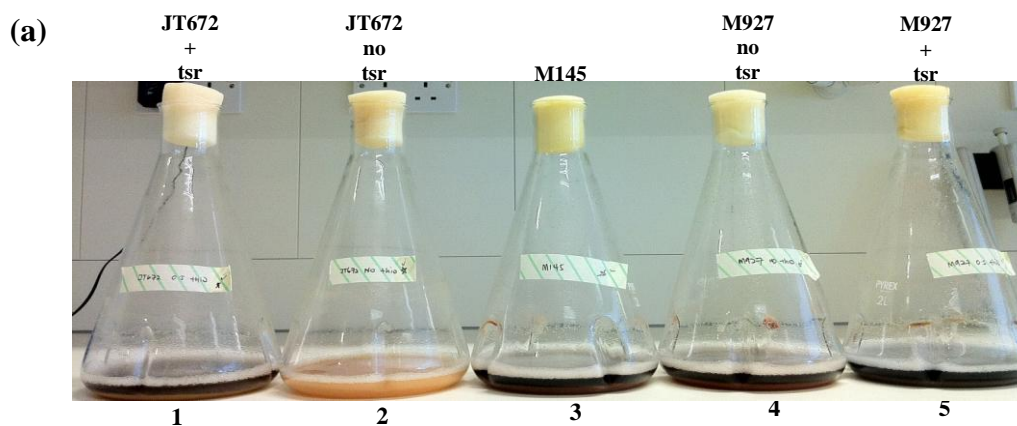
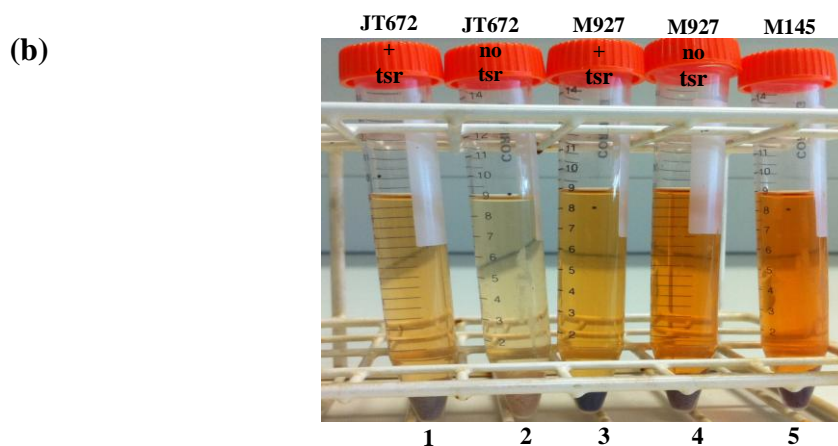


Figure 68: Alteration of *pss* expression affects growth of JT672 in mid-log phase. Dry weight growth curves of JT672, M927 and M145 grown in liquid YEME with time-points at 8, 12, 18, 21, 24, 27, 30 and 36 hours on (a) linear scale Y-axis and (b) log scale Y-axis. Partial depletion of Pss resulted in slightly slower growth rate of JT672 in mid-log phase compared to M145. The addition of 0.5  $\mu\text{g/ml}$  thiostrepton to JT672 resulted in a growth spurt between 12 to 18 hours compared to the uninduced mutant and the controls. A mid-log transition phase was observed for both induced (18 to 21 hours) and uninduced JT672 (21 to 24 hours) but not in the controls.



Flask	Strains	Actinorhodin concentration ( $\mu\text{M}$ )
1	JT672 + 0.5 $\mu\text{g/ml}$ thiostrepton	8.06
2	JT672	1.59
3	M145	14.5
4	M927	12.4
5	M927 + 0.5 $\mu\text{g/ml}$ thiostrepton	28.9



Tube	Strain	Undecylprodigiosin concentration ( $\mu\text{M}$ )
1	JT672 + 0.5 $\mu\text{g/ml}$ thiostrepton	1.53
2	JT672	0.60
3	M927 + 0.5 $\mu\text{g/ml}$ thiostrepton	2.31
4	M927	4.60
5	M145	4.99

Figure 69: (a) Actinorhodin (blue) production and (b) undecylprodigiosin (red) production in JT672 (+/- 0.5  $\mu\text{g/ml}$  thiostrepton), M927 (+/- 0.5  $\mu\text{g/ml}$  thiostrepton) and M145 grown in liquid YEME after 56 hours. Uninduced JT672 had reduced actinorhodin and undecylprodigiosin productions compared to M927 and M145. The addition of 0.5  $\mu\text{g/ml}$  thiostrepton increased the production of both antibiotics compared to the uninduced mutant but was still lower than that of M927 and M145. Antibiotics production of both M927 and M145 were comparable but the addition of 0.5  $\mu\text{g/ml}$  thiostrepton to M927 appeared to raise the production of actinorhodin but lower the undecylprodigiosin production compared to M145.

## **6.6 Enhanced green fluorescent protein (EGFP) tagging of Psd and Pss as a mode to analyse protein localization within bacterial cells**

### **6.6.1 Introduction**

Fluorescent proteins are powerful reporter tools in molecular biology frequently used in gene analysis. The discovery of green fluorescent protein (GFP) in the jellyfish *Aequorea victoria* has led to its wide usage as a marker for gene expression and protein localization within prokaryotic and eukaryotic cells (Chalfie *et al.*, 1994). The aim of this section is to produce a C-terminal *egfp*-tagged *psd* and *pss* mutants as a mode to visualize their cellular expression and localization within *S. coelicolor* through fluorescence microscopy. In the context of drug discovery, the changing fluorescence pattern in the presence of possible protein inhibitors could be utilized as data to corroborate the ligand-protein interaction findings in MIC assay.

### **6.6.2 Construction of the *egfp*-tagged cosmids of *psd* and *pss***

The basis behind designing of primers for *egfp*-tagging of *psd* and *pss* is shown in Figure 70. The forward primers for *psd/pss* (89 nt) had 5' 39 nt matching the *S. coelicolor* sequence (coding strand) at the end of *psd/pss* with stop codon changed from TGA to TGG, 10 amino acids linker associated with the pIJ786, 3' 20 nt matching the *egfp* at the start of the cassette (in pIJ786) with respect to the correct reading frame to the *psd/pss*. The reverse primers for *psd/pss* (58 nt) on the other hand, had 5' 39 nt matching the *S. coelicolor* sequence (complementary strand) adjacent to the end of *psd/pss* and 3' 19 nt matching the end of P1 in the cassette (pIJ786). The sequences of primers used for PCR amplification of the extended EGFP cassette are shown in Table 18.

PCR amplification of extended cassette was first done using high fidelity polymerase, Accuzyme™ DNA Polymerase to prevent possible point mutation

during the amplification process. The fragments were then gel-purified before electrotransformation into *E. coli* BW25113/pIJ790/St9C7. Homologous recombination between the linear DNA with *S. coelicolor* cosmid, St9C7 resulted in C-terminal *egfp* tagging of *psd* /*pss* in the cosmid via a 10 amino acids linker. These cosmids ST9C7E67(B) and ST9C7E68(B) were then verified using various restriction digests (Figure 71 & 72 respectively) before being used for *egfp*-tagging of *psd* and *pss* in *S. coelicolor* chromosome.

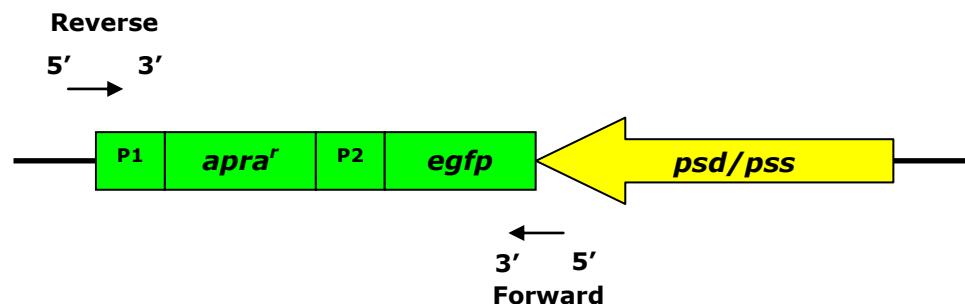


Figure 70: General design of primers for *egfp*-tagging of *psd* and *pss* using pIJ786 as amplification template. **Forward primers for *psd/pss* (89 nt)**: 5' 39 nt matching the *S. coelicolor* sequence (coding strand) at the end of *psd/pss* with stop codon changed from TGA to TGG), 10 amino acids linker associated with the pIJ786, 3' 20 nt matching the *gfp* the start of the cassette (in pIJ786) with respect to the correct reading frame to the *SCO6467/68*. **Reverse primers for *psd/pss* (58 nt)**: 5' 39 nt matching the *S. coelicolor* sequence (complementary strand) adjacent to the end of *psd/pss*, 3' 19 nt matching the end of P1 in the cassette (pIJ786).

Table 18: Forward and reverse PCR primers for *pss/psd* flanked extended *egfp* cassette to be used for homologous recombination. Black font: gene of interest to be linked with *egfp*; orange font: 10 amino acids linker; blue font: *egfp* gene sequence.

Oligo Name	Sequence (5' to 3')	Temp (°C)
6467F	GACAACCGACGGGAGGCGCGGGCGGCAG TTGCCGTGGCTGCCGGGCCGGAGCTGCCGGGC CCGGAGGTGAGCAAGGGCGAGGAGCT (89)	>75
6467R	CGAACCCGACCCGGGTCCGGGGCCCCACCCAG CGGA GCGATTCCGGGGATCCGTCGAC (58)	>75
6468F	AAGACGGTGGCTGGGGTGACTCGAATT GACCGTGATTGGCTGCCGGGCCGGAGCTG CCGGGCCCGGAGGTGAGCAAGGGCGAGGAG CT (89)	>75
6468R	TCGTCCGGCTCCGGCACCCATCCGGCCTGG GTCTGTGGAATTCCGGGGATCCGTCGAC (58)	>75



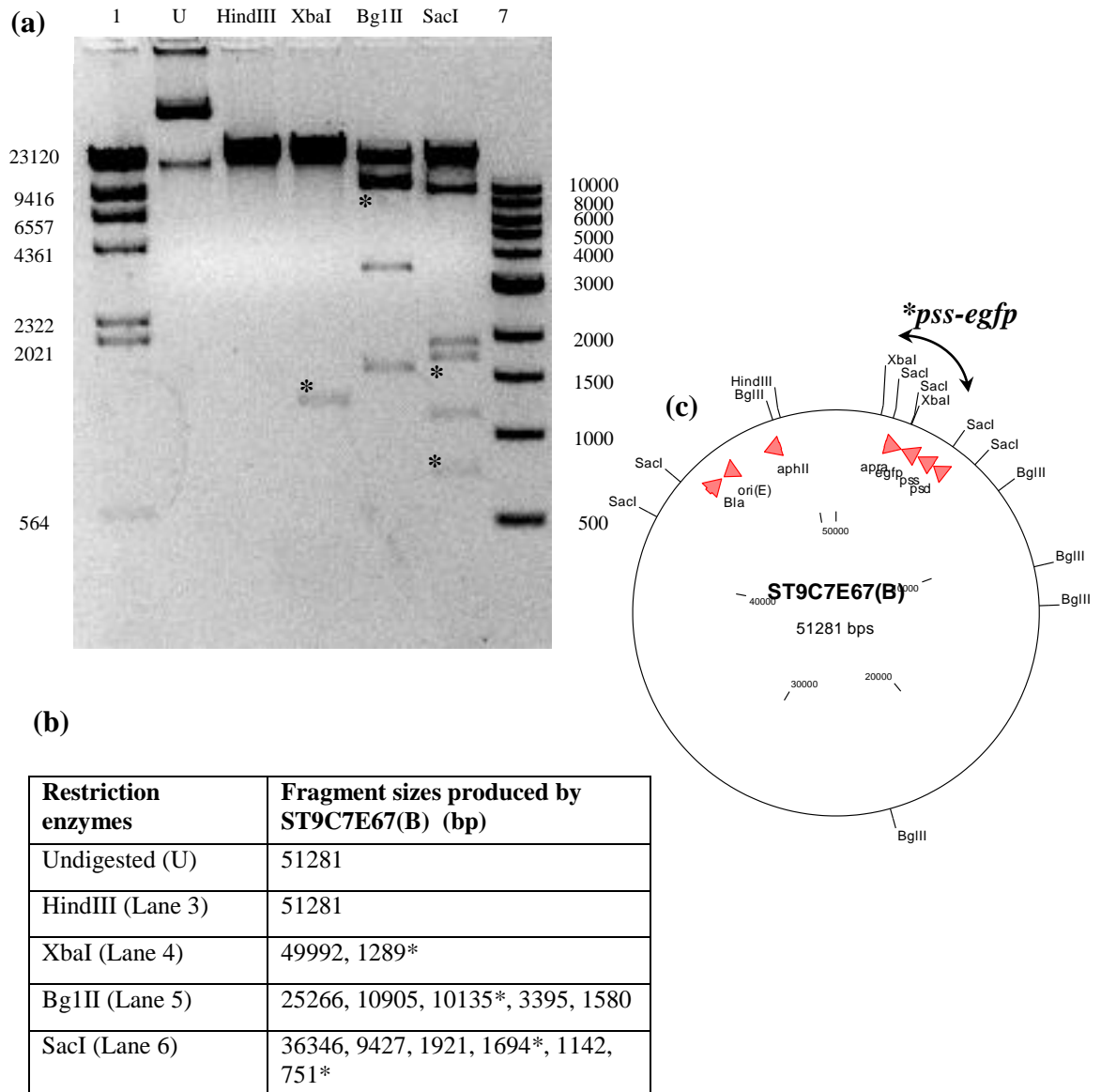


Figure 71: Electrophoresis gel of cosmid ST9C7E67(B). (a) Lane 1 & 7:  $\lambda$  HindIII DNA ladder and 1Kb ladder (Promega) respectively; Lane 2: undigested cosmid; Lane 3: HindIII digested cosmid; Lane 4: XbaI digested cosmid; Lane 5: BglII digested cosmid; Lane 6: SacI digested cosmid. (b) Fragments produced by different restriction enzymes. (c) The map of ST9C7E67(B) with (\*) sign indicating the diagnostic band containing the *pss-egfp* fragment.

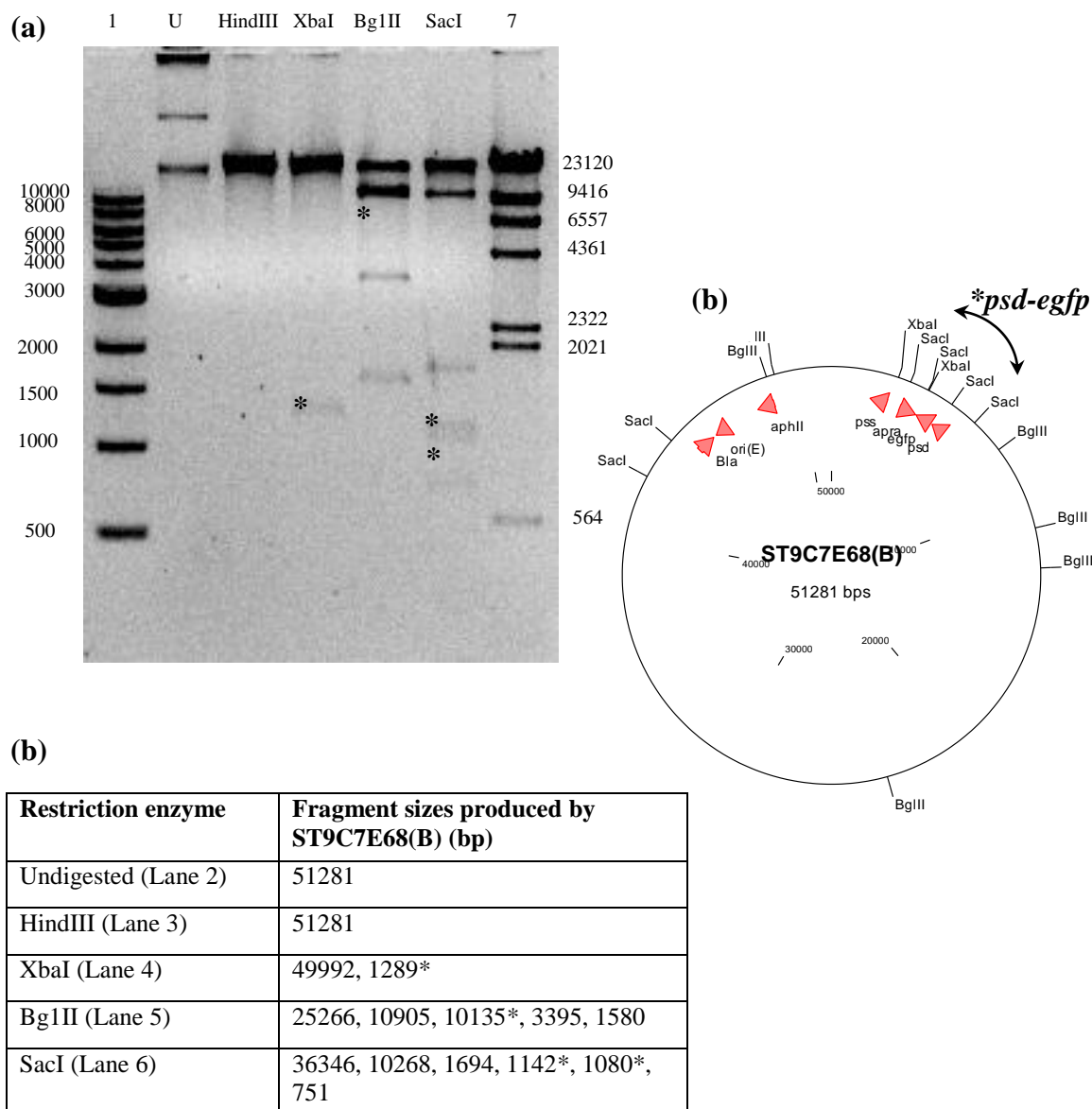


Figure 72: Electrophoresis gel of cosmid ST9C7E68(B) (*psd-egfp*). (a) Lane 1 & 7: 1 kb ladder (Promega) and  $\lambda$ HindIII DNA ladder; Lane 2: undigested cosmid; Lane 3: HindIII digested cosmid; Lane 4: XbaI digested cosmid; Lane 5: BglII digested cosmid; Lane 6: SacI digested cosmid. (b) Fragments produced by different restriction enzymes. (c) The map of ST9C7E68(B) with (\*) sign indicating the diagnostic band containing the *psd-egfp* fragment.

### 6.6.3 C-terminal *egfp*-tagging of *psd* or *pss* in *S. coelicolor*

To determine the cellular expression and localization of Psd and Pss through fluorescence microscopy, *egfp* tagging of the C-terminal end of the corresponding gene in *S. coelicolor* chromosome had to be carried out. The recombinant cosmids created previously were conjugally transferred into *S. coelicolor* for homologous recombination. 1000 exconjugants were then patched onto two replica MS agar plate added with either kanamycin (50 µg/ml) or apramycin (50 µg/ml) to screen for double crossover exconjugants *apra*<sup>r</sup>, *km*<sup>s</sup> which had undergone the allelic replacement. Unfortunately, only double crossover exconjugants were obtained for *pss* but not *psd* (Figure 73). Similar to the previous PCR-directed mutagenesis assay, the reason for our inability to obtain *egfp*-fused *psd* mutant remained uncertain. The *pss-egfp* mutant, ME67 was then verified via PCR before being analyzed via fluorescence microscopy.

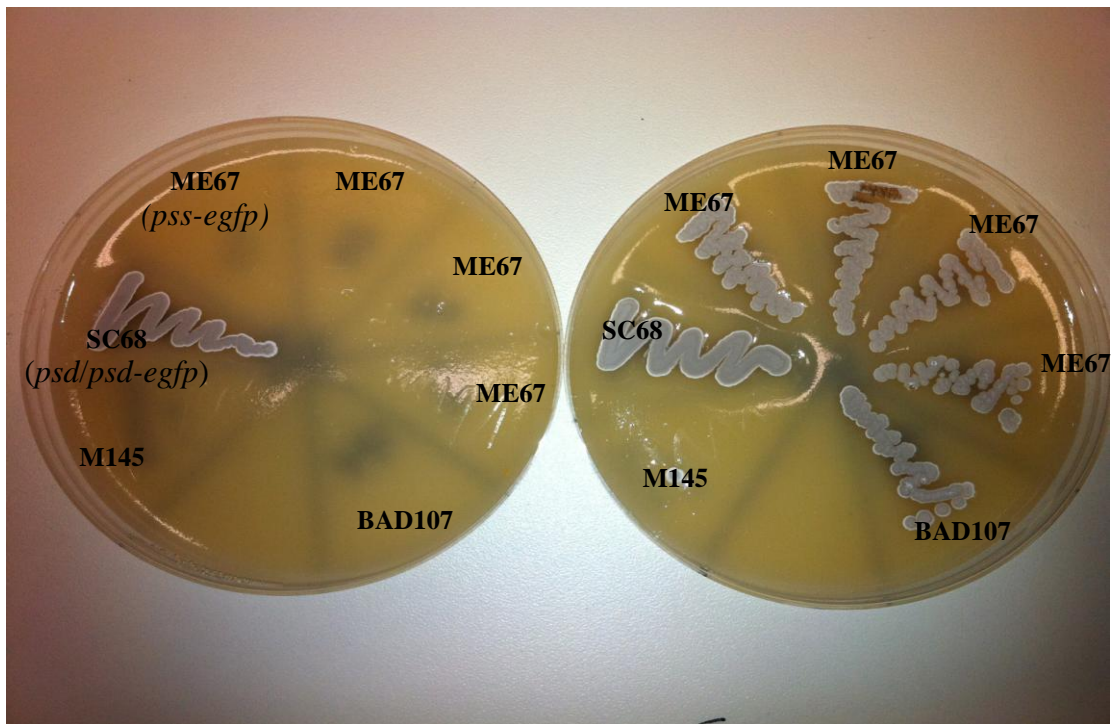
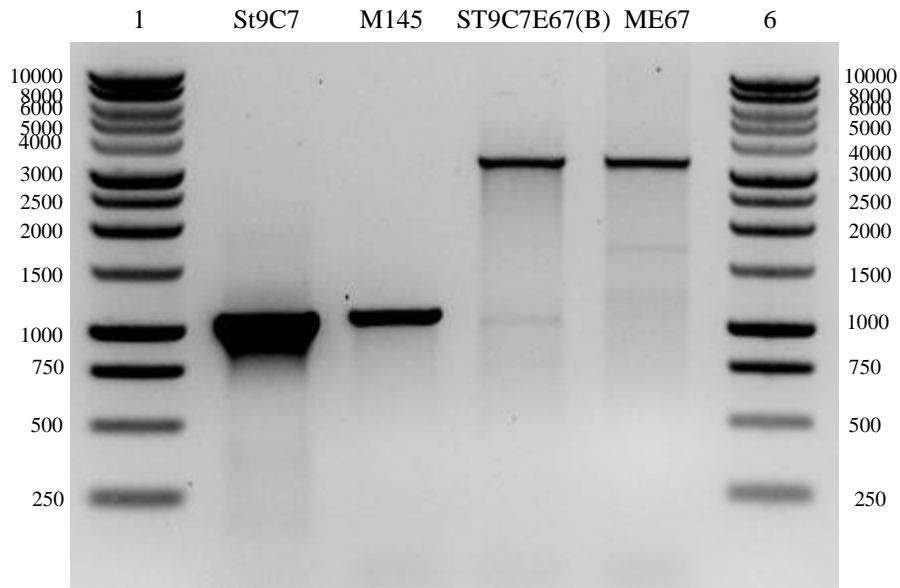


Figure 73: Double crossover exconjugant ME67,  $\text{apra}^r$ ,  $\text{km}^s$  (*pss-egfp*), single crossover exconjugant SC68,  $\text{apra}^r$ ,  $\text{km}^r$  (*psd/psd-egfp*) as well as the controls, BAD107,  $\text{apra}^r$ ,  $\text{km}^s$  and M145,  $\text{apra}^s$ ,  $\text{km}^s$  grown on replica plate of MS agar + 50 µg/ml apramycin/kanamycin

## 6.7 PCR-verification of ME67 (*pss-egfp*)

A set of primers (L2 and R1) was designed for the PCR-verification of ME67. The sequences of the primers used in the verification assay are shown in Table 15, Section 3.22. The primers primed from the sequences upstream and downstream of *pss-egfp* yielding a 3.26 kb fragment in the mutant vis-à-vis 1.056 kb in M145 (Figure 74). PCR-verification was carried out on ME67 against various controls (*pss-egfp* recombinant cosmid, ST9C7E67(B), the parenteral cosmid St9C7 and M145). The presence a 3.26 kb amplicon *in lieu* of the 1.056 kb amplicon (Lane 5 vs Lane 3 of Figure 74) indicated the *egfp* tagging of the chromosomal *pss* in ME67.



Lane	Strain/plasmid	Expected size (kb)	Actual Size (kb)
2	St9C7	1.056	1.056
3	M145	1.056	1.056
4	ST9C7E67(B)	3.260	3.260
5	ME67	3.260	3.260

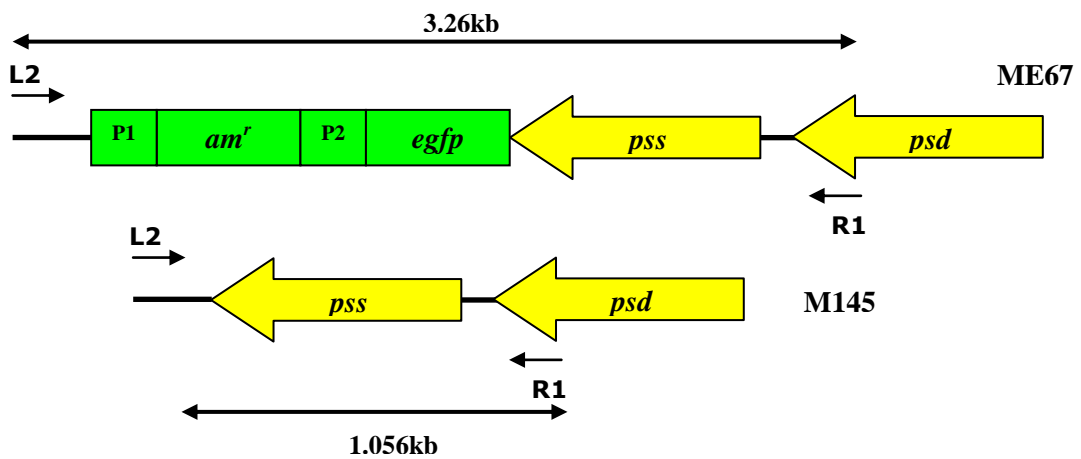


Figure 74: PCR–confirmation of *pss-egfp* tagged mutant, ME67 The second set of primers primed from upstream gene *psd* and the downstream flanking sequence. The presence of a 3.26 kb fragment *in lieu* of the 1.056 kb fragment in M145 further confirmed the mutant. The primers (L2+R1) used in the verification assay are shown in Table 15, Section 3.22.

## 6.8 Microscopy analysis of ME67 and JT672 (Kieser *et al.*, 2000; Jyothikumar *et al.*, 2012).

Samples were inoculated on coverslips inserted 45° diagonally into 3MA plate. The inoculums were incubated at 30 °C and coverslips with samples were removed daily for fixation and staining prior to microscopy analysis using Nikon TE2000S inverted microscope at 100x magnification via different filters. Both Pss-EGFP in ME67 and Vancomycin-FL staining of JT672 were visualized with FITC filter, Syto42 staining with DAPI filter and FM4-64 staining with TRITC filter. Measurement of morphological parameters (tip to first lateral branch distance, inter-branch distance, inter-septum distance and spore width) were carried out and the multiple data sets were analysed using Minitab (ANOVA) and bar charts with their standard errors were constructed using Microsoft Excel 2003.

The effect of altering the expression of *pss* on growth and morphology was investigated by growing M145, M927 and JT672 on 3MA in the presence or absence of thiostrepton. Staining using fluorescent dyes such as Syto42, FM4-64 and Vancomycin-FL aided the visualization of nucleoids, membranes and sites of peptidoglycan incorporation respectively. Concurrent statistical analysis of a number of key growth parameters (such as inter-branch distance, distance between hyphal tip to first lateral branch, inter-septum distance and spore width) that defined the overall architecture of the bacteria was also conducted.

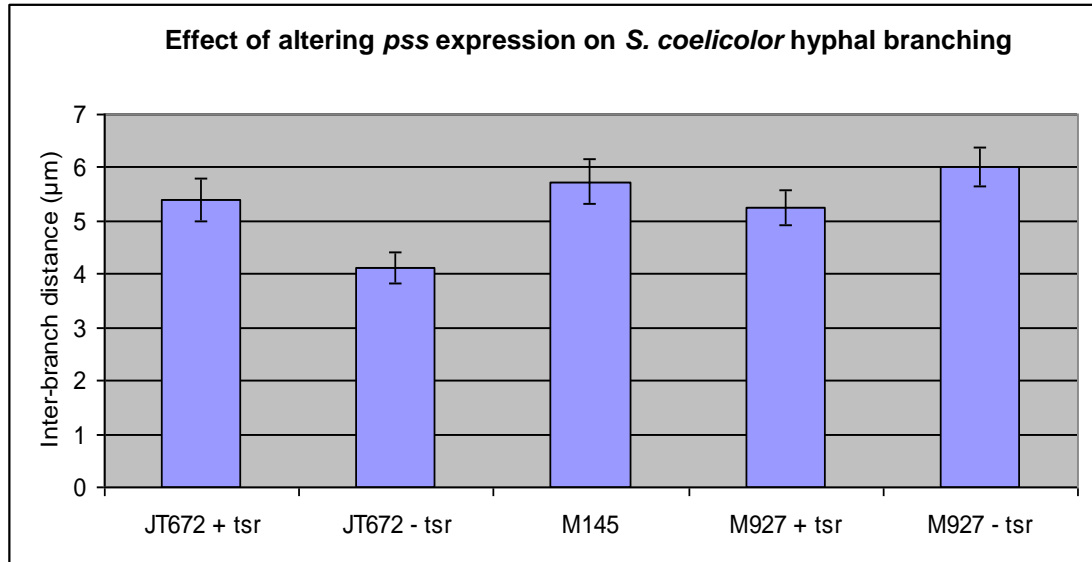
Alteration of *pss* expression affected hyphae growth, branching, septation and sporulation. Partial depletion of Pss led to increased hyphal branching (Figure 75a & 75b). In the absence of thiostrepton, inter-branch distance was significantly reduced compared to the wild type (JT672 vs M145: 4.13 ( $\pm$  0.29)  $\mu$ m vs 5.74 ( $\pm$  0.41)  $\mu$ m  $p$  < 0.05). The addition of thiostrepton increased the inter-branch distance close to that of the wild type (JT672 vs M145: 5.39 ( $\pm$  0.41)  $\mu$ m vs 5.74 ( $\pm$  0.41)  $\mu$ m  $p$  > 0.05). Partial repression of *pss* in JT672 also resulted in the significant increase in the distance between the hyphal tip and the first lateral branch (JT672 vs M145: 14.57 ( $\pm$  0.94)  $\mu$ m vs 11.50 ( $\pm$  0.65)  $\mu$ m  $p$  < 0.05) as shown in Figure 76a & 76b. This was restored close to that of the wild type with the addition of thiostrepton (JT672 vs

M145:  $10.26 (\pm 0.53) \mu\text{m}$  vs  $11.50 (\pm 0.65) \mu\text{m}$   $p > 0.05$ ). Uninduced mutant also failed to form spore chain although erection of aerial hyphae was observed (Figure 78b).

Unfortunately, triple staining using Cyto42, FM4-64 and Vancomycin-FL did not yield useful images due to some unknown problems with the DAPI and TRITC filters. However, Vancomycin-FL staining revealed the shortening of the inter-septum distance in the *pss* under-expressed mutant (JT672 vs M145:  $3.68 (\pm 0.16) \mu\text{m}$  vs  $6.60 (\pm 0.34) \mu\text{m}$   $p < 0.05$ ) as shown in Figure 77a & Figure 77b. The addition of thiostrepton on the other hand significantly lengthened the inter-septum distance compared to M145 (JT672 vs M145:  $8.36 (\pm 0.34) \mu\text{m}$  vs  $6.60 (\pm 0.34) \mu\text{m}$   $p < 0.05$ ). The use of the integrative vector did not affect any of the growth parameters mentioned but the addition of thiostrepton did significantly increase the width of the spores compared to M145 (JT672 + *tsr* vs M145:  $1.08 (\pm 0.01) \mu\text{m}$  vs  $1.01 (\pm 0.01) \mu\text{m}$   $p < 0.05$ ; M927+ *tsr* vs M145:  $1.07 (\pm 0.01) \mu\text{m}$  vs  $1.01 (\pm 0.01) \mu\text{m}$   $p < 0.05$ ) as shown in Figure 78a.

M145 was used as control in the fluorescence microscopy of ME67 for microscope exposure adjustment in order to minimize the faint background auto-fluorescence often observed in vegetative hyphae of *S. coelicolor* grown on 3MA. Unlike the diffuse nature of ClsA (Jyothikumar *et al.*, 2012), cellular localisation of Pss-EGFP in ME67 was observed at discrete locations mainly along vegetative hyphae near branching points and hyphal tip ends (Figure 79). This further substantiated the role of Pss in both branching and tip growth demonstrated previously in staining microscopy.





Strain	Sample size (N)	Mean	St. Error (SE)	Grouping*
JT672 - tsr	110	4.13	0.29	B
JT672 + tsr	109	5.39	0.41	A B
M145	109	5.74	0.41	A
M927 - tsr	111	6.01	0.36	A
M927 + tsr	110	5.25	0.34	A B

\* Means that do not share a letter are significantly different ( $p < 0.05$ )

Figure 75a: Statistical analysis of the inter-branch distance of JT672, M145 and M927 using ANOVA. Alteration of *pss* expression in *S. coelicolor* resulted in changing inter-branch distance. Partial depletion of Pss in JT672 significantly shortened inter-branch distance compared to the M145 whereas the addition of thiostrepton restored the inter-branch distance close to that of the wild type.

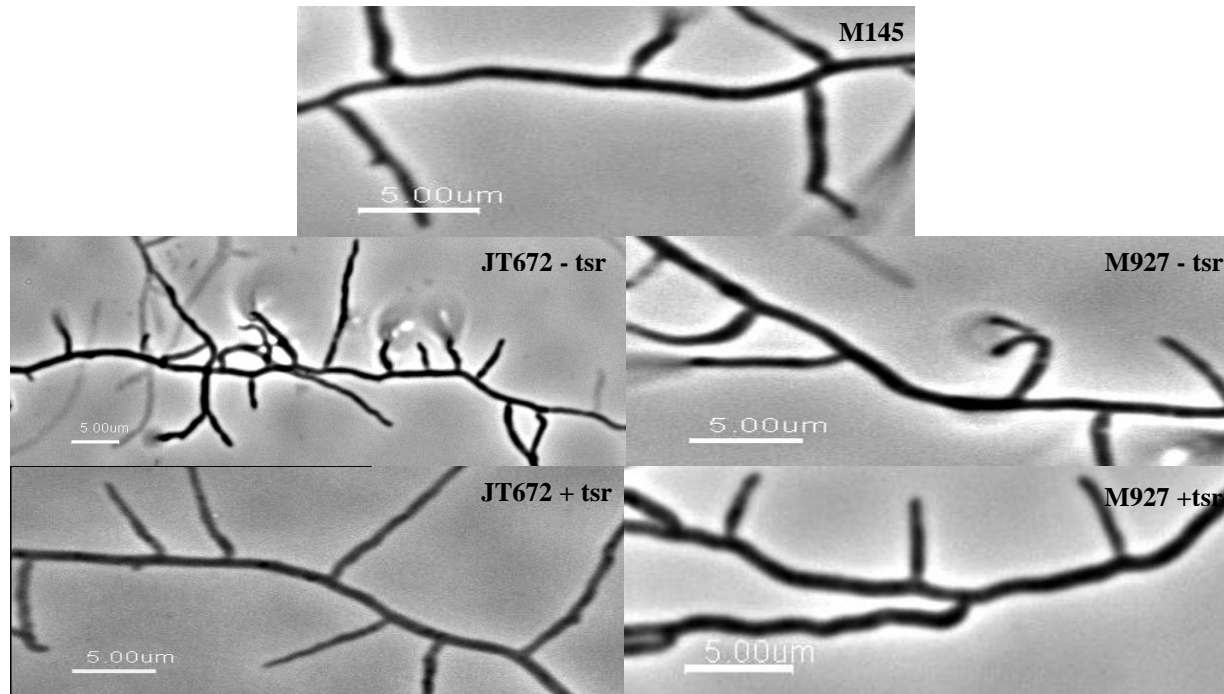
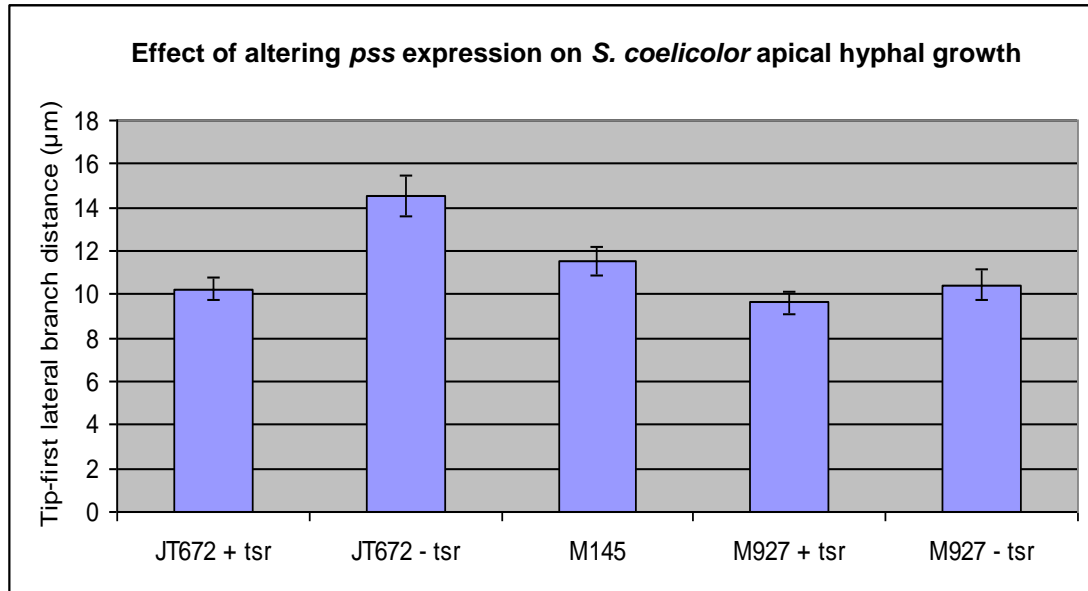


Figure 75b: Phase contrast microscopy of JT672, M145 and M927. Alteration of *pss* expression affected branching in *S. coelicolor*. Partial depletion of Pss in JT672 caused an increase in branching whereas the addition of thiostrepton restored the phenotype close to that of the wild type.



Strain	Sample size (N)	Mean	St. Error (SE)	Grouping*
JT672 - tsr	105	14.57	0.94	A
JT672 + tsr	105	10.26	0.53	B
M145	105	11.50	0.65	B
M927 - tsr	107	10.42	0.69	B
M927 + tsr	108	9.63	0.54	B

\* Means that do not share a letter are significantly different ( $p < 0.05$ )

Figure 76a: Statistical analysis of the tip-first lateral branch distance of JT672, M145 and M927 using ANOVA. Alteration of *pss* expression in *S. coelicolor* resulted in changing tip-to-first lateral branch distance. Partial depletion of Pss in JT672 significantly lengthened the tip-to-first lateral branch distance compared to the M145 whereas the addition of thiostrepton restored the distance close to that of the wild type.

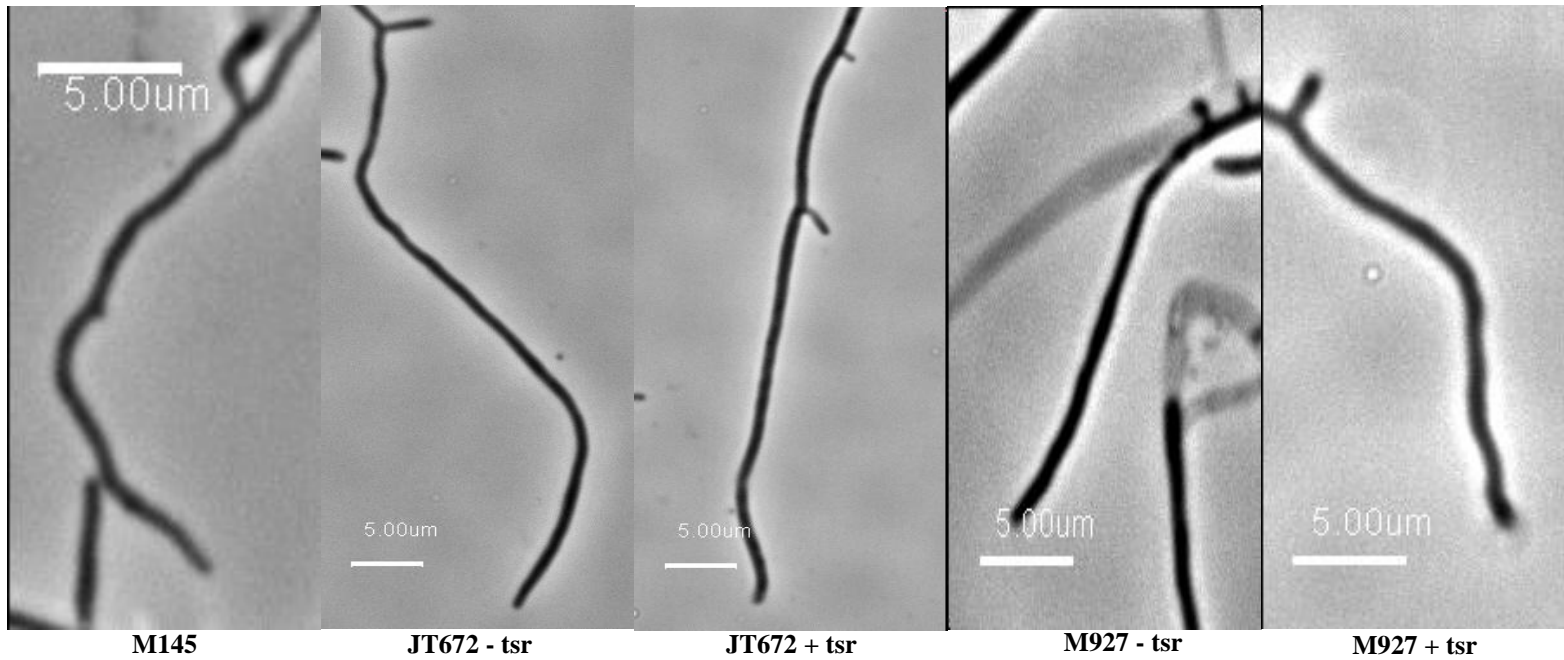
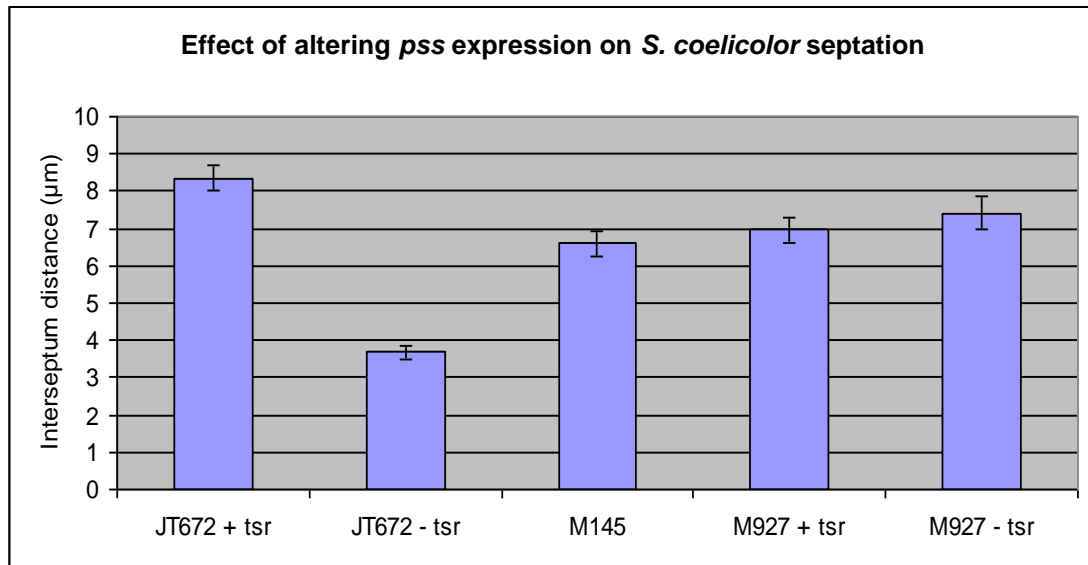


Figure 76b: Phase contrast microscopy of JT672, M145 and M927. Alteration of *pss* expression affected hyphal tip growth in *S. coelicolor*. Partial depletion of Pss in JT672 significantly increased the apical tip growth hence lengthened the tip-to-first lateral branch distance compared to the M145 whereas the addition of thiostrepton restored the phenotype close to that of the wild type.



Strain	Sample size (N)	Mean	St. Error (SE)	Grouping*
JT672 - tsr	110	3.68	0.16	C
JT672 + tsr	110	8.36	0.34	A
M145	110	6.60	0.34	B
M927 - tsr	110	7.42	0.45	A B
M927 + tsr	114	6.97	0.34	B

\* Means that do not share a letter are significantly different ( $p < 0.05$ )

Figure 77a: Statistical analysis of the inter-septum distance of JT672, M145 and M927 using ANOVA. Alteration of *pss* expression in *S. coelicolor* resulted in changing inter-septum distance. Partial depletion of Pss in JT672 significantly shortened the inter-septum distance compared to the M145 whereas the addition of thiostrepton significantly lengthened the inter-septum distance compared to that of the wild type.

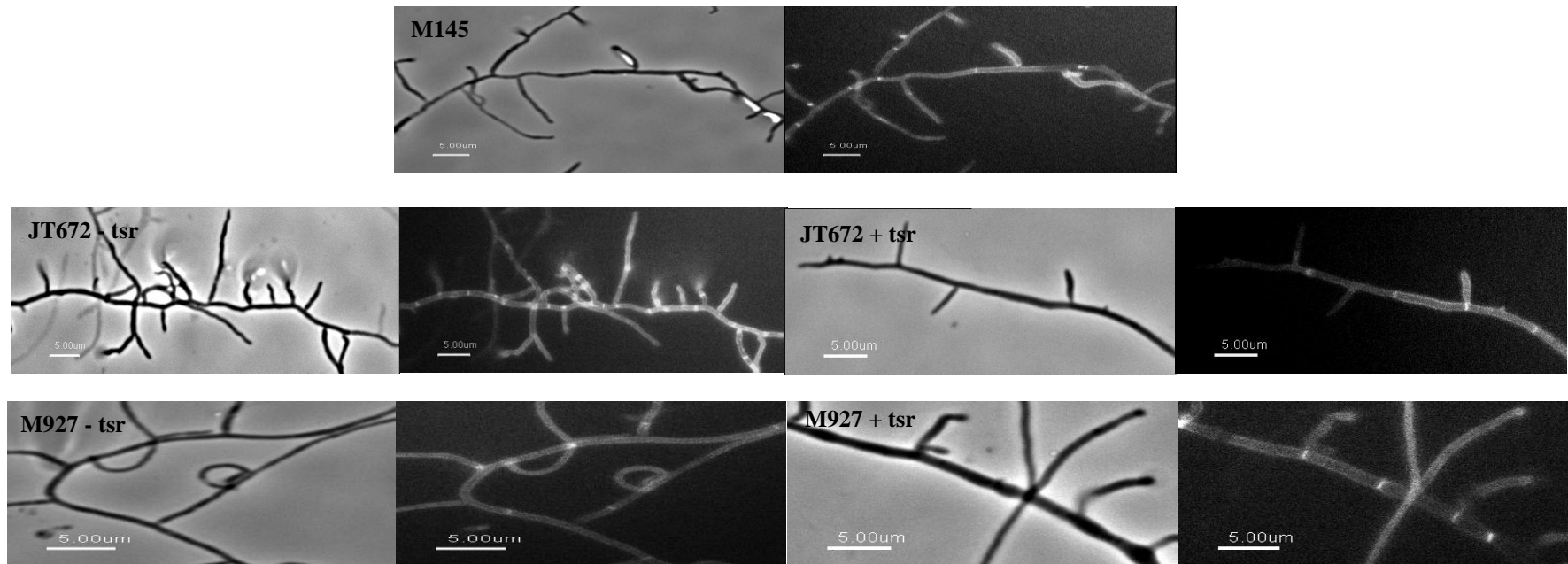
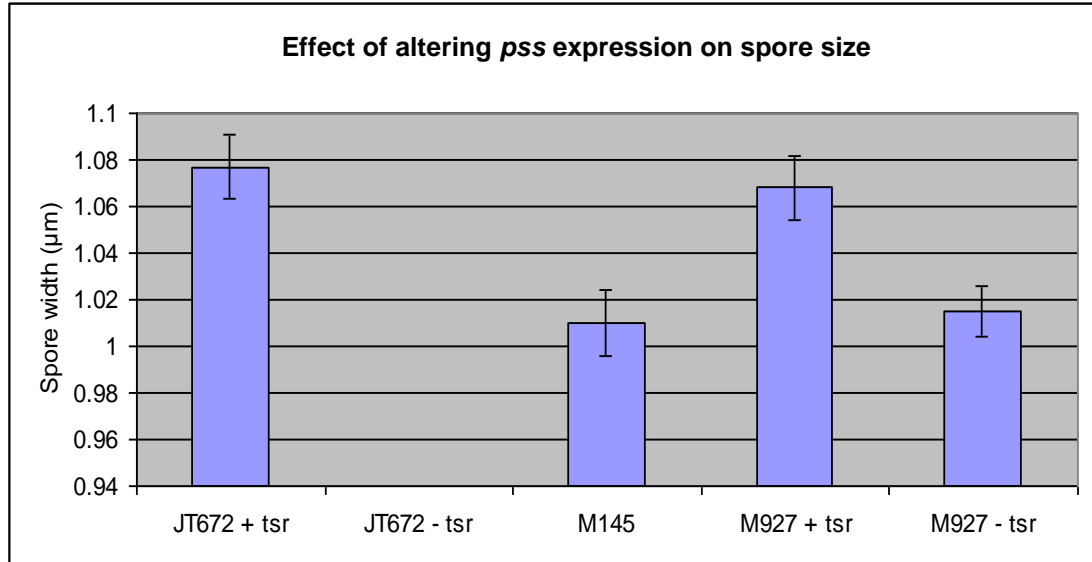


Figure 77b: Phase contrast and fluorescence microscopy of Vancomycin-FL stained JT672, M145 and M927. Alteration of *pss* expression affected septation in *S. coelicolor*. Partial depletion of Pss in JT672 caused an increase in septation compared to the M145 whereas the addition of thiostrepton significantly reduced septation compared to that of the wild type.



Strain	Sample size (N)	Mean	St. Error (SE)	Grouping*
JT672 - tsr	NIL	NIL	NIL	NIL
JT672 + tsr	110	1.08	0.01	A
M145	109	1.01	0.01	B
M927 - tsr	111	1.02	0.01	B
M927 + tsr	108	1.07	0.01	A

\* Means that do not share a letter are significantly different  $p < 0.05$

Figure 78a: Statistical analysis of the spore width of JT672, M145 and M927 using ANOVA. The addition of 0.5 µg/ml to *S. coelicolor* resulted in changing spore width. The addition of thiostrepton resulted in significant increase in the width of the spores of both JT672 and M927 compared to M145. Partial depletion of Pss in JT672 prevented spore formation.

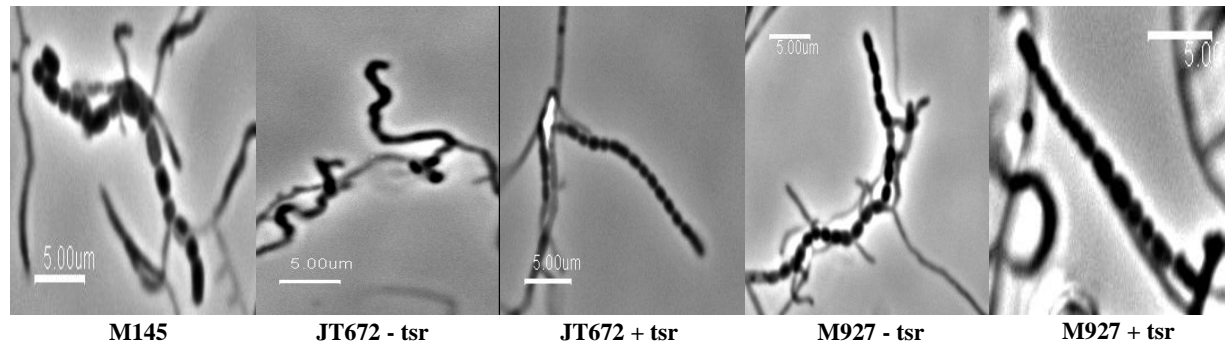


Figure 78b: Phase contrast of JT672, M145 and M927. Alteration of *pss* expression affected sporulation in *S. coelicolor*. Partial depletion of Pss in JT672 prevented the formation of spore chain whereas the addition of thiostrepton restored the wild type morphology.



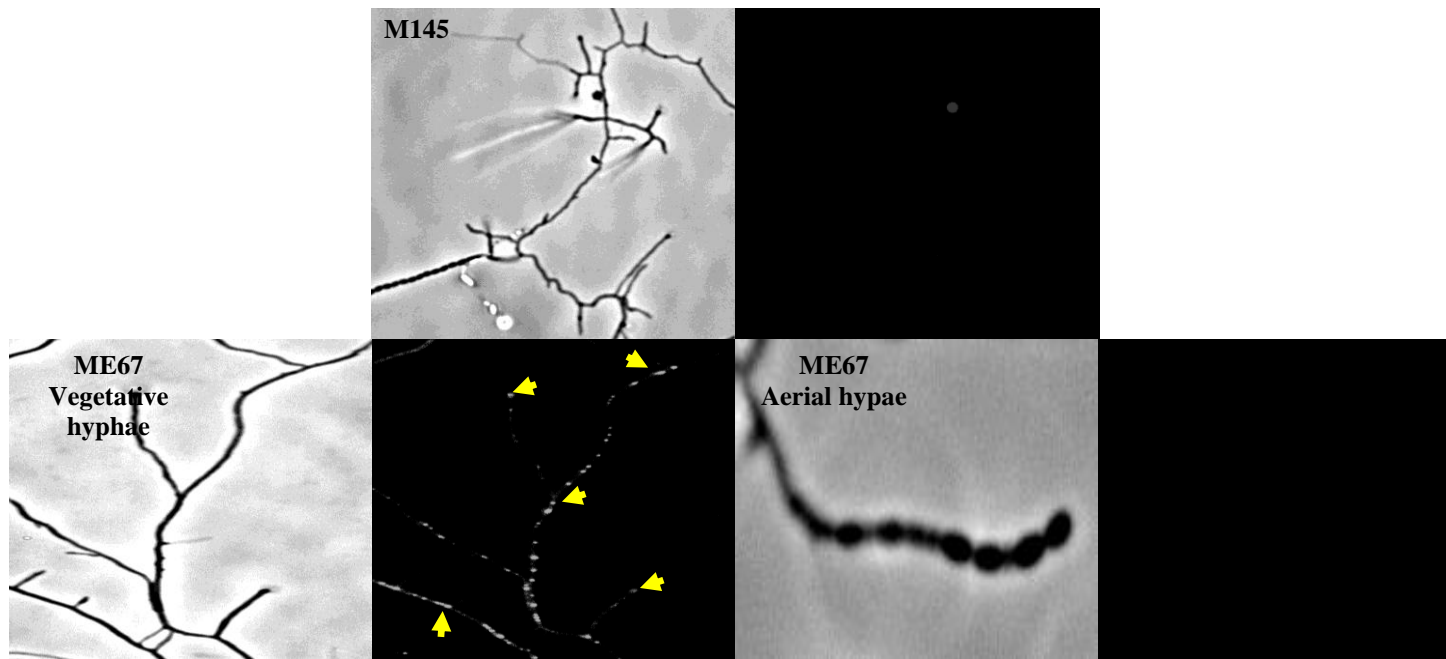


Figure 79: Phase contrast and fluorescence microscopy of M145 and ME67. Localization of Pss was observed on discrete locations mainly along the vegetative hyphae especially at branching points and tip ends (yellow arrows).

## 6.9 Discussion and conclusion

In view of the involvement of phospholipids in many of the important cellular processes required to maintain viability, artificial alteration imposed on the balanced composition via genetic approach may disrupt not only the cell integrity but many related physiological processes (Dowhan 1997). Genetic mutation of phospholipid biosynthetic enzymes causes not only the deficiency in the corresponding phospholipid but significantly affects other membrane lipid components (Lopez *et al.*, 2006). Therefore, morphological and biochemical analyses were conducted on the *pss* mutant, JT672 in order to elucidate the function of this gene and the overall effects of its repression in *S. coelicolor*. The *pss* controlled-expression assay conducted previously (chapter 5) clearly demonstrated the role of Pss (hence the major zwitterionic phospholipid, PE) in the physiology and morphological differentiation of *S. coelicolor*. This was evident with the steady increase of aerial hyphae formation as well as reduction in antibiotic production with the gradual increase in the concentration of thiostrepton added to the solid growth medium, 3MA.

### 6.9.1 Effect of varying expression of *pss* on RT-PCR and phospholipid profiles of *S. coelicolor*

RT-PCR and TLC analyses carried out on both 3MA and YEME grown JT672 confirmed the thiostrepton-dependence of *ptipA-pss* expression although there were marked differences in the level of gene expression between solid and liquid media at different concentrations of inducer. An RT-PCR product was still observed in the absence of thiostrepton for the 3MA grown JT672 suggesting the leaky nature of this promoter. Surprisingly, similar analysis of the liquid grown JT672 demonstrated full repression of the promoter in the absence or even at 0.005 µg/ml of thiostrepton. Moreover, full level of *pss* expression was also achieved at different concentrations i.e. 0.05 µg/ml vs 0.5 µg/ml for 3MA and YEME respectively.

This could largely be due to variation in terms of growth media used, duration of incubation (60 hours for 3MA vs 24 hours for liquid YEME), sample preparation/purification and many more factors which were inherent to this method (Gause & Adamovicz, 1994). The leaky profile of the inducible-promoter may also be more apparent with longer incubation time (Shibuya *et al.*, 1985). Furthermore, it is also worth noting that detected PCR amplicon intensity may even vary for the same set of primers run at different times due to differences in the efficiency of the PCR reaction of that particular run and the settings of imaging system used (Al-Khatib & Carr, 2003). Nevertheless, we were more convinced of the leaky nature of the *ptipA* shown by the 3MA grown JT672 which was consistent with previous findings (Holmes *et al.*, 1993; Flardh, 2003a; Ali *et al.*, 2002).

The phospholipid profile of the liquid grown JT672 sometimes showed the presence of a faint spot corresponding to the PE standard in the absence of inducer which was also indicative of the basal activity of the uninduced promoter. Nevertheless, it should be noted that in some instances, trace amount of phospholipid might still be detected in the absence of its biosynthetic enzyme activity in growth medium supplemented with the divalent cation,  $Mg^{2+}$  (DeChavigny *et al.*, 1991) which in this case is a component used in preparing YEME. It is also worth pointing out that there was always an overlap between CL and PE spots in solvent system (2) hence the observed faint spot might well be the CL spot which could be verified by mass spectrometry.

Concurrent analysis of phospholipid profile of JT672 via TLC further corroborated the thiostrepton– dependent induction of *ptipA-pss* shown in the RT-PCR assay. Repression and overexpression of *pss* caused significant changes in the phospholipid profile of JT672 compared to wild type *S. coelicolor* despite the inability to conclusively identify all spots via TLC. There was also remarkable difference between the solid-grown and liquid-grown phospholipid profiles in terms of the balance between the zwitterionic and anionic phospholipids.

In solid-grown cultures, the depletion of Pss caused the depletion of only PE which was restored with the addition of thiostrepton but the overexpression of *pss* at concentration of 0.05 µg/ml or higher might have caused the channelling of common phospholipid biosynthesis precursor, CDP-DAG into the PE biosynthesis pathway. Consequently, the exhaustion of this branch point substrate, might have resulted in the restoration of PE at the expense of PG. In liquid-grown cultures, depletion of PE also resulted in concurrent loss of the anionic phospholipid PG which was restored only at higher concentrations of thiostrepton (> 0.5 µg/ml). This could be taken as a hint of the possible structural and morphological diversity between the solid-grown and the liquid-grown mutant. The change in phospholipid profile of liquid-grown mutant appeared to be more drastic perhaps due to the need of more stringent control of the balance in phospholipid composition to maintain the overall membrane fluidity, membrane potential and its permeability since the bacteria were constantly submerged in liquid.

To further understand the phospholipid metabolism in *S. coelicolor*, TLC analysis was also carried out on *S. coelicolor clsA* mutant, RJ118b ( $\Delta clsA /tcp830-clsA$ ); (Jyothikumar, *et al.*, 2012). Similarly, depletion of ClsA in YEME-grown RJ118b not only resulted in deficiency of the anionic CL, but simultaneous depletion of the zwitterionic phospholipid PE. In other words, straightforward depletion of a particular phospholipid (especially in liquid-grown cultures) might not be the sole outcome of the disruption of the corresponding enzyme involved in its biosynthesis since a cascade of compensatory reactions might also be triggered in response to this event causing significant alteration to the overall membrane lipid composition. This indicates the presence of a cross –regulatory mechanism in membrane lipid pathways involved in keeping the balance between anionic and zwitterionic phospholipids which is crucial for maintaining the membrane integrity, fluidity and functionality (Smith, T. personal communication). This also concurs with several previous findings (Shibuya, 1992; Saha *et al.*, 1996a; Lopez *et al.*, 2006).

In *E. coli* for instance, it is believed that the regulation of the phospholipid metabolism occurred at the enzyme level since overexpression of *E. coli pss* by up to

100-fold did not significantly alter the phospholipid composition. With the demonstration of transcription-dependent synthesis of PE by *E. coli*  $\Delta pss$  mutant possessing a copy of the *pssB* from *B. subtilis* (which encodes an integral membrane protein), it was proposed that association of soluble cytosolic Pss to the acidic phospholipid components is essential for its catalytic property. A defective PgsA in *E. coli* on the other hand, caused not only a reduction in PG synthesis but 10-fold decrease in PE despite normal level of Pss activity hence further supporting the proposed model. Defective PssA however did not alter the anionic phospholipid content in *E. coli* suggesting a one-sided feedback mechanism (Saha *et al.*, 1996a). The question remains as to how a non-reciprocal regulatory system could maintain the balance between two major classes of phospholipids. Furthermore, the evidence of the validity/applicability of this model especially to those species of bacteria with membrane-bound Pss such as *Streptomyces coelicolor* and *Bacillus subtilis* is still lacking.

### **6.9.2 Adaptation of JT672 to different external growth pressures.**

The altered osmosensitivity of the *pss* mutant to KCl as well as changing tolerance of the spores to SDS and heat treatments further demonstrated the structural and physiological role of PE in *S. coelicolor*. High concentration of KCl is known to trigger  $\sigma^B$  which acts as the master regulator that modulates  $\sigma^B$ -regulon in *S. coelicolor*, one of which is the morphological differentiation needed in response to oxidative and osmotic stresses (Lee *et al.*, 2004). Some 287 genes are induced by  $\sigma^B$  as an osmotic response but the prominent ones include  $\sigma^L$  and  $\sigma^M$  which together with  $\sigma^B$  itself are responsible for aerial hyphae formation ( $\sigma^B$ ) and sporulation ( $\sigma^L$  and  $\sigma^M$ ) (Lee *et al.*, 2005). Although present evidences are pointing towards the involvement of only anionic phospholipids (CL and PG) in osmotolerance (Miller, 1985; Lopez *et al.*, 2006) we suspect that PE also plays direct role in the osmoadaptation of *S. coelicolor*. This conclusion was drawn based on several observations; reduced osmotolerance towards KCl in the partial Pss-depleted mutant which was reversed with the addition of thiostrepton as well as the involvement of this phospholipid in

the erection of aerial hyphae and sporulation which in itself is a form of sigma factors-dependent adaptation to adverse environmental condition (Willey *et al.*, 2006). This is further supported by the previous finding of the  $\sigma^B$ -dependence of *psd* promoter (Lee *et al.*, 2004) which is directly involved in the biosynthesis of PE.

As one of the major building blocks in the phospholipid bilayers of cell membrane, PE depletion is predicted to bring significant alteration to the integrity of the cell barriers. The spore sensitivity assay conducted on JT672 yielded several insights into the physical function of PE. Increased sensitivity of mutant to SDS (which is an anionic surfactant that disrupts the non-covalent bonds of the phospholipid bilayers and possibly the integral proteins via electrostatic repulsion) revealed by the spore sensitivity assay suggested that there might be a change in the overall structure and composition of the mutant/spore membrane. The raised heat resistance of the spore of JT672 observed in the heat sensitivity assay further supported this hypothesis.

Cell membranes are delicate barriers which are sensitive to temperature change. The application of heat or increase in the environmental temperature will increase the fluidity of phospholipids hence compromising the integrity of the barrier. Bacteria alter the membrane lipid composition in order to attain the physical characteristics and membrane fluidity needed for proper membrane function at a given temperature (Sinensky, 1974; Cronan & Gelman, 1975; Miller, 1985). Nevertheless, current evidences are contradicting when it comes to the role of PE in bacterial thermoadaptation (Souza *et al.*, 1974; Hasegawa *et al.*, 1980; Miller, 1985). Hence, it is difficult to draw a general conclusion based on this preliminary observation.

There was no significant difference between JT672 and the wild types in terms of sensitivity to DMSO which is a polar aprotic solvent known to alter membrane fluidity. Perhaps this membrane property was maintained via an internal compensatory mechanism despite the change in the overall structure/composition of membrane suggested previously. This concurred with the cross-regulatory

mechanism proposed in Section 6.9.1. Finally, there was also little change in the sturdiness of the mutant/spore cell wall compared to the wild type as revealed by the lysozyme (peptidoglycan hydrolase that can damage the bacterial cell wall via hydrolysis of the 1,4-beta-linkages between N-acetyl-D-glucosamine and N-acetylmuramic acid residues) and sonication sensitivity assays.

### **6.9.3 Effect of varying expression of *pss* on growth curve and antibiotic production of JT672**

*S. coelicolor* establishes a lifecycle that is both complex and similar to that of filamentous fungi. Morphological development/differentiation is often related to the transition from primary to secondary metabolism resulting in the production of secondary metabolites such as antibiotics (Chater, 1993; Huang *et al.*, 2001). A mid-log transition phase was apparent from the growth curve of both induced (18 to 21 hours) and uninduced JT672 (21 to 24 hours) which corresponded to the shift from primary to secondary metabolism in the mutant (Huang *et al.*, 2001). Increased in *pss* expression also caused an increased growth rate of the mutant in the exponential phase which was similarly observed in *E. coli* with overexpressed *pss<sub>BS</sub>* (Saha *et al.*, 1996a). Partial depletion of PE on the other hand, significantly reduced the growth rate which may suggest the role of the major membrane phospholipid, PE in actively growing *S. coelicolor* in the mid-log phase. This concurred with the observations made in mycobacteria (Morita *et al.*, 2005) and *B. Subtilis* (Lopez *et al.*, 2006). Perhaps *pss* (and probably *psd*) is one of the many genes which are up-regulated in the mid-log growth phase of *S. coelicolor* (Huang *et al.*, 2001) in order to supply adequate amount of PE to cater for the need of the growing and dividing cell.

Antibiotic production in the partially repressed *pss* mutant, JT672 was less pronounced in liquid YEME compared to the 3MA-grown mutant which further points to the physiological difference between the liquid and solid grown mutant. In the absence of thiostrepton, JT672 had markedly reduced actinorhodin and undecylprodigiosin productions compared to the controls. Partial restoration was observed with the addition of thiostrepton. Thiostrepton also affected the production

of both antibiotics as seen in M927 + 0.5 µg/ml of thiostrepton. The pleiotropic effect of thiostrepton could be due to its low affinity to the methylated ribosomes in the resistant strains (Dixon *et al.*, 1975) which could significantly influence the overall metabolism in the bacteria.

#### **6.9.4 Microscopy analysis of ME67 and JT672**

Although streptomycetes grow by means of hyphal tip extension and branching, our understanding of the precise mechanisms underlying such polarised growth remains limited (Flardh, 2003b). Cell wall material and presumably phospholipids are deposited at the extending apical tip as well as the newly formed cross walls (Daniel & Errington, 2003; Flardh, 2003b) consequently implying the presence of a unique scheme that coordinates this process. Our recent work with *Pss<sub>S.coelicolor</sub>* which catalyzes the committed step to the synthesis of PE suggests the role of the zwitterionic phospholipid in regulating this dynamic cellular process.

The partial Pss (hence PE) depleted mutant, JT672 exhibited an increase in hyphal branching, tip-to-first lateral branch length, septation as well as hindered spore chain formation (depicted by the cartoon shown in Figure 80(a)) compared to M145 (Figure 80(b)) and the reversal of the mutant phenotypes with the addition of thiostrepton. Fluorescence microscopy carried out on the *pss-egfp* mutant, ME67 on the other hand revealed the cellular localization of Pss on discrete locations along the vegetative hyphae especially near the hyphal tips and branching points (Figure 80(c)). Taking all these observations into account, we suspect the involvement of PE in modulating hyphae growth and branching as well as cross wall formation in *S. coelicolor* via interaction with DiVIVA (Flardh, 2003a; Hempel *et al.*, 2008; Flardh & Buttner, 2009) and FtsZ (McCormick *et al.*, 1994; Schwedock *et al.*, 1997) which are two of the main molecular entities involved in regulating these cellular processes.



We propose the role of PE as a topological regulator that coordinates the placement of both FtsZ and DivIVA in *S. coelicolor*. Consequently, reduction of PE following Pss partial depletion would result in aberrant cellular localization of these two proteins. The exaggerated septation might be caused by the eccentric positioning of FtsZ along the lateral length of substrate hyphae in the presence of low amount of PE which acts as a negative regulator. The longer tip-to-first lateral branch length could be ascribed in part to the increased frequency of septa placement along the vegetative hyphae since it has been shown previously that there is correlation between the rate of Z-ring progression and rate of hyphal tip extension (Jyothikumar *et al.*, 2008). Perhaps the increased in septation stimulates hyphal tip growth in an unknown mechanism in order to maintain a desirable distance between the tip and the first lateral cross wall. PE might also be involved in guiding the movement of this Z-ring forming protein from vegetative hyphae into aerial hyphae hence in its absence, spore chain formation is hindered. Although it is difficult to exclude the direct role of PE in the erection of aerial hyphae, there is possibility of interaction between PE with other molecular components which are responsible for such morphological development (Willey *et al.*, 2006).

Increased hyphal branching and tip growth in mutant with low PE content could be attributed to the role of this phospholipid as a negative regulator of the polar growth determinant protein, DivIVA and its polarisome assembly. Recent findings had suggested the possible role of DivIVA in apical tip extension (Flardh, 2003a) Perhaps, the unchecked polarisome-splitting mechanism (Hempel *et al.*, 2008; Hempel *et al.*, 2012) could have caused an intensified precipitation of flexible cell wall material at the growing hyphal tip hence stimulating the rate of tip extension by mean of turgor pressure. Hyper-branching is the result of an excessive tip-focus splitting mechanism which marked more sites along the lateral wall of the vegetative hyphae for new branch formation. Moreover, the subapical daughter cell which is cut off by the hyphal cross wall is unable to grow further other than switching its polarity to generate a new lateral branch with extending tip (Flardh, 2003b), thus exaggerated septation described previously could have further stimulated branching.

Since *de novo* incorporation of peptidoglycan precursors is required at the new cell wall (Braña *et al.*, 1982; Gray *et al.*, 1990; Prosser & Tough, 1991 & Miguélez *et al.*, 1992), the involvement of PE in modulating this process should not be discounted. It is also interesting to see how PE could affect nucleoid migration due to its influence over DivIVA and FtsZ. Nevertheless, the precise role of PE and its interaction with other related developmental proteins such as SsgA (VanWezel *et al.*, 2000), SsgB (Keijser *et al.*, 2003) and AfsK (Hempel *et al.*, 2012)) remains to be investigated.

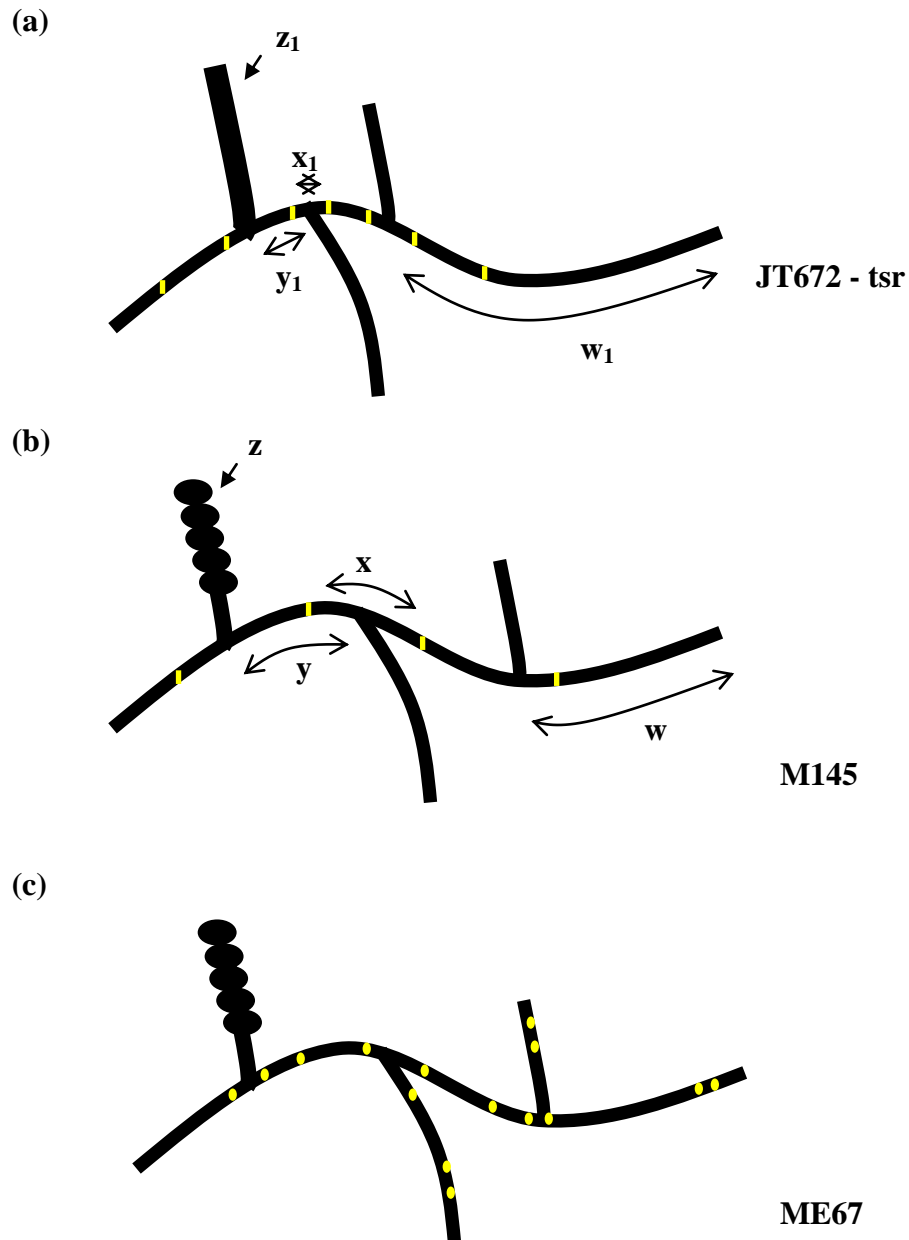


Figure 80: **(a)** JT672 in the absence of thiostrepton, **(b)** M145 and **(c)** ME67 with discrete localization of Pss along the vegetative hyphae especially at branch points and hyphal tips. Partial depletion of Pss in JT672 causes increased in hyphal tip growth  $w_1 > w$ , increased in septation  $x_1 < x$ , hyperbranching  $y_1 < y$  and hindered the formation of spore chain ( $z_1$  vs  $z$ ).

**7.0 Results**  
**Screening for novel anti-TB compounds targeting**  
**Psd and Pss in *S.coelicolor***

## 7.1 Introduction

The role of phospholipids in bacterial survival has attracted immense attention since they are known to be essential building blocks of bacterial membrane and in some cases confer virulence (Jackson *et al.*, 2000). The aim of our drug discovery programme is to design novel anti-TB compounds using chemical genetics and computational approaches targeting Psd and Pss in *M. tuberculosis*. Since experimental work on the clinical pathogen is often restricted to the confine of CL3 facilities, our preliminary research had to be carried out on an evolutionary related bacterium, *S. coelicolor* which is both safe and faster growing “surrogate” of *M. tuberculosis*.

As described in Section 1.4, drug discovery is a lengthy process that entails a multi-disciplinary approach. In addition, not every drug discovery project has the luxury of known 3D structure of target protein or inhibitor(s) hence the strategy employed may differ depending on the circumstances. In the absence of known inhibitor and 3D structures of both Psd and Pss, we expected our drug discovery scenario to be highly challenging since none of the classical approaches (structure based or ligand based method) is applicable.

Our approach was limited to the use of the natural substrate of target protein as template for virtual screening of various compound databases. Knowledge of the catalytic mechanism of the enzyme or the binding pattern of the natural substrate to amino acid moieties within the active site is of great importance in mapping out the possible pharmacophores needed to confer the inhibitory properties. In this process, the identified compounds were tested for their antibacterial activities against various bacteria. Compounds with interesting inhibitory activity would further be used to query the compound libraries to obtain more analogues with their structures as diverse as possible from one another to maximize the chance of obtaining a real ‘hit’ for the optimization phase.

## 7.2 The rationale behind choosing natural substrate of target protein as template for virtual screening

Psd is an important enzyme involved in the synthesis of PE through decarboxylation of its natural substrate, PS. Although *E.coli* Psd has little specificity in terms of the type of fatty acid residues attached to its substrate, it is believed to catalyze only the decarboxylation of lipid – linked serine moiety (Dowhan *et al.*, 1974). This remains to be investigated but could be taken as a hint that the probable ligand pharmacophores would be the lipid side chains as well as the serine moiety that should be included in the 2D similarity screening process.

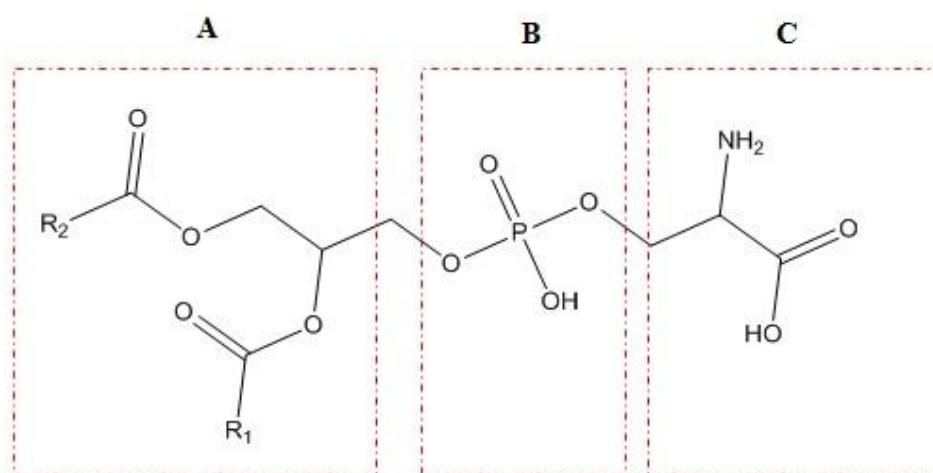
Pss which catalyzes the committed step to the synthesis of PE is found upstream of Psd in the zwitterionic phospholipid biosynthesis pathway. It is involved in the *de novo* biosynthesis of PS from CDP-DAG and L-serine. There is suggestion of the weak role of Pss in catalyzing the synthesis of CL via phosphatidyl transfer from CDP-DAG to PG in the absence of a functional Cls (Shibuya *et al.*, 1985; Nishijima *et al.*, 1988). Nonetheless, the screening process was complicated by the fact that little is known about the catalytic mechanism or ligand binding properties of this protein (Saha *et al.*, 1996b).

With no clue of the possible pharmacophore of Pss ligand, we decided to proceed with only the screening process of potential inhibitors of Psd in the first instance. Since no known structure of ligand/inhibitor was identified previously, we utilized the natural substrate of Psd i.e. PS (Figure 81) as the template for 2D screening of various libraries of compounds.

### 7.3 2D similarity screening of potential inhibitor(s) of Psd

For the purpose of querying the different libraries of compounds (Maybridge, ChemDiv, CNS\_SDF, IBS2009 and Keyorganic 2008), PS was used as template for 2D similarity searching using Pipeline Pilot Student Edition (Accelrys). In this empirical approach, the structure of PS was dissected into three further substructures (Figure 81) to be used as separate inputs in the screening process. This approach was taken since searches based on the whole 2D structure of the substrate generated too many unspecific/unrelated compounds in return. In order to narrow down our search, we fed these substructures into 3 different filters and the screenings were done in different combinations of these filters (Figure 82). Substructure A and C were believed to be the important pharmacophores since it was proposed that the decarboxylation could only happen in the presence of lipid-linked serine moiety whereas the amine group of the serine moiety was known to form a Schiff base with the pyruvate coenzyme within the active site of Psd during the catalytic process (Satre & Kennedy, 1978; Voelker, 1997; Barker *et al.*, 2009). It is still uncertain whether or not substructure A is needed in the binding affinity of PS to Psd in the catalytic domain or is merely important in conferring the required thermodynamic properties for the ligand to gain access to the active site of the protein.

Database querying based on different combination of these three substructures generated several compounds with related structures which were then clustered into five groups based on the core structures shown in Figure 83. Four of the compounds were selected from the list for further testings i.e. *O*-phospho-L-serine, diethyl aminomalonate, 3-ethoxy-2-methyl-3-oxo-1-phenylpropyl heptanoate and *O*-phospho-L-tyrosine (highlighted in Table 19). Selection was done based on the structural features which is discussed in the discussion section. Any observed inhibitory activity from these four compounds may shed some lights on the importance of each substructure of PS in functioning as a natural substrate. This could serve as an important piece of information in the structure optimization process based on the QSAR model and pharmacophore modelling which are most widely utilized techniques in ligand-based drug design (Acharya *et al.*, 2011).



R<sub>1</sub> = Oleate  
 R<sub>2</sub> = Palmitate

Figure 81: Chemical structure of PS. The molecule was divided into 3 substructures A, B and C to be used in 2D similarity search of library of compounds. Substructure A and C were hypothesized to be the important pharmacophores. Substructure C was believed to be essential for Schiff base formation with the pyruvate –containing active site of Psd.



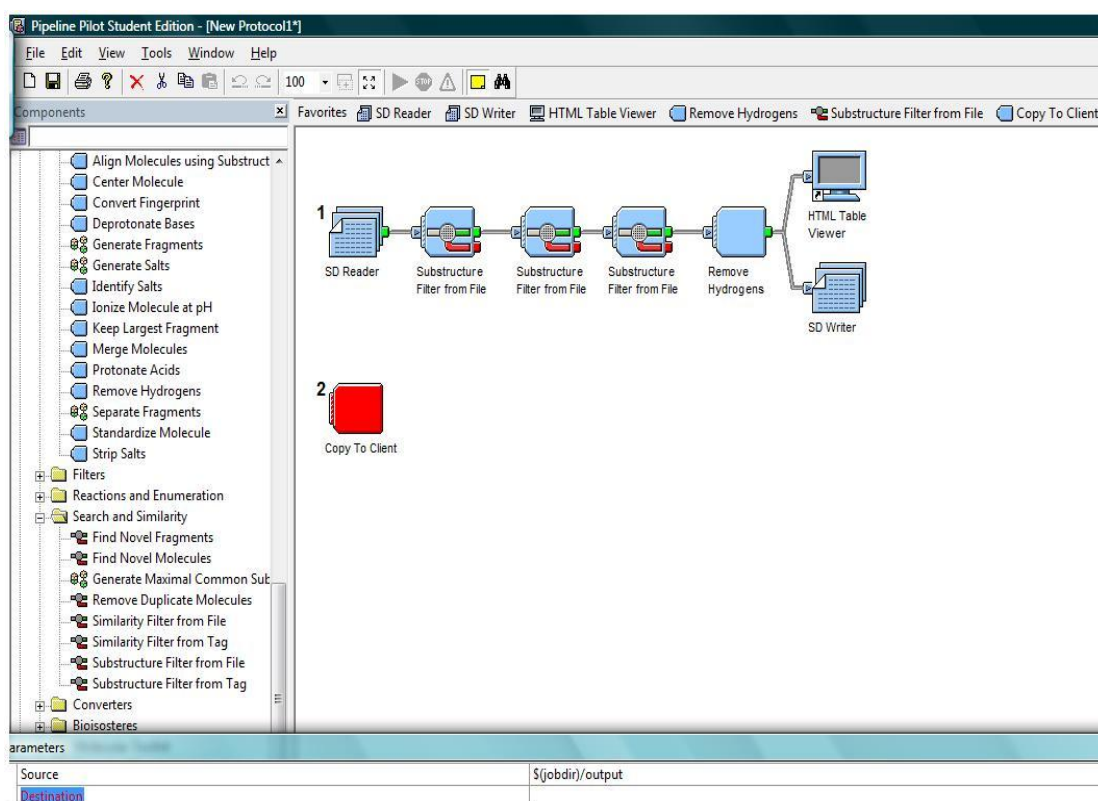


Figure 82: The user interface of Pipeline Pilot Student Edition. The library of compounds would be inserted into SD Reader whereas the substructure A, B and C of a PS used for database querying would be inserted into different filter(s). The filter(s) would be connected to a “Remove Hydrogens” node to remove all hydrogen atoms to simplify the structure of ligands obtained.

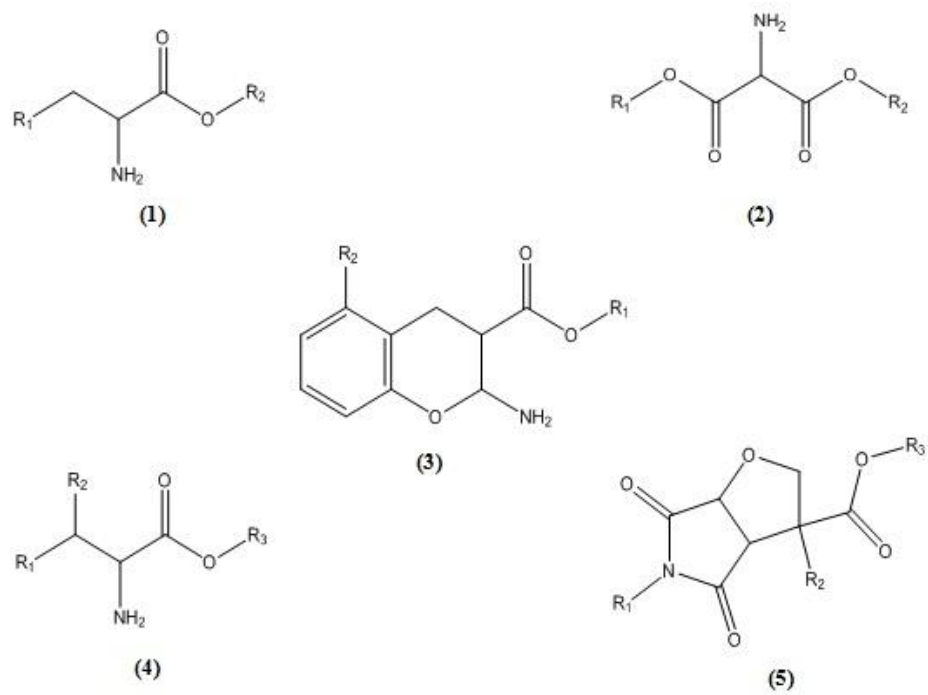
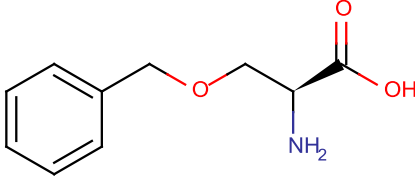
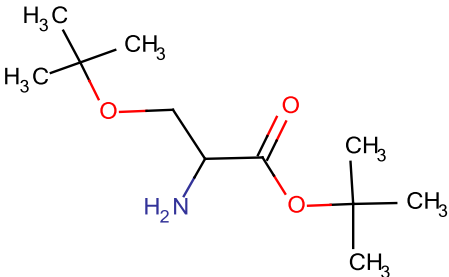
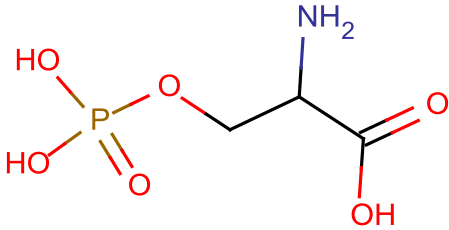
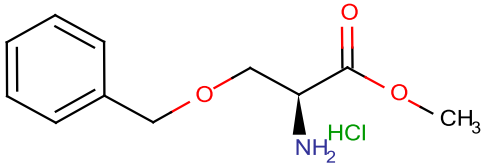
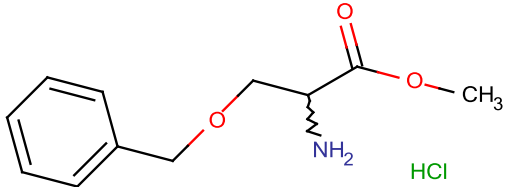
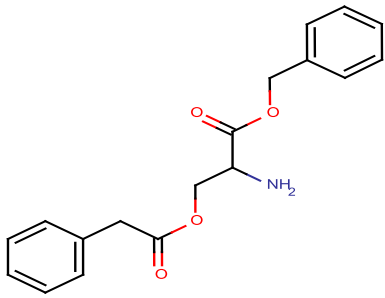
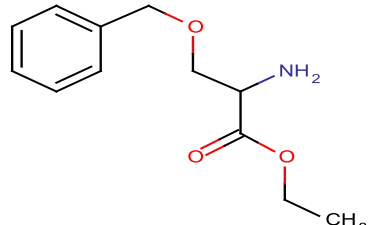
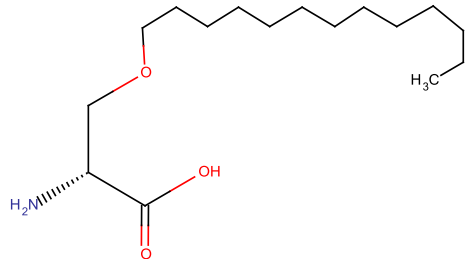
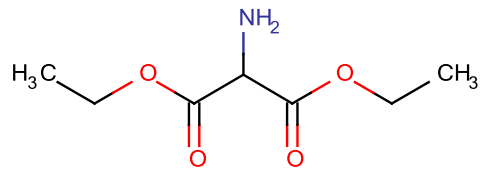
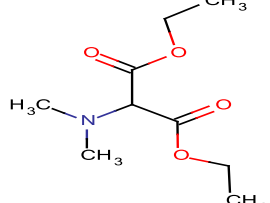
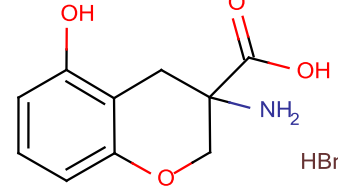
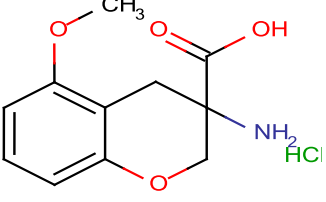
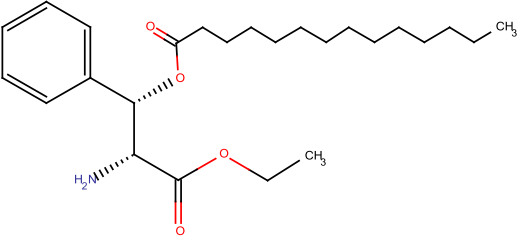
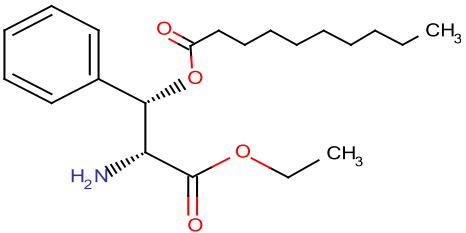
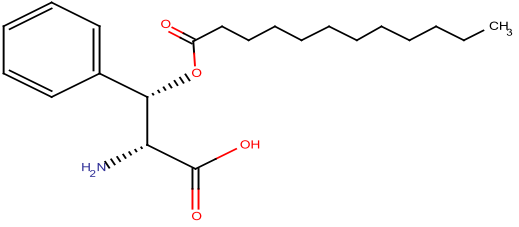
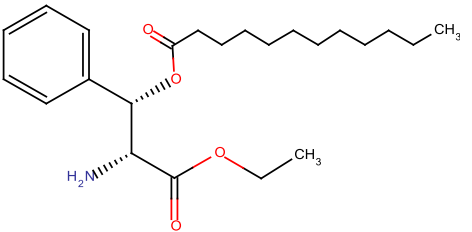
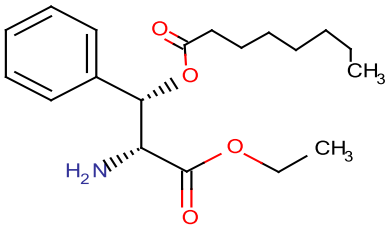


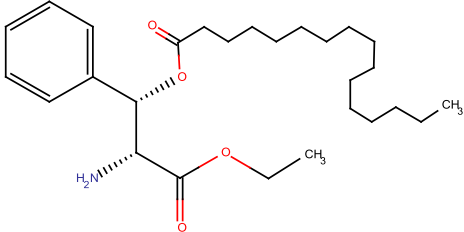
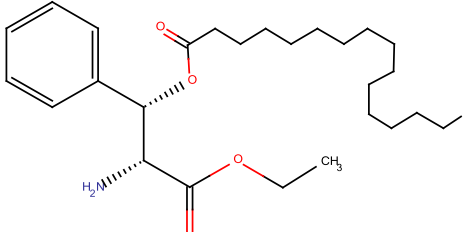
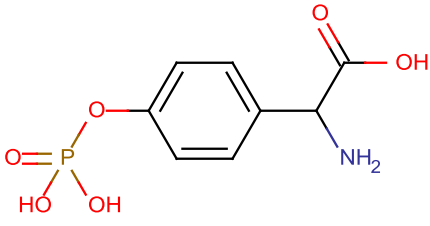
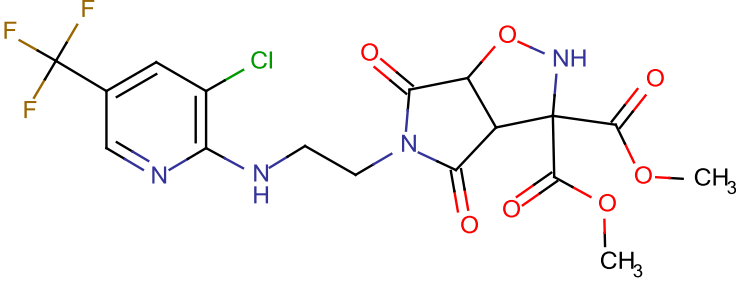
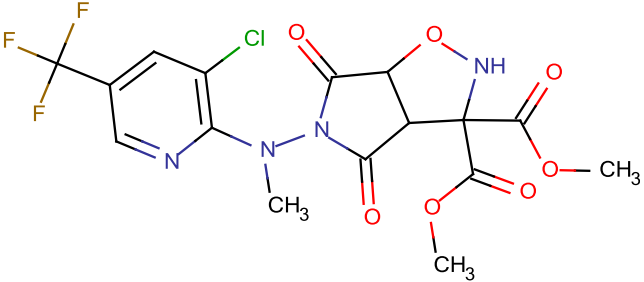
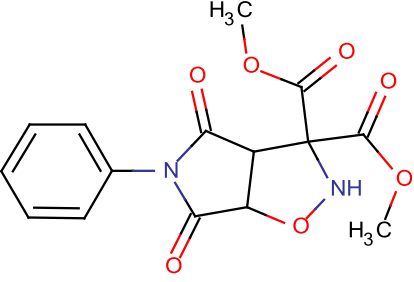
Figure 83: The core structures of five clusters of compounds obtained from querying of various databases using PS substructure(s) as template.  $R_1$ ,  $R_2$  and  $R_3$  represented the three sites of variable side chains.

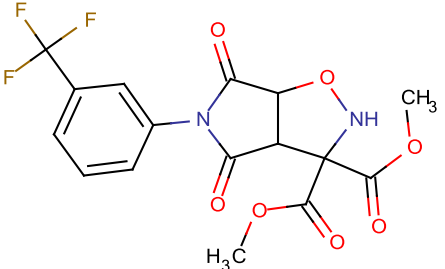
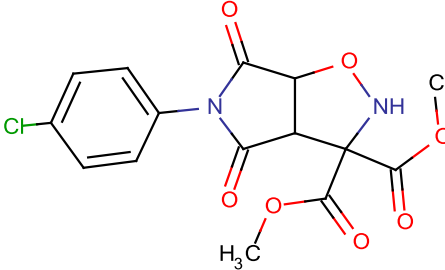
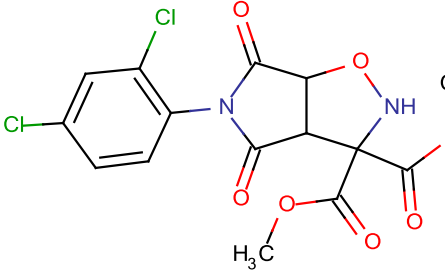
Table 19: The list of compounds obtained from the querying of various databases using PS structure/substructures as template. The compounds were sorted based on their core structures with information of their ID and the database which they were taken from. Diethyl aminomalonate, *O*-phospho-L-tyrosine, 3-ethoxy-2-methyl-3-oxo-1-phenylpropyl heptanoate and *O*-phospho-L-serine (in bold) were chosen for further testing.

Structures	Database/Code/Cluster
	Maybridge RJC 01683 1
	ChemDiv 0256-0011 1
	<b>CN_SDF</b> <b>AB-00016728</b> <b>1</b> <b>(<i>O</i>-phospho-L-serine)</b>
	CN_SDF AB-00027746 1
	CN_SDF AB-00027829 1

 <p style="text-align: right;">HC</p>	<p>CN_SDF AB-00004365 1</p>
 <p style="text-align: right;">HCl</p>	<p>CN_SDF AB-00028256 1</p>
	<p>IBS2009_full STOCK1N-04209 1</p>
<p style="text-align: center;">HCl</p> 	<p><b>Maybridge</b> <b>SB 00700</b> 2 <b>(diethyl aminomalonate)</b></p>
	<p>Maybridge XBX 00203 2</p>
 <p style="text-align: right;">HBr</p>	<p>CN_SDF AB-00006622 3</p>

	<p>CN_SDF AB-00006592 3</p>
	<p>IBS2009_full STOCK1N-02779 4</p>
	<p>IBS2009_full STOCK1N-04389 4</p>
	<p>IBS2009_full STOCK1N-09516 4</p>
	<p>IBS2009_full STOCK1N-10752 4</p>
	<p>IBS2009_full STOCK1N-07951 4 (3-ethoxy-2-methyl-3-oxo-1-phenylpropyl heptanoate)</p>

	<p>IBS2009_full STOCK1N-11553 4</p>
	<p>ibs2009apr_natural STOCK1N-11553 4</p>
	<p><b>Sigma-aldrich</b> <b>O-phospho-L-tyrosine</b> 4</p>
	<p>Keyorganic2008 11G-958 5</p>
	<p>Keyorganic2008 1J-920 5</p>
	<p>Keyorganic2008 3G-916 5</p>

 <p>The structure shows a bicyclic core with a blue nitrogen atom bonded to a phenyl ring substituted with three fluorine atoms (CF<sub>3</sub>). The core includes a red oxygen atom, a blue nitrogen atom bonded to a methyl group (CH<sub>3</sub>), and a red oxygen atom bonded to a methyl group (H<sub>3</sub>C).</p>	<p>Keyorganic2008 4G-910 5</p>
 <p>The structure is similar to the first one, but the phenyl ring is substituted with a chlorine atom (Cl) instead of a trifluoromethyl group.</p>	<p>Keyorganic2008 4G-911 5</p>
 <p>The structure is similar to the first one, but the phenyl ring is substituted with two chlorine atoms (Cl) at the 2 and 6 positions.</p>	<p>Keyorganic2008 7G-912 5</p>

## 7.4 Analogues of thiolactomycin (TLM): 2-amino-5-methylthiazole-4-carboxylate (ATC) derivatives.

### 7.4.1 Introduction

TLM is a well-known natural compound with a broad range of medicinal properties i.e. antibacterial activity (against Gram negative and Gram positive including mycobacteria) (Noto *et al.*, 1982; Hamada *et al.*, 1990; Slayden *et al.*, 1996), encouraging anti-malarial activity as well as potential for chemotherapeutic protection (prophylaxis against intraperitoneal and urinary tract infection) (Waller *et al.*, 1998; Morita *et al.*, 2000). TLM is known to specifically target the mycobacterial acyl carrier protein-dependent type II fatty acid synthase (FAS-II) in mycobacteria. Such inhibition affects the synthesis of longer chain di-unsaturated  $\alpha$ -mycolates and epoxy-mycolates with no known effect on the synthesis of shorter chain mono-unsaturated  $\alpha$ -mycolates (Slayden *et al.*, 1996).

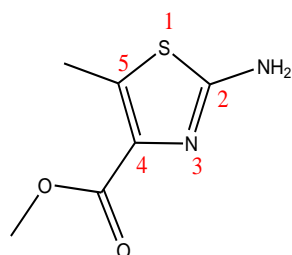
In a previous TB drug discovery project carried out in the medicinal chemistry department of University of Strathclyde, the ATC derivatives were synthesized by substituting the thiolactone scaffold of TLM with structurally similar aminothiazole ring resulting in the synthetically-less challenging analogues (due to the absence of the chiral centre in the aminothiazole ring) with an improved antimycobacterial potency. Although these ATC derivatives showed interesting anti-TB properties (MIC within the  $\mu$ M range), their cellular target within *M. tuberculosis* remain unknown (Al-Balas *et al.*, 2009). In order to investigate the biological target of these compounds and their involvement in Psd/Pss, the synthesis of these ATC derivatives were scaled up and included in our screening process.



## 7.4.2 Chemical synthesis of ATC derivatives

The detailed synthetic strategies for all the ATC derivatives are outlined in Section 3.31. After the chemical synthesis, a number of standard chemical analyses i.e. melting point determination, elemental analysis, NMR spectroscopy and mass spectrometry were conducted on these compounds in order to determine their purity. Their profiles were summarized as follow. With the purity of these compounds validated, screening for their antibacterial properties was then initiated (described in next section).

### (a) Methyl 2-amino-5-methylthiazole-4-carboxylate (QAB004)



**Physical appearance:** White powder

**Melting point:** 165-166 °C.

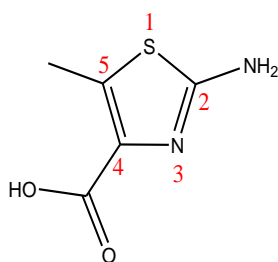
**MS:** Calculated  $C_6H_8N_2O_2S$  (M+H): 173.0; found: 173.0

**$^1H$  NMR ( $\delta$ ):** 2.50 (3H,  $CH_3$ -Ar); 3.75 (3H,  $OCH_3$ ); 6.92 (2H,  $NH_2$ ).

**$^{13}C$  NMR ( $\delta$ ):** 12.3 ( $CH_3$ Ar); 51.7 ( $OCH_3$ ); 134.9 ( $C_4$ ); 137.1 ( $C_5$ ); 163.6 ( $CO$ ); 167.1 ( $C_2$ ).

**CHN Analysis:** Found: C, 42.13; H, 4.77; N, 15.92; S, 18.39 (Calculated:  $C_6H_8N_2O_2S$ : C, 41.85; H, 4.68; N, 16.27; S, 18.62).

**(b) 2-amino-5-methylthiazole-4-carboxylic acid (QAB004A)**



**Physical appearance:** White powder

**Melting point:** 321-323 °C.

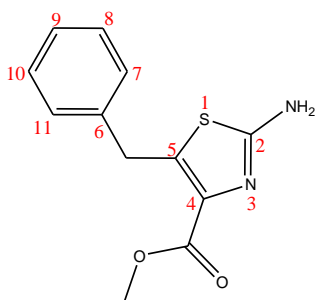
**MS:** Calculated C<sub>5</sub>H<sub>6</sub>N<sub>2</sub>O<sub>2</sub>S (M+H): 159.1; found: 159.1

**<sup>1</sup>H NMR (δ):** 2.60 (3H, CH<sub>3</sub>-Ar); 6.95 (2H, NH<sub>2</sub>).

**<sup>13</sup>C NMR (δ):** 12.3 (CH<sub>3</sub>Ar); 134.9 (C<sub>4</sub>); 137.2 (C<sub>5</sub>); 163.8 (CO); 167.7 (C<sub>2</sub>).

**CHN Analysis:** Found: C, 34.27; H, 3.18; N, 15.21; S, 17.79 (Calculated: C<sub>5</sub>H<sub>6</sub>N<sub>2</sub>O<sub>2</sub>S: C, 37.97; H, 3.82; N, 17.71; S, 20.27).

(c) methyl 2-amino-5-benzylthiazole-4-carboxylate (QAB008)



**Physical appearance:** White crystal

**Melting point:** 127- 128 °C.

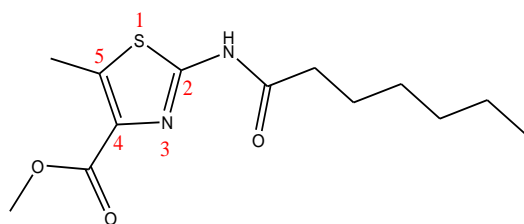
**MS:** calculated C<sub>12</sub>H<sub>12</sub>N<sub>2</sub>O<sub>2</sub>S (M+H): 249.1; found: 249.1

**<sup>1</sup>H NMR (δ):** 3.87 (3H, OCH<sub>3</sub>); 4.42 (2H, CH<sub>2</sub>-Ar); 5.30 (2H, NH<sub>2</sub>); 7.20-7.40 (5H, multiplet, Ar).

**<sup>13</sup>C NMR (δ):** 32.6 (Ar-CH<sub>2</sub>-); 51.9 (OCH<sub>3</sub>); 127.1 (Ar C<sub>9</sub>); 128.9, 129.1 (C<sub>7</sub>,C<sub>8</sub>,C<sub>10</sub>,C<sub>11</sub>); 136.4 (C<sub>4</sub>); 137.3 (C<sub>5</sub>); 140.7 (C<sub>6</sub>); 163.2 (CO); 165.3 (C<sub>2</sub>).

**CHN Analysis:** Found: C, 58.26; H, 4.26; N, 11.03; S, 12.11 (Calculated: C<sub>12</sub>H<sub>12</sub>N<sub>2</sub>O<sub>2</sub>S: C, 58.05; H, 4.87; N, 11.28; S, 12.91).

(d) methyl 2-heptanamido-5-methylthiazole-4-carboxylate (QAB014)



**Physical appearance:** White fuzzy solid

**Melting point:** 83.5-85.5 °C.

**MS:** calculated C<sub>13</sub>H<sub>20</sub>N<sub>2</sub>O<sub>3</sub>S (M+H): 285.2; found: 285.2

**<sup>1</sup>H NMR (δ):** 0.92 (3H, triplet, CH<sub>3</sub>(CH<sub>2</sub>)<sub>4</sub>CH<sub>2</sub>-); 1.23-1.34 (6H, multiplet, CH<sub>3</sub>(CH<sub>2</sub>)<sub>3</sub>CH<sub>2</sub>CH<sub>2</sub>-); 1.58 (2H, multiplet, CH<sub>3</sub>(CH<sub>2</sub>)<sub>3</sub>CH<sub>2</sub>CH<sub>2</sub>); 2.51 (2H, triplet, CH<sub>3</sub>(CH<sub>2</sub>)<sub>3</sub>CH<sub>2</sub>CH<sub>2</sub>-); 2.83 (3H, singlet, CH<sub>3</sub>Ar); 3.93 (3H, singlet, OCH<sub>3</sub>).

**<sup>13</sup>C NMR (δ):** 12.5 (CH<sub>3</sub>Ar); 14.4 (CH<sub>3</sub>(CH<sub>2</sub>)<sub>4</sub>CH<sub>2</sub>-); 23.2 (CH<sub>3</sub>CH<sub>2</sub>(CH<sub>2</sub>)<sub>3</sub>CH<sub>2</sub>-); 25.1 (CH<sub>3</sub>CH<sub>2</sub>CH<sub>2</sub>(CH<sub>2</sub>)<sub>2</sub>CH<sub>2</sub>-); 29.4 (CH<sub>3</sub>(CH<sub>2</sub>)<sub>2</sub>CH<sub>2</sub>CH<sub>2</sub>CH<sub>2</sub>-); 32.7 (CH<sub>3</sub>(CH<sub>2</sub>)<sub>2</sub>CH<sub>2</sub>CH<sub>2</sub>CH<sub>2</sub>-); 37.1 (CH<sub>3</sub>(CH<sub>2</sub>)<sub>2</sub>CH<sub>2</sub>CH<sub>2</sub>CH<sub>2</sub>-); 52.9 (OCH<sub>3</sub>); 135.5 (C<sub>4</sub>); 139.8 (C<sub>5</sub>); 154.9 (C<sub>2</sub>); 163.9 (COOCH<sub>3</sub>); 173.7 (CONH).

**CHN Analysis:** Found: C, 54.53; H, 7.21; N, 9.54; S, 11.09 (Calculated: C<sub>13</sub>H<sub>20</sub>N<sub>2</sub>O<sub>3</sub>S: C, 54.91; H, 7.09; N, 9.85; S, 11.28).

## 7.5 Screening of compounds for antibacterial activities

After obtaining all the compounds needed, screening for their antibacterial properties was carried out against *S. coelicolor*, *E. coli*, *B. subtilis* and *S. aureus* at a concentration of 100 µg/ml via disc diffusion assay (Bauer *et al.*, 1966). The purpose of this preliminary screening was to identify any compound which not only possessed antibacterial activity but exhibited inhibitory effect only against *S. coelicolor* since Psd and Pss are non-essential in *E. coli* and *B. subtilis* (Shibuya *et al.*, 1985; DeChavigny *et al.*, 1991; Saha *et al.*, 1996a; Matsumoto *et al.*, 1998). Any lead ligand obtained from this endeavour will be used for further querying of databases for more related compounds before structural optimization phase.

Apart from the 4 compounds obtained from the databases (diethyl aminomalonate, *O*-phospho-L-tyrosine, 3-ethoxy-2-methyl-3-oxo-1-phenylpropyl heptanoate and *O*-phospho-L-serine) and the synthesized ATC derivatives (QAB004, QAB004A, QAB008 and QAB014) (Al-Balas *et al.*, 2009), many different plant extracts (such as andrographolide, deoxyandrographolide, neoandrographolide, spiculosporic acid, surfactin sodium, glycyrrhizin, glycyrrhetic acid, petai seed extract and all the coded compounds) were included in the screening programme as they were available in the laboratory. Some of the plants where the compounds were extracted were traditionally used in treatments of various infections or were speculated to possess antibacterial activities. The identities of all the coded compounds were withheld for IP protection purpose. The antibacterial activities of these compounds are summarized in Table 20.

Unfortunately, none of these compounds appeared to match the desired profile described previously. An alternative approach must be undertaken since random screening being both expensive and time consuming is not a feasible method in the context of drug discovery.

Table 20: The list of compounds being tested against *E. coli*, *S. coelicolor*, *B. Subtilis* and *S. aureus* via disc diffusion assay. All the compounds were tested at a concentration of 100µg/ml. The first 4 compounds with coded names i.e. QAB004, QAB004A, QAB008 and QAB014 were synthetic compounds with known activity against *M. tuberculosis* H<sub>37</sub>R<sub>v</sub>. Diethyl aminomalonate hydrochloride, 3-ethoxy-2-methyl-3-oxo-1-phenylpropyl heptanoate, *O*-phospho-L-serine and *O*-phospho-L-tyrosine were analogues of PS obtained from the libraries of compounds. All the other compounds on the list thereafter are plant extracts from various sources.

Compounds	<i>E. coli</i>	<i>S. coelicolor</i>	<i>B. subtilis</i>	<i>S. aureus</i>
<b>QAB004</b>	inactive	inactive	inactive	inactive
<b>QAB004A</b>	inactive	inactive	inactive	inactive
<b>QAB008</b>	inactive	inactive	inactive	inactive
<b>QAB014</b>	inactive	inactive	inactive	inactive
<b>Diethyl aminomalonate hydrochloride</b>	inactive	inactive	inactive	inactive
<b><i>O</i> -phospho-L-serine</b>	inactive	inactive	inactive	inactive
<b><i>O</i> -phospho-L-tyrosine</b>	inactive	inactive	inactive	inactive
<b>3-ethoxy-2-methyl-3-oxo-1-phenylpropyl heptanoate</b>	inactive	inactive	inactive	inactive
<b>Andrographolide</b>	inactive	inactive	inactive	inactive
<b>Deoxyandrographolide</b>	inactive	inactive	inactive	inactive
<b>Neoandrographolide</b>	inactive	inactive	inactive	inactive
<b>Spiculosporic acid</b>	inactive	inactive	inactive	inactive
<b>Surfactin sodium</b>	inactive	inactive	inactive	inactive
<b>Glycyrrhizin</b>	inactive	inactive	inactive	inactive
<b>Glycyrrhetic acid</b>	inactive	inactive	inactive	inactive
<b>Petai seed extract</b>	inactive	inactive	inactive	inactive
<b>LXE-1</b>	inactive	inactive	inactive	inactive
<b>EPX-1</b>	inactive	inactive	inactive	inactive
<b>F16-17</b>	inactive	active	active	active
<b>F18-19</b>	inactive	active	active	active
<b>ACM 12-13</b>	inactive	inactive	inactive	inactive
<b>SHME 1-44</b>	inactive	inactive	inactive	inactive
<b>TAMDM-4W</b>	inactive	inactive	inactive	inactive
<b>TAMCF</b>	inactive	inactive	inactive	inactive
<b>ECMB</b>	inactive	inactive	inactive	inactive
<b>WSM-WASH</b>	inactive	inactive	inactive	inactive
<b>TASX-5</b>	inactive	inactive	inactive	inactive
<b>MFHE 84-89</b>	active	active	active	inactive
<b>MFHE 90-94</b>	active	inactive	active	inactive
<b>NME 31-37</b>	inactive	inactive	active	inactive
<b>C-6N</b>	inactive	inactive	inactive	inactive
<b>NPE 49.5</b>	inactive	inactive	inactive	inactive
<b>CSE-10</b>	inactive	inactive	inactive	inactive
<b>AMH 1</b>	inactive	inactive	inactive	inactive

<b>Compounds</b>	<b><i>E. coli</i></b>	<b><i>S. coelicolor</i></b>	<b><i>B. subtilis</i></b>	<b><i>S. aureus</i></b>
<b>CSM-23</b>	inactive	inactive	inactive	inactive
<b>NPE 8R</b>	inactive	inactive	inactive	inactive
<b>CPE-5</b>	inactive	inactive	active	active
<b>NPE-7</b>	inactive	inactive	inactive	inactive
<b>NMET 3</b>	inactive	inactive	inactive	inactive
<b>NMET 4</b>	inactive	inactive	inactive	inactive
<b>R56</b>	inactive	inactive	inactive	inactive
<b>R52-55</b>	inactive	inactive	inactive	inactive
<b>R26-49</b>	inactive	inactive	inactive	inactive
<b>R75-82</b>	inactive	inactive	inactive	inactive
<b>R60-62</b>	inactive	inactive	inactive	inactive
<b>TASX-2</b>	inactive	inactive	inactive	inactive
<b>R63-68</b>	inactive	inactive	active	inactive
<b>R60-65</b>	inactive	inactive	active	inactive
<b>CSE-11</b>	inactive	inactive	active	inactive
<b>NPE-8</b>	inactive	inactive	inactive	inactive
<b>NPRE-3</b>	inactive	inactive	inactive	inactive
<b>NPP81-89</b>	inactive	inactive	inactive	inactive
<b>TAMDM-2W</b>	inactive	inactive	active	inactive
<b>LLBE-39</b>	inactive	inactive	active	inactive
<b>LLBH-46</b>	inactive	inactive	inactive	inactive
<b>LLBH-42</b>	inactive	inactive	inactive	inactive
<b>FEBH-2</b>	inactive	inactive	inactive	inactive
<b>R9-14</b>	inactive	inactive	inactive	inactive
<b>R58-59</b>	inactive	inactive	inactive	inactive
<b>R7-9</b>	inactive	inactive	inactive	inactive
<b>CPE-6</b>	inactive	inactive	active	inactive

## 7.6 Discussion and conclusion

### 7.6.1 Chemical mechanism involved in the synthesis of ATC derivatives

The chemical synthesis of ATC derivatives is a well-established method involving a two-steps reaction (Zhang *et al.*, 2007; Al-Balas *et al.*, 2009; Chen *et al.*, 2010). The first step involves the Darzens reaction between methyl dichloroacetate and an aldehyde in the presence of sodium methoxide (base) as shown in Figure 84. The reaction proceeds through the resonance-stabilized enolate resulting in two intermediates; the  $\alpha$ -halo glycidic ester as the major product and  $\beta$ -halo  $\alpha$ -oxo ester as the minor product. Due to the reactivity of sodium methoxide, the whole reaction has to be carried out at 0 °C under anhydrous conditions to ensure optimal yields.

In the second-step, thiourea is added to these intermediates and refluxed in methanol. The  $\alpha$ -halo glycidic ester reacts with isothiuronium ion where the thiolate acts on the unstable epoxide ring releasing a chloride ion. The liberated chloride ion helps to stabilize the charge on isothiuronium salt via hydrogen extraction.  $S_N2$  nucleophilic attack of the amine group on the carbonyl group results in the formation of a thiazolidine ring. Finally, two double bonds are formed via the acid-catalyzed reaction which aromatizes the thiazolidine into the final thiazole product (major product) shown in Figure 85. The  $\beta$ -halo  $\alpha$ -oxo ester (minor product) forms the final thiazole product in a similar manner albeit involving a different starting product. The nucleophilic attack of the isothiuronium ion on the  $\beta$ -halo  $\alpha$ -oxo ester occurs in exactly the same mechanism as the major product to form the 4-carboxylate thiazole (Figure 86).



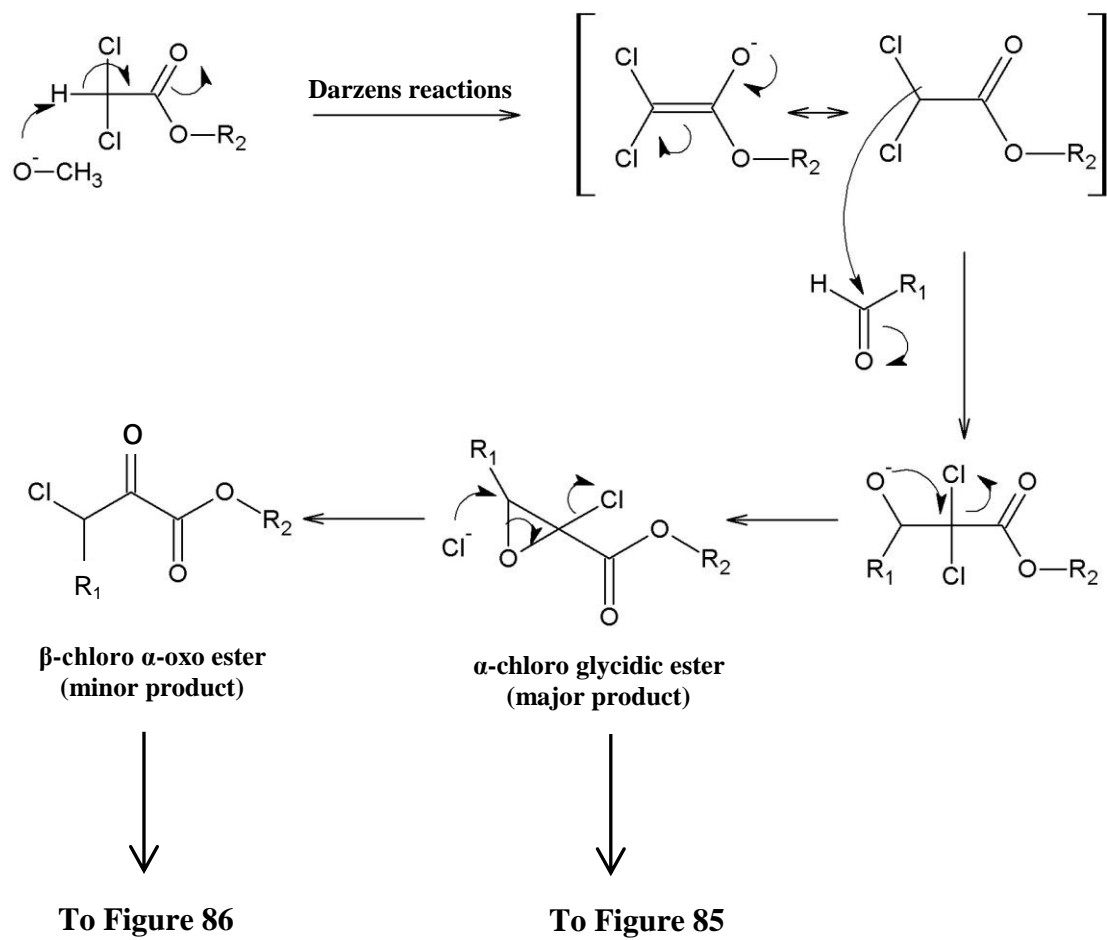


Figure 84: Darzens reaction involving methyl dichloroacetate and an aldehyde that resulted in the production of  $\alpha$ -halo glycidic ester as the major product and  $\beta$ -halo  $\alpha$ -oxo ester as the minor product.

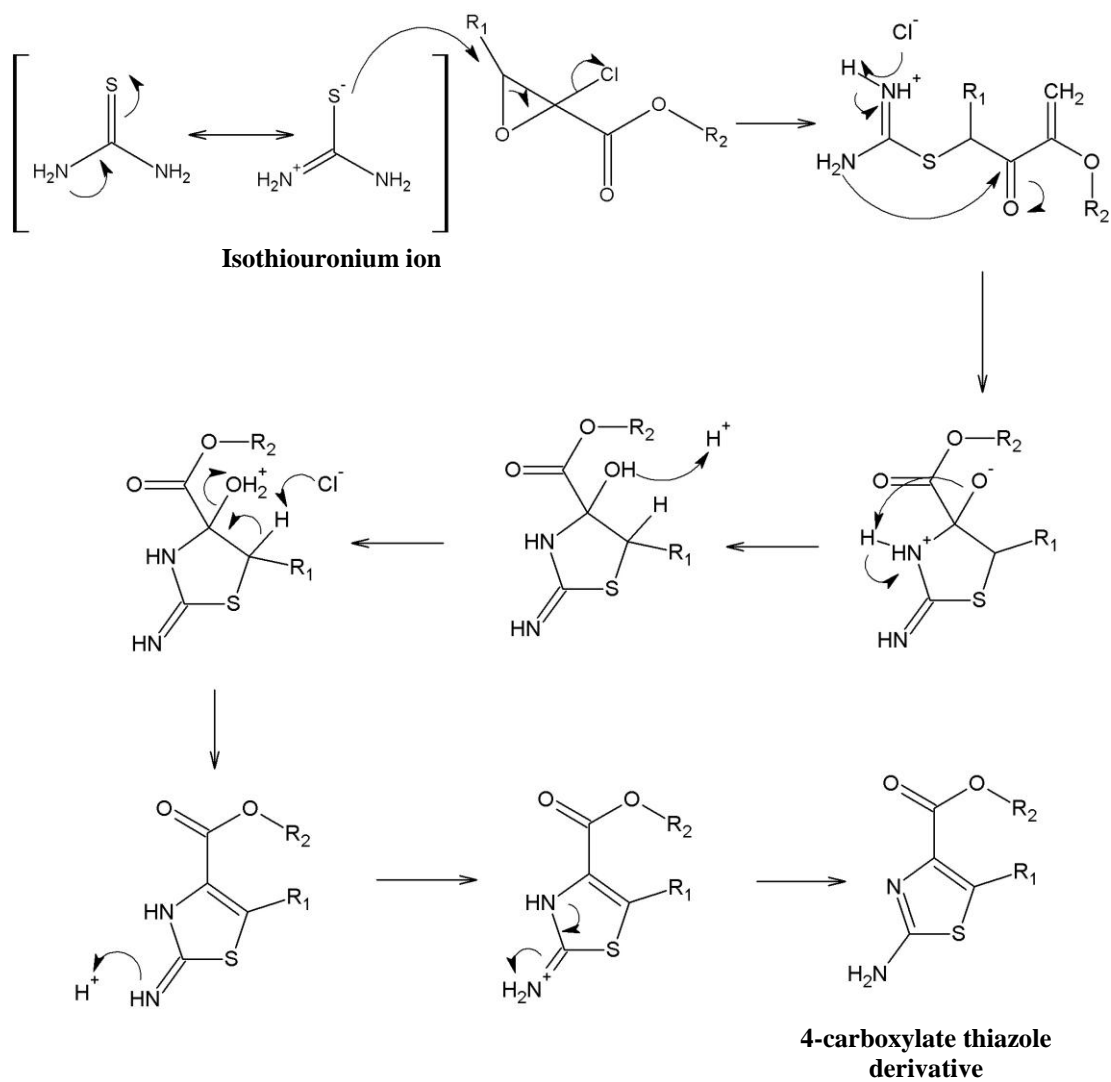


Figure 85: Mechanism involved in the formation of the final thiazole product from  $\alpha$ -halo glycidic ester (major product) and thiourea.

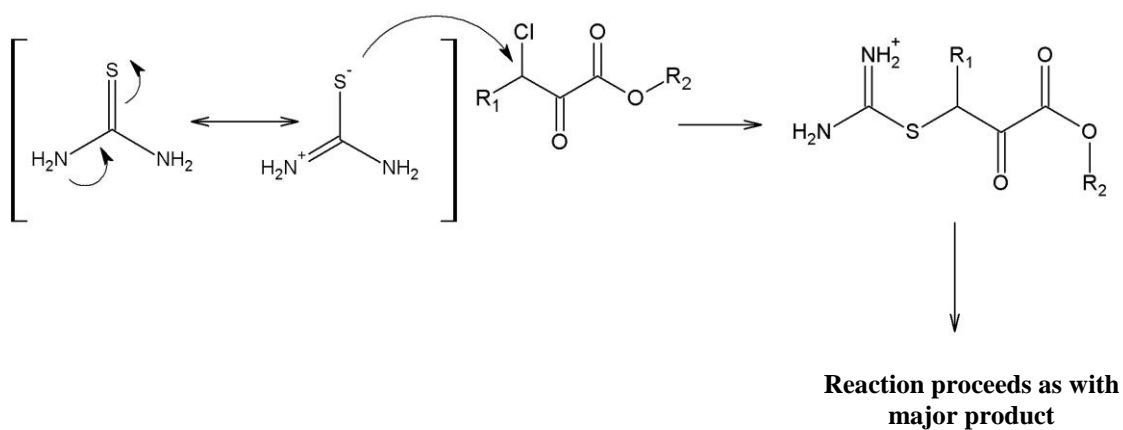


Figure 86: Mechanism involved in the formation of the final thiazole product from  $\beta$ -halo  $\alpha$ -oxo ester (minor product) and thiourea

## 7.6.2 Screening for potential inhibitors of Psd

With little knowledge of the exact binding domain and amino acid residues involved in the catalysis of our drug target, Psd (Chapter 4) an understanding of the overall catalytic mechanism could provide crucial insights into the nature of the interactions between drug target and ligand molecule besides the generation of predictive models suitable for lead compound optimization. Fortunately, the catalytic mechanism of Psd was proposed recently (Voelker, 1997). The mechanism of formation of the functional pyruvoyl prosthetic group ( $\alpha$  subunit) from its proenzyme and the catalytic mechanism of Psd are shown in Figure 87.

The cleavage of the catalytic  $\alpha$ -subunit from the zymogen begins with the serinolysis of the peptide bond between glycine and serine within the conserved 4 LGST motif (Chapter 4). Subsequent hydration and deamination of the  $\alpha$ -subunit leads to the generation of the active enzyme with the exposed pyruvoyl carbonyl functional group. The first step of the catalytic reaction commences with the binding of PS primary amine to the pyruvoyl carbonyl group forming a Schiff base with the  $\alpha$ -subunit. The decarboxylation reaction proceeds through the electron rearrangement resulting in azomethine intermediate with consecutive protonation forming the Schiff base linked Psd - PE complex. Finally, the hydration of the Schiff base liberates PE from the enzyme whilst regenerating the pyruvoyl prosthetic group for subsequent decarboxylation reaction.

The proposed catalytic model suggested the carbonyl group containing  $\alpha$ -subunit as the catalytic centre of Psd. Taking this idea onboard, we believed that the Schiff base forming serine moiety is the important pharmacophore of the natural substrate. However, with limited knowledge of the substrate recognition site in the bacterial Psd, the dispensability of other substructures had to be investigated. Therefore, the screening of the analogues obtained from the library of compounds relied on the omission/modification of substructure(s) of the natural substrate to investigate the effect of such alteration to the decarboxylation process.

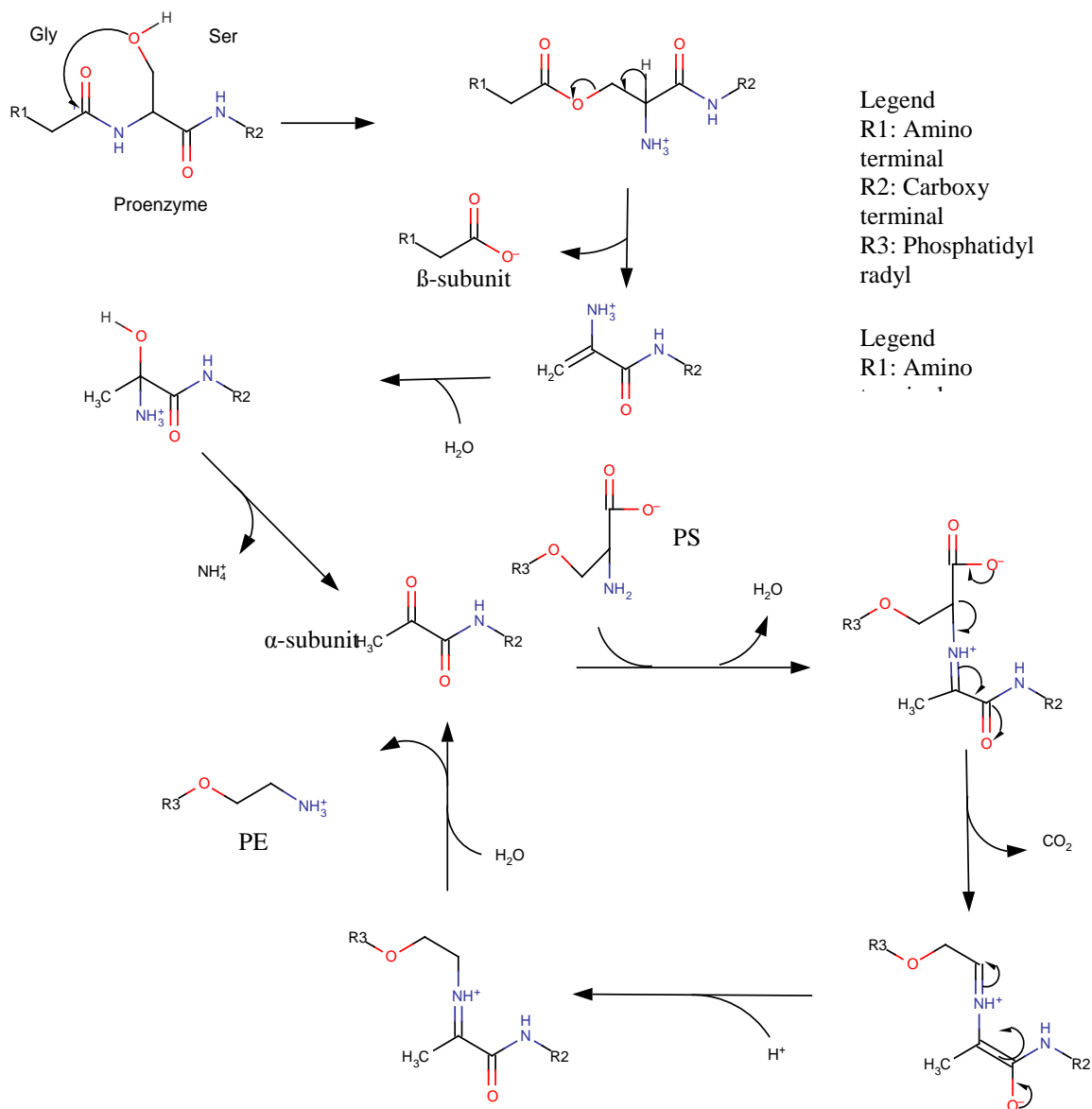


Figure 87: Mechanism of formation of the functional pyruvoyl prosthetic group ( $\alpha$  subunit) from its proenzyme and the decarboxylation mechanism of Psd in generation of PE from PS (adapted from Voelker, 1997).

The aim was to obtain a lead compound with adequate level of binding affinity which could compete with the natural substrate for the active site and block the decarboxylation process.

*O*-phospho-L-serine and *O*-phospho-L-tyrosine were chosen to assess the effect of omitting the lipid-side chains. Diethyl aminomalonate and *O*-phospho-L-tyrosine were tested to investigate the consequence of serine moiety replacement. 3-ethoxy-2-methyl-3-oxo-1-phenylpropyl heptanoate and diethyl aminomalonate both possessed the esterified carbonyl group in place of the free carboxyl group which could hopefully block the decarboxylation process since it was apparent from the proposed scheme that only free carboxyl group could be utilized in the catalytic process. 3-ethoxy-2-methyl-3-oxo-1-phenylpropyl heptanoate was also used to gauge the effect of phosphate group exclusion. Obtaining a possible 'hit' in the process would be a huge step forward since this could lead us to the ligand-based drug design approach. Understanding the structural and physico-chemical properties of the ligands which correlate with the desired inhibitory activity of those ligands based on the QSAR model might help in the lead optimization process (Acharya *et al.*, 2011).

Unfortunately, this approach had proven to be futile since none of the 4 compounds appeared to exhibit any sort of inhibitory activity. Structural modifications could be done on some of these compounds to alter their Log P values and/or their spatial orientations/shapes to address the possible pharmacodynamic issues (active site affinity/accessibility hindrance or membrane permeability) related to their lack of antibacterial activity.

Random screening of the natural plant extracts also did not yield any useful result. Although some compounds exhibited possible antibacterial activities, none fit the profile of being active against *S. coelicolor* but not *E. coli* and *B. subtilis* since Psd and Pss are non-essential in the latter two (Shibuya *et al.*, 1985; DeChavigny *et al.*, 1991; Saha *et al.*, 1996a; Matsumoto *et al.*, 1998). Screening of more compounds could be considered but an alternative approach should be undertaken since random

screening being both expensive and time consuming is not a feasible method in drug discovery.

A stronger approach would be to perform a protein X-ray crystallography or saturation-transfer difference (STD) NMR spectroscopy (Viegas *et al.*, 2011) on both Psd and Pss to characterize the atomic structure of these proteins. *In silico* design and optimization of ligands based on the important binding moieties within the active sites coupled with the calculated protein-ligand docking algorithm using software such as GOLD would increase the chance of obtaining a ‘hit’ and further improve upon the potency of potential inhibitors. Such method has gained importance in drug design since it complements and improves upon the role of traditional techniques like chemical synthesis and biological experimentation which necessitate a great deal of time and resources.

Finally, any compound with possible antibacterial activity obtained in the future would be tested on the mutant screen, JT672 designed previously. Elevation of the MIC in the mutant strain with the over-expressed protein in comparison to the wild type *S. coelicolor* could be a good indication of the protein targeting characteristic of the compound. Parallel testing should also be done on *M. tuberculosis* which is our target pathogen. Ultimately, structural optimization should be carried out on the identified antibacterial compounds to make them more drug-like in terms of their safety index, pharmacokinetic and pharmacodynamic properties prior to animal testing.

## **8.0 Conclusion and future work**



## 8.0 Conclusion and future work

We were able to verify the essentiality of both *psd* and *pss* hence validating the use of their gene products as potential drug targets within the phospholipid biosynthesis pathways. The main setback we faced was the inability to disrupt *S. coelicolor psd* despite numerous attempts. A new approach currently in sight involves the replacement of the promoter of *psd* in its native locus with an inducible promoter.

Even though we were successful in the construction of *pss* mutant, much work remains to be done especially when it comes to elucidation of the gene function. Since preliminary data suggested the involvement of PE in the morphology of *S. coelicolor* i.e. vegetative hyphae branching, septation and sporulation, the topological influence PE has over other cellular entities such as DivIVA (and its polarisome) and FtsZ which are the two main developmental regulators that govern these morphological processes could be investigated. This may involve the concurrent use of mCherry and EGFP to study the cellular co-localization of these molecules and how the alteration of *pss* expression would affect the overall fluorescence patterns. Fluorescence microscopy should also be carried out on the fluorescence dyes-stained JT672 (Cyto42, FM4-64, Vancomycin-FL and Ro09-0198 (Ro)) to visualize the co-placement of nucleoid, membrane, septum and PE in the partial depleted or overexpressed Pss mutant.

In the drug discovery programme, ‘hit identification’ process was started with the virtual screening of several libraries of compounds for potential inhibitors of Psd and the subsequent identification of four analogues of PS (i.e. diethyl aminomalonate hydrochloride, 3-ethoxy-2-methyl-3-oxo-1-phenylpropyl heptanoate, *O*-phospho-L-serine and *O*-phospho-L-tyrosine. Unfortunately, these analogues together with numerous other natural products and synthetic compounds (ATC derivatives) were either devoid of antibacterial property or did not match the required inhibitory profile i.e. selective only against *S. coelicolor*. Screening of more compounds should be carried out in conjunction with structural modification of the

four identified analogues to address the possible pharmacodynamic issues. Protein X-ray crystallography and/or saturation transfer difference - NMR should also be considered in order to characterize the atomic structure of the protein and its ligand - binding moieties which would help the computer-assisted drug design.

## **9.0 References**

## 9.0 References

- Abdallah, A.M., van Pittius, N.C.G., Patricia A. DiGiuseppe Champion, P.A.D., Cox, J., Luirink, J., Vandenbroucke-Grauls, C., Appelmek, B.J., & Bitter, W. (2007) Type VII secretion — mycobacteria show the way. *Nature Reviews Microbiology* **5**: 883-891
- Acharya, C., Coop, A., Polli, J.E., & MacKerell Jr, A.D. (2011) Recent Advances in Ligand-Based Drug Design: Relevance and Utility of the Conformationally Sampled Pharmacophore Approach. *Curr Comput Aided Drug Des* **7(1)**: 10-22
- Al-Balas, Q., Anthony, N.G., Al-Jaidi, B., Alnimr, A., Abbott, G., Brown, A.K., Taylor, R.C., Besra, G.S., McHugh, T.D., Gillespie, S.H., Johnston, B.F., Mackay, S.P., & Coxon, G.D. (2009) Identification of 2-Aminothiazole-4-Carboxylate Derivatives active against *Mycobacterium tuberculosis H37Rv* and the  $\beta$ -ketoacyl-ACP synthase mtFabH. *Plos one* **4(5)**: 1-9
- Ali, N., Herron, P.R., Evans, M.C., & Dyson, P.J. (2002) Osmotic regulation of the *Streptomyces lividans* thiostrepton-inducible promoter *Ptipa*. *Microbiology* **148**: 381-390
- Al-Khatib, K., & Carr, D.J.J (2003) Relative quantification of mRNA Real-Time PCR vs End- point PCR. *Bio-Rad Laboratories, Inc (USA)*. **2003**:2915
- Amaral, L., Boeree, M.J., Gillespie, S.H., Udwardia, Z.F., & van Soolingen, D. (2010) Thioridazine cures extensively drug-resistant tuberculosis (XDR-TB) and the need for global trials is now! *Int. J. Antimicrob. Agents* **35(6)**: 524–526
- Andries, K., Verhasselt, P., Guillemont, J., Gohlmann, H.W., Neefs, J.M., Winkler, H., Van Gestel, J., Timmerman, P., Zhu, M., Lee, E., Williams, P, de

- Chaffoy, D., Huitric, E., Hoffner, S., Cambau, E., Truffot-Pernot, C., Lounis, N., & Jarlier, V. (2005) A diarylquinoline drug active on the ATP synthase of *Mycobacterium tuberculosis*. *Science* **307(5707)**: 223–227
- Bakala N'Goma, J. C., Schue, M., Carriere, F., Geerlof, A., Canaan, S. (2010) Evidence for the cytotoxic effects of *Mycobacterium tuberculosis* phospholipase C towards macrophages. *Biochimica et Biophysica Acta* **1801**: 1305 - 1313
- Barak, I., Muchova, K., Wilkinson, A.J., O'Toole, P.J., & Pavlendova, N. (2008 ) Lipid spirals in *Bacillus subtilis* and their role in cell division. *Molecular Microbiology* **68**: 1315-1327
- Barker, *et al.* (2009) Novel S-Adenosylmethionine Decarboxylase Inhibitors for the Treatment of Human African Trypanosomiasis. *ANTIMICROBIAL AGENTS AND CHEMOTHERAPY* **53(5)**: 2052–2058
- Bateman, B. T., Donegan, N.P., Jarry, T.M., Palma, M. & Cheung, A.L. (2001) Evaluation of a Tetracycline-Inducible Promoter in *Staphylococcus aureus* *In Vitro* and *In Vivo* and Its Application in Demonstrating the Role of *sigB* in Microcolony Formation. *Infection and Immunity* **69(12)**: 7851–7857
- Bauer, A. W., Kirby, W.M., Sherris, J.C., & Turck, M. (1966) Antibiotic susceptibility testing by a standardized single disk method. *Am J Clin Pathol* **45(4)**: 493-496
- Bayer, R., & Wilkinson, D. (1995) Directly observed therapy for tuberculosis: history of an idea. *Lancet* **345(8964)**: 1545–1548
- Bell, R. M. (1974) Mutants of *Escherichia coli* defective in membrane phospholipid synthesis: macromolecular synthesis in an sn-glycerol 3-phosphate acyltransferase Km mutant. *J Bacteriol* **117(3)**: 1065-1076

- Bentley, S. D., Chater, K.F., Cerdeño-Tárraga, A.M., Challis, G.L., Thomson, N.R., James, K.D., Harris, D.E, *et al* (2002) Complete genome sequence of the model actinomycete *Streptomyces coelicolor* A3(2). *Nature* **417**: 141-147
- Bibb, M. J., Janssen, G.R., & Ward, J.M. (1985) Cloning and analysis of the promoter region of the erythromycin resistance gene (*ermE*) of *Streptomyces erythraeus*. *Gene* **38(1-3)**: 215-226.
- Birnboim, H.C., & Doly, J. (1979) A rapid alkaline extraction procedure for screening recombinant plasmid DNA. *Nucleic Acids Res* **7(6)**: 1513-1523
- Bishop, A., Fielding, S., Dyson, P., & Herron, P.R (2004) Systematic insertional mutagenesis of a streptomycete genome: a link between osmoadaptation and antibiotic production. *Genome Research* **14**: 893-900
- Bligh, E. G., & Dyer, W.J. (1959) A rapid method of total lipid extraction and purification. *Can J Biochem Physiol* **37**: 911-917
- Boccard, F., Smokvina, T., Pernodet, J.L., Friedmann, A., & Guerineau, M. (1989) The integrated conjugative plasmid pSAM2 of *Streptomyces ambofaciens* is related to temperate bacteriophages. *EMBO J* **8**: 973 - 980
- Bogdanova, M., Heacock, P., Guan, Z., & Dowhan, W. (2010) Plasticity of lipid-protein interactions in the function and topogenesis of the membrane protein lactose permease from *Escherichia coli*. *doi: 10.1073/pnas.1006286107*
- Braña, A. F., Manzanal, M.B., & Hardison, C. (1982) Mode of cell wall growth of *Streptomyces antibioticus*. *FEMS Microbiol Lett* **13**: 231-235
- Bucca, G., Laing, E., Mersinias, V., Allenby, N., Hurd, D., Holdstock, J., Brenner, V., Harrison, M., & Smith, C.P. (2009). Development and application of

versatile high density microarrays for genome-wide analysis of *Streptomyces coelicolor*: characterization of the HspR regulon. *Genome Biol* **10**: R5

- Burman, W. J., Goldberg, S., Johnson, J.L., Muzanye, G., Engle, M., Mosher, A.W., Choudhri, S., Daley, C.L., Munsiff, S.S., Zhao, Z., Vernon, A., & Chaisson, R.E. (2006) Moxifloxacin versus ethambutol in the first 2 months of treatment for pulmonary tuberculosis. *Am Respir Crit Care Med* **174(3)**: 331–338.
- Bustin, S. A., & Dorudi, S. (1998) Molecular assessment of tumour stage and disease recurrence using PCR-based assays. *Molecular Medicine Today* **4**: 389–396
- Buttner, M. J., Chater, K.F., & Bibb, M.J. (1990) Cloning, disruption and transcriptional analysis of three RNA polymerase sigma factor genes of *Streptomyces coelicolor* A3(2). *J Bacteriol* **172(6)**: 3367-3378.
- Bystrykh, L. V., Fernández-Moreno, M.A., Herrema, J.K., Malpartida, F., Hopwood D.A., & Dijkhuizen, L. (1996) Production of actinorhodin-related "blue pigments" by *Streptomyces coelicolor* A3(2). *J Bacteriol* **178(8)**: 2238-2244
- Capstick, D. S., Willey, J.M., Buttner, M.J., Elliot, M.A. (2007) SapB and the chaplins: connections between morphogenetic proteins in *Streptomyces coelicolor*. *Molecular Microbiology* **64**: 602 - 613
- Chalfie, M., Tu, Y., Euskirchen, G., Ward, W., & Prasher, D. (1994) Green fluorescent protein as a marker for gene expression. *Science* **263 (5148)**: 802–805
- Champness, W.C. (1988) New loci required for *Streptomyces coelicolor* morphological and physiological differentiation. *J Bacteriol* **170**: 1168-1174

- Chang, Y.Y., & Kennedy, E.P. (1967a) Biosynthesis of phosphatidyl glycerophosphate in *Escherichia coli*. *J Lipid Res* **8**: 447-455
- Chang, Y.Y., & Kennedy, E.P. (1967b) Pathways for the synthesis of glycerophosphatides in *Escherichia coli*. *Journal of Biological Chemistry* **242(3)**: 516-519
- Chater, K. F. (1993) Genetics of differentiation in *Streptomyces*. *Annu Rev Microbiol* **47**: 685-713
- Chen, B.C., Zhao, R., Wang, B., Droghini, R., Lajeunesse, J., Sirard, P., Endo, M., Balasubramanian, B., & Barrisha, J.C. (2010) A new and efficient preparation of 2-aminothiazole-5-carbamides: applications to the synthesis of the anti-cancer drug dasatinib. *ARKIVOC* **vi**: 32- 38.
- Chiu, M.L., Folcher, M., Griffin, P., Holt, T., Klatt, T., & Thompson, C.J. (1996) Characterization of the covalent binding of thiostrepton to a thiostrepton-induced protein from *Streptomyces lividans*. *Biochemistry* **35**: 2332 - 2341
- Chiu, M.L., Folcher, M., Katoh, T., Puglia, A.M., Vohradsky, J., Yun, B.S., Seto, H., & Thompson, C.J. (1999) Broad spectrum thiopeptide recognition specificity of the *Streptomyces lividans* TipAL protein and its role in regulating gene expression. *J Biol Chem* **274**: 20578 - 20586
- Claessen, D. *et al.* (2002) Two novel homologous proteins of *Streptomyces coelicolor* and *Streptomyces lividans* are involved in the formation of the rodlet layer and mediate attachment to a hydrophobic surface. *Molecular Microbiology* **44**: 1483 – 1492
- Claessen, D., Rink, R., Jong, W.D., Siebring, J., Vreugd, P.D, Boersma, F.G.H., Dijkhuizen, L., & Wo sten, H.A.B. (2003) A novel class of secreted hydrophobic proteins is involved in aerial hyphae formation in *Streptomyces*



coelicolor by forming amyloid-like fibrils. *Genes & Development* **17**: 1714–1726.

Claessen, D. *et al.* (2004) The formation of the rodlet layer of streptomycetes is the result of the interplay between rodlines and chaplins. *Molecular Microbiology* **53**: 433 - 443

Combes, P., Till, R., Bee, S., & Smith, M.C.M. (2002). The *Streptomyces* Genome Contains Multiple Pseudo-attB Sites for the phiC31-Encoded Site-Specific Recombination System. *J Bacteriol* **184(20)**: 5746–5752.

Corbeil, C. R., & Moitessier, N. (2009) Docking Ligands into Flexible and Solvated Macromolecules. 3. Impact of Input Ligand Conformation, Protein Flexibility and Water Molecules on the Accuracy of Docking Programs. *J Chem Inf Model* **49**: 997- 1009

Cotes, K., Bakala N'Goma, C., Dhouib, J.R., Douchet, I., Maurin, D., Carriere, F., Canaan, S. (2008) Lipolytic enzymes in *Mycobacterium tuberculosis*. *Appl. Microbiol. Biotechnol* **78**: 741 - 749

Cronan, J. E., & Gelman, E.P. (1975) Physical properties of membrane lipids: biological relevance and regulation. *Bacteriol Rev* **39**: 232-256.

Cullis, P.R., Verkleij, A.J., & Ververgaert, P.H. (1978a) Polymorphic phase behaviour of cardiolipin as detected by <sup>31</sup>P NMR and freeze-fracture techniques. Effects of calcium, dibucaine and chlorpromazine. *Biochim Biophys Acta* **513(1)**: 11-20

Cullis P.R., & De Kruijff, B. (1978b) The polymorphic phase behaviour of phosphatidylethanolamines of natural and synthetic origin. A <sup>31</sup>P NMR study. *Biochim Biophys Acta* **513(1)**: 31-42

- Daniel, R. A., & Errington, J. (2003) Control of Cell Morphogenesis in Bacteria: Two Distinct Ways to Make a Rod-Shaped Cell. *Cell* **113(6)**: 767–776
- Datsenko, K.A., & Wanner, B.L. (2000). One-step inactivation of chromosomal genes in *Escherichia coli* K-12 using PCR products. *Proc Natl Acad Sci U.S.A.* **97(12)**: 6640-6645
- De Carvalho, L. P., Lin, G., Jiang, X., & Nathan, C. (2009) Nitazoxanide kills replicating and nonreplicating *Mycobacterium tuberculosis* and evades resistance. *J Med Chem* **52(19)**: 5789–5792
- De Sol, R., Pitman, A., Herron, P., & Dyson, P. (2003) The product of a developmental gene, *crgA*, that coordinates reproductive growth in *Streptomyces* belongs to a novel family of small actinomycete-specific proteins. *J Bacteriol* **185**: 6678 – 6685
- De Sol, R., Mullins, J.G.L., Grantcharova, N., Flardh, K., & Dyson, P. (2006) Influence of CrgA on Assembly of the Cell Division Protein FtsZ during Development of *Streptomyces coelicolor*. *J Bacteriol* **188(4)**: 1540–1550.
- DeChavigny, A., Heacock, P.N., & Dowhan, W. (1991) Sequence and inactivation of the *pss* gene of *Escherichia coli*. Phosphatidylethanolamine may not be essential for cell viability. *J Biol Chem* **266**: 5323 - 5332
- Desjardin, L.E., Perkins, M.D., Wolski, K., Haun, S., Teixeira, L., Chen, Y., Johnson, J.L., Ellner, J.J., Dietze, R., Bates, J., Cave, M.D., & Eisenach, K.D. (1999) Measurement of sputum *Mycobacterium tuberculosis* messenger RNA as a surrogate for response to chemotherapy. *American Journal of Respiratory and Critical Care Medicine* **160**: 203–210

- Dixon, P. D., Beven, J.E., & Cundliffe, E. (1975) Properties of the ribosomes of antibiotic producers: effects of thiostrepton and micrococcin on the organisms which produce them. *Antimicrob Agents Chemother* **7(6)**: 850-855
- Dorman, S. E., Johnson, J.L., Goldberg, S., Muzanye, G., Padayatchi, N., Bozeman, L., Heilig, C.M., Bernardo, J., Choudhri, S., Grosset, J.H., Guy, E., Guyadeen, P., Leus, M.C., Maltas, G., Menzies, D., Nuermberger, E.L, Villarino, M., Vernon, A., & Chaisson, R.E. (2009) Substitution of moxifloxacin for isoniazid during intensive phase treatment of pulmonary tuberculosis. *American Journal of Respiratory and Critical Care Medicine* **180(3)**: 273–280
- Dover, L.G., & Coxon, G.D. (2011) Current Status and Research Strategies in Tuberculosis Drug Development. *Journal of Medicinal Chemistry* **54**: 6157–6165
- Dower, W.J., Miller, J.F., & Ragsdale, C.W. (1988) High-efficiency transformation of *Escherichia coli* by high-voltage electroporation. *Nucleic Acids Research* **16**: 6127-6145
- Dowhan, W. (1997) MOLECULAR BASIS FOR MEMBRANE PHOSPHOLIPID DIVERSITY: Why Are There So Many Lipids? *Annu Rev Biochem* **66**: 199 – 232
- Dowhan, W., Wickner, W.T., & Kennedy, E.P. (1974) Purification and properties of phosphatidylserine decarboxylase from *Escherichia coli*. *The Journal of Biological Chemistry* **249(10)**: 3079-3084
- Dubnau, E., Chan, J., Raynaud, C., Mohan, V. P., Laneelle, M.A., Yu, K., Quemard, A., Smith, I., & Daffe, M. (2000). Oxygenated mycolic acids are necessary for virulence of *Mycobacterium tuberculosis* in mice. *Mol Microbiol* **36**: 630–637

- Dutt, A., & Dowhan, W. (1981) Characterization of a membrane-associated cytidine diphosphate-diacylglycerol-dependent phosphatidylserine synthase in Bacilli. *J Bacteriol* **147**: 535 - 542
- Dye, C., Scheele, S., Dolin, P., Pathania, V., & Raviglione, M.C. (1999) Consensus statement. Global burden of tuberculosis: estimated incidence, prevalence, and mortality by country. WHO Global Surveillance and Monitoring Project. *The Journal of American Medical Association* **282(7)**: 677-686
- Elliot, M. A., Karoonuthaisiri, N., Huang, J., Bibb, M.J., Cohen, S.N., Kao, C.M., & Buttner, M.J. (2003) The chaplins: a family of hydrophobic cell-surface proteins involved in aerial mycelium formation in *Streptomyces coelicolor*. *Gene Dev* **17(14)**: 1727-1740
- Emoto, K., Kobayashi, T., Yamaji, A., Aizawa, H., Yahara, I., Inoue, K., & Umeda, M. (1996) Redistribution of phosphatidylethanolamine at the cleavage furrow of dividing cells during cytokinesis. *Proc Natl Acad Sci USA* **93**: 12867-12872
- Enguita, F.J., de la Fuente, J.L., Martin, J.F., & Liras, P. (1996) An inducible expression system of histidine-tagged proteins in *Streptomyces lividans* for one-step purification by Ni<sup>2+</sup> affinity chromatography. *FEMS Microbiol Lett* **137**: 135-140
- Espinal, M.A. (2003) The global situation of MDR-TB. *Tuberculosis* **83(1-3)**: 44-51
- Felsenfield, G. (1992) Chromatin as an essential part of the transcriptional mechanism. *Nature* **355**: 219-224

- Ferrara, P., Gohlke, H., Price, D.J., Klebe, G., & Brooks, C.L. (2004) Assessing Scoring Functions for Protein-Ligand Interactions. *J Med Chem* **47**: 3032-3047
- Ferrari, G., Naito, M., Langen, H., & Pieters, J. (1999) A coat protein on phagosomes involved in the intracellular survival of mycobacteria. *Cell* **97**: 435-447
- Flardh, K., Findlay, K.C., & Chater, K.F. (1999) Association of early sporulation genes with suggested developmental decision points in *Streptomyces coelicolor* A3(2). *Microbiology* **145**: 2229-2243
- Flardh, K., Leibovitz, E., Buttner, M.J., Chater, K.F. (2000) Generation of a non-sporulating strain of *Streptomyces coelicolor* A3(2) by the manipulation of a developmentally controlled *ftsZ* promoter. *Molecular Microbiology* **38(4)**: 737-749
- Flardh, K. (2003a) Essential role of DivIVA in polar growth and morphogenesis in *Streptomyces coelicolor* A3(2). *Molecular Microbiology* **49(6)**: 1523–1536
- Flardh, K. (2003b) Growth polarity and cell division in *Streptomyces*. *Current Opinion in Microbiology* **6**: 564-571
- Flardh, K., & Buttner, M.J. (2009) *Streptomyces* morphogenetics: dissecting differentiation in a filamentous bacterium. *Nat Rev Microbiol* **7**: 36-49
- Fratti, R. A., Chua, J., Vergne, I., & Deretic, V. (2003) *Mycobacterium tuberculosis* glycosylated phosphatidylinositol causes phagosome maturation arrest. *Proc Natl Acad Sci USA* **100**: 5437-5442
- Funk, C.R., Zimniak, L., & Dowhan, W. (1992) The *pgpA* and *pgpB* genes of *Escherichia coli* are not essential: evidence for a third phosphatidylglycerophosphate phosphatase. *J Bacteriol* **174(1)**: 205-213

- Ganong, B.R., Leonard, J.M., & Raetz, C.R.H (1980) Phosphatidic acid accumulation in the membranes of *Escherichia coli* mutants defective in CDP-diglyceride synthetase. *Journal of Biological Chemistry* **255(4)**: 1623-1629
- Gao, L.Y., Laval, F., Lawson, E.H., Groger, R.K., Woodruff, A., Morisaki, J.H., Cox, J.S., Daffe, M., & Brown, E.J. (2003) Requirement for *kasB* in *Mycobacterium* mycolic acid biosynthesis, cell wall impermeability and intracellular survival: implications for therapy. *Molecular Microbiology* **49(6)**: 1547–1563
- Gatfield, J., & Pieters, J. (2000) Essential role for cholesterol in entry of mycobacteria into macrophages. *Science* **288**: 1647-1650
- Gause, W.C., & Adamovicz, J. (1994) The use of the PCR to quantitate gene expression *Genome Research* **3**: 123-135
- Ghossein, R. A., & Rosai, J. (1996) Polymerase chain reaction in the detection of micrometastases and circulating tumor cells. *Cancer* **78**: 10-16
- Grant, S.G., Jessee, J., Bloom, F.R., & Hanahan, D. (1990) Differential plasmid rescue of *fmr* transgenic mouse DNAs into *Escherichia coli* methylation-restriction mutants. *Proceedings of the National Academy of Sciences of the United States of America*. **87**: 4645-4649
- Grantcharova, N., Lustig, U., & Flärdh, K. (2005) Dynamics of FtsZ assembly during sporulation in *Streptomyces coelicolor* A3(2). *J Bacteriol* **187(9)**: 3227-3237
- Gray, D.I., Gooday, G.W., & Prosser, J.I. (1990) Apical hyphal extension in *Streptomyces coelicolor* A3 (2). *J Gen Microbiol* **136**: 1077–1084

- Gregory, M.A., Till, R., & Smith, M.C.M. (2003) Integration site for *Streptomyces* phage phiBT1 and development of site-specific integrating vectors. *Journal of Bacteriology* **185**: 5320-5323
- Grosset, J. (2003) *Mycobacterium tuberculosis* in the extracellular compartment: an underestimated adversary. *Antimicrob Agents Chemother* **47**: 833-836
- Gruenberg, J., & Stenmark, H. (2004) The biogenesis of multivesicular endosomes. *Nat Rev Mol Cell Biol* **5**: 317-323
- Gust, B., Challis, G.L., Fowler, K., Kieser, T., & Chater, K.F. (2003) PCR-targeted *Streptomyces* gene replacement identifies a protein domain needed for biosynthesis of the sesquiterpene soil odor geosmin. *Proc Natl Acad Sci USA* **100**: 1541–1546
- Hamada, S., Fujiwara, T., Shimauchi, H., Ogawa, T., Nishihara, T., Koga, T., Nishihara, T. & Matsuno, T. (1990) Antimicrobial activities of thiolactomycin against gram-negative anaerobes associated with periodontal disease. *Oral Microbiol Immunol* **5**: 340-345
- Hanahan, D. (1983) Studies of transformation of *Escherichia coli* with plasmids. *Journal of Molecular Biology* **166**: 557-580
- Harries, A. D., & Dye, C. (2006) Tuberculosis. *Annals of Tropical Medicine and Parasitology* **100(17)**: 415-431
- Hasegawa, Y., Kawada, N. & Nosoh, Y. (1980) Change in chemical composition of membrane of *Bacillus caldotenax* after shifting the growth temperature. *Arch Microbiol* **126**: 103-108

- Hawrot, E., & Kennedy, E.P (1975) Biogenesis of membrane lipids: mutants of *Escherichia coli* with temperature-sensitive phosphatidylserine decarboxylase. *Proc Natl Acad Sci USA* **72**: 1112-1116
- Hawrot, E., & Kennedy, E.P (1976) Conditional lethal phosphatidylserine decarboxylase mutants of *Escherichia coli*. Mapping of the structural gene for phosphatidylserine decarboxylase. *Mol Gen Genet* **148**: 271-279
- Hawrot, E., & Kennedy, E.P (1978) Phospholipid Composition and Membrane Function in Phosphatidylserine Decarboxylase Mutants of *Escherichia coli*. *The Journal of Biological Chemistry* **253(22)**: 8213-8220
- Heacock, P.N., & Dowhan, W. (1987) Construction of a lethal mutation in the synthesis of the major acidic phospholipids of *Escherichia coli*. *Journal of Biological Chemistry* **262(27)**: 13044-13049
- Hempel, A.M., Wang, S., Letek, M., Gil, J.A., & Flardh, K. (2008) Assemblies of DivIVA mark sites for hyphal branching and can establish new zones of cell wall growth in *Streptomyces coelicolor*. *JOURNAL OF BACTERIOLOGY* **190(22)**: 7579–7583
- Hempel, A. M., Cantlay, S., Molle, V., Wang, S.B., Naldrett, M.J., Parker, J.L., Richards, D.M., Jung, Y.G., Buttner, M.J., & Flardh, K. (2012) The Ser/Thr protein kinase AfsK regulates polar growth and hyphal branching in the filamentous bacteria *Streptomyces*. *Proc Natl Acad Sci USA* **109(35)**: E2371-2379.
- Herron, P.R., Hughes, G., Chandra, G., Fielding, S., & Dyson, P.J. (2004) Transposon Express, a software application to report the identity of insertions obtained by comprehensive transposon mutagenesis of sequenced genomes: analysis of the preference for *in vitro* Tn5 transposition into GC-rich DNA. *Nucleic Acids Research* **32**



- Hill, W. E. (1996). The polymerase chain reaction: applications for the detection of food borne pathogens. *Critical Reviews in Food Science and Nutrition* **36**: 23–173
- Hirschberg, C.B., & Kennedy, E.P. (1972) Mechanism of the enzymatic synthesis of cardiolipin in *Escherichia coli*. *Proc Natl Acad Sci USA* **69**: 648-651
- Hobbs, G., Frazer, C.M., Gardner, D.C.J., Cullum, J.A., & Oliver, S.G. (1989). Dispersed growth of streptomycetes in liquid culture. *Appl Microbiol Biotechnol* **31**: 272-277
- Hoischen, C., Gura, K., Luge, C., & Gumpert, J. (1997). Lipid and Fatty Acid Composition of Cytoplasmic Membranes from *Streptomyces hygroscopicus* and Its Stable Protoplast-Type L Form. *JOURNAL OF BACTERIOLOGY* **179(11)**: 3430–3436
- Holmes, D.J., Caso, J.L. & Thompson, C.J. (1993) Autogenous transcriptional activation of a thiostrepton-induced gene in *Streptomyces lividans*. *EMBO J* **12**: 3183 - 3191
- Holodniy, M. (1994) Clinical application of reverse transcription-polymerase chain reaction for HIV infection. *Clinical and Laboratory Medicine* **14**: 335–349
- Hopwood, D.A. (1967) Genetic analysis and genome structure in *Streptomyces coelicolor*. *Bacteriol Rev* **31**: 373-403
- Hopwood, D.A., & Wright, H.M. (1978) Bacterial protoplast fusion: recombination in fused protoplasts of *Streptomyces coelicolor*. *Mol Gen Genet* **162**: 307-317

- Hoskisson, P. A., Hobbs, G., & Sharples, G.P. (2000) Response of *Micromonospora echinospora* (NCIMB 12744) spores to heat treatment with evidence of a heat activation phenomenon. *Letters in Applied Microbiology* **30**: 114-117
- Houben, E.N., Nguyen, L., & Pieters, J. (2006) Interaction of pathogenic mycobacteria with the host immune system. *Current Opinion in Microbiology* **9**: 76 - 85
- Huang, J., Lih, C., Pan, K., & Cohen, N. (2001) Global analysis of growth phase responsive gene expression and regulation of antibiotic biosynthetic pathways in *Streptomyces coelicolor* using DNA microarrays. *Genes & Development* **15**: 3183-3192
- Huang, K.C., Mukhopadhyay, R., & Wingreen, N.S. (2006) A curvature-mediated mechanism for localization of lipids to bacterial poles. *PloS Comput Biol* **2**: 1357-1364
- Igarashi, K., Kaneda, M., Yamaji, A., Saido, T.C., Kikkawa, U., Ono, Y., Inoue, K., & Umeda, M. (1995) A Novel Phosphatidylserine-binding Peptide Motif Defined by an Anti-idiotypic Monoclonal Antibody. Localization of phosphatidylserine-specific binding sites on protein kinase C and phosphatidylserine decarboxylase. *The Journal of Biological Chemistry* **270(49)**: 29075–29078
- Jackson, B. J., & Kennedy, E.P (1984) The biosynthesis of membrane-derived oligosaccharides: a membrane-bound phosphoglycerol transferase. *Journal of Biological Chemistry* **258**: 2394-2398
- Jackson, M., Crick, D.C., & Brennan, P.J. (2000) Phosphatidylinositol Is an Essential Phospholipid of Mycobacteria. *THE JOURNAL OF BIOLOGICAL CHEMISTRY* **275(39)**: 30092–30099

- Jyothikumar, V., Tilley, E.J., Wali, R., & Herron, P.R. (2008). Time-Lapse Microscopy of *Streptomyces coelicolor* Growth and Sporulation. *APPLIED AND ENVIRONMENTAL MICROBIOLOGY* **74(21)**: 6774-6781
- Jyothikumar, V., Klanbut, K., Tiong, J., Roxburgh, J.S., Hunter, I.S., Smith, T.K. & Herron, P.R. (2012) Cardiolipin synthase is required for *Streptomyces coelicolor* morphogenesis. *Molecular Microbiology* **84(1)**: 181 – 197
- Kanfer, J., & Kennedy, E.P (1963) Metabolism and function of bacterial lipids. *The Journal of Biological Chemistry* **238(9)**: 2919-2922
- Kanfer, J., & Kennedy, E.P (1964) Metabolism and function of bacterial lipids II. *The Journal of Biological Chemistry* **239(6)**: 1720-1726
- Kang, J.G., Hahn, M.Y., Ishihama, A., & Roe, J.H. (1997) Identification of sigma factors for growth phase-related promoter selectivity of RNA polymerases from *Streptomyces coelicolor* A3(2). *Nucleic Acids Research* **25**: 2566-2573
- Kang, S. G., Jin, W., Bibb, M. & Lee, K.J. (1998) Actinorhodin and undecylprodigiosin production in wild-type and *relA* mutant strains of *Streptomyces coelicolor* A3(2) grown in continuous culture. *FEMS Microbiol Lett* **168**: 221 – 226
- Kapetanovic, I.M. (2008) Computer - aided drug discovery and development (CADD): *in silico* - chemico - biological approach. *Chem Biol Interact* **171(2)**: 165-171
- Karnezis, T., Fisher, H.C., Neumann, G.M., Stone, B.A & Stanisich, V.A. (2002) Cloning and Characterization of the Phosphatidylserine Synthase Gene of *Agrobacterium* sp. Strain ATCC 31749 and Effect of Its Inactivation on Production of High-Molecular-Mass (1->3)-b-d-Glucan (Curdlan). *J Bacteriol* **184(15)**: 4114-4123

- Katzung, B.G. (2004) Antibacterial Agents III. Basic and Clinical Pharmacology. USA, Appleton & Lange. **8th Edition:** 793-802
- Kawai, F., Shoda, M., Harashima, R., Sadaie, Y., Hara, H., & Matsumoto K. (2004) Cardiolipin domains in *Bacillus subtilis* Marburg membranes. *J Bacteriol* **186:** 1475-1483
- Keijser, B. J., Noens, E.E., Kraal, B., Koerten, H.K., & van Wezel, G.P. (2003) The *Streptomyces coelicolor* *ssgB* gene is required for early stages of sporulation. *FEMS Microbiol Lett* **225:** 59-67
- Kelemen, H. G., & Buttner, M.J. (1998) Initiation of aerial mycelium formation in *Streptomyces*. *Current Opinion in Microbiology* **1:** 656-662
- Khaleel, T., Younger, E., McEwan, A.R., Varghese, A.S., & Smith, M.C.M. (2011) A phage protein that binds phi C31 integrase to switch its directionality. *Molecular Microbiology* **80:** 1450-1463
- Kikuchi, S., Shibuya, I., & Matsumoto, K. (2000) Viability of an *Escherichia coli* *pgsA* Null Mutant Lacking Detectable Phosphatidylglycerol and Cardiolipin. *J Bacteriol* **18(2):** 371-376
- Kieser, T., Bibb, M.J., Buttner, M.J., Chater, K.F., & Hopwood, D.A. (2000) *Practical Streptomyces Genetics*. John Innes Foundation, Norwich, UK
- Kochi, A. (1994) Tuberculosis: distribution, risk factors, mortality. *Immunobiology* **191(4- 5):** 325-336
- Kodani, S., Hudson, M.E., Durrant, M.C., Buttner, M.J., Nodwell, J.R., & Willey, M.J. (2004) The SapB morphogen is a lantibiotic-like peptide derived from

the product of the developmental gene *ramS* in *Streptomyces coelicolor*. *Proc Natl Acad Sci USA* **101**: 11448-11453

- Kuge, O., Nishijima, M., & Akamatsu, Y. (1986) Phosphatidylserine biosynthesis in cultured Chinese hamster ovary cells III. Genetic evidence for utilization of phosphatidylcholine and phosphatidylethanolamine as precursors. *J Biol Chem* **261(13)**: 5795-5798.
- Kuge, O., Saito, K., & Nishijima, M. (1997) Cloning of a Chinese hamster ovary (CHO) cDNA encoding phosphatidylserine synthase (PSS) II, overexpression of which suppresses the phosphatidylserine biosynthetic defect of a PSS I-lacking mutant of CHO-K1 cells. *J Biol Chem* **272(31)**: 19133-19139.
- Larkin M.A., Blackshields G., Brown N.P., Chenna R., McGettigan P.A., McWilliam H., Valentin F., Wallace I.M., Wilm A., Lopez R., Thompson J.D., Gibson T.J., & Higgins D.G. (2007) ClustalW and ClustalX version 2. *Bioinformatics* **23(21)**: 2947-2948.
- Lawn, S.D., & Wilkinson, R. (2006) Extensively drug resistant tuberculosis. *British Medical Journal* **333**: 559-560
- Lee, E.J., Cho, Y.H., Kim, H.S., & Roe, J.H. (2004) Identification of  $\sigma^B$ -dependent promoters using consensus-directed search of *Streptomyces coelicolor* genome. *The Journal of Microbiology* **42(2)**: 147-151
- Lee, E.J, Karoonuuthaisiri, N., Kum, H., Park, J., Cha, C., Kao, C.M., & Roe, J. (2005) A master regulator  $\sigma^B$  governs osmotic and oxidative response as well as differentiation via a network of sigma factors in *Streptomyces coelicolor*. *Molecular Microbiology* **57(5)**: 1252-1264
- Leskiw, B.K., Bibb, M.J., & Chater, K.F. (1991) The use of a rare codon specifically during development? *Molecular Microbiology* **5**: 2861–2867

- Li, Q. X., & Dowhan, W. (1988) Structural characterization of *Escherichia coli* phosphatidylserine decarboxylase. *J Biol Chem* **263**: 11516–11522
- Lopez, C.S., Alice, A.F., Heras, H., Rivas, E.A., & Sanchez-Rivas, C. (2006) Role of anionic phospholipids in the adaptation of *Bacillus Subtilis* to high salinity. *Microbiology* **152**: 605-616
- Matsumoto, K., Okada, M., Horikoshi, Y., Matsuzaki, H., Kishi, T., Itaya, M. & Shibuya, I. (1998) Cloning, sequencing, and disruption of the *Bacillus subtilis* *psd* gene coding for phosphatidylserine decarboxylase. *J Bacteriol* **180(1)**: 100-106
- Mazodier, P., Thompson, C. & Boccard, F. (1990) The chromosomal integration site of the *Streptomyces* element pSAM2 overlaps a putative tRNA gene conserved among actinomycetes. *Mol Gen Genet* **222**: 431 - 434
- McArthur, M., & Bibb, M. (2006 ) *In vivo* DNase I sensitivity of the *Streptomyces coelicolor* chromosome correlates with gene expression: implications for bacterial chromosome structure. *Nucleic Acids Research* **34(19)**: 5395-5401
- McCormick, J.R., Su, S.P, Driks, A., & Losick, R. (1994) Growth and viability of *Streptomyces coelicolor* mutant for the cell division gene *ftsZ*. *Molecular Microbiology* **14**: 243-254
- McCormick, J.R. (2009) Cell division is dispensable but not irrelevant in *Streptomyces*. *Current Opinion in Microbiology* **12**: 689-698
- Merrick, M.J. (1976) A morphological and genetic mapping study of bald colony mutants of *Streptomyces coelicolor*. *J Gen Microbiol* **96**: 299-315

- Mersinias, V. (2003) Total RNA isolation from *Streptomyces* cultures with RNeasy protect bacteria kit . In.: UniS *Streptomyces* microarray group, pp.
- Metcalf, T., Wang, J.L., & Schindler, M. (1986) Lateral diffusion of phospholipids in the plasma membrane of soybean protoplasts: evidence for membrane lipid domains. *Proc Natl Acad Sci USA* **83**: 95-99
- Michener, C., & Sokal, R. (1957) A quantitative approach to a problem in classification. *Evolution* **11**: 130-162.
- Mitchison, D.A. (1979) Basic mechanisms of chemotherapy. *Chest* **76(6)**: 771–781
- Mitchison, D. A. (2000) Role of individual drugs in the chemotherapy of tuberculosis. *Int J Tuberc Lung Dis* **4(9)**: 796-806
- Miguélez, E.M., Martín, C., Manzanal, M.B., & Hardison, C. (1992) Growth and morphogenesis in *Streptomyces*. *FEMS Microbiol Lett* **100**: 351–360
- Miller, K.J. (1985) Effects of Temperature and Sodium Chloride Concentration on the Phospholipid and Fatty Acid Compositions of a Halotolerant *Planococcus* sp. *J Bacteriol* **162(1)**: 263-270
- Mills, N. (2006). ChemDraw Ultra 10.0. *J. Am. Chem. Soc.* **128 (41)**: 13649–13650
- Molle, V., Palframan, W.J., Findlay, K.C., & Buttner, M.J. (2000) WhiD and WhiB, homologous proteins required for different stages of sporulation in *Streptomyces coelicolor* A3(2). *J Bacteriol* **182(5)**: 1286-1295
- Montgomery, R.A., & Dallman, M.J. (1997) Semi-quantitative polymerase chain reaction analysis of cytokine and cytokine receptor gene expression during thymic ontogeny. *Cytokine* **9**: 717–726

- Mori, T. (2007) MDR-TB - Its characteristics and control in Asia-Pacific rim symposium in USJCMSP 10th international conference on emerging infectious diseases in the Pacific rim. *Tuberculosis* **87**: S5-S9
- Morita, Y.S., Paul, K.S. & Englund, P.T. (2000) Specialized fatty acid synthesis in African trypanosomes: myristate for GPI anchors. *Science* **288**: 140-143
- Morita, Y.S. *et al.* (2005). Compartmentalization of Lipid Biosynthesis in Mycobacteria. *THE JOURNAL OF BIOLOGICAL CHEMISTRY* **280(22)**: 21645–21652
- Morrison, N. (2012). <http://www.in-pharmatechnologist.com/Processing-QC/Accelrys-moves-into-Pharma-QA-QC-with-VelQuest-acquisition>. *in-pharma technologist*. Retrieved: 15/11/2012
- Murakami, T., Holt, T. G. & Thompson, C. J. (1989). "Thiostreptoninduced gene expression in *Streptomyces lividans*." *J Bacteriol* 171: 1459 - 1466.
- Munro, S. (2003) Lipid rafts: elusive or illusive? *Cell* **115**: 377-388
- Nikawa, J. I., Kodaki, T., & Yamashita, S. (1988) Expression of the *Saccharomyces cerevisiae* *PIS* gene and synthesis of phosphatidylinositol in *Escherichia coli*. *J Bacteriol* **170(10)**: 4727-4731
- Nishibori, A., Kusaka, J., Hara, H., Umeda, M., & Matsumoto, K. (2005) Phosphatidylethanolamine domains and localization of phospholipids synthases in *Bacillus subtilis* membranes. *J Bacteriol* **187**: 2163-2174
- Nishijima, S., Asami, Y., Uetake, N., Yamagoe, S., Ohta, A., & Shibuya, I. (1988) Disruption of the *Escherichia coli* *cls* gene responsible for cardiolipin synthesis. *J Bacteriol* **170(2)**: 775-780



- Noto, T., Miyakawa, S., Oishi, H., Endo, H. & Okazaki, H (1982) Thiolactomycin, a new antibiotic. III. In vitro antibacterial activity. *J Antibiot* **35**: 401-410
- Ohta, A., & Shibuya, I. (1977). Membrane phospholipid synthesis and phenotypic correlation of an *Escherichia coli* pss mutant. *J Bacteriol* **132**: 434 - 443
- Okada, M., Matsuzaki, H., Shibuya, I., & Matsumoto, K. (1994). Cloning, sequencing and expression in *Escherichia coli* of the Bacillus subtilis gene for phosphatidylserine synthase. *J Bacteriol* **176**: 7456-7461
- Okanishi, M., Suzuki, K., & Umezawa, H. (1974) Formation and reversion of streptomycete protoplasts: cultural conditions and morphological study. *J Gen Microbiol* **80**: 389-400
- Okuyama, H., & Wakil, S.J. (1973) Positional specificities of acyl coenzyme A: glycerophosphate and acyl coenzyme A: monoacylglycerophosphate acyltransferases in *Escherichia coli*. *Journal of Biological Chemistry* **248**: 5197-5205
- Parry, C., & Davies, P.D. (1996) The resurgence of tuberculosis. *Soc Appl Bacteriol Symp Ser* **25**: 23s - 26s
- Peyron, P., Bordier, C., N'Diaye, E.N., & Maridonneau-Parini, I. (2000) Nonopsonic phagocytosis of *Mycobacterium kansasii* by human neutrophils depends on cholesterol and is mediated by CR3 associated with glycosylphosphatidylinositol-anchored proteins. *J Immunol* **165**: 5186-5191
- Philips, J.A., Rubin, E.J., & Perrimon, N. (2005) Drosophila RNAi screen reveals CD36 family member required for mycobacterial infection. *Science* **309**: 1251-1253

- Pieringer, R.A., Bonner, H., Jr., & Kunnes, R.S. (1967) Biosynthesis of phosphatidic acid, lysophosphatidic acid, diglyceride and triglyceride by fatty acyltransferase pathway in *E. coli*. *Journal of Biological Chemistry* **242(11)**: 2719-2724
- Pluschke, G., Hirota, Y., & Overath, P. (1978) Function of phospholipids in *Escherichia coli*. Characterization of a mutant deficient in cardiolipin synthesis. *Journal of Biological Chemistry* **253(14)**: 5048-5055
- Price, B., Adamidis, T., Kong, R., & Champness, W. (1999) A *Streptomyces coelicolor* Antibiotic Regulatory Gene, *absB*, Encodes an RNase III Homolog. *J Bacteriol* **181(19)**: 6142–6151
- Prosser, J.O., & Tough, A.J. (1991) Growth mechanics and growth kinetics of filamentous microorganisms. *Crit Rev Biotech* **10(10)**: 253-274
- Raetz, C.R.H., & Kennedy, E.P. (1972) The association of phosphatidylserine synthase with ribosomes in extracts of *Escherichia coli*. *Journal of Biological Chemistry* **247**: 2008-2014
- Raetz, C.R.H., & Kennedy, E.P. (1973) Function of cytidine diphosphate-diglyceride and deoxycytidine diphosphate-diglyceride in the biogenesis of membrane lipids in *Escherichia coli*. *Journal of Biological Chemistry* **248(3)**: 1098-1105
- Raetz, C.R.H. (1976) Phosphatidylserine synthetase mutants of *Escherichia coli*. Genetic mapping and membrane phospholipid composition. *Journal of Biological Chemistry* **251**: 3242-3249
- Rampini, C., Barbu, E., & Polonovski, J. (1970) Metabolisme du disphosphatidyl-glycerol d'*E.coli* K 12 apres l'arret, par incubation en milieu sans source d'energie, du developpement des bacteries. *C R Acad Sci* **270**: 882-885

- Rando, R.R. (1988) Regulation of protein kinase C activity by lipids. *The FASEB Journal* **2(8)**: 2348-2355
- Rappolee, D.A., Mark, D., Banda, M.J., & Werb, Z. (1988) Wound macrophages express TGF-alpha and other growth factors in vivo: analysis by mRNA phenotyping. *Science* **241**: 708–712
- Redenbach, M., Kieser, H.M., Denapaite, D., Eichner, A., Cullum, J., Kinashi, H., & Hopwood, D.A. (1996) A set of ordered cosmids and a detailed genetic and physical map for the 8 Mb *Streptomyces coelicolor* A3(2) chromosome. *Mol Microbiol* **21**: 77–96
- Rodriguez-Garcia, A., Combes, P., Perez-Redondo, R., Smith, M.C.A. & Smith, M.C.M. (2005) Natural and synthetic tetracycline-inducible promoters for use in the antibiotic-producing bacteria *Streptomyces*. *Nucleic Acids Research* **33(9)**: 1-8
- Romantsov, T., Helbig, S., Culham, D.E., Gill, C., Stalker, L., & Wood, J.M. (2007) Cardiolipin promotes polar localization of osmosensory transporter ProP in *Escherichia coli*. *Molecular Microbiology* **64**: 1455-1465
- Romantsov, T., Stalker, L., Culham, D.E., & Wood, J.M. (2008) Cardiolipin controls the osmotic stress response and the subcellular location of transporter ProP in *Escherichia coli*. *J Biol Chem* **283**: 12314-12323
- Rozen, S., & Skaletsky, H.J (2000) Primer3 on the WWW for general users and for biologist programmers. In: Krawetz S, Misener S (eds) *Bioinformatics Methods and Protocols: Methods in Molecular Biology*. Humana Press, Totowa, NJ, 365-386

- Saha, S.K., Nishijima, S., Matsuzaki, H., Shibuya, I., & Matsumoto, K. (1996a) A regulatory mechanism for the balanced synthesis of membrane phospholipid species in *Escherichia coli*. *Bioscience, Biotechnology, and Biochemistry* **60(1)**: 111-116
- Saha, S.K., Furukawa, Y., Matsuzaki, H., Isao Shibuya, I., & Matsumoto, K. (1996b) Directed Mutagenesis, Ser-56 to Pro, of *Bacillus subtilis* Phosphatidylserine Synthase Drastically Lowers Enzymatic Activity and Relieves Amplification Toxicity in *Escherichia coli*. *Bioscience, Biotechnology, and Biochemistry* **60(4)**: 630-633
- Saitou, N., & Nei, M. (1987). The neighbor-joining method: a new method for reconstructing phylogenetic trees. *Mol Biol Evol* **4(4)**: 406-425
- Sambrook, J., Fritsch, E.F., & Maniatis, T. (1989). Molecular cloning a laboratory manual. *Cold Spring Harbour Laboratory Press*.
- Sandoval - Calderon, M., Geiger, O., Guan, Z., Barona-Gomez, F., & Sohlenkamp, C. (2009) A Eukaryote-like Cardiolipin Synthase Is Present in *Streptomyces coelicolor* and in Most Actinobacteria. *Journal of Biological Chemistry* **284(26)**: 17383 - 17390
- Satre, M., & Kennedy, E.P. (1978) Identification of Bound Pyruvate Essential for the Activity of Phosphatidylserine Decarboxylase of *Escherichia coli*. *THE JOURNAL OF BIOLOGICAL CHEMISTRY* **253(2)**: 479 - 483
- Scherr, N., & Nguyen, L. (2009) *Mycobacterium* versus *Streptomyces* - we are different, we are the same. *Current Opinion in Microbiology* **12**: 699-707
- Schuiki, I., & Daum, G. (2009) Phosphatidylserine decarboxylases, key enzymes of lipid metabolism. *IUBMB Life* **61(2)**: 151-162.

- Schwedock, J., McCormick, J.R., Angert, E.R., Nodwell, J.R., & Losick, R. (1997) Assembly of the cell division protein FtsZ into ladder-like structures in the aerial hyphae of *Streptomyces coelicolor*. *Molecular Microbiology* **25(5)**: 847-858
- Shibuya, I. (1992) Metabolic regulations and biological functions of phospholipids in *Escherichia coli*. *Progress in Lipid Research* **31**: 245-299
- Shibuya, I., Miyazaki, C., & Ohta, A. (1985) Alteration of phospholipid composition by combined defects in phosphatidylserine and cardiolipin synthases and physiological consequences in *Escherichia coli*. *J Bacteriol* **161(3)**: 1086-1092
- Sinensky, M. (1974) Homeoviscous adaptation: a homeostatic process that regulates the viscosity of membrane lipids in *Escherichia coli*. *Proc Natl Acad Sci USA* **71**: 522-525.
- Singer, S. J., & Nicolson, G.L. (1972) The Fluid Mosaic Model of the Structure of Cell Membranes. *Science* **175(4023)**: 720-731
- Slayden, R.A., Lee, R.E., Armour, J.W., Cooper, A.M., Orme, I.M., Brennan, P.J., & Besra, G.S. (1996) Antimycobacterial action of thiolactomycin: an inhibitor of fatty acid and mycolic acid synthesis. *Antimicrob Agents Chemother* **40**: 2813-2819
- Smokvina, T., Mazodier, P., Bocard, F., Thompson, C. J., & Guerineau, M. (1990) Construction of a series of pSAM2-based integrative vectors for use in actinomycetes. *Gene* **94(1)**: 53-59
- Sneath, P., & Sokal, R. (1973) Numerical Taxonomy. *Freeman*, San Francisco.

- Souza, K.A., Kostiw, L.L., & Tyson, B.J. (1974) Alteration in normal fatty acid composition in a temperature sensitive mutant of a thermophilic bacillus. *Arch Microbiol* **97**: 89-102
- Sparrow, C.P., & Raetz, C.R.H. (1985) Purification and properties of the membrane-bound CDP-diglyceride synthetase from *Escherichia coli*. *Journal of Biological Chemistry* **260(22)**: 12084-12091
- Sumartojo, E.(1993) When tuberculosis treatment fails. A social behavioural account of patient adherence. *American review of respiratory diseases* **147**: 1311-1320
- Sun, J., Kelemen, G.H., Fernandez-Abalos, J., & Bibb, M.J. (1999) Green fluorescent protein as a reporter for spatial and temporal gene expression in *Streptomyces coelicolor* A3(2). *Microbiology* **145**: 2221–2227
- Stover, C.K., Warrener, P., VanDevanter, D.R., Sherman, D.R., Arain, T.M., Langhorne, M.H., Anderson, S.W., Towell, J.A., Yuan, Y., McMurray, D.N., Kreiswirth, B.N., Barry, C.E., & Baker, W.R. (2000) A small-molecule nitroimidazopyran drug candidate for the treatment of tuberculosis. *Nature* **405(6789)**: 962–966
- Takano, E., Gramajo, H.C., Strauch, E., Andres, N., White, J., & Bibb, M.J. (1992) Transcriptional regulation of the *redD* transcriptional activator gene accounts for growth-phase-dependent production of the antibiotic undecylprodigiosin in *Streptomyces coelicolor* A3(2). *Molecular Microbiology* **6(19)**: 2797-2804
- Takano, E., White, J., Thompson, C.J., & Bibb, M.J. (1995) Construction of thiostrepton-inducible, high-copy-number expression vectors for use in *Streptomyces* spp. *Gene* **166**: 133 - 137

- Thompson, C.J., Ward, J.M., & Hopwood, D.A. (1980) DNA cloning in streptomycetes - resistance genes from antibiotic - producing species. *Nature* **286**: 525-527
- Trotter, P.J., Pedretti, J., & Voelker, D.R. (1993) Phosphatidylserine Decarboxylase from *Saccharomyces cerevisiae*. *THE JOURNAL OF BIOLOGICAL CHEMISTRY* **268(28)**: 21416-21424
- Vaillancourt, P.G., Costa, G.L., & Weiner, M.P. (1994) Vector systems for directional and bidirectional cloning of PCR-generated DNA fragments and high-level protein expression. *Abstr Pap Am Chem Soc* **207**: 123-BIOT
- Vance, J. E., & Steenbergen, R. (2005) Metabolism and functions of phosphatidylserine. *Progress in Lipid Research* **44**: 207-234
- VanWezel, G.P., Meulen, J., Luiten, R.G.M., SHINICHI Kawamoto, S., Koerten, H.K., & Kraal, B. (2000) *ssgA* is essential for sporulation of *Streptomyces coelicolor* A3(2) and affects hyphal development by stimulating septum formation. *J Bacteriol* **182(20)**: 5653–5662
- Vasilenko, I., De Kruijff, B., & Verkleij, A.J. (1982) Polymorphic phase behaviour of cardiolipin from bovine heart and from *Bacillus subtilis* as detected by <sup>31</sup>P-NMR and freeze-fracture techniques. Effects of Ca<sup>2+</sup>, Mg<sup>2+</sup>, Ba<sup>2+</sup> and temperature. *Biochim Biophys Acta* **684(2)**: 282-286
- Vergne, I., Chua, J., Lee, H.H., Lucas, M., Belisle, J., & Deretic, V. (2005) Mechanism of phagolysosome biogenesis block by viable Mycobacterium tuberculosis. *Proc Natl Acad Sci USA* **102**: 4033-4038
- Viegas, A., Manso, J., Nobrega, F.L., & Cabrita, E.J. (2011) Saturation-Transfer Difference (STD) NMR: A Simple and Fast Method for Ligand Screening and Characterization of Protein Binding. *J. Chem. Educ.* **88(7)**: 990-994

- Voelker, D.R. (1997) Phosphatidylserine decarboxylase. *Biochimica et Biophysica Acta (BBA) - Lipids and Lipid Metabolism* **1348(1-2)**: 236–244
- Volmink, J., & Garner, P. Directly observed therapy for treating tuberculosis. Cochrane Database of Systematic Reviews 2007, Issue 4. Art. No.: CD003343. DOI: 10.1002/14651858.CD003343.pub3
- Wade, M.M., & Zhang, Y. (2004) Anaerobic incubation conditions enhance pyrazinamide activity against *Mycobacterium tuberculosis*. *J Med Microbiol* **53(8)**: 769–773
- Walburger, A., Koul, A., Ferrari, G., Nguyen, L., Prescianotto-Baschong, C., Huygen, K., Klebl, B., Thompson, C., Bacher, G., & Pieters, J. (2004) Protein kinase G from pathogenic mycobacteria promotes survival within macrophages. *Science* **304**: 1800 - 1804.
- Waller, R.F., Keeling, P.J., Donald, R.G., *et. al.* (1998) Nuclear-encoded proteins target to the plastid in *Toxoplasma gondii* and *Plasmodium falciparum*. *Proc Natl Acad Sci USA* **95**: 12352-12357
- Weintraub, H., & Groudine, M. (1976) Chromosomal subunits in active genes have an altered conformation. *Science* **193**: 848-856
- Weis, J.H., Tan, S.S., Martin, B.K., & Wittwer, C.T. (1992) Detection of rare mRNAs via quantitative RT-PCR *Trends in Genetics* **8**: 263–264
- Willey, J., Santamaria, R., Guijarro, J., Geistlich, M., & Losick, R. (1991) Extracellular Complementation of a Developmental Mutation Implicates a Small Sporulation Protein in Aerial Mycelium Formation by *S. coelicolor*. *Cell* **65**: 641-650



- Willey, J.M., Willems, A., Kodani, S., & Nodwell, J.R. (2006) Morphogenetic surfactants and their role in the formation of aerial hyphae in *Streptomyces coelicolor*. *Molecular Microbiology* **59(3)**: 731–742
- Williams, R.P., Green, J.A., & Rappoport, D.A. (1956) Studies on pigmentation of *Serratia marcescens*. 1. Spectral and paper chromatographic properties of prodigiosin. *J Bacteriol* **71**: 115-120
- Winer, J., Jung, C.K., Shackel, I., & Williams, P.M. (1999) Development and validation of real-time quantitative reverse transcriptase-polymerase chain reaction for monitoring gene expression in cardiac myocytes in vitro. *Analytical Biochemistry* **270**: 41-49
- WHO. (2008) Tuberculosis. *Who Health Organization Fact Sheet* N°104. Geneva.: World Health Organization.
- WHO. (2010) Treatment of tuberculosis guidelines 4<sup>th</sup> Edition. Geneva.: World Health Organization.
- WHO. (2011). Global tuberculosis control. Geneva.: World Health Organization
- WHO. (2011). Tuberculosis MDR-TB and XDR-TB 2011 Progress Report. Geneva.: World Health Organization
- Wright, A., Zignol, M., Deun, A.V., Falzon, D., Gerdes, S.R., Feldman, K., Hoffner, S., Drobniewski, F., Barrera, L., Soolingen, D.V, Boulabhal, F., Paramasivan, C.N., Kam, K.M., Mitarai, S., Nunn, P., Raviglione, M. (2009) Epidemiology of antituberculosis drug resistance 2002–07: an updated analysis of the Global Project on Anti-Tuberculosis Drug Resistance Surveillance. *The Lancet* **373**: 1861-1873

- Xia, W. M., & Dowhan, W. (1995) Phosphatidylinositol cannot substitute for phosphatidylglycerol in supporting cell growth of *Escherichia coli*. *J Bacteriol* **177(10)**: 2926-2928
- Xu, H., Chater, K., Deng, Z., & Tao, M. (2008) A cellulose synthase-like protein involved in hyphal tip growth and morphological differentiation in *Streptomyces*. *J. Bacteriol* **190**: 4971-4978
- Xu, W., Lu, W., Zhou, Y., Zhu, L., Shen, H., & Wang, J. (2009) Adherence to anti-tuberculosis treatment among pulmonary tuberculosis patients: a qualitative and quantitative study. *BMC Health Services Research* **9(169)**: 1-8
- Yanisch-Perron, C., Vieira, J., & Messing, J. (1985) Improved M13 phage cloning vectors and host strains: Nucleotide sequences of the M13mp18 and pUC19 vectors. *Gene* **33**: 103–119
- Yu, F., Inouye, S., & Inouye, M. (1986) Lipoprotein-28, a cytoplasmic membrane lipoprotein from *Escherichia coli*. Cloning, DNA sequence, and expression of its gene. *Journal of Biological Chemistry* **261(5)**: 2284-2288.
- Zager, E. M., & McNerney, R. (2008). Multidrug-resistant tuberculosis. *BMC Infectious Diseases* **8(10)**: 1-5
- Zamorano, P.L., Mahesh, V.B., & Brann, D.W. (1996) Quantitative RT-PCR for neuroendocrine studies. A minireview. *Neuroendocrinology* **63**: 397–407
- Zhang, A., Li, F., Ding, C., Yao, Q., Knapp, B.I., Bidlack, J.M., & Neumeyer, J.L. (2007) Synthesis and Pharmacological Evaluation of 6,7-Indolo/Thiazolo-Morphinans Further SAR of Levorphanol. *J Med Chem* **50**: 2747-2751

Zignol, M., Hosseini, M.S., Wright, A., Weezenbeek C.L., Nunn P., Watt C.J., Williams B.G., & Dye, C. (2006) Global incidence of multidrug-resistant tuberculosis. *The Journal of Infectious Diseases* **194(4)**: 479-485